The Development and Application of an *In Vitro* Model of Coronary Lesion Thrombosis

by

Kumaran Kolandaivelu

B.S. Mechanical Engineering
Massachusetts Institute of Technology, 1995

M.S. Mechanical Engineering
Massachusetts Institute of Technology, 2003

SUBMITTED TO THE DEPARTMENT OF HEALTH SCIENCES AND TECHOLOGY
IN PARTIAL FULFILLMENT OF THE REQUIREMENTS FOR THE DEGREE OF

DOCTOR OF PHILOSOPHY IN MEDICAL ENGINEERING MEDICAL PHYSICS
AT THE MASSACHUSETTS INSTITUTE OF TECHNOLOGY

MAY 2005 [June 2005]

Signature of Author: _____
Department of Health Sciences and Technology
May 16, 2005

Certified by: _____
Elazer R. Edelman
Thomas D. and Virginia W. Cabot Professor
Division of Health Sciences and Technology
Thesis Supervisor

Accepted by: _____
Martha L. Gray, Ph.D.
Edward Hood Taplin Professor of Medical and Electrical Engineering
Director, Harvard-MIT Division of Health Sciences and Technology

The Development and Application of an *In Vitro* Model of Coronary Lesion Thrombosis

by Kumaran Kolandaivelu

Submitted to the Department of Mechanical Engineering on May 16, 2005 in Partial Fulfillment of the Requirements for the Degree of Doctor of Philosophy in Medical Engineering Medical Physics

Abstract

Thrombosis is an initiating response to vascular injury. Physiologically, this process aids in the repair and remodeling of the vessel wall. However, if left unchecked, luminal occlusion may rapidly occur. The coronary vascular bed is a life-sustaining environment in which pathological thrombosis can lead to devastating outcomes such as acute coronary syndromes or post-interventional thrombosis. In order to study these coronary thrombotic reactions, it is essential to consider the physical environment in which they occur. We have developed an *in vitro* method for creating pulsatile flows to mimic the coronary hemodynamic setting on a beat-to-beat basis. Furthermore, he have developed techniques and protocols to parametrically vary both the biological and physical aspects of thrombosis and in doing so, have investigated the effects of real-world temporal and spatial flow perturbations on local site platelet adhesion. Not only do such variations create quantitative differences in local reactions, but qualitative differences as well as various receptors must interact to create stable adhesions in a given hemodynamic environments. These findings have implications on the propensity for certain individuals to form clot under certain condtitions, as well as the environment-dependent efficacy of various clinically relevant anti-thrombotic strategies

Thesis Supervisor: Elazer R. Edelman
Thomas D. and Virginia W. Cabot Professor of Health Sciences and Technology

Acknowledgments

First and foremost, I would like to thank my mentor, Prof. Elazer R. Edelman who through a perfect balance of guidance, acceptance and support over the past six years has guided me over an improbable path towards an impossible goal. Thanks to his tremendous foresight and insight, I have, in hindsight, enjoyed all that I have seen along the way.

I would also like to thank my thesis committee: Prof. Roger D. Kamm who has been a beacon on the often choppy waters of fluid mechanics, Dr. Fredrick D. Welt whose ability to mix the intricacies of cardiovascular biology with an all around good nature provide on inspiration for the years that lie ahead, and Dr. Robert D. Handin who helped me begin to appreciate the important distinctions between a scientific and engineering approach.

I give special thanks to Nick Houstis, Siraj Ali, two great friends with whom I have been stumbling with for the past seven years, and undoubtedly will stumble with for many more. Also, I would like to thank Mercedes for being a great friend and a portal to a Spanish sun-- to endless rays of light and laughter which have illuminated even my darkest days (and nights) as a researcher. Viva la Spain! And of course, my partner-in-crime, Bobbie Bushiae-- without whom I would have likely finished a year or two ago, but with whom I would gladly spend a lifetime more. Viva la Bobbie Bushaie!

Last, I dedicate this thesis to my mom and dad, who have taught me above all else to take them for granted. You are my foundation.

Table of Contents

List of Figures

List of Tables

CHAPTER 1 Background and Significance

1.1 Coronary Thrombosis

1.1.1 Pathophysiology

The vital coronary arteries transport freshly oxygenated blood to the heart (see Fig. 1.1). These vessels branch off of the aorta, curving over the epicardial surface while bifurcating and providing tributaries to the ever-beating myocardial tissue. Such complex geometries and the pulsing intramural pressures create a high degree of spatial and temporal diversity in the local hemodynamic environment, resulting in a unique vascular setting.

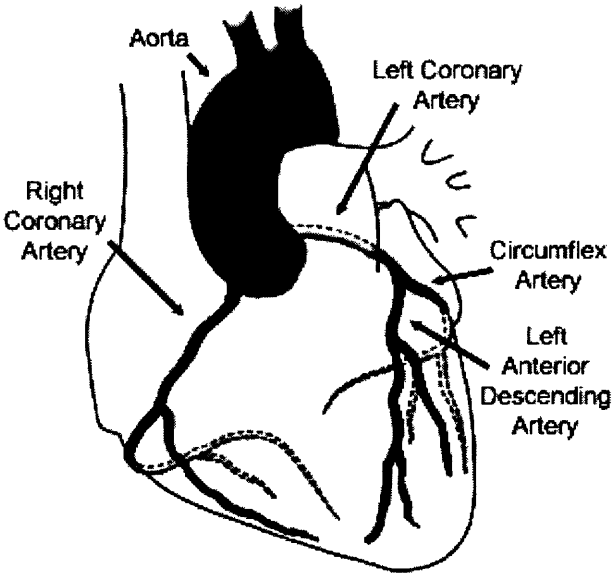

Figure 1.1 Schematic diagram of the heart and major overlying coronary arteries.

In states of health, the coronary vessels, as all parts of the vasculature, are lined with a protective endothelial barrier that separates the highly reactive vessel wall and contained blood compartments. Traversing through these conduits, changes in the vascular environment are accompanied by changes in the phenotypes of these cells [1]. Gene expression patterns, surface receptor expression, and a slew of other cellular mechanisms are tightly linked to the environment and work to keep this living surface appropriately matched with local needs.

Within the first decades of life, nearly ubiquitous environmental and genetic stresses conspire to create loci of low-grade injury to the protective endothelial surface allowing the accumulation of subendothelial deposits of lipids and lipid-laden

macrophages [2-6]. These minor breaches instigate a complex cycle of chronic inflammation and immune recruitment through endothelial activation, smooth muscle cell proliferation and migration, extracellular matrix turnover, and the build up of cellular and necrotic debris. Over time, such processes transform into full fledged atherosclerotic disease and luminal stenosis. Figure 1.2 *a*, *b* depicts a healthy vessel and one whose lumen has been diminished by atherosclerotic plaque burden.

a. Healthy **b. Diseased**

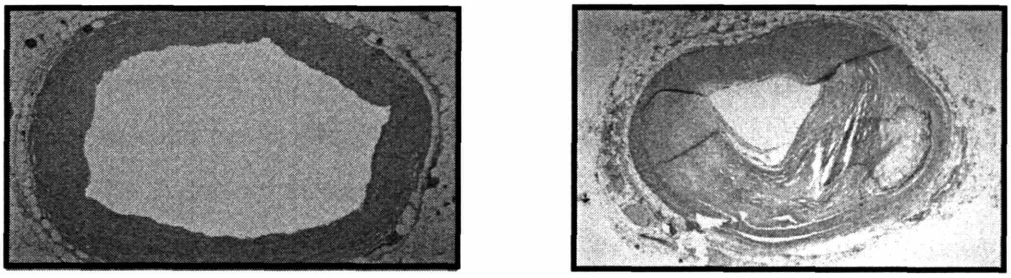

Figure 1.2. a. Healthy coronary artery with patent lumen; b. Atherosclerotic coronary artery with luminal stenosis

Typically, the plaques are characterized by a lipid-laden, highly thrombogenic, necrotic core, covered by a fibrous cap region. As the plaques continue to grow, regulatory mechanisms are often able to compensate and uphold the balance between blood supply and myocardial demand. While such progressive, chronic, atherosclerotic processes can eventually lead to significant, uncompensatable disease (> 75% area reduction) characterized by ischemic episodes and stable angina (exertional chest pain), a far more devastating and unpredictable outcome is plaque rupture or endothelial erosion (see Fig 1.3) [2-4, 7, 8].

Under such circumstances, the protective endothelial layer is acutely disrupted, exposing highly reactive subendothelial, atheromatous components. A rapid, thrombotic process ensues which can either exacerbate disease progression or lead to acute coronary syndromes (ACS) such as unstable angina, acute myocardial infarction, or ischemic sudden death.

1.1.2 Treatments

Prevention is the preferred treatment option for coronary disease. Epidemiological studies have generated a great deal of information regarding the different genetic and environmental risk factors involved in coronary disease progression [9-11]. Accordingly, appropriate measures can be taken to minimize risk. Currently, our cellular and molecular based understanding of the etiology of atherosclerosis and thrombosis has also allowed the use of relatively safe, long-term drug strategies. Perhaps the most notable example is the widespread use of aspirin in treating populations at risk of coronary disease. By targeting platelet responsiveness (a key component of the arterial thrombotic response), aspirin has offered a 25% relative risk reduction of severe cardiovascular incidence (vascular death, MI, stroke) becoming a nearly ubiquitously used background therapy [12]. A battery of such agents (statins, etc) has shown great risk benefit, with novel drugs, either targeting new mechanisms for reducing the complications of pre-existing ones, constantly emerging [13, 14].

Unfortunately, many cases of coronary disease are brought on unexpectedly (ACS), or are simple too far progressed (severe luminal stenosis), necessitating more intensive strategies. In cases of thrombosis, highly potent anti-thrombotics and fibrinolytic agents (which prevent the build up and promote the dissolution of clots respectively) have proven highly effective if administered within critical windows [15]. Such powerful, systemic agents are not suitable for sustained therapy do to excessive complications, and while these provide immediate, life-saving benefit, the underlying problems of atherosclerosis and plaque instability remain [16, 17]. The supply/demand mismatch accompanying severe stenosis can also often be managed medically with agents such as nitroglycerin which, up to a point, can aid innate autoregulatory mechanisms [18]. While such therapies may provide immediate relief, the chronic need for medication often indicates a need for more invasive revascularization procedures. Coronary bypass arterial grafting (CABG) has long been the standard revascularization procedure [19, 20]. However, the advent of minimally-invasive, ever-improving, catheter-based therapies has transformed the state of coronary disease management. Two wide spread approaches include angioplasty, which mechanically disrupts the atherosclerotic segment through balloon expansion, and stenting, which involves the co-

expansion of a permanent, rigid, foreign structure adding post-procedural, luminal support. Although the benefits offered by such treatments are indisputable, changes in the biological and physical environment accompanying mechanical disruption of the endothelial barrier and insertion of a foreign structure, even as minor as a intravascular wire, can lead to deleterious complications by iatrogenically creating an ACS-like state.

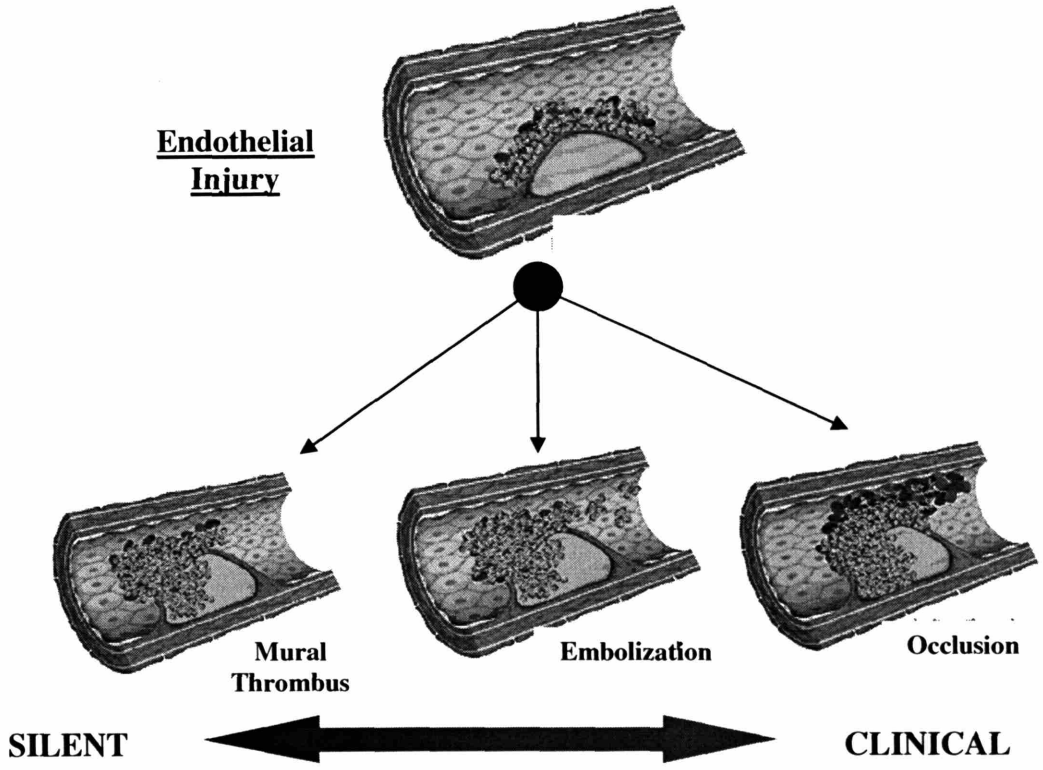

Figure 1.3. Clinical and silent (subclinical) thrombotic outcomes of vascular injury.

Much effort has been placed in understanding and controlling the complex, pathophysiological mechanisms of atherosclerotic disease and its devastating outcome, coronary thrombosis. Still, in westernized societies, such endovascular disease processes account for close to 50% of all deaths [6]. For continued improvement of safe, efficacious management of coronary events (pathological and iatrogenic), it is important to gain further understanding into the mechanisms and events leading up to acute thrombosis within the vital coronary arterial setting.

1.2 The Platelet

While a multitude of biological effectors are involved in vascular thrombosis, we will focus on the platelet as an essential mediator of the biological response to vascular injury. Platelets are circulating cells (1.5-4.5 X 10^8/ml) which bud off from megakaryocytes resident in the bone marrow [21]. Although anucleate, platelets are highly responsive to their environment. A multitude of surface receptor interactions, second messenger pathways, pre-packaged granule release substances (Fig 1.4), and translatable proteins allow these cells to provide constant monitor of the vascular environment and play a key role in initiating biological responses.

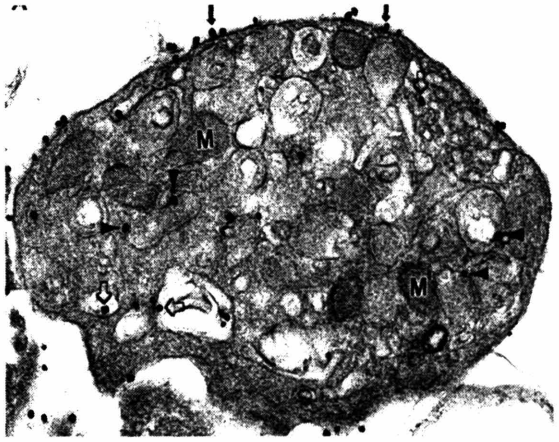

Figure 1.4 Tunneling electron microscope image of anucleate platelet depicting numerous internal storage granules and canalicular system (image reproduced from Feng D, et al. Blood. 99(11), 2002).

The importance of platelets in arterial thrombosis cannot be overstated as attested to by the clinical effectiveness of anti-platelet therapies in minimizing arterial thrombotic risk [22]. Upon binding to an injured wall, they alter their expression of surface molecules and release substances which both attract and adhere to flowing cells, as well as promote the enzymatically driven coagulative response. Accordingly, platelet wall reactions and subsequent component interactions are essential to understand when considering the thrombotic response to vascular injury.

1.2.1 Platelet Reactions

Platelet/wall reactions classically take place in a series of steps, beginning with initial contact, followed by a sequence of activation, firm adhesion, cell spreading, and aggregation (Fig. 1.5).

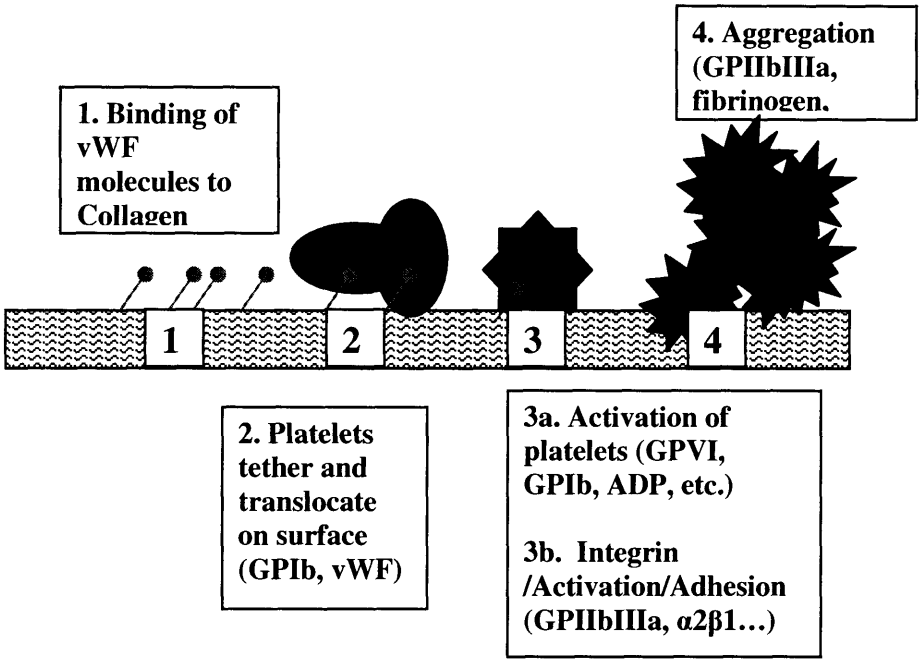

Figure 1.5. Sequence of platelet/vessel wall reactions.

Tethering/Activation

The platelet glycoprotein Ib (GPIb; in complex with GPIX, GPV) and von Willebrand's Factor (vWF) are important components in enabling initial platelet/surface contact in arterial, high flow environments [23, 24]. Upon endothelial breach, platelets tether to sub-endothelial matrix vWF (either directly present or adsorbed to matrix collagen from the blood) via fast on-off rate GPIb bonds [25]. The speed of these bonds is an essential quality of this interaction in allowing the platelets to grab onto the surface under high shear conditions [26-28]. Several studies have shown that these tethering interactions become increasingly important at shear rates above 300 s^{-1}, becoming essential at shears above 1500 s^{-1} in reducing the platelet relative wall velocity in a start-stop type dynamic [26, 29]. As the platelet slows and translocates, a multitude of other activating responses take place. The GPIB-vWF bond itself is known to be one of these activating pathways by interacting with internal, second messenger machinery [28, 30-32]. Concurrently, autocrine and paracrine substances, such as ADP, thrombin, thromboxane, and epinephrine, bind to specific receptors, further potentiating platelet activation [21, 33].

Recently, the importance of the collagen activating receptor GPVI has also been shown to provide a physiologically essential activating interaction with exposed collagen and vWF surfaces [34]. It is an integration of these coalescing, outside-in, activating pathways that dictate the final activation decision.

Firm adhesion/Spreading

An essential outcome of platelet activation in supporting shear dependent thrombosis is the modulation of platelet integrin receptors from their low to high affinity state. Integrins are cell surface molecules, composed of an α and β subunit, and support adhesion to particular substrates [35]. The major platelet integrins are αIIbβIII, α2β1, and αVβ3 [35, 36]. Upon activation, these receptors support the firm adhesion of platelets onto fibrinogen, collagen, and fibronectin surfaces respectively. However, the existence of other, less prevalent integrins and substrate cross reactivity create redundancy in the adhesion pathways and while providing a safety net given the importance of adequate platelet adhesion, dramatically complicating the mechanistic picture.

After firm adhesion, internal processes that are not fully characterized lead to filipodial extensions and cell spreading [37]. Such cytoskeletal rearrangement allows more complete surface contact, enhanced integrin binding, and increased binding strength of the adherent platelets.

Aggregation

Platelet shape change is accompanied by granular exocytosis which helps to transform the local biological milieu by the release of substances such as ADP and thromboxane [21]. Free-stream platelets are potentiated and activated in this pro-thrombotic environment. As induced during surface interactions, such activation enables high affinity integrin conformations. Platelet-derived fibrinogen and vWF add to pre-existing, local plasma concentrations of these proteins, enhancing binding to activated αIIbβIII integrin receptors [21, 38]. These protein/receptor interactions mediate inter-platelet cross-linking and aggregation, forming what is commonly referred to as the primary hemostatic plug.

1.2.2 Platelet Interactions

Though platelets play an essential, initiating role in arterial thrombosis, they are far from the only participants. Numerous interactions with other blood-borne cellular and protein components have long been recognized as mediators of thrombotic disease.

Coagulation

When platelets are activated, negatively charged phospholipids, such as phosphotidylcholine and phosphotidylserine, are externally presented, localizing various enzymatic reaction complexes of the coagulation cascade to the platelet surface [21, 33, 39]. This sequestration keeps the reactants in close proximity to one another, while protecting them from other free-stream anti-coagulative mechanisms. Upon association with the platelet membrane, conformational changes in enzyme/substrate complexes also dramatically accelerate the reactions [21, 39]. Such localization and catalysis are essential for the successful progression of coagulation under flow conditions where convective mass transport would otherwise wash away the formed products [21].

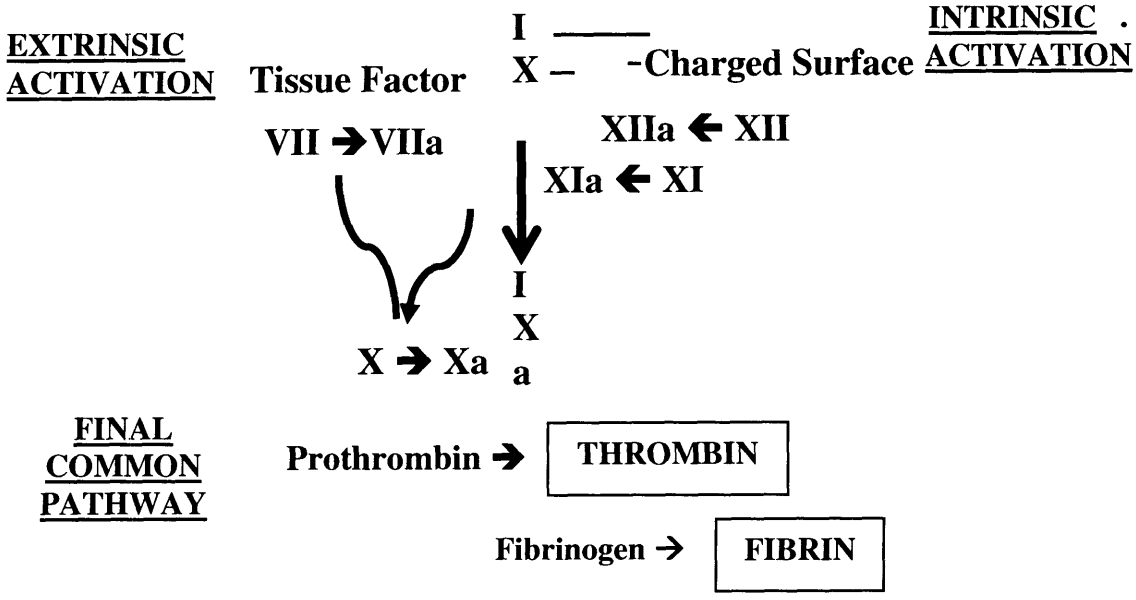

Fig 1.6. Classical reactions of the coagulation cascade commensing with the exposure of tissue factor (Extrinsic activation) and/or an appropriate surface (Intrinsic activation), leading to the explosive, proteolytic production of thrombin and fibrin

While platelets are necessary in supporting coagulative propagation, the products of the coagulation cascade in turn play a critical role in potentiating and stabilizing primary, platelet-driven hemostasis. The key reactions of this proteolytic pathway are shown in Figure 1.6 [21, 39]. Classically, coagulation is initiated via the extrinsic or intrinsic pathways, merging into the common pathway with the eventual production of thrombin which catalyzes the conversion of monomeric fibrinogen to fibrin. While numerous interactions exist, thrombin and fibrin are two of the most important and well characterized links between platelet function and coagulation.

Thrombin is known to be a potent activator of platelets through a variety of mechanisms. Protease activated receptors (PAR-1, 4) have been characterized on the surface of platelets [40-42]. Using a unique cleavage mechanism, thrombin causes receptor self-association and activation. Interestingly, the various PARs are functionally activated at different threshold concentrations of thrombin, while additional interactions with the GPIb receptor have been recently recognized to affect platelet activation [42-45]. Such connections allude to the delicate control structures poised between the coagulative network and platelet function.

While the physiological relevance of thrombin-activation has been shown, its catalytic conversion of fibrinogen to fibrin also plays a critical role in platelet-driven thrombosis. Once formed, monomeric fibrin quickly polymerizes into a mesh-like network of filaments. Platelets can adhere to this fibrin mesh via αIIbβIII receptor linkage, greatly strengthening the cohesiveness of the aggregating, hemostatic plug (Fig. 1.7) [46].

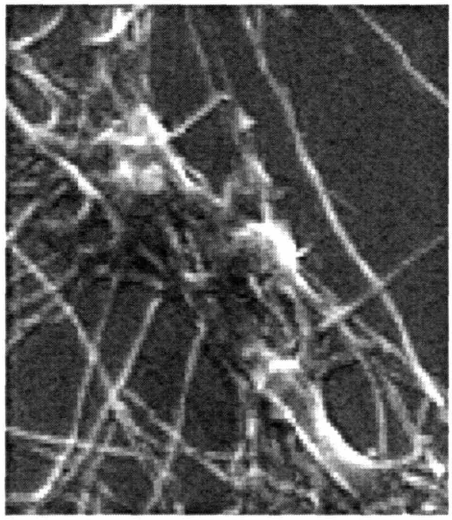

Figure 1.7 .Platelets 'entangled' in fibrin mesh (surface electron microsopy; image by Alisa Morss)

Though these classical platelet/coagulation interactions are key mediators of physiological thrombus formation, they are only representative

of a long list of interactions, many of which are characterized, and a great many of which undoubtedly remain to be found.

Leukocytes

Leukocytes are the cellular mediators of the inflammatory and immune responses. In blunt categorizations, these responses have often been considered as separate to the thrombotic reactions. However, upon closer examination, the great deal of interactions between these biological processes has grayed the distinction. As with coagulation, a variety of platelet processes are involved in initiating inflammatory responses and vice-versa. Upon vessel wall injury and platelet recruitment, P-selectin is rapidly presented on the surface of the activated platelet layer. Surface expression of this selectin is able to recruit various leukocytic cells. Neutrophils and monocytes initially adhere via P-selectin glycoprotein ligand-1 (PSGL-1), tethering in a manner analogous to the GPIb-vWF interactions of platelets [25, 47]. Again, outside-in signaling causes leukocytic activation and integrin modulation enabling firm adhesion. The importance of platelets in heralding such inflammatory processes is witnessed in the effectiveness of P-selectin blockade or powerful platelet inhibition on limiting the development of chronic vascular inflammatory processes such as atherosclerosis or the neointimal formation after interventional treatments [48].

Just as platelets play a critical role in inflammation, the importance of inflammatory mediators in thrombosis is now being recognized. Cytokines produced during inflammatory processes such as tumor necrosis factor (TNF), interlukin-1 (IL-1), monocytic chemoattractant protein-1 (MCP-1), and IL-6, have all been found to upregulate the expression of tissue factor (TF) on endothelial and monocytic surfaces. TF is the key initiating factor in extrinsic activation (see Fig. 1.6), and it is becoming recognized that such cytokine-mediated expression of TF acts as a primary initiator of thrombosis by shifting the vascular environment into a prothrombotic state [49].

Erythrocytes

Erythrocytes (red blood cells; RBCs) are also important in modulating arterial thrombotic events. Being the most numerous blood cell, RBCs dramatically alter the fluidic

properties of blood. Flow-dependent gradients in erythrocyte distribution marginalize the platelets to the flow periphery, dramatically increasing local platelet wall concentrations [50, 51]. Further, by increasing the viscous forces of blood, erythrocytes dramatically affect the shear force at a given shear rate which can have significant impact on biophysical processes such as thrombosis.

RBCs are also one of the primary, physiological sources of ADP, a potent activator of platelets. Under conditions of shear, ADP pathways have been shown to greatly enhance platelet activation and adhesion [52, 53]. The relevance of this mechanism in arterial thrombus formation is attested to by the efficacy of ADP receptor blockade via thienopyridine derivatives (i.e. clopidogrel, ticlopidine) in minimizing post-interventional thrombotic risk [53, 54].

In this section, we have described the fundamental processes underlying platelet/wall adhesion, which serves an essential, initiating role in arterial thrombus formation. We have also introduced some of the classic interactions that platelets undergo with other blood-borne, vascular components. While these interactions only breach the surface of the thrombotic response, they point to the complexity of the biological issue and the need to develop controllable systems where parameters can be sufficiently isolated, allowing tractable, mechanistic studies to be performed.

1.3 The Local Hemodynamic Setting

It is important to recognize that biological interactions both occur in and react to their physical surroundings. In vascular environments, flow is one of the critical physical parameters that helps to maintain vascular diversity and dictate vascular responses. The coronary environment provides a distinctive setting where curving vessels, numerous branch points, geometric pathologies and the time-dependent nature of the driving pressure create highly unique, complex flow patterns (see Fig. 1.8) [1, 55-58].

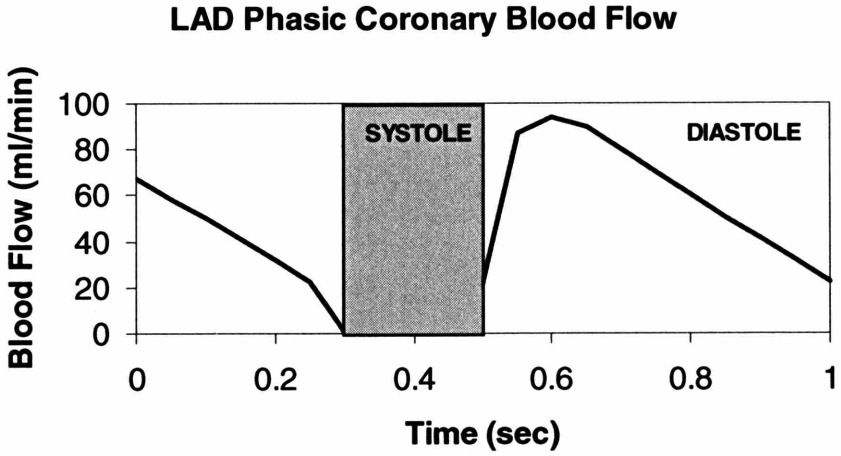

Figure 1.8. Typical phasic coronary flow profile in the left anterior descending coronary branch (LAD). In supplying blood to the beating myocardial wall, coronary flow principally occurs during diastolic relaxation, being driven to a halt with rising, systolic, intramural pressures.

These spatially and temporally diverse conditions must be appreciated when considering highly flow-sensitive events such as thrombosis. Here, we introduce some of the mechanisms whereby physical flow parameters may interact with biological factors and the manner by which the local hemodynamic environment can be altered in states of disease.

1.3.1 Local Flow Interactions

Flow can affect biological interactions on variety of levels, from molecular to microscopic to macroscopic scales. Often times these dependencies stem from basic physical concepts such as mass transport and physical forces. However, given the long time scales that these biological mechanisms have been interacting within relatively stable physical environments, selective pressures have also enabled biological systems to evolve sophisticated machinery, allowing them to respond and adapt to their surroundings in a more complex manner.

Molecular Interactions

The mass transport of molecular substances to and from an activating locus plays an important role in thrombus formation. In flowing environments, fleeting conditions are setup as diffusive and convective forces transport substances to and from the reactive site. The mass flux, J, of a substance reacting at a surface has been shown to be:

$$J(x,t) = \frac{C_0}{\frac{1}{k_w} + \frac{1}{k_l(x,t)}} \qquad (1)$$

for arteries of diameter > 0.1mm [59]. This relation shows that the flux is dependent on the mean bulk concentration C_O, the wall reactivity of the substance, k_w, as well as the mass transport coefficient, k_l. In cases where the wall reactivity is very low compared to the mass transport coefficient, the flux is said to be reaction limited. Alternatively, with low mass transport coefficients, transport dictates the surface flux.

Flow affects this relation implicitly through k_l, which, in the case of the entrance region in large cylindrical arteries, is given by:

$$k_l = .5K\left(\frac{\gamma D^2}{x}\right)^{\frac{1}{3}} \qquad (2)$$

where D is the diffusion constant, K is a proportionality constant dependent on geometry and boundary conditions, x is the axial distance from the start of the region, and γ is the wall shear rate [59]. Thus, when substances are transport limited ($J \rightarrow C_0 k_l$), flow modulates the surface flux. This becomes highly relevant in cases of static or recirculant flows such as those which are often established in the complex coronary vasculature (particularly given the autocatalytic nature of many blood-borne reactions). That the physiological reactions of thrombosis globally function in this flow dependent regime is revealed by the morphological differences in thrombus formation under venous (low) and arterial (high) flow systems and by observations such as the increased likelihood of post-interventional acute thrombotic events in poorly perfused vessels [21, 60-62].

Microscopic Interactions

Cellular Transport (k_m)

Just as reactive molecules are transported to and from the reactive surfaces, so are cellular components. However, due to special non-Newtonian properties of blood, the effective diffusion coefficient, D, of cells is itself a function of erythrocyte concentration and flow parameters. As blood flows through the vasculature, RBCs migrate towards the flow axis creating a flow-dependent, radial concentration gradient. As a result, platelets are marginalized to the flow periphery, increasing the shear dependence of platelet mass flux. [50]. Various studies of platelet wall interactions have shown surface accumulation to be largely dependent on flow parameters, implicating the importance of transport phenomena and the underlying diffusion limitations involved in this process [50].

Wall Reactivity (k_w)

While cells and molecules must be transported to the wall, they must also be able to react when appropriate, and the wall reactivity, k_w, can also be considered a complex function of fluid flow. Local shear stresses and pressure forces have been shown to greatly affect vessel wall morphology. Endothelial cells and wall smooth muscle cells are able to sense these physical forces and respond with directed genotypic and phenotypic changes. When activated, these cells alter their expression of surface adhesion molecules [1, 63]. These, along with numerous other changes (i.e. TF, vWF, tissue plasminogen activator,

platelet activating factor-1, thrombospondin, RANTES, monocytic chemoattractant protein-1), alter the local environment creating a generalized, prothrombotic, proinflammatory state [1, 58, 64-66].

The paradigm of vascular cell adhesion to this reactive wall in flowing environments parallels the scheme outlined for platelet adhesion (recall Fig. 1.5), beginning with the presentation of a particular class of surface adhesion molecules called selectins (or vWF in the case of platelets). Various cell types express various types of selectins. These molecules interact with respective ligands on free-stream cells, thereby recruiting them to the vessel wall. Selectin/ligand interactions are characterized by fast binding constants, and are thus able to catch flowing cells under high shear conditions [25]. While necessary in supporting the initial cell/wall contact under flow, they do not bind tightly, and instead produce a rolling motion as bonds are sequentially broken and formed. During this slowed, translocation, several other pathways cause vascular cell activation, resulting in integrin receptor activation and firm, shear-resistant adhesion to surface ligands [67]. These prototypical flow mediated interactions are representative of vascular cell/wall interactions, with the exact receptor/ligand interactions dependent on the particular cell type and substrate under consideration.

Macroscopic Interactions

On macroscopic scales, shear stresses can integrate to create high local forces which can have a significant impact on the pathogenic progression of vascular disease. Atherosclerotic plaques are characterized by atheromatous core regions, covered by a fibrous cap. Acute thrombotic events often occur when such plaques rupture by sudden fracture of the cap region and currently there is much interest in studying the strength of the cap as varied biological properties can affect plaque stability [68-71]. However, the final rupture event is predicated on the fact the cap strength is too weak in relation to local fluidic forces.

As cells and molecules aggregate on the reactive wall via the flow-dependent processes outlined above, larger mural thrombus develops and is increasingly subject to macroscopic embolizing forces. As in the case of plaque rupture, embolization is known to be highly dependent on shear rates, with embolic stresses varying linearly with wall

shear at thrombus heights less than 0.1 mm and quadratically at larger heights as a result of flow separation [72, 73]. In either situation, the rheological situation dictates the removal forces that help to determine detachment probability.

1.3.2 Local Geometric Environment

Local fluid flow plays an important role in directing the thrombotic response. By prescribing the flow boundary conditions, the local physical geometry is critical to determining the contained flow field, and thus also plays a crucial role. These geometries can be dramatically altered in states of disease or intervention, having great impact on the local hemodynamic environment and the tightly dependent biological outcomes.

Physiological Geometries

Physiological vascular properties such as curvature, branching, and tapering are all highly relevant in establishing the local flow environment, particularly in the coronary bed where the arteries coarse over the curved epicardial surface, supplying numerous braches to the demanding myocardial wall (Fig. 1.9) [74].

In purely axial flows, radial and circumferential symmetry ensure purely axial pressure gradients and relatively simple flow profiles. However, in more complex, curved flow streams, adverse axial and orthogonal pressure gradients are established, creating secondary flow fields and zones of recirculation (Fig. 1.10*a*, *b*) [56, 75, 76]. These can have significant impacts on local wall shear stresses and through the

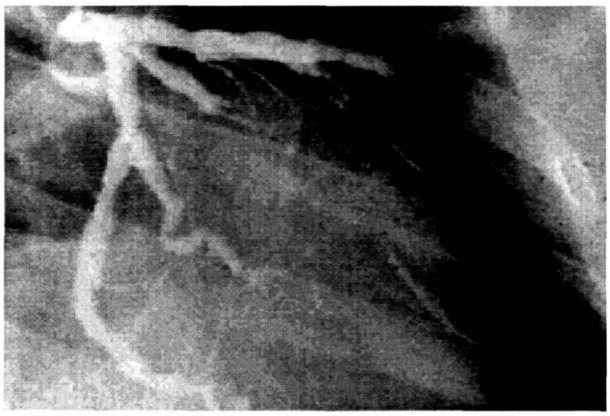

Figure 1.9. Angiogram of coronary arteries depicting highly branching, curving geometries overlying and penetrating the heart tissue (image reproduced from Dhond, MK, et. al. Clinical

biophysical connections outlined above, orchestrate local biological responses.

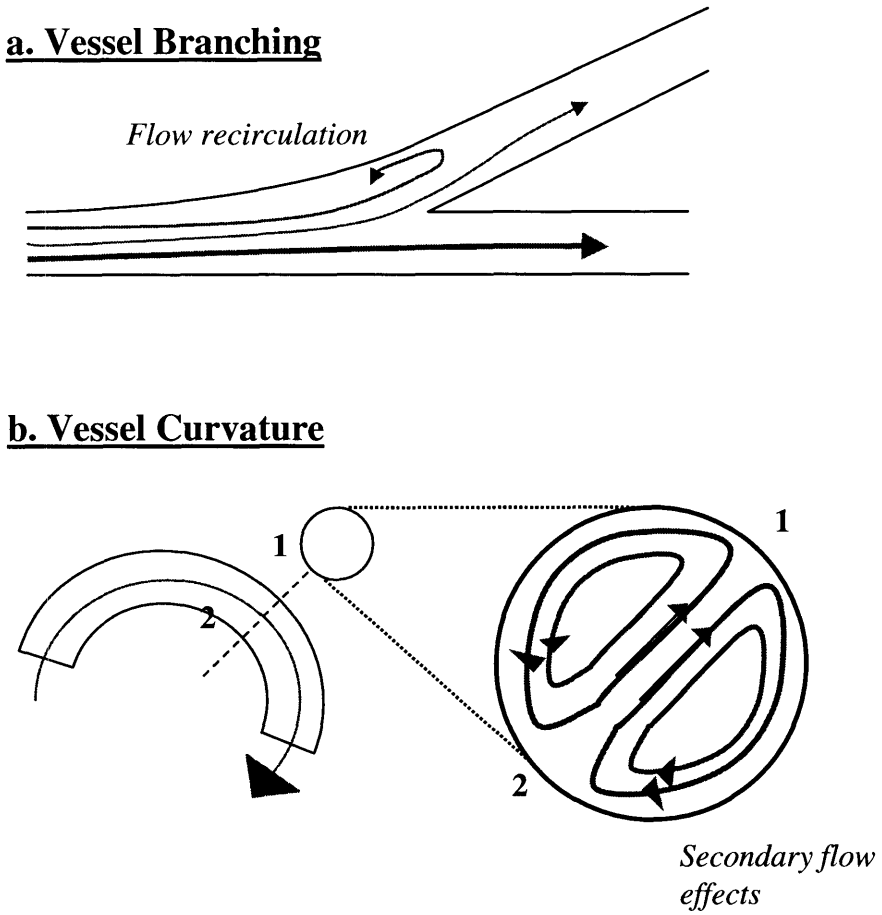

Figure 1.10. Examples of vessel architecture leading to complex flow patterns. a. Vessel branching and axial flow reversal and recirculation; b. Vessel curvature and transverse, secondary flows.

Such responses are essential in vascular remodeling and maintaining healthy vessels. However, when inappropriately harnessed, they can also lead to vascular disease progression. The effect of local, physiological geometries and the resultant flow fields in vascular pathology is well recognized, as indicated by the frequent initiation of atherosclerosis at sites of vessel branching or the increased atherosclerotic burden observed on the inner curvature of coronary vessels [77, 78].

Pathological Geometries

While physiological geometries correlate well with disease initiation, local geometries can be significantly altered with disease progression, often compounding the detrimental effects. As cellular and necrotic debris accumulate within the wall, volume constraints result in either inward (stenotic) or outward (aneurismal) remodeling of the vessel wall. In cases of compensatable stenosis, mass conservation implies increased flow velocities for a given total flow rate, with wall shear rates at times exceeding 10,000 s^{-1} (typically < 600 s^{-1} in the coronary arteries) [51, 52, 79]. Under such pathological conditions, free-stream vascular cell activation and erythrocyte hemolysis can significantly alter volumetric blood status leading to both local and far-reaching systemic effects [79, 80]. When the total flow rate can no longer be maintained due to excessive stenotic flow resistance, severe decompensation can conversely result in dramatically reduced flows. Indeed, when plaques rupture and mural thrombus occludes the lumen, increased resistance can totally eliminate blood flow, quickly potentiating further thrombus growth. Alternatively, under aneurismal conditions, flow rheology can also be significantly affected. As a result of reduced transport and embolic forces in recirculant zones, significant, venous-like mural thrombus formation is often observed, creating a nidus for thromboembolic disease [21, 59].

Interventional Geometries

Significant geometry-altering vascular disease is often treated with interventional revascularization techniques which can in themselves affect the local geometry and hemodynamic environment. Stenting involves the placement of an intravascular structure that props open the vessel lumen. The post-interventional luminal shape is determined by the overall profile of the implanted stent device, and has been shown to have an impact on long-term biological outcomes, likely due in part to alterations in fluid flow [81]. Furthermore, in order to provide sufficient radial support, stents are typically made of a mesh work of steel struts on the order of 100 μm thick. While this thickness is relatively small compared to the entire flow diameter (> 2 mm), their juxtaposition next to the vessel wall can significantly alter local wall shear stresses, with complex flow patterns developing in the inter-strut regions [82-85]. Berry et. al. have shown that

changes in stent geometry, can dramatically affect these flow fields and resultant mass transport parameters [82].

The effects of stent placement can also be more pronounced depending on implantation technique. Significant over-expansion can lead to aneurismal-like conditions, while insufficient expansion can results in significant flow abnormalities. Indeed, such improper expansions have been associated with the high acute thrombotic rates observed in the early clinical stenting experience [61, 86].

While the placement of intravascular objects can create altered local flow, a more subtle point is that revascularization itself alters the geometry and `expected' flow field of the vessel due to the significant biological adaptations that occur during disease progression. Recently, Richter and Edelman (unpublished observations, 2003) have shown that such acute interventional revascularization can lead to adverse, unexpected outcomes.

We have briefly described some of the key mechanisms by which flow can interact with the thrombotic processes. Furthermore, we have discussed how the physical, geometric environment can have a significant impact on flow parameters under physiological, pathological and interventional conditions. Considering these significant interactions, an attempt to study thrombotic reactions in the coronary setting would hopefully take these physical parameters into account, allowing them to be manipulated and studied in a controlled fashion, along with the pertinent biological components.

1.4 Methods of studying flow dependent thrombosis

A variety of methods have been utilized to investigate thrombotic reactions under appropriate hemodynamic conditions. These methods include both *in vivo* and *ex vivo* models, as well as bench-top *in vitro* setups. Each of these methodologies has offered unique insights by virtue of inherent advantages, though often these same advantages limit the types of information that can be gleaned from their use. It has been a combined use of these techniques, along with an appreciation of their limitations that has contributed greatly to our current understanding of vascular biology. Here, we present various methodologies that have been and are currently being used to study flow-dependent thrombotic reactions and the types of advances they have provided.

1.4.1 *In Vivo* Models (Realistic)

In vivo models offer a degree of realism and physiological relevance unattainable in bench-top models, and when chosen appropriately, allow thrombotic outcomes to be assessed in relevant hemodynamic conditions. The two most basic types of *in vivo* study include clinical trials and animal studies.

Human Studies/Clinical Trials

Human studies and clinical trials generate immediately applicable, clinical information, inherently taking into account the complex biological interactions at work in the human body. Such studies allow integrated, relevant, systemic and long-term processes to be observed, offering clear cut advantages over other systems when considering actual disease characterization, patient risk stratification, and the efficacy of therapeutic options. Historically, mechanistic insights have been obtained from observing the human condition, often times becoming evident when systems overtly fail. Indeed, many important processes of the thrombotic response have been initially discovered through clinical presentation (GPVI deficiency, Glanzmann's thrombasthenia, Bernard-Soulier, GPIb deficiency, vWF disease, etc.) [21]. While such accidental observations are predicated on patients and patience to search the space of biological processes, they are implicitly of great relevance.

Human studies and clinical trials are by definition the most relevant to the human condition. However, as the primary goal is to benefit the immediate patient, making clear scientific progress is difficult at best. The lack of ideal controls and patient variability (particularly given the optimizing nature of medical advance) causes such trials to be expensive and long, oftentimes yielding unclear conclusions. Further complicating the issue is that as trials are performed, the evolving ground of clinical experience often races by, altering the clinical relevance, therapeutic dogmas and potentially, for patient benefit, the clinical trials themselves.

Animal Studies

One step removed, animal models of physiology and pathology allow detailed observation of complex biological situations while offering a more controlled setting than human studies. Though ethical considerations and respect must always accompany the experimental use of living organisms, an accepted goal in animal use is the progress of scientific understanding for human benefit, thus allowing intensive, well-controlled, prospective studies to be carried out to completion.

Animal models of thrombosis span the evolutionary ladder, from the use of non-human primates to mice. Architectural similarity and flow conditions in large animals allow highly relevant studies of thrombotic processes under appropriate hemodynamic settings. Alternatively, the ease of manipulation and relatively low cost of small animal studies enable more fundamental questions to be epistatically probed, dramatically accelerating the pace of scientific discovery and understanding. However, the relevance to the human condition varies tremendously as a result of species-specific biological and physical differences and the often crude models used to approximate human vascular disease. Furthermore, while offering greater experimental possibilities than human trials, there are still limitations in the parameters that can be reasonably manipulated in living animals, particularly when considering complex traits such as the hemodynamic environment [79, 87-89].

1.4.2 *In Vitro* Models (Perturbable)

To gain detailed mechanistic insight into the rheological dependence of thrombosis, it is important to have parametric control over the hemodynamic and complex biological environments. *In vitro* models allow powerful manipulations to be performed on isolated biological components under highly consistent, prescribed physical conditions, thus offering a degree of versatility not attainable with *in vivo* settings. Such models can broadly be categorized into systems that maintain physical geometric properties and those that maintain flow conditions.

Maintaining Geometry

Geometrically relevant *in vitro* systems maintain realistic vascular dimensions and have been applied towards various issues, from endovascular device thrombogenicity to cellular adhesion in vascular deformities. One limitation in these models has been in developing suitable bench-top mechanisms of flow actuation and control. While some setups have employed gravity to provide a pressure head for generating blood flow, the need for sizable, static holding volumes in these one-pass systems significantly constrains the allowable flow rates and experimental run times [89]. Alternatively, loops partially filled with blood and mounted on a tilted turntable have been employed to create relative wall motion. This method allows the use of small blood volumes, though effects of blood recirculation and the required air-fluid interface must be considered when interpreting results [90-92]. Moreover, the constant flow potential of these gravity-driven systems results in restricted control of the flow environment. To establish more controllable flows, the most basic approach has been to use pumps to drive blood through a model flow circuit [93, 94]. However, even external peristaltic drives have generated excessive background levels of activation, proving too traumatic in setting up arterial-like flow conditions.

Maintaining Flow

Strategies that attempt to maintain geometry are typically constrained by the need to create high flow rates to generate arterial-like conditions. In order to study flow effects, laxness in the physical circuit architecture has enabled alternate schemes to be employed.

The use of small circuit geometries such as narrow, parallel-plate flow chambers, allows high shear rates to be developed under relatively low flow conditions [26, 83, 95-97]. Such *in vitro* systems allow great control of the biological environment while enabling microscopic visualization of surface-cellular interactions in real time. As a result of their controllability and observability, these studies have greatly enhanced our fundamental understanding of shear-dependent, thrombotic surface reactions.

Techniques such as cone-plate or annular ring devices create relative motion between two fluid-contacting surfaces, thus generating Cuvette-type flow. These models can establish well-described surface and volumetric shear profiles. Furthermore, while these Cuvette-systems dramatically change the physical flow shape, suitable scaling and experimental design have allowed certain geometrically relevant questions to be asked under appropriate flow settings [58, 98].

1.4.3 Proposed Flow System

Table 1.1 compares prior model systems that have been employed to study the hemodynamics of thrombosis with respect to the human condition.

		Complex Interactions	Physiol. Shear	Physiol. Geom.	Parametric Analysis (Biological)	Parametric Analysis (physical)	Signal/ Noise	Cost
In Vivo	**Clinical Trials**	+++	+++	+++	---	---	---	---
	Large Animal Studies	++	++	++	--	--	--	--
	Small Animal Studies	+	+	-	+	--	-	-
In Vitro	**Gravity Driven Systems**	--	-	++	+	-	+	+
	Peristaltic Systems	--	--	++	++	-	-	++
	Parallel Plate Chambers	--	++	--	++	-	++	++
	Cuvette-Systems	--	++	-	++	-	+	++
Ex Vivo	**Ex-Vivo Circuits**	-	++	++	-	+	+	--

Table 1.1. Comparison of prior methods showing an incomplete niche for experimental strategies supporting the simultaneous parametric analysis of biological and physical systems. (Subjective scale, using clinical trials to reference extremes ratings: +++ → ---; Excellent → Poor).

Combining the information obtained from these systems has lead to great leaps in our understanding of acute thrombosis. *Ex vivo* hybrids, where external sections are placed in-line with a natural circulation, have helped to bridge the gap where *in vivo* and *in vitro* models do not meet [51]. Still, cracks remain and alternative models addressing new

issues are needed. One particular niche which we hope to address in this work is the need for systems that concurrently retain significant control of both the biological and physical axes, specifically with regards to the human coronary setting. The key selection criterion we considered when developing the system were:

1.) Generating and controlling physiologically relevant flows
2.) Creating versatile, geometrically relevant circuits
3.) Retaining control of the biological setting
4.) Maximizing the biological signal/circuit background noise ratio

After considering various strategies, we developed a novel, inertial mechanism that could produce highly controllable flows in relevant arterial geometries while maximizing the biological signal to background noise ratio by minimizing the circuit length and surface discontinuities. Briefly, fluid-filled loops are spun about their axis in a prescribed and controlled fashion to modulate relative fluid/wall motions through transmitted shear forces. This method further allows us to maintain low test volumes and cost, enabling reasonable parametric analysis of the biological and physical settings.

CHAPTER 2 Flow System Design

2.1 Theory

2.1.1 Description

In order to create the desired flow profiles, a fluid-filled torus (figure 4) is rotated about its axis. When impulsively started, there is inertial fluid motion relative to the toroid wall: With time, the fluid is accelerated due to momentum transfer into the fluid bulk via shear forces. Lyne has previously analogized such fluid motion to pressure driven flows where, moving in a reference frame with the wall (WRF), the acceleration takes on the driving character of a body force [99]. While the absolute fluid velocity in an inertial reference frame (IRF) may change under pressure driven or accelerating wall conditions, it is the maintenance of the velocity gradients, or shear, that is important in the flow-dependent thrombotic reactions [21, 50, 59]. Rather than fluid being conducted to and from a reactive wall surface, the relevant reaction control volumes are conducted away from the lagging fluid.

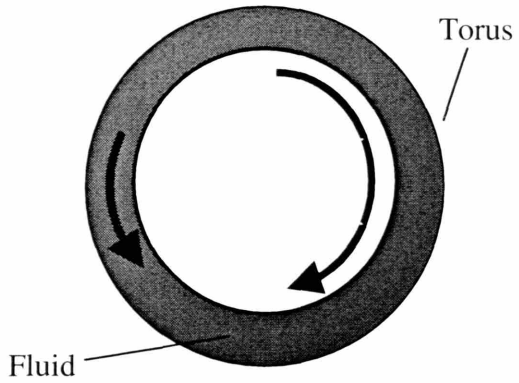

FIGURE 2.1. Fluid-filled torus. Clockwise motion of the torus causes relative counter-clockwise inertial motion of the contained fluid and vice versa.

Using such a technique, we hoped to create time-varying flows whose characteristics, as defined by the dimensionless mean Reynolds ($\overline{Re}$; based on an absolute velocity) and Womersley (α) parameters were typical of coronary flows, as well as estimate the secondary flow effects of curvature by considering the peak Dean number (κ_{peak}) associated with our system (see Table 2.1).

Dimensionless #	Definition	Typical Coronary Values (LAD)
Mean Reynolds # ($\overline{\mathrm{Re}}$)	$\frac{2a\overline{V_{fluid}}}{\nu}$	153±64
Womersley # (α)	$a\sqrt{\omega/\nu}$	1.5±0.27
Peak Dean # (κpeak)	$Max\left(\frac{2aV_{fluid}}{\nu}\sqrt{a/R}\right)$	95Ψ

Table 2.1. List of the dimensionless parameters considered, along with customary definitions and typical values found in the left anterior descending coronary branch (LAD) [13]. V_{fluid} is the mean cross-sectional axial velocity of the fluid, ν is the kinematic viscosity, ω is the flow oscillatory frequency, a is the vessel radius, and R is the radius of curvature of the loop. Ψ This value for κ_{peak} was calculated assuming a peak Re of twice the $\overline{\mathrm{Re}}$ and a aspect ratio, R/a, of 10 as suggested by Chang and Tarbell [15].

Table 2.1 defines these conventional dimensionless parameters [100]. In each of these parameters, a Newtonian approximation for the kinematic viscosity, ν, is used, as has been shown to be valid for high shear conditions (> 100 s^{-1}) and often applied when considering coronary flow [76, 78, 101, 102].

2.1.2 Analytical, Straight Tube Approximation

Equations

Simplifying to a linearly accelerating, straight tube model (Fig. 2.2), streamline curvature effects can be neglected and only the axial (z) component of the Navier-Stokes equation for cylindrical coordinates need be considered:

$$\left(\frac{\partial V_z}{\partial t}+V_r\frac{\partial V_z}{\partial r}+\frac{V_\theta}{r}\frac{\partial V_z}{\partial \theta}+V_z\frac{\partial V_z}{\partial z}\right)=-\frac{1}{\rho}\frac{\partial P}{\partial z}-\frac{d^2Z}{dt^2}+\upsilon\left(\frac{\partial^2 V_z}{\partial r^2}+\frac{1}{r}\left(\frac{\partial V_z}{\partial r}\right)+\frac{1}{r^2}\left(\frac{\partial^2 V_z}{\partial \theta^2}\right)+\frac{\partial^2 V_z}{\partial z^2}\right) \quad (3)$$

where V_z, V_r, and V_o are the velocity components in the axial (z), radial (r) and tangential (θ) directions respectively, t is time, ρ is the fluid density, $\delta P/\delta z$ is the axial pressure gradient, and d^2Z/dt^2 is the axial wall acceleration.

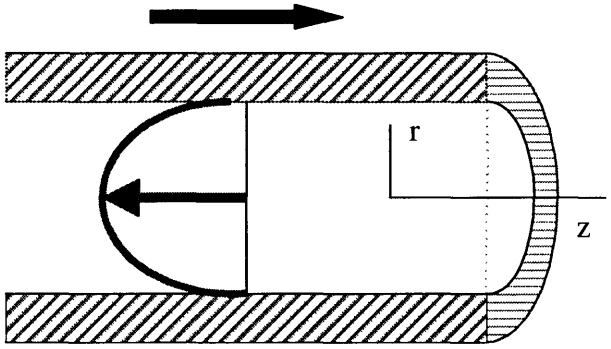

Figure 2.2. Theoretical system assuming linear rather than angular motions.

In the special case of flow in a circular pipe of constant cross sectional area, circumferential and axial symmetry allow several dependencies to be eliminated, leaving only an axial velocity component, V_z, dependent on r and t, and the driving pressure and acceleration terms. These considerations yield the equation:

$$\frac{\partial V_z}{\partial t}=-\frac{1}{\rho}\frac{\partial P}{\partial z}-\frac{d^2Z}{dt^2}+\upsilon\left(\frac{\partial^2 V_z}{\partial r^2}+\frac{1}{r}\left(\frac{\partial V_z}{\partial r}\right)\right) \quad (4)$$

By prescribing periodic functions for the driving terms of the form,

$$\frac{1}{\rho}\frac{\partial P(t)}{\partial z}=\sum_{n=1}^{\infty}G_n e^{in\omega t} \quad (5)$$

$$\frac{d^2Z(t)}{dt^2} = \sum_{n=1}^{\infty} A_n e^{in\omega t} \qquad (6)$$

analytical solutions with appropriate wall and centerline boundary conditions ($V_z(R, t)=0$; $dV_z/dr\ (0,t)=0$; where R is the tube radius) have been derived elsewhere [101, 103-105], yielding:

$$V_z(r,t) = \frac{-(G_0 + A_0)}{4\upsilon}\left(R^2 - r^2\right) + \sum_{n=1}^{\infty} \frac{(G_n + A_n)}{in\omega}\left[1 - \frac{J_0\left(i^{3/2} r\sqrt{\frac{n\omega}{\upsilon}}\right)}{J_0\left(i^{3/2} R\sqrt{\frac{n\omega}{\upsilon}}\right)}\right] e^{inwt} \qquad (7)$$

where the axial flow velocity, $V_z(r, t)$ is a function of radius and time, and can be driven by pressure gradients (Eq. 5) or wall accelerations (Eq. 6). G_n and A_n represent the amplitudes for the Fourier components of the nth harmonic of ω for the pressure gradient and wall acceleration respectively, while G_o and A_o are the steady forcing terms. From this straight tube model we see that identical relative flow profiles can be obtained through either pressure gradients or wall accelerations given the interchangeability of G and A.

Solutions

Using this linearly accelerating straight tube approximation, we can analytically study the nature of the contained flows under various prototypical forcing conditions. By applying an acceleration impulse of the form:

$$\frac{d^2Z(t)}{dt^2} = \sum_{n=1}^{\infty} e^{in\omega t} \qquad (8)$$

and solving equation 7 for $V_z(r, t)$ using R=0.16 cm (typical of coronary geometries), and a Newtonian approximation for the blood viscosity, υ=0.04 dynes cm/sec (valid for arterial type flows), we obtain the solution shown in figure 2.3.

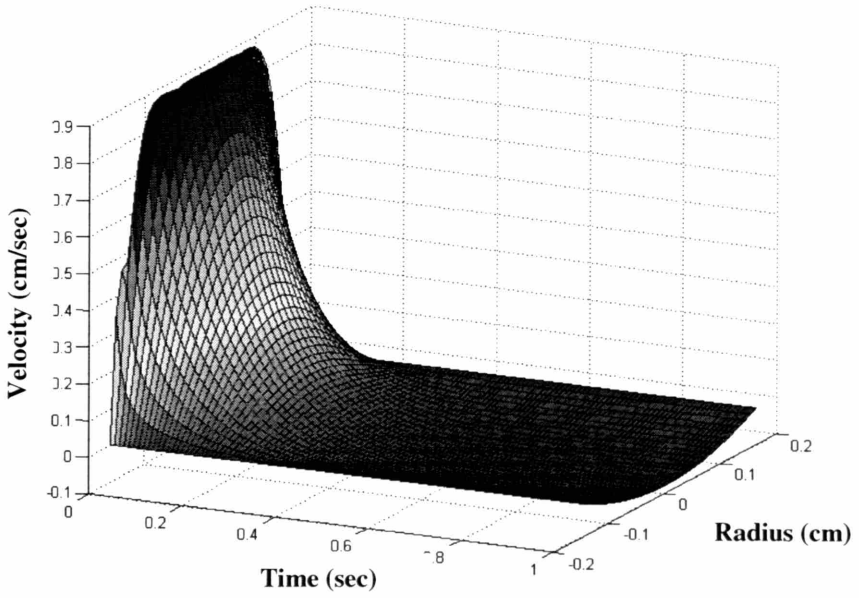

Figure 2.3. Evolution of the axial velocity profiles relative to the wall in a radial distribution over time given an impulsive wall acceleration.

We see that there is an initial spike of relative fluid motion which decays as shear forces propagate through the fluid, quickly establishing radially parabolic, axial velocities profiles. It is important to note that an impulse of wall acceleration leads to a step in wall velocity, and while this means that there continues to be fluid motion in the IRF, relative wall motion is not sustained through constant wall velocities. The impulsive decay is governed by a time constant dependent on the fluid viscosity and square of the tube radius (see Eq. 7) which we find to be equal to ~ 0.1 sec (time to 36.7% of peak value). While different amplitudes of acceleration can be used to drive the contained flow, this characteristic time remains unchanged so long as the fluid and tube properties remain constant.

In order to maintain a relative fluid/wall motion, the tube wall must continue to accelerate. For the case of constant acceleration,

$$A_0 = 628 cm/\sec^2 \qquad (9)$$

we can plot the radial, relative velocity profiles with time in the WRF (solid surface), along with the velocity profiles in an IRF (mesh surface; Fig. 2.4).

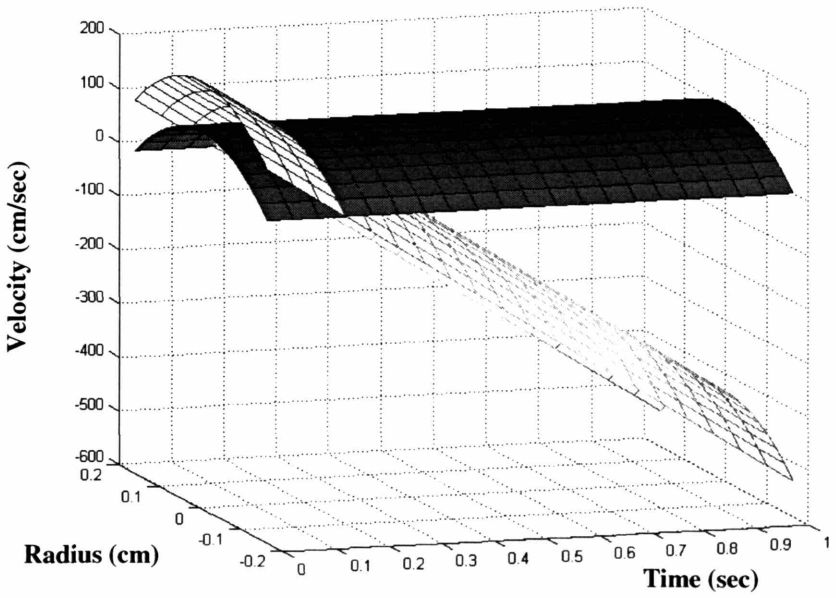

Figure 2.4. Parabolic axial velocity profiles in a radial distribution over time due to a constant wall acceleration in both a relative wall (solid) and inertial reference frame (mesh); R=0.16 cm; v=0.04 dynes cm/sec

As predicted, the induced, relative, constant velocity profiles are parabolic in nature, paralleling pressure-driven Pousille flows. While such relative flows can be created and maintained through wall accelerations, the continuous acceleration leads to unbounded wall and IRF fluid velocities. More generally, net positive flows require net positive accelerations. Thus any motor used to drive such a system would quickly reach its operating limit.

While this situation poses a problem, the unique coronary flow which we hope to emulate is highly pulsatile, as a systolic rise in intramural pressure drives the flow to a halt (recall Fig. 1.8). This creates a situation where relative wall motions and tube accelerations are reduced to zero. If the time for flow decay is gradual and greater than approximately

three system time constants, the flow can be reduced to within 5% of its peak value without having to decelerate the tube walls, while slower decay profiles can be quasi-statically accommodated by modulating the wall motions. On the other hand, rapid flow decelerations would create flow reversal and more complex flow patterns. Although identical, repeating acceleration profiles could maintain unidirectional flow pulses, this situation would lead to impractical, compounding wall velocities in the IRF. Rather, introducing a one-way valve or allowing bi-directional flow offers two potential solutions.

By incorporating a one-way valve, the walls can be rapidly brought to a halt once the contained fluid has reached solid body motion. This action essentially creates a negative impulsive wall acceleration that would normally drive rapid relative retrograde flow. However, by virtue of the one-way valve, the fluid can be kept motionless in the WRF and brought to rest in the IRF. Thus, unidirectional flow pulses can be maintained without a net compounding wall velocity.

There are various drawbacks to this method. Designing a one-way valve of sufficiently low profile is difficult, and would itself generate unwarranted resistance and hemodynamic effects. Even though the flow could be stopped in solid body rotation via a one-way valve, the imposed pressure wave created in the fluid due to the sudden deceleration could have consequences on the thrombotic process. As a principle goal of this system is to reduce noise and minimize external sources of thrombotic activation to allow sensitive, flow dependent studies, such disruptions are undesirable.

Alternatively, bi-directional flow at one half the frequency (ω_{system}) of the desired heart rate ($\omega_{coronary}$) can be established by following each tube acceleration profile with a symmetric deceleration. Such an action would create a flow of identical magnitude though in the opposite direction, at the end of which the tube would have no net change in momentum. This limits the maximal required speed of the motor to some value dependent solely of the characteristics of a single pulse, and is minimized by setting the bounds symmetrically about a zero angular velocity.

To observe the nature of this type of oscillatory flow, we can model wall velocities assuming a sinusoidal motion

$$\frac{dZ(t)}{dt} = \frac{A_1}{\omega_{system}} e^{i\omega_{system}t} \qquad (10)$$

$$\frac{d^2Z(t)}{dt^2} = A_1 e^{i\omega_{system}t} \qquad (11)$$

where we only consider one harmonic, ω_{system}, which is equal to the frequency of oscillation (heart rate/2=π). A_1/ω_{system} is the amplitude of the wall velocity, and A_1 gives the corresponding wall acceleration amplitude (200π cm/sec^2). Again solving equation 7 for the radial velocity profiles, w(r, t), we obtain the solution shown in figure 2.5.

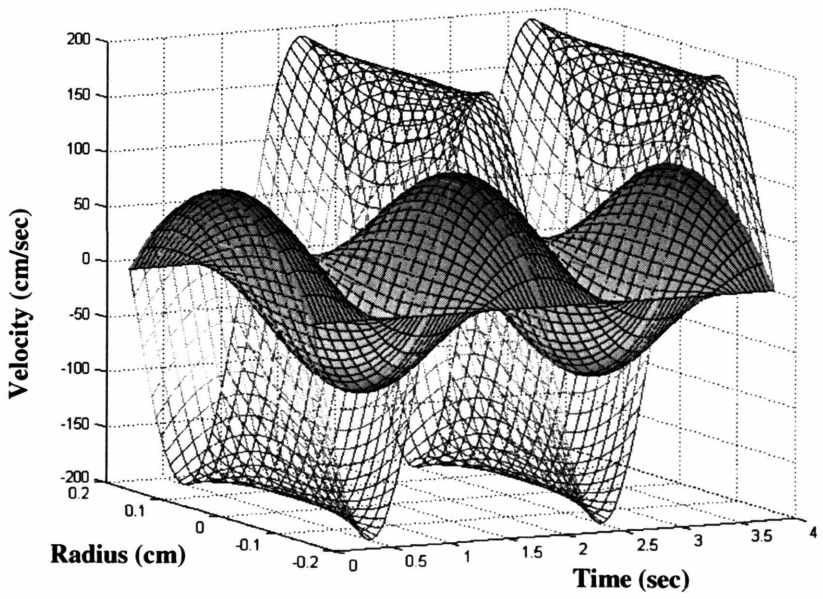

Figure 2.5. Solid surface depicts the relative axial fluid velocity in a radial distribution as a function of time given a sinusoidal wall motion while the mesh surface depicts the fluid velocity in the inertial reference frame; R=0.16 cm, v=0.04 dynes cm/sec.

Here, we see that oscillatory flows can readily be generated, and moreover, that given the relatively fast system time constants as compared to physiological pulse rates, the fluid/wall motion can be smoothly transitioned from beat to beat, with negligible flow at the beginning of each new pulse. While this example considers a simple, sinusoidal

forcing function, more complex forcing functions (Eq. 6) can be used to generate more complex flows.

An extreme case is that of square wave wall accelerations where otherwise steady absolute wall accelerations are interrupted with discontinuous jumps to motions of equal magnitude but opposite direction. Such a driving wall motion is given by:

$$\frac{d^2Z(t)}{dt^2} = \sum_{n=1,3,5...}^{\infty} \frac{A_1}{n} e^{in\omega t} \tag{12}$$

driving the axial velocity profiles shown in figure 2.6. Here, we note that the profile reaches a uniform, parabolic condition after a time delay of ~0.3 sec (3 time constant, as expected from our impulsive response, Fig. 2.3). However, the presence of the rapid directional transition creates brief moments of flow reversal, which can be observed in the radial profiles.

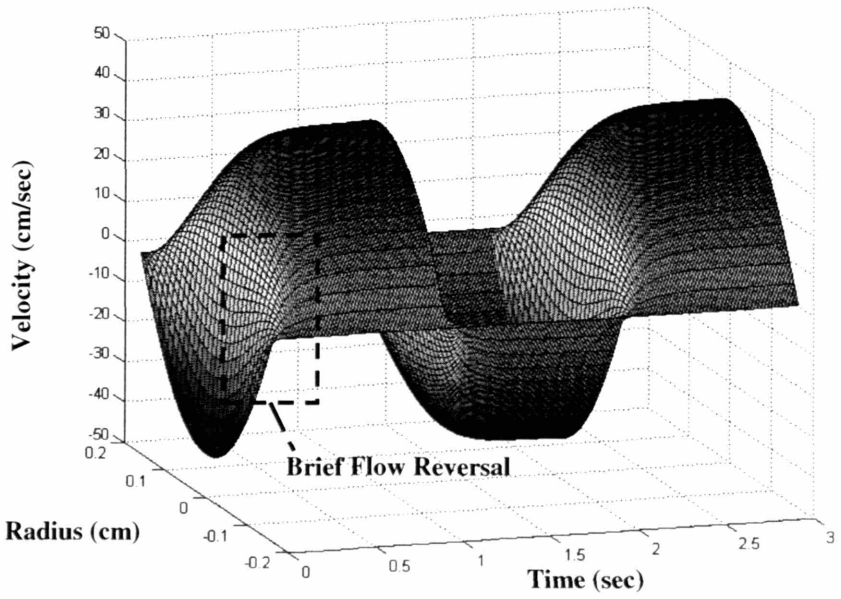

Figure 2.6. Solid surface depicts the relative axial fluid velocity in a radial distribution as a function of time given a square bulk fluid flow; R=0.16 cm, v=0.04 dynes cm/sec.

2.1.3 Curvature Effects

These solutions cover the case of straight tube, axial wall motions. However, both the coronary arteries and our toroidal loop model (adopted for low blood volumes and practical use) have inherent curvature which can have effects on the internal flow. Curving flow streams are affected by centrifugal forces which can establish secondary, off-axis, flow fields when interacting within viscous boundary layers. The magnitudes of these secondary flows are governed by the dimensionless Dean #, κ, which is a function of the secondary inertial and viscous damping forces, and the main stream centrifugal force. However, the customary definition of κ (see Table 2.1) is not applicable in the rotating toroid case, as the relevant velocity term must take into account the fluid's axial velocity in an inertial reference frame (V_{fluid}) which gives rise to the centrifugal forces and a different wall velocity (V_{wall}). It is the difference in these components that gives rise to the relative wall velocity (V_{rel}) and hence, the centrifugal pressure mismatch leading to secondary flows.

To determine a modified κ_{peak} number (κ'_{peak}) for comparison with the nominal conditions of table 2, we can consider the definition of κ as a ratio of the square root of the product of the secondary flow inertial and centrifugal forces to the viscous forces [100], where

$$Inertial\ forces \rightarrow \frac{\rho V_{secondary}^{2}}{2a} \tag{13}$$

$$Centrifugal\ forces \rightarrow \frac{\rho\left(\left|V_{fluid}^{2} - V_{wall}^{2}\right|\right)}{2R} \tag{14}$$

$$Viscous\ forces \rightarrow \frac{\mu V_{secondary}}{(2a)^{2}} \tag{15}$$

which have been determined from an order of magnitude consideration of the relevant quantities [106]. In these equations, $V_{secondary}$ represents a typical secondary fluid

velocity, ρ is the density of the fluid, and μ is the dynamic viscosity of the fluid. The use of tube and loop diameters (2a, 2R) rather than radii have been used to allow reduction into a quantitatively conventional form. The differential term in the centrifugal relation accounts for the relative centripetal motions in an inertial frame. When both motions are present, κ'_{peak} becomes

$$\kappa'_{peak} = Max\left(\left[\frac{2a\left(\left|V_{fluid}{}^{2} - V_{wall}{}^{2}\right|\right)^{1/2}}{\upsilon}\right]\left[\frac{a}{R}\right]^{1/2}\right) \qquad (16)$$

When V_{wall} is zero, as in the case of forced flow through a curved, stationary pipe, κ'_{peak} reduces to the standard form given in table 2.1 The magnitudes and effects of these secondary flows an the embodied device are discussed further in section 3.1.2.

While a thorough, quantitative description of the time-dependent fluid flow profiles within the rotating toroidal case would require more extensive numerical techniques, we satisfied ourselves with the straight tube characterization and the practical goal of matching the critical dimensionless Reynolds, Womersley, and modified peak Dean numbers to those observed in typical coronary flow settings on a beat to beat basis.

2.2 Embodiment

2.2.1 Prototype evolution

In order to create the inertially driven, relative flows, we needed to develop a suitable system that could maintain the required, toroidal angular motion profiles. Generally, such a system requires a rotor, a suitable strategy of inducing motion and a technique for monitoring the contained flow. In sections 2.2.2-2.2.6, we give a thorough description of the current system embodiment and composite parts. First, we give a brief prototype evolution of the developmental stages.

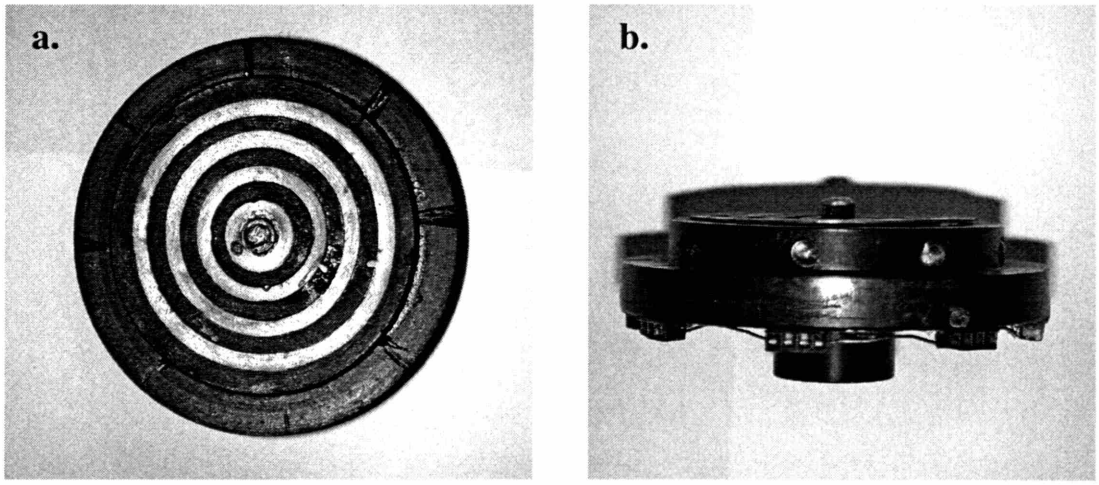

Figure 2.7. Single fluid loop, infra-red sensing rotor stage. a. Top view; b. Side view.

To verify the inertial method of relative flow induction, we developed a system that could spin a single fluid loop. An Electro-Craft® NEMA42C motor (selected using a similar design rational as detailed in section 2.2.4) rotated a rotor stage through a prescribed motion profile utilizing the control system described in section 2.2.5. The initial prototype utilized a rotor stage with equi-spaced infra-red (IR) sensors and detectors positioned around its perimeter, with the held fluid loop passing in between the IR beam (Fig. 2.7). To detect fluid motion, a small particle of equi-fluid density (typically a fibrin clot) was placed within the fluid loop. With relative fluid motion, the particle would cut the IR beam and its velocity could be determined by observing sequential deflections of

IR detector output. Although this method roughly indicated the suitablilty and practicality of generating relative flows, the inclusion of a tracer particle with in the actual flow field interacts with both the biological and physical environments. Such disturbances could dramatically affect both the observation and performance of the test system.

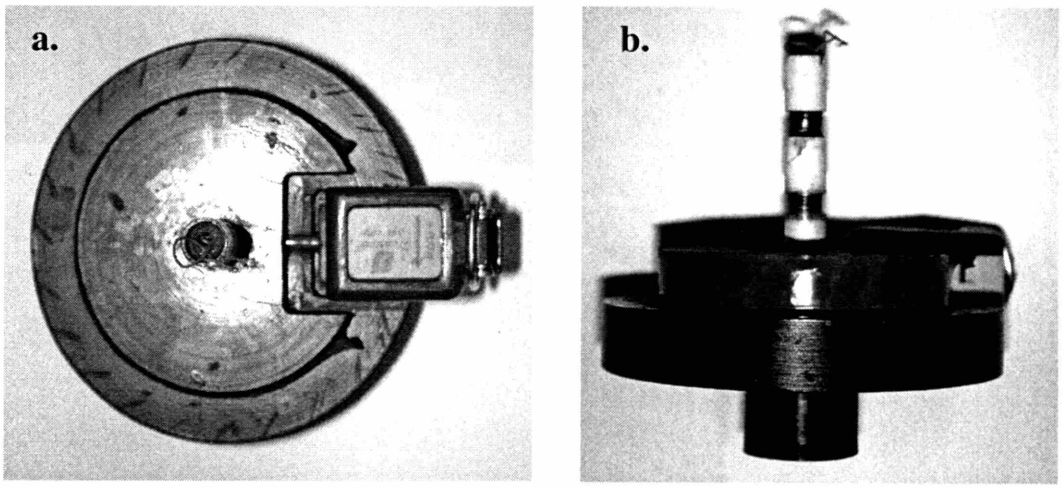

Figure 2.8. Single fluid loop rotor stage with ultrasound flow probe. a. Top view; b. Side view

A second prototype was developed which utilized a rotor stage incorporating an external ultrasound flow probe (see section 2.2.6) to measure relative fluid flows, using the same motor/controller system used for the IR rotor (Fig. 2.8). The external nature of the probe allowed unperturbed flows to be measured with greater granularity and precision than the relatively crude IR technique while verifying the ability to pass the probe signals between rotating and inertial reference frames for this unorthodoxed use.

These systems have utilized a single rotor stage to create motions within a single fluid loop. In order to perform parametric, mechanistic studies into complex phenomena such as vascular thrombosis, it is important to be able to perform many experiments and developed models and strategies must take this into account. Practically speaking, high throughput systems allow studies to be perform quickly and efficiently. Speed becomes an even greater issue when investigating blood. Upon removal from its natural vascular

environment, it rapidly begins to change. On this shifting ground, studies must be performed soon after withdrawal to maintain study accuracy and temporally close together for precision. To enhance our ability to probe vascular situations, we developed a multi-rotor system which supported six rotors on a single axis allowing six fluid flops to be spun simulataneously (Fig. 2.9). While the motor needed to be reconsidered to support the increased requirements (section 2.2.4), the single rotor control structures could be maintained.

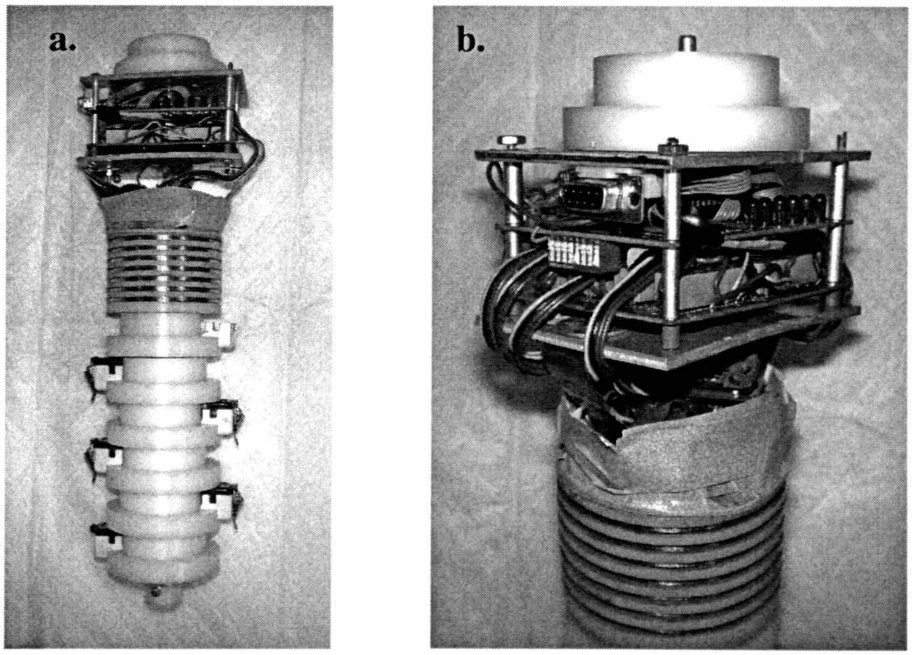

Figure 2.9. Multi-rotor system. a. Side view showing six, stacked rotor stages with alternating ultrasound flow probes; b. Close-up view of on board probe multiplexer

Using the same evolutionary pressure of study speed and efficiency, we modified the multi-rotor design to enhance modularity and ease of incorporation onto a multi-axis system, thus allowing multiple simultaneous flow profiles to be considered (Fig. 2.10). We now discuss the multi-rotor embodiement in greater detail.

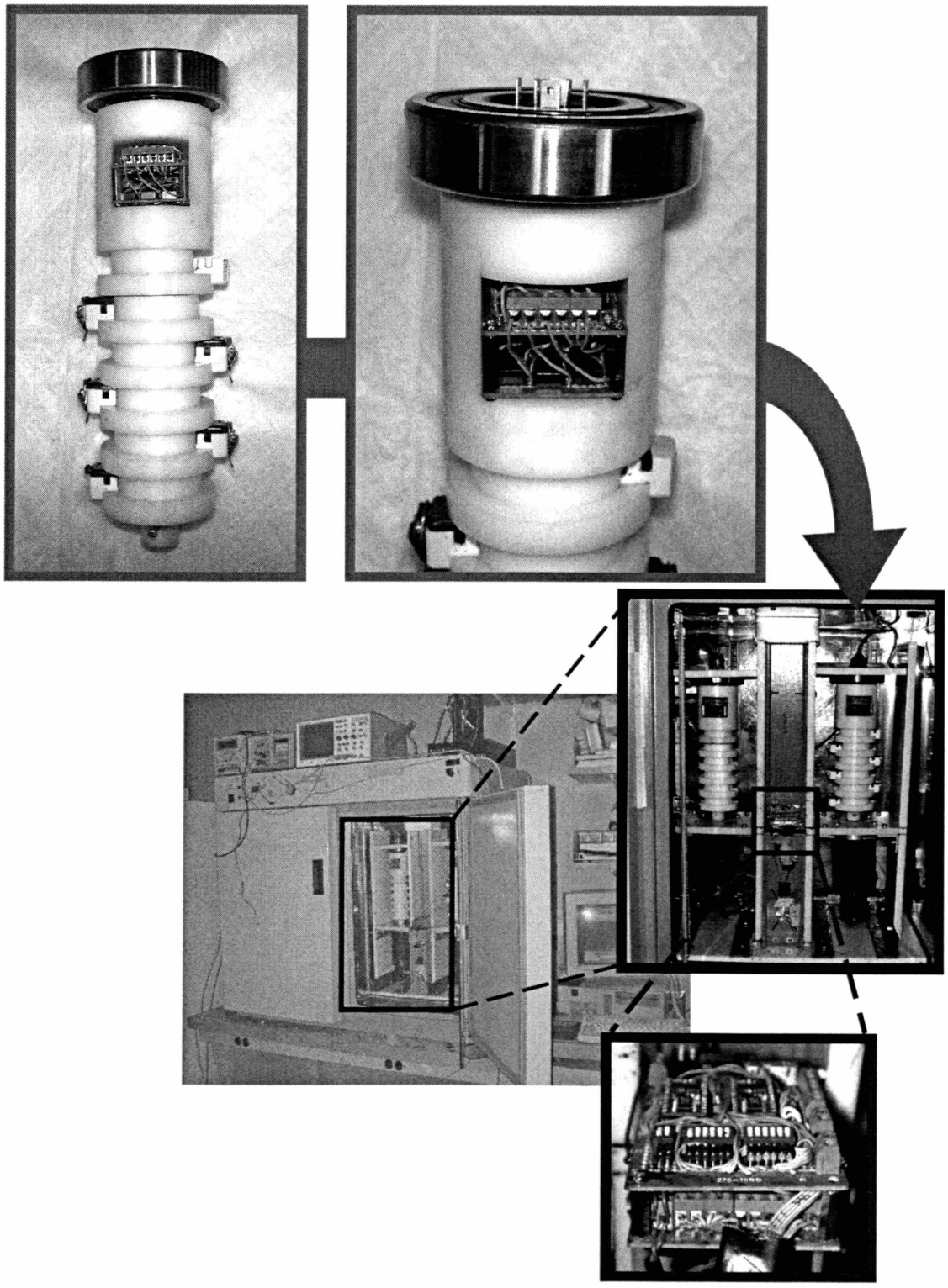

Figure 2.10. Current system embodiment with two axes, each holding upto six rotors stages. Much of the electronics have been consolidated into the inertial reference frame, increasing the modularity of system to support future expansions.

System Overview

A system was developed in order create the inertially driven flow profiles discussed in section 2.1. Figure 2.11 shows the key components of the system, which include a fluid loop, rotor-stage, driving motor, motion controller, and a measurement system.

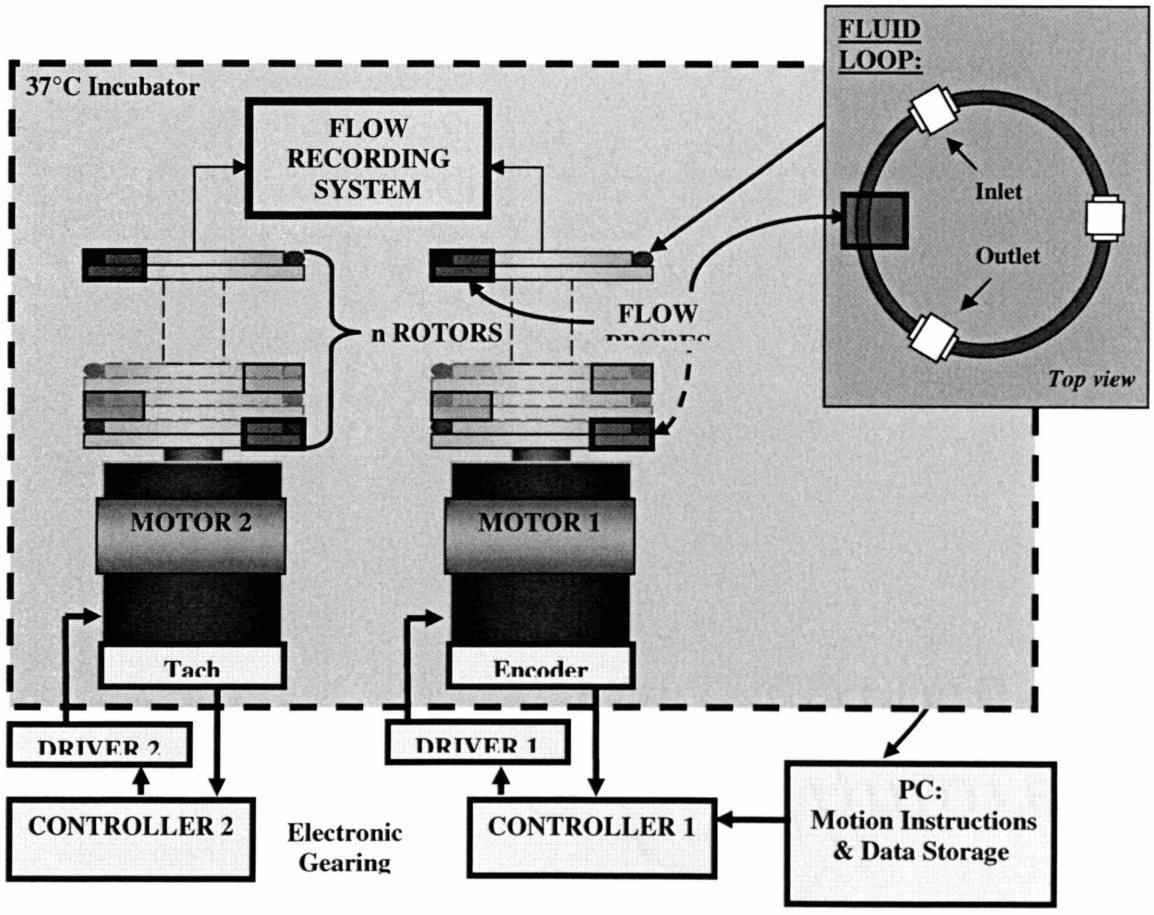

Figure 2.11. General mutlti-axis, multi-rotor flow system schematic.

platform and is placed in axial alignment with other loops to be tested under the same flow conditions. Although any number of loops is allowed, the embodied system allows six simultaneous runs via six modular rotor platforms per axis. The entire rotor system is then driven through a desired angular motion profile via the motor and controller system. This motion creates internal flows, which are measured via onboard flow transducers built into the rotor stages. Each transducer sends the flow measurements of a particular fluid loop to the measuring/recording system, which can be used to instantaneously

monitor the flow profiles and fluidity of the blood. A detailed description of these components and a rational for there selection follows.

2.2.2 Fluid Loops

Design

A schematic of the basic fluid torus is show in figure 2.12. The loops are made of a 24 cm length of 1/8 " ID::5/32" OD 3350 Tygon silicon tubing. The connecting ends of the tube are squarely cut, orthogonal to the axial dimension to ensure a matching end-to-end fit. This connection is held via a 1.5 cm overlapping segment of S-50-HL Tygon tubing (3/16" ID; 5/16" OD.) The close OD/ID match provides a compression fit and axial alignment of the juxtaposed ends. Further support is provided by a 1 cm elastic band of silicon tubing (Silastic; ¼" ID; 3/8" OD) placed coaxially over the 1.5 cm joiner segment, thus radially compressing the junction.

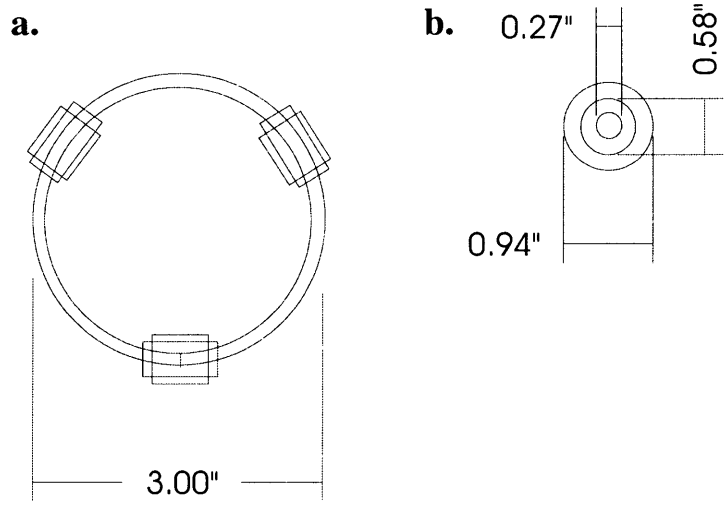

Figure 2.12.. Fluid loop design. a. Loop format with three coaxial sleeves, one for maintaing loop format and two as inlet and outlet ports; b. Coaxial sleeve cross-sectional profile.

Two similar structures are slid onto the 1/8" loop at equally spaced 120 degree intervals serving as outlet and inlet ports for the replacement of the loop's contained air by the desired fluid. Briefly, a needle is slid under the outer most elastic sleeve and then driven

into the lumen through the middle sleeve and inner loop layers. To minimize possible disturbances to the loop's inner, fluid-contact surface, small gauge needles are used. While a 26+ gauge needle is suitable for air evacuation, 19 or 20 gauge needles are used for the untraumatic injection of blood components (Fig. 2.13).

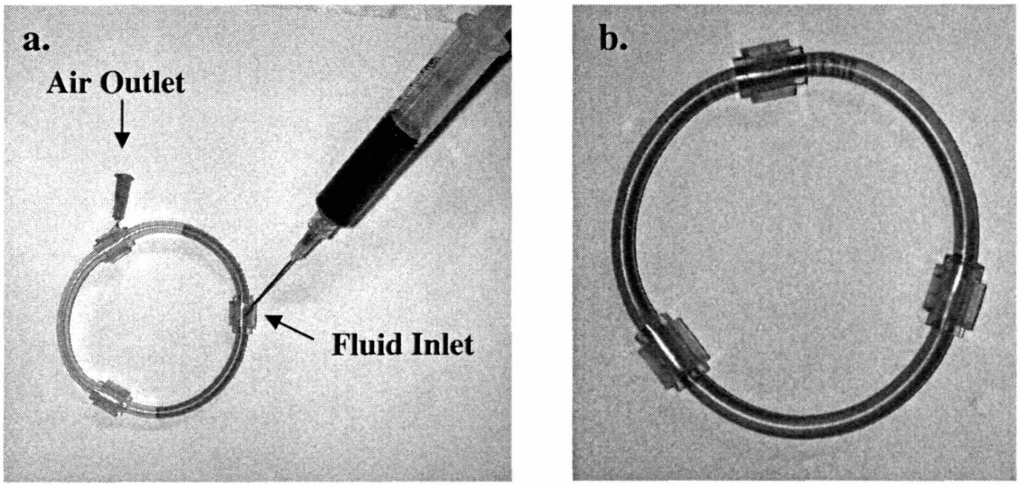

Figure 2.13. a. Filling of fluid loop; b. Filled loop. Note the absence of fluid/air interface.

Rational

.In settling on these embodied loop dimensions, a primary concern was to match the physiological diameters, typical of a coronary setting (3-3.5 mm; LAD). The 1/8" ID tube was chosen as it fell neatly within this range (3.175 mm), with the 5/32" OD imposed by specifications of the flow probes (discussed below in section 2.2.6).

The overall 24 cm length was determined by balancing the desire to minimize blood contact surface and blood volume (both to maximize the biological signal to circuit noise ratio, while enabling practical biological manipulation) with the need to keep loop curvature at reasonable levels to dimensionally consider secondary flow effects.

The final consideration in tubing selection was the 3350 Tygon silicon tubing chosen for its low bioreactivity and suitable gas permeability. However, given the inertial mechanisms driving the flow, any desirable tube could be used (i.e. rigid vs. compliant). Furthermore, the tubing can readily be replaced (i.e. vascular graft material,

ex vivo arterial sections, etc.) or simply coated with a test substance (i.e. proteins, cells, polymers, etc.) whose thrombotic properties are to be specifically studied.

2.2.3 Rotors

Rotor stage design

The rotors are the platforms upon which the fluid loops are held. In the current embodied system, each axis holds 6 rotors. Figure 2.14 depicts the design of an individual rotor (3 orientation A; 3 orientation B per flow axis). Each rotor was manufactured out of a stock of 3" diameter delrin plastic chosen for its machinability and ease of handling. The key features of the rotor are a resting stage for the fluid loop, an axial hole for alignment of the rotors, a notch for the placement of the flow transducer, and a shaft through which the transducer connections may be passed.

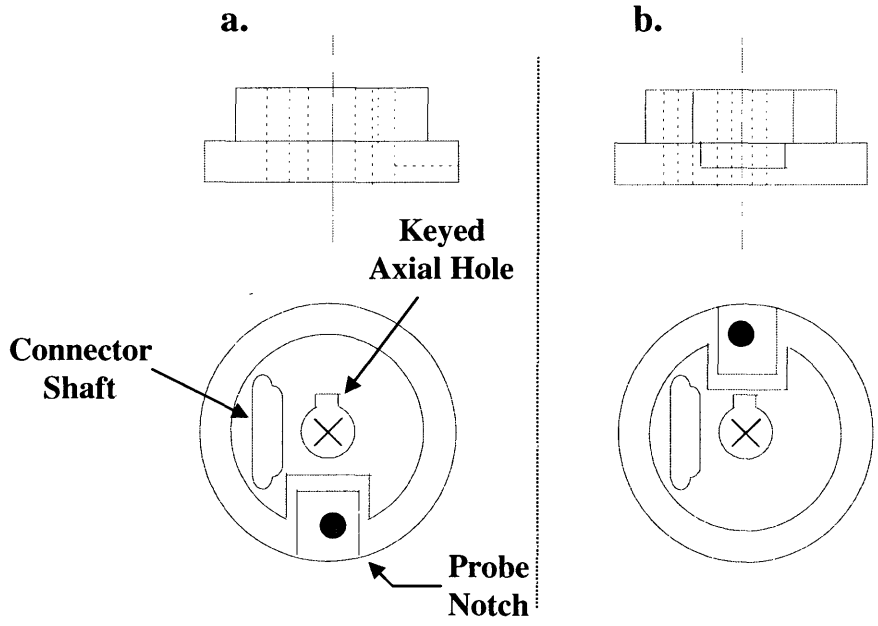

Figure 2.14. Schematic drawing of a single rotor-stage. a. Orientation A; b. Orientation B. Note the chirality of the probe notch.

The stage was designed to fit the embodied fluid loops. As such, they snuggly fit the inner most diameter (5.75 mm) of the loop which is outlined by the outer most Silastic tubing layer of the fluid loop's inlet, outlet, and junction structures. Only this Silastic

band is in contact with the stage, thus suspending the fluid loop. The notch for the flow probe accommodates a Transonic 3CA flow probe (described in further detail in section 2.2.6), and its dimensions were defined by the need to allow the suspended 1/8" ID, 5/32" OD fluid loop to pass through the flow probe's sensor (Fig. 2.15). As shown in figure 2.13, two chiral rotor conformations exist, based upon notch orientation. This chirality allows the probes to face opposite directions as the rotors are sequentially stacked, thus minimizing asymmetrical, processional loading.

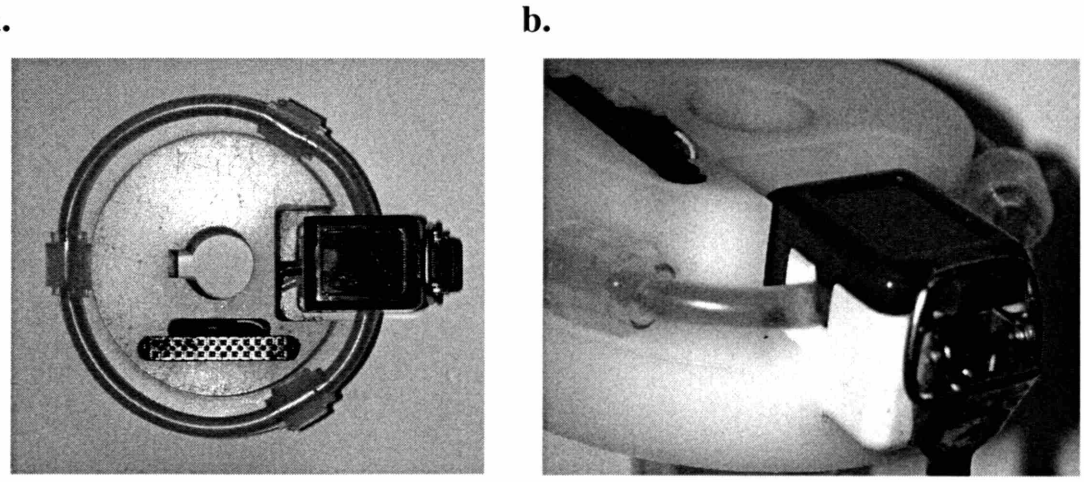

Figure 2.15. Fluid loop positioned on rotor stage. a. Top view showing coaxial positioning; b. Fluid loop passing through the probe's sensor.

The shaft for the transducer connections was designed to accommodate a specialized connector (described in section 2.2.6) which relays real-time flow information. A 1/8" hole connects this shaft to the probe's notch serving as a conduit for essential wires.

Rotor shaft design

The rotor axis is shown in figure 2.16, along with a diagram depicting six stacked, alternating rotor stages. The shaft was machined from a 1" diameter stock of delrin and consists of two sections. The top section has been lathed down to a diameter of ¾", with a milled ¼" groove running its entire length to accommodate a strip of nylon. This strip protrudes from the shaft and serves as a key to hold the rotor stages in axial alignment via a matching perimeter center-hole in each rotor stage as shown in figure 2.8. The square key design holds each stage in tight tolerance while undergoing angular accelerations. The bottom section remained at the initial stock diameter of 1". Into it, a centered 1/2" hole allows communication with the driving axis (see Section 2.2.4 for motor selection). To ensure a non-slip junction, a screw key was also placed to grip the motor shaft.

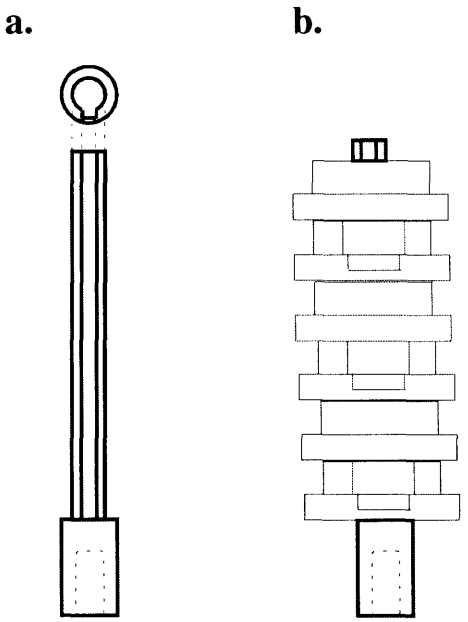

Figure 2.16. a. Rotor shaft; b. Shaft w/ six stacked rotor stages

A final caveat that can be observed in figure 2.16 is that the shaft extends past the length of six combined rotor heights. This is critical in allowing for the fit of a cap structure that houses on-board instrumentation for the flow transducers (see Section 2.2.6).

2.2.4 Motor Selection

The driving motor is an Electro-Craft® E643 DC servo-brush motor. The critical design parameters that were considered were the peak torque and maximum operating speed which were estimated from the straight tube, Newtonian fluid approximation outlined in

the previous section, augmented by an impedance factor to account for curvature effects as suggested by Chang and Tarbell [76].

The peak torque was determined from the maximum angular acceleration required to drive the fluid, which in turn was constrained by the desired flow rates. Peak physiological flow rates are around 100 ml/min in the coronary arteries. While the actual profiles are highly pulsatile, the extreme steady flow case (see Fig. 2.4) can be obtained using a constant wall acceleration of 6.28 m/sec^2. For the embodied loop diameter of 0.0762 m (3"), this axial wall motion transforms into an angular acceleration (α; $A/2\pi r$), of 26.2 sec^{-2}. This value can further be augmented by an impedance factor as suggested by Chang and Tarbell [76] to account for curvature effects [100, 104], as well as compounded to allow more extreme flow rates and varying blood conditions (i.e. increased hematocrit), yielding a critical design α of 40 sec^{-2} .

The torque, T, needed to drive the system at this angular acceleration is given by:

$$T = I\alpha \qquad (17)$$

where I is the moment of inertia of the rotor system. I was estimated to be 7.26X10^{-4} kg m^2 assuming the rotor was a solid delrin cylinder 0.0762 m in diameter (m~1 kg; $I=1/2mR^2$), resulting in a peak torque of 0.029 Nm.

The maximal operating speed was estimated from the rotor speed required to accommodate one acceleration pulse. With a physiological rate of 60 bpm, we again over-designed our criteria by considering a 2 second pulse duration (30 bpm). This yields a maximum angular velocity of 500 rad/sec (4775 RPM).

The Electro-Craft® E643 model satisfies these criteria, supplying a peak torque of 0.16 Nm and a maximum operating speed of 4800 RPM. A chassis was built to house the motor in a vertical configuration, allowing the rotor system to mount directly on top. It was decided to allow the rotor to communicate directly with the drive shaft, given both the heavy duty nature of the E643 motor and the care taken in axial alignment and minimizing asymmetrical loading. Still, a bearing system to accommodate off-axis loading could be used in future designs.

2.2.5 Control System

Single Axis

In order to control the Electro-Craft® E643 DC servo-brush motor, the control structure shown in figure 2.17 was developed. The components of the motor control system integrate readily and allow specific flow profiles to be generated. These components include a Renco RM15 Encoder, an Electro-Craft® IQ-550 Position Control Module, an Electro-Craft® Max-100 PWM Servo Drive, and a Windows compatible PC terminal running IQ Master software.

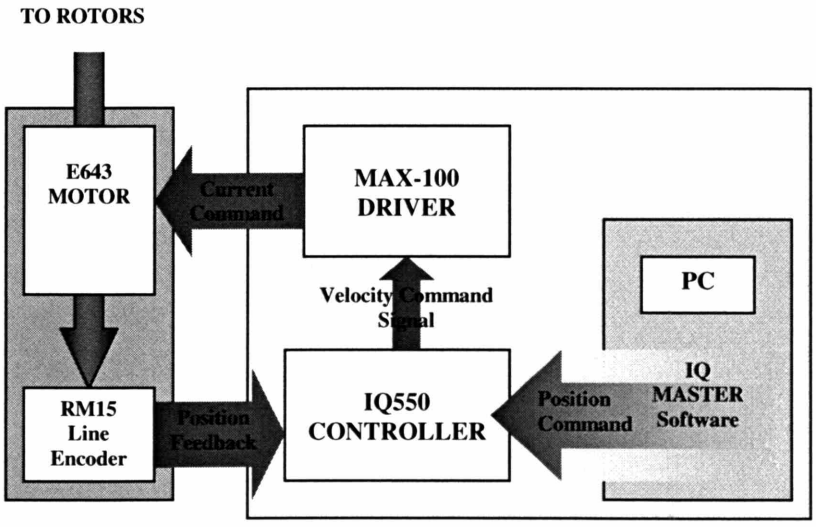

Figure 2.17. Control schematic for single axis

The RM15 Encoder is a 1000 line encoder that is placed in axial alignment with the drive, transducing rotor position. This position signal is then sent to the IQ-550 which sends a +/-10 volt analog velocity command signal to control the motion of the motor. The analog signal is dictated by a program written in the IQ Master programming language and stored on the IQ-550's EPROM. This velocity command is relayed to the MAX-100 drive which serves as a power amplifier, supplying up to +/-3 amps of continuous current to drive the motor.

The rational for choosing these components was their integratability and the ease with which the motor's motion profile could be adjusted via software rather than hardware means, allowing various flow profiles to be readily generated and modified according to the desired experiment. Specific IQ Master programs used to create the various flow profiles used in the current work are given in the Appendix.

Multiple Axes

While this control structure allows the control of a single rotor axis and hence one flow profile, we wanted the ability to drive multiple *flow profiles* simultaneously to increase the precision and accuracy of our model in studying flow

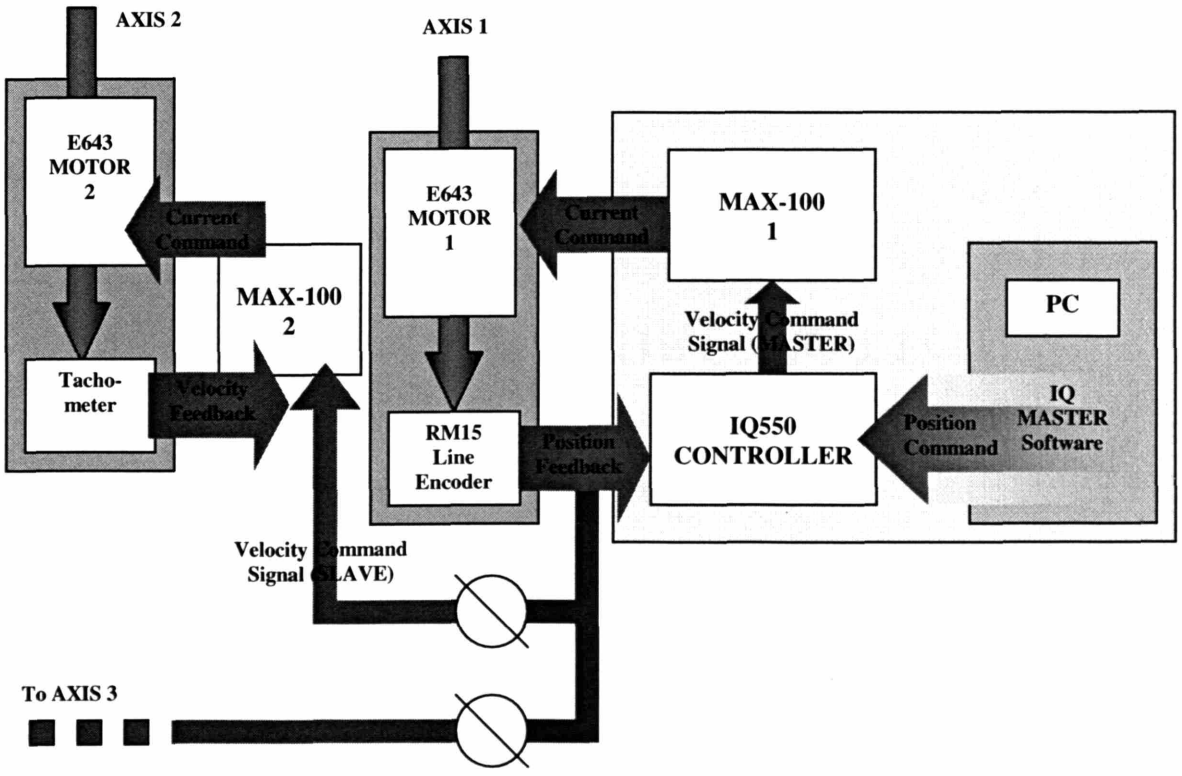

Figure 2.18. Control schematic for multiple-slaved axes.

dependent processes. The most versatile option would be to have multiple IQ-550 controllers, each driving an individual axis via a specific, implanted IQ program.

However, a simple, cost-effective method to control multiple *flow rates* at once is to `slave' additional motor axes to the controlled, master motor's velocity profile which can be obtained directly from the line-encoder output on the master motor (Fig. 2.18). By using a slaved velocity command signal that is a variable ratio of the master motor's profile, proportional velocities, accelerations, and hence flow rates can be easily generated. For each additional axis, a motor and feedback tachometer is required, along with a driving MAX-100 whose on-board control structures can accept velocity feedback to maintain the slaved velocity command signal.

2.2.6 Measurement/Recording System

In order to measure and record the flow profiles, the outlay shown in figure 2.19 developed. The components of the system are the Transonic 3CA

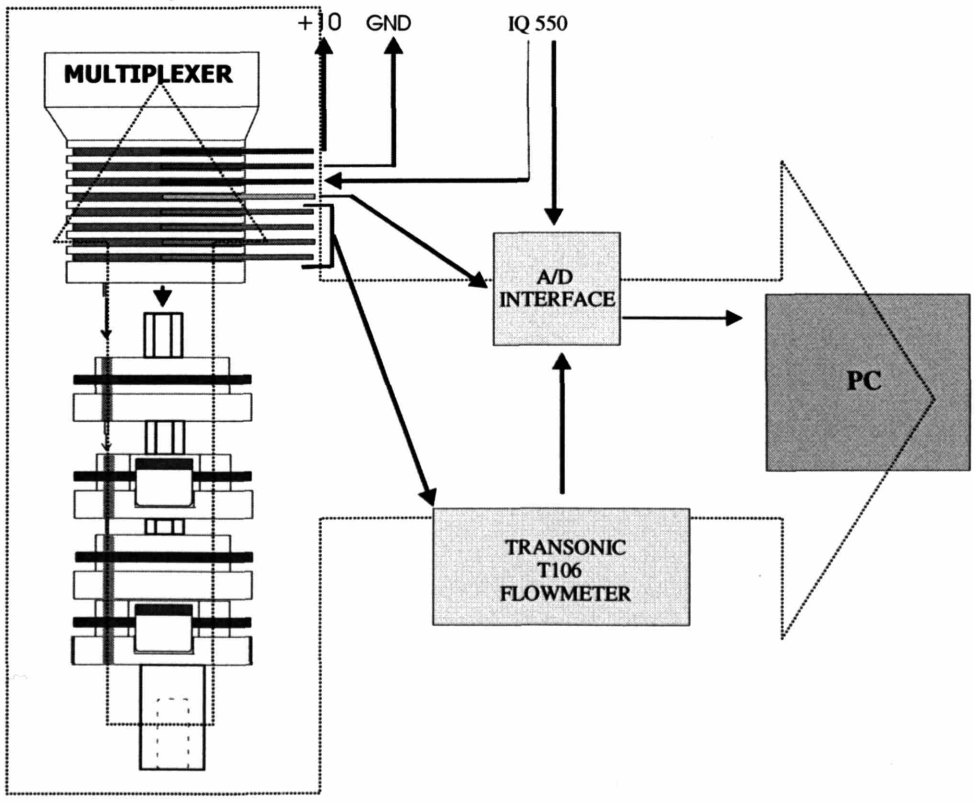

Figure 2.19. Measurement/Recording system schematic and information flow.

flow probes, probe multiplexer, rotary junctions, 10 volt Tecma power supply, Transonic T106 Flowmeter, and a Windows compatible PC equipped with a National Instruments® LAB-PC A/D interface and LABTECH Version 8.1 software package (Laboratory Technologies Corporation ©)

Probes

The Transonic flow probes measure bi-directional flow via an ultrasound transit time method. Typically, four piezoelectric transducers are positioned around the tube. These elements pass ultrasound beams in alternating up- and downstream directions through the fluid, each serving as a transmitter and receiver in turn. The differential, directional transit time can then be used to measure the bulk flow in the tube. The probes were specifically calibrated for use with the 1/8"ID/5/32" OD 3350 Tygon tubing used for the fluid loops, and further modified so that only 2 of the transducers were required (1 upstream, 1 downstream) allowing 4 connections per transducer rather than 8. Accordingly, the total number of connections on a six rotor/six probe axis was reduced from 48 to 24. This reduction, though not necessary, greatly simplified the construction and wiring of the embodied system.

On each rotor stage, the four transducer leads were passed to the connector shaft and soldered onto a given pin on a specially constructed 24 pin connector (Fig. 2.20). Once the proper connections were made, these pieces were press fit into the connector shaft on the corresponding rotor stage. Upon stacking, the male junctions on a given rotor stage communicates with the female junctions on stage immediately below it. Thus, each stacked rotor stage is hardwired to all of the probes via the 24 pin connections. This design allows the stages to be modular for loading and possible future expansion purposes, with the top most stage relaying all probe signals to the probe multiplexer.

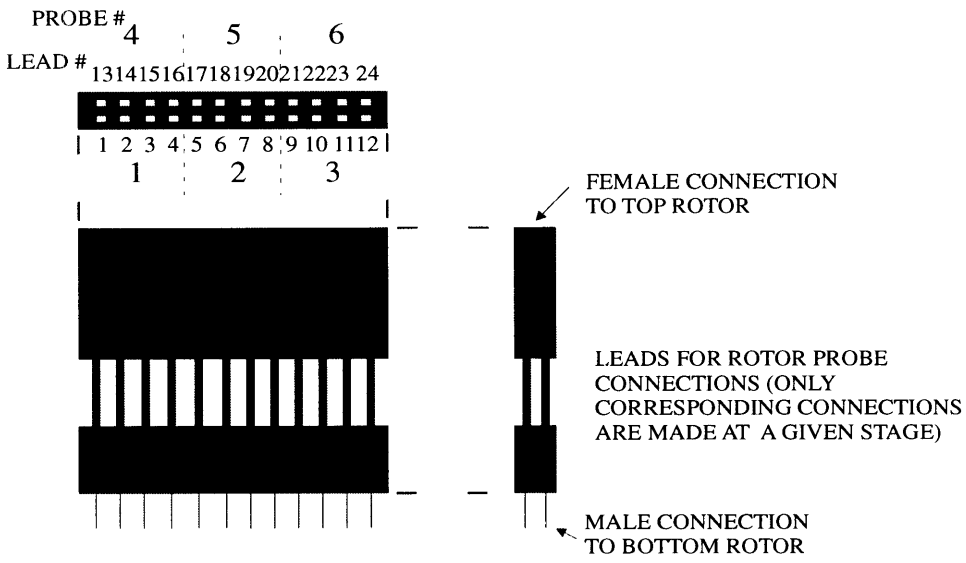

Figure 2.20. Measurement/Recording system schematic and information flow.

Multiplexer

The multiplexer (Fig. 2.21) sequentially passes individual flow signals to a Transonic T106 Flowmeter which outputs a voltage signal, recordable on a computer via the LAB-PC A/D interface and LABTECH software. The trigger to sequentially switch probes is provided after each flow cycle by the high to low or low to high state change of a digital output pin on the IQ 550 controller. In this method, all of the probes' signals are merged into a continuous waveform. A final signal is passed from the multiplexer to the computer encoding a specific probe label. Therefore, with the waveform and corresponding probe label information, an individual fluid loop can be monitored throughout the time course of a given run. When recording from multiple axes, a similar measurement strategy of cycling between individual probes is applied, with an additional multiplexing layer added to cycle between the various axes

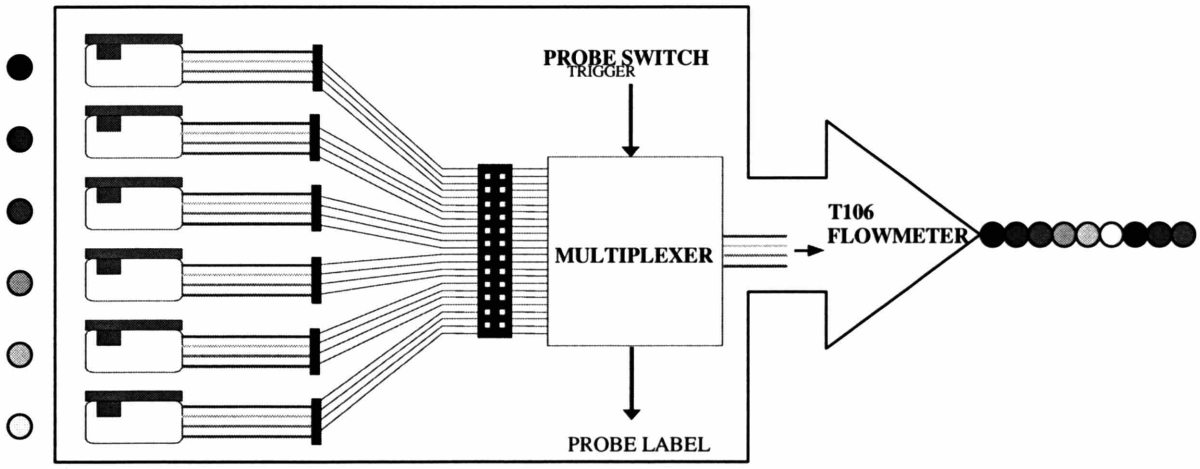

Figure 2.21. Multiplexing schematic; Six probe signals are merged into one continuous waveform and subsequently decoded using concurrently recorded probe label information.

A rotary electrical coupling interfaces the rotating loop reference frame with the inertial frame. To limit the number of rotary junctions, the probe multiplexing stage is located on the rotor frame itself (Fig 2.18), thus reducing the required number of rotary junctions from 24 to 8 (or 7 in the multi-axes scenario as some functions could be consolidated onto inertial frame circuitry). The onboard multiplexer probe output is wired to four of the rotary couplings. Three additional couplings provide power (+10V, GND) to the multiplexer as well as information on the probe label. A final connection is required to pass the probe switch trigger in cases when multiplexing logic is distributed to individual axes in the rotating reference frames.

Although this measurement system can monitor and record the full flow profiles in the fluid loops, often times only the peak flow values are stored to disk. This data compression is performed in real-time using the LABVIEW software capabilities. To do this, the IQ550 was programmed to send a brief 5V pulse to the PC during peak acceleration, signaling an appropriate, consistent point in each flow pulse to be sampled. Thus, even if the flow is significantly reduced (as in thrombotic loop occlusion), consistent portions of the cycle can still be recorded.

2.2.7 Design Summary

The system described allows an oscillating type flow of a prescribed flow pattern to be produced in fluid loops. The manner in which the flow is produced is atraumatic, thus allowing delicate processes such as thrombosis to be studied in a low noise setting, even under high flow rates. Furthermore, this strategy allows the entire fluid contact surface to be prescribed and minimized, without the use of valves, connectors, or other potential disturbances, further reducing potential sources of background noise. By readily allowing changes in flow profiles, the system also allows the thorough, parametric investigation of how flow may interact with biological processes such as thrombosis.

While the current embodiment allows multiple, 1/8" ID loops to be run under two simultaneous, bidirectional flow rates, various modifications can be readily made to extend the system's applicability. More axes can easily be added (Fig. 2.17), allowing multiple, simultaneous comparisons at several flow rates. By incorporating additional IQ550 Controllers, these flow variations can be extended to include not only flow rates, but profiles as well. Altering rotor and loop characteristics, can also offer a wide degree of variation in the geometric properties. Furthermore, incorporating a one-way valve could be used to allow unidirectional flows, though the impact of such a structure on the hemodynamic loop environment would have to be considered as discussed in section 2.1.2. It is important to recognize that each of these adjustments would also require reconsidering the embodied motor specifications and other aspects of the system design.

CHAPTER 3 Flow System Testing

3.1 Mechanical validation

To demonstrate the range of system capabilities, a single fluid loop was filled with a 6:4 water/glycerol mix to match the Newtonian approximation blood viscosity under arterial flow conditions (0.04 cm^2s^{-1}) [78] and placed on a rotor stage. The rotor was driven through a variety of motion profiles to generate impulse, square, triangle, sinusoidal, and coronary-type flows. The full flow profiles, rather than just peak data, were recorded via the LABTECH software.

3.1.1 Flow profiles

The impulsive response of the system was examined after a brief burst of torque was supplied to the rotor. Some points to note in this profile (Fig. 3.1) are the 0-135 ml/min rise time of 0.1 sec and a decay time constant of 0.1 sec, which matches fairly well with the value obtained from our theoretical, linear approximation (Fig. 2.3). The finite rise

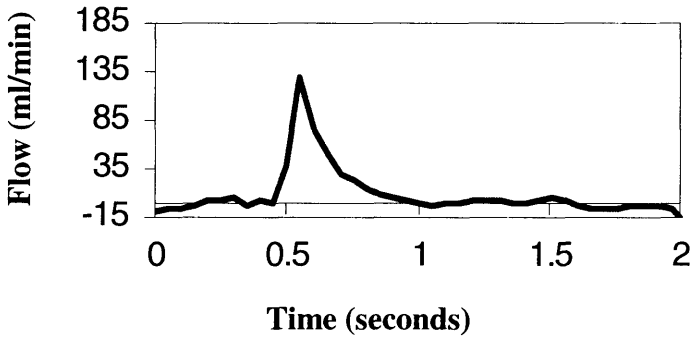

Figure 3.1. Relative fluid flow to impulsive wall accelerations.

time was a result of the limitations of rotor inertia, friction, and peak obtainable torque. If a quicker response is required, these parameters can be adjusted through design modifications. The decay time constant on the other hand, being constrained by the

vessel radius and kinematic fluid viscosity, is not readily subject to change. Therefore, relative flows decaying to nearly zero (<5% peak) in times less than 3 time constants are not possible without some flow reversal or the incorporation of a directional valve. These parameters help to characterize the realistic impulse response achievable with the current setup, which serves as the limiting building block from which other functions can be composed.

Some examples (square, triangular, sine waves) of other possible flows are shown in figure 3.2 a-c. Here, the periodic, bi-directional nature of the flow is evident. Again, this type of oscillation is necessary in the methodology used to create flow, as no valves were present in the circuit.

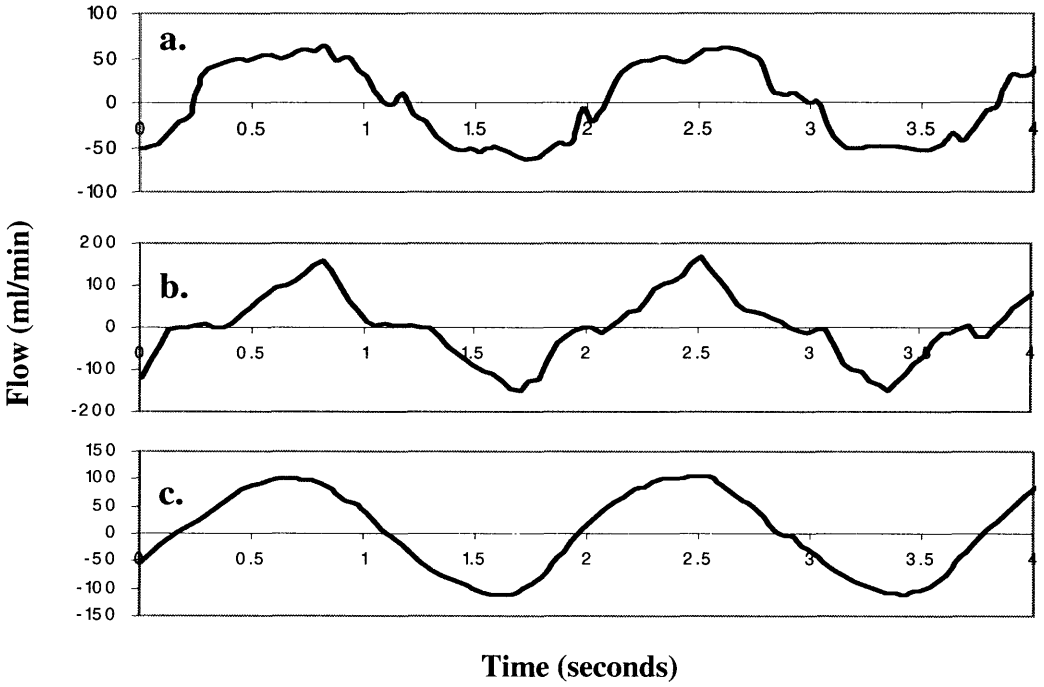

Figure 3.2. Various flow profiles depicting the easily alterable flows. a. Square; b. Triangular; c. Sinusoidal profiles. **It should be noted that the square profile depicted in panel a is blunted at the corners. This is a result of the inherent time decay in the system, as shown computationally in Fig. 2.6. More accurate square profiles can be discussed through the use of more complex driving functions as discussed in later in section 6.1.1.

3.1.2 Coronary-Flow

Since we hope to investigate coronary arterial events, a coronary flow pattern [19] (scaled to a 60 bpm frequency) was approximated with our bi-directional model (Fig. 3.3*a*). Figure 3.3*b* gives the driving wall velocities, V_{wall}, required to achieve this coronary-type flow, V_{rel}, and the derived absolute fluid velocity in the inertial frame, V_{fluid}.

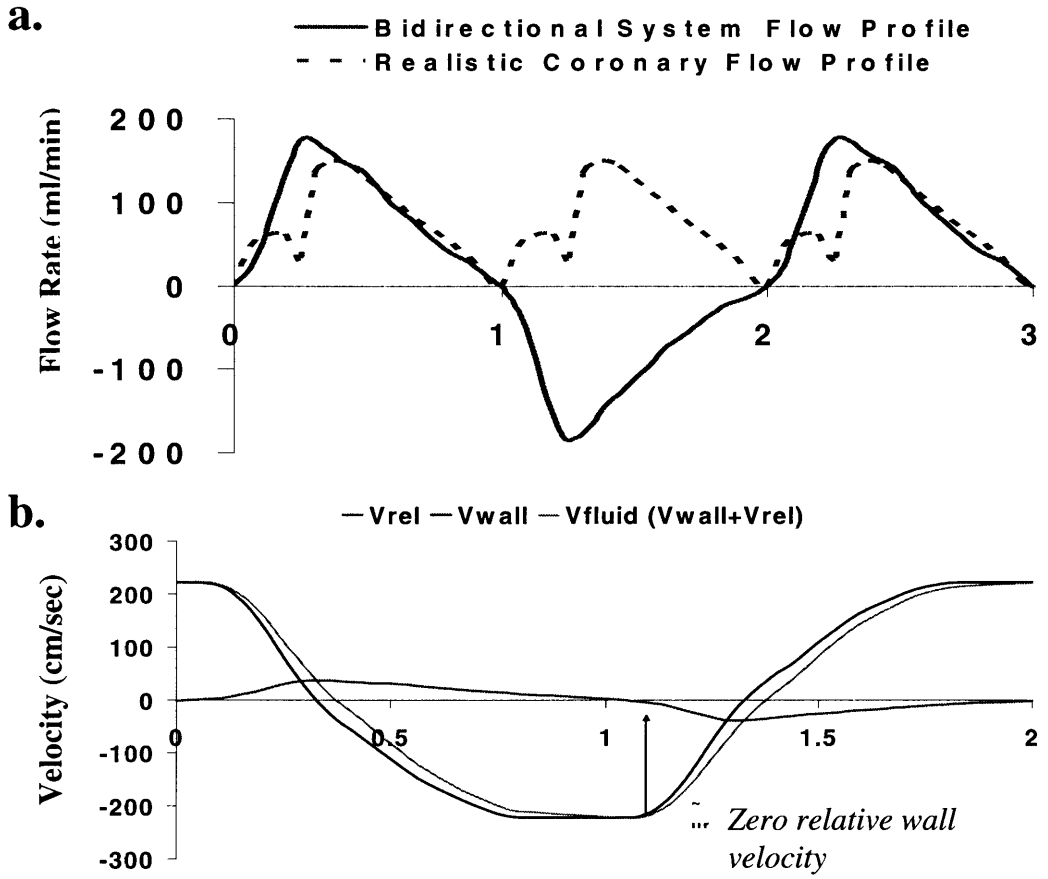

Figure 3.3 Generating coronary type flows. a. Bidirectional bulk flow rate relative to the rotating wall (solid line), superimposed on idealized coronary pulse (dashed line); b. The wall and fluid velocities in the inertial reference frame (blue, magenta lines respectively) in phase with the target, relative, peak fluid velocity (red line; derived from bulk flows assuming parabolic motion, justified for low Wormesley # flows). Prior to a new pulse, there is no fluid motion relative to the wall.

This simulated coronary-type flow is characterized by a $\overline{Re}$ of 150 (based on $|V_{rel}|$), an α of 2 (based on a $\omega_{coronary}$), and a κ'_{peak} of 135 (as defined by equation 1). $\overline{Re}$ and α, when compared with table 2.1, indicate the ability to achieve coronary-type principle flows while keeping secondary flow effects (as estimated by κ'_{peak}) to within physiological levels. The relatively low α (which compares the magnitude of the driving frequency to the system frequency response) indicates that the flows are, for the most part, driven in a relatively quasi-steady manner. This is further indicated experimentally in Figure 5b, which shows that the relative flow velocity is approximately zero by the time the wall velocity begins to initiate a new pulse.

While V_{rel} essentially resets to zero initial conditions after each unidirectional pulse, we must again point out that the created flows are bi-directional in nature. Though many of the thrombotic protein and cellular surface reactions have been shown to be dependent on shear (Section 1.3.1) which we attempt to approximate by matching beat-to-beat dimensionless parameters, the potential influences of such oscillation on factors such as mass transport [59] and cellular function (adhesion, activation, response) [23] may eventually need to be considered.

Another aspect of the flow that is altered is the secondary flow. Physiologically, such flows in curved vessel geometries have been shown to be up to 5% of the axial flow velocity, shifting the peak of the velocity contour towards the outer wall via half-tube, single vortex flows (recall Fig. 1.7*c*). Peak wall shear rates due to these flows can be up to 40% of the peak axial wall shear rates [76]. While precise determination of these secondary flow fields through numerical simulation would be interesting and of value in finding the exact time-dependent wall shear rates, we have found that the magnitude of the secondary flows in our system (as determined by comparing κ_{peak} values observed in the coronary setting with κ'_{peak} values in our system using equation 16) are comparable to those found in a coronary setting of similar axial flows. Qualitatively, a deviation in the secondary flow pattern results from a disconnect between the centrifugal force and the relative wall velocity (which are normally linked in stationary wall flows). During part of the cycle, the bulk fluid velocity is greater than the wall-boundary layer velocity as is

typically the case [76]. However, in our rotational system, there are also times when the wall-boundary layer velocity in the IRF is greater than the bulk fluid's, resulting in a counter-rotating secondary flow drive. Considering these effects, we see that we can minimize the secondary flows as well as maintain beat-to-beat symmetry by using a zero DC component of V_{wall}. If needed, redesigning the fluid loop characteristics to have a larger curvature to tube radius ratio (R/a) can further reduce the magnitudes of these flows.

The versatility of the system allows fundamental wave characteristics such as amplitude and frequency to be readily varied as desired. Figures 3.4 *a* and *b* depict such profile manipulations as the amplitude is varied by a factor of 2. Furthermore, the system allows for tailoring of more detailed parameters such as the systolic:diastolic ratio if desired

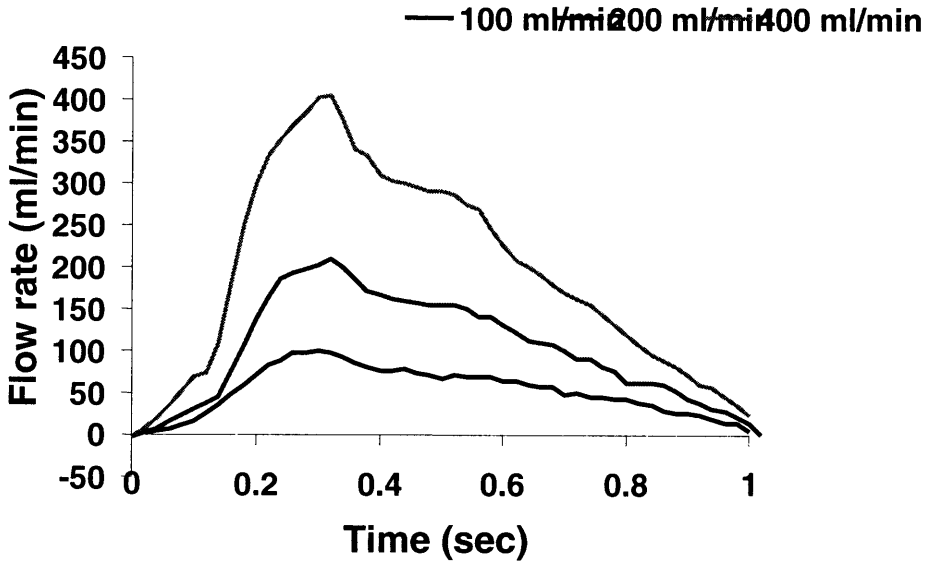

Figure 3.4. Changing amplitude of coronary type flow (100, 200, 400 ml/min peak flow rates in a triangular (Tri) profile).

3.2 Biological validation

We performed an initial assessment of the model's suitability to study issues of vascular thrombosis by observing the impact of endoluminal stenting on thrombotic outcomes. In this preliminary study, we evaluated loop occlusion times as a straightforward, integrated, measure of thrombosis. This evaluation allowed us to address the system's repeatability, as well as background levels of circuit thrombotic activation. Together, these qualities play a major role in determining the system's signal to noise ratio. As a concrete example of this, we compared the loop occlusion times of stents of dissimilar surfaces.

3.2.1 Materials

Blood Source

In this preliminary study, surplus American Red Cross blood products were used to obtain quantities sufficient to allow several experiments to be performed on the same batch of blood for precision testing. Fresh frozen plasma and fresh platelet concentrates (both anticoagulated with 10mmol acid citrate dextrose; ACD) were utilized as these contained the key ingredients of classical thrombosis, neglecting the erythrocytic and leukocytic components in this first level of study. Type AB+ fresh frozen plasma (FFP) with a prescribed storage life of 6 months post-collection was stored at –20 °C. The plasma was thawed in a 37 °C water bath for 45 minutes and then spun down at 10000 G to eliminate debris such as preformed platelet micro-particles. The supernatant was filtered 4 times through a 0.2 μm low protein binding filter to further ensure clean FFP. The platelets (type AB+ PRP) were obtained within one day of collection and stored on a 70 RPM rocker at room temperature. These were used within the first two days post-collection as was justified from adequate functional comparisons with freshly drawn volunteer platelets.

One hour before a planned experiment, the platelets were added to the FFP at a constant ratio of 1:4 PRP to FFP and returned to the rocker for equilibration. Each loop required 2.5 ml of the FFP/platelet mix to ensure proper filling. To reduce experimental

error from mixing and handling variation, the total volume of the suspension for a given run (15 ml; 2.5 X 6) was pooled and prepared in a single tube.

Stented Loops

7-9 stainless steel NIR® endovascular stents were obtained from Medinol Ltd. (Jerusalem, ISRAEL). While the platelets were equilibrating in the filtered FFP, the stents were expanded within the 1/8" tubing midway between two coaxial sleeves via a 36mm MaxxumTM 3.5 SCIMED® balloon catheter under a pressure of 12 atm (see Fig. 3.5). The tubes were closed into their loop format ensuring a gapless fit. When the

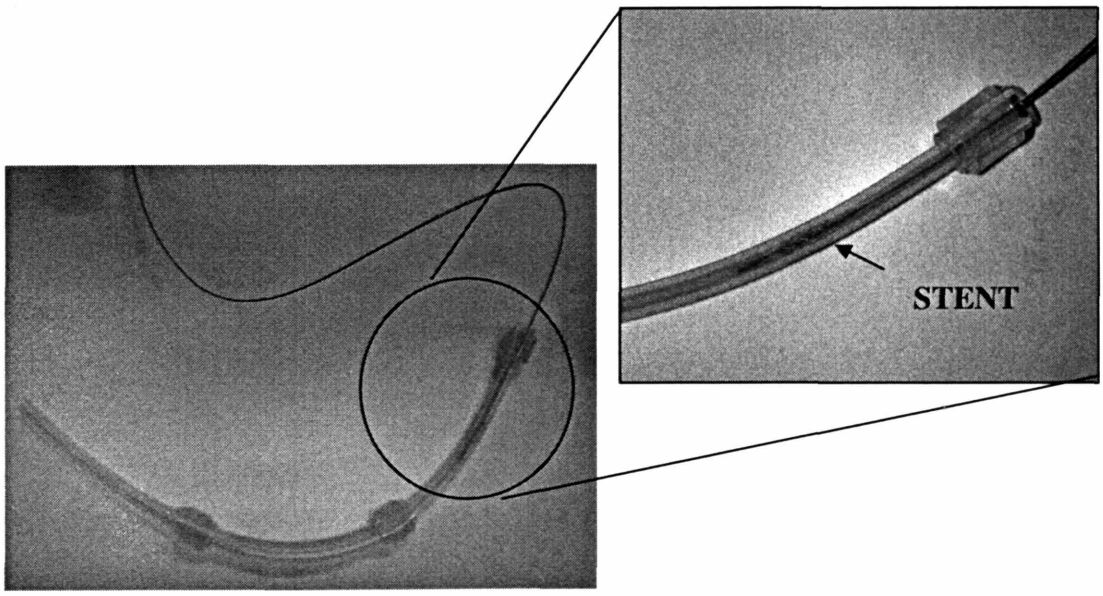

Figure 3.5. Picturte of stent placement within fluid loop.

plasma/platelet mix was ready, 5M Ca2+ was added to bring the sample to an additional 10mmol Ca2+ concentration, negating the citrate's anticoagulant, calcium chelating effect. The stented loops were then filled with the plasma/platelet mix as described above and placed onto the rotors. This process was sequentially performed as rapidly as possible (~15 sec/loop) while ensuring safe handling of the blood components and proper filling of the tubes (no air bubbles). Once complete, the rotors were placed onto the rotor

shaft and spun under a coronary-like motion profile (150 ml/min peak flow) within the 37 °C incubator.

3.2.2 Systemic Noise Characterization

Precision/Variance

As a preliminary test of systemic noise, six stents were positioned in their respective fluid loops and run through the described coronary flow protocol. The results obtained after

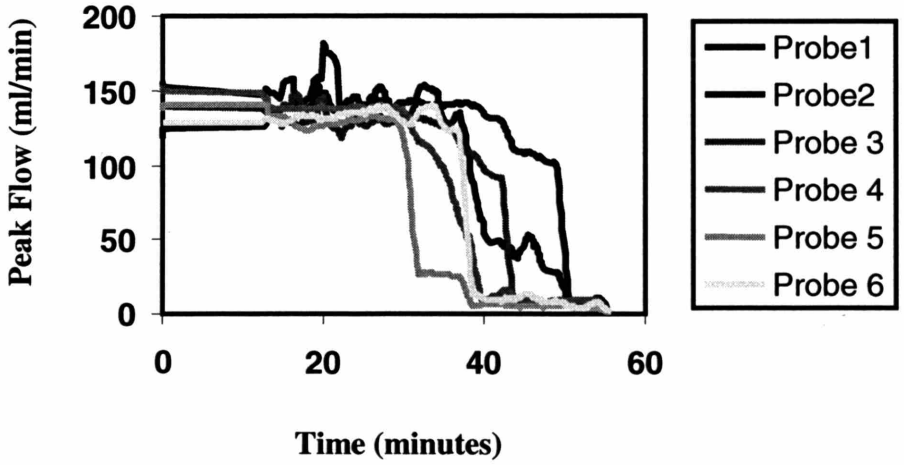

Figure 3.6. System precision. Single run of 6 identical stainless steel stents, showing recorded peak flow profiles and loop occlusion times.

parsing the data into individual loop, peak flow profiles (as discussed in Section 2.2.6) show a constant flow rate followed by a fairly rapid drop to zero flow (Fig. 3.6). The actual initial flows in each loop are identical as they have the same dimensions, fluid properties, and driving motion profiles. Variation in the measured start-up flow rates arises from the hard-wire calibration of the meter for a specific flow probe's signal while our system employs six different probe signals. To account for this, each signal can be re-calibrated according to these initial deviations where identical fluid conditions are known to exist. The drop-off point indicates when the thrombus is occluding the stent. If

a zero-flow condition is taken as the end point, the average occlusion time for this run is 43.1 ± 6.8 min (mean ± standard error).

Circuit Background Noise

As another initial test of the system, we compared a trial of three stented tubes to three empty control tubes. The transformed peak flow data for such a run is given in figure 3.7. As above, the initial flow period followed by a drop-off is witnessed in the stented samples, with an average clotting time of 39.1 +/- 1.7min. The stentless controls remained patent for the +2 hour duration of the test, indicating low levels of circuit thrombotic noise.

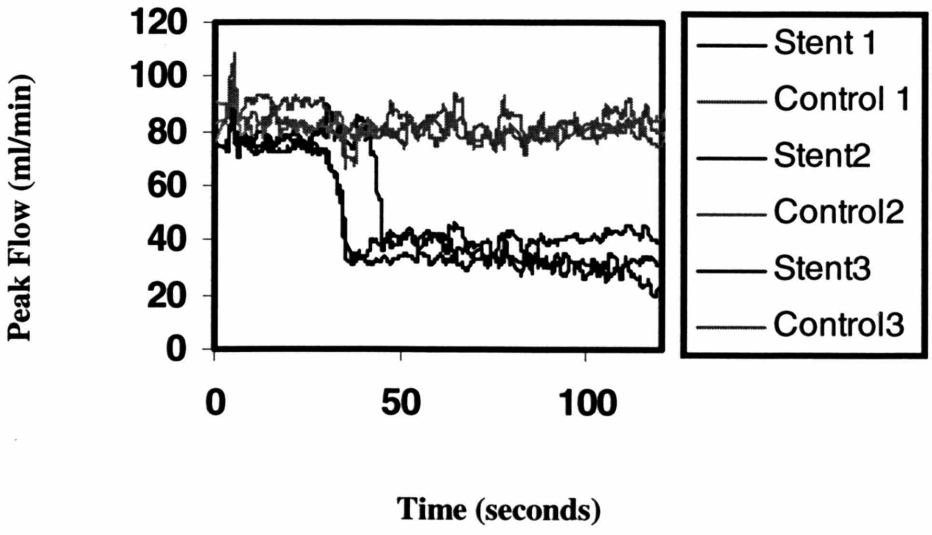

Figure 3.7. Background thrombotic noise levels. Peak flow tracings for stented and control, non-stented loops.

3.2.3 Signal to Noise

These results give insight into the important characteristics of the system's precision and background noise levels. Maximizing precision and minimizing background noise potentiates high signal to noise ratios which enable effective, powerful, parametric studies. We investigated the preliminary effectiveness of our *in vitro* method in creating

sufficient signal to noise ratios by exploring the loop occlusion times of 7-9 NIR® stents of dissimilar surfaces properties. Four kinds of stent surface treatments were selected as motivated by clinical and industrial perspectives: untreated stainless steel, standard electropolished stainless steel, gold-coated (7 ± 2 μm), and gold-coated + heat treatment.

Effects of polishing on loop occlusion times

We first tested the occlusion times between untreated stainless steel stents with those put through a standard, electropolishing procedure which has been shown to significantly reduce surface roughness. To minimize possible bias due to placement order, 3 polished and 3 untreated stents were loaded in an alternating pattern (#1,3,5 polished; #2,4,6 untreated or vice versa) and run under the prescribed coronary-type flows. Three runs were performed in total, yielding a sample size of 9 untreated and 9 polished stents. To correct for variability in blood samples, all occlusion time values were normalized to the average, polished stent clotting time for each run. Figure 3.8 shows that the non-polished stents took significantly less time to clot than polished stents (unpolished, 0.73 +/- .06 normalized mean run steel occlusion time; two-tailed t-test, $p < .05$). Therefore, when looking at end point, loop occlusion time as a measure of thrombogenicity, the positive effects of polishing on stent thrombotic potential can be seen.

Effects of gold-coating on loop occlusion times

Gold-coating is a desirable surface property due to increased radio-opacity and easier stent placement. However, such processing has been shown to alter other surface parameters (i.e. roughness, surface energy, etc.) which can have detrimental side effects [107]. By subsequently heat-treating the coated stents, roughness is significantly reduced to precoating levels. Thus, we tested the loop occlusion times between standard, polished stainless steel with and without gold coating, along with the post-coating, heat processed devices.

Comparisons were performed on the stent types, using the average run, polished steel surface as a normalization control to account for inter-run variability. Stents were loaded (standard vs. gold-coated; standard vs. processed gold) and run in an alternating 1, 3, 5 / 2, 4, 6 pattern as in the preceding trial. From figure 3.8, we see that basic gold-

coating significantly reduced the normalized loop occlusion times (gold, 0.68 +/- 0.03 normalized mean run steel occlusion time; two tailed t-test p-value < .01), while the heat-processing treatment was able negate this pro-thrombotic effect (heat+ gold, 1.0. +/- .05 normalized mean run steel occlusion time ; two tailed t-test p value --). Comparing the normalized, gold-coated pre- and post- treatment results, we see that the treatment effect is significant (two-tailed t-test, p <.02).

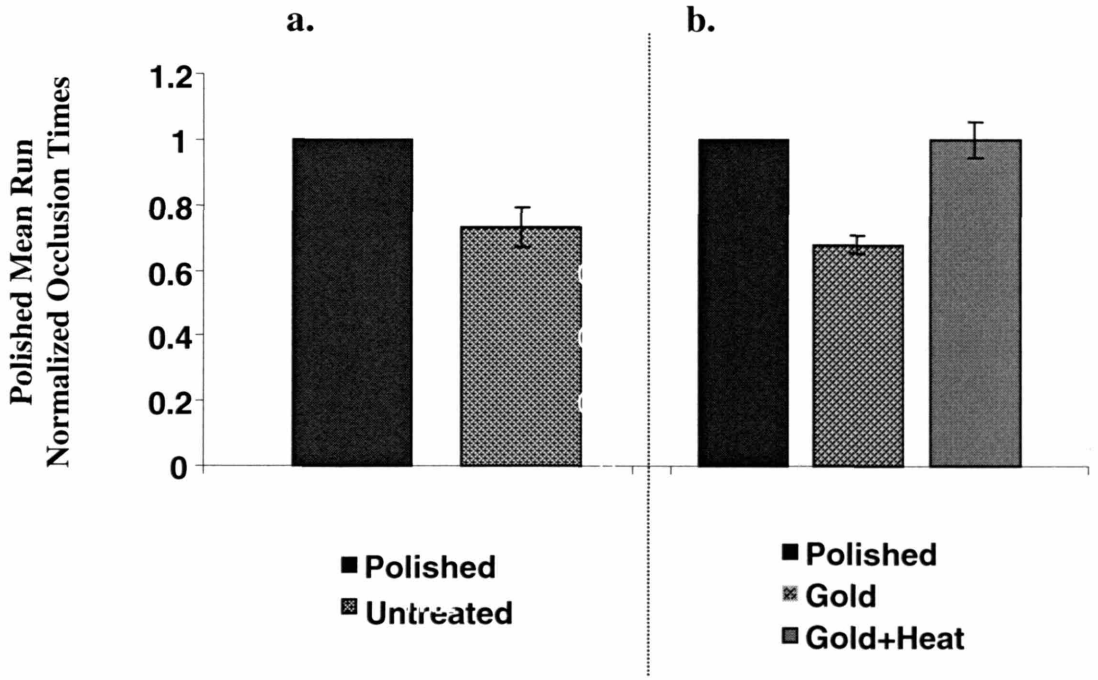

Figure 3.8. Inter-stent studies. a. Polished vs. Untreated; b. Polished vs. Gold vs. Gold + Heat Treatment. Note that the Polished steel values are by definition 1.

When designing tests, it is important to consider a studies power, which is a function of the differences that are trying to be measured (signal), the inherent variance in the measurement (noise), and the number of trials that must be performed to be relatively certain that observed differences are real rather than merely a consequence of measurement error. At one extreme, clinical trials are plagued with high variance. As a result, they typically require massive trials of hundreds to thousands of human subjects to sift through this noise for relevant signals. The expense and time needed for such trials

creates very real, practical limitations on the types of studies that can be performed. *In vitro* methods are often able to significantly reduce such population variance by offering greater experimental control. In our studies, we see that significant results (as indicated by the p values) could be obtained with relatively small sample sizes (~10).

Having powerful methods is essential to explore complex biological situations where isolation and directed manipulation of variables with observable outcomes enable epistatic pathway dissection. While sufficient power is only definable in reference to a particular signal of interest, our preliminary case studies of endovascular stent loop occlusion times add confidence that similar techniques will allow for other mechanistic investigations of coronary thrombotic events and processes.

In this section, we have tested our model flow system and found it to be suitable for reproducing coronary-type flow patterns on a beat to beat basis as judged by dimensional consideration. We have further applied this system towards an investigation of endovascular device thrombosis by considering acute loop occlusion times as a measure of the thrombotic response. The approximate 40-minute stent occlusion times that we observed are phenomenological findings that occur in our model system. *In vivo* thrombotic occlusion occurs at a much lower rate and generally takes place subacutely over the course of several days. There are various potential explanations for such observational discrepancies. The clinical situation has both innate and external counter measures, such as a reactive endothelial layer and drug therapies that help to regulate thrombosis. Indeed, with the advent of suitable drug regimes and implantation techniques, the thrombosis rate has dropped from nearly 25% in initial studies to its current low levels (<5%) [86, 108, 109]. Furthermore, our system is a closed, *in vitro* model where produced substances are not cleared. This could not only help to explain the regularity of clotting seen within our system, but also the fairly rapid drop to zero flow as confined, explosive reactions could augment rapidly due to positive feedback processes.

Due to such differences between our model and the physiological situation, we hope not to study the physical occurrence of end-state occlusion (though this is an important preliminary observation), but the cellular and protein factors leading up to thrombosis. Such dependencies are not only key mediators of occlusive events, but essential in vascular remodeling and sub-clinical responses to injury.

CHAPTER 4 Parameterizing the Thrombotic Response

There are many components and interactions involved in the thrombotic response to injury (section 1.2). In the previous chapter (section 3.2), we have used our flow model to investigate an integrated, loop occlusion response to endovascular stenting. Such overt occlusion occurs as platelets and enzymatic mediators interact with both the device surface and with each other to mediate thrombosis. When observing such complex, high level outcomes, these interactions may be significantly misrepresented in model systems. Rather than observing phenomenological loop occlusion times, we hope to develop a deeper level of understanding of the thrombotic response, initially focusing on the platelet as essential component of vascular thrombosis (section 1.2). Upon binding to an injured wall, platelets alter their expression of surface molecules and release substances which both attract and adhere to flowing cells while promoting the enzymatically driven coagulative response. The richness and importance of this platelet level demands the pursuit of understanding how this component interacts within its hemodynamic environment to promote vascular thrombosis. To accomplish this, methods of observation and control are required.

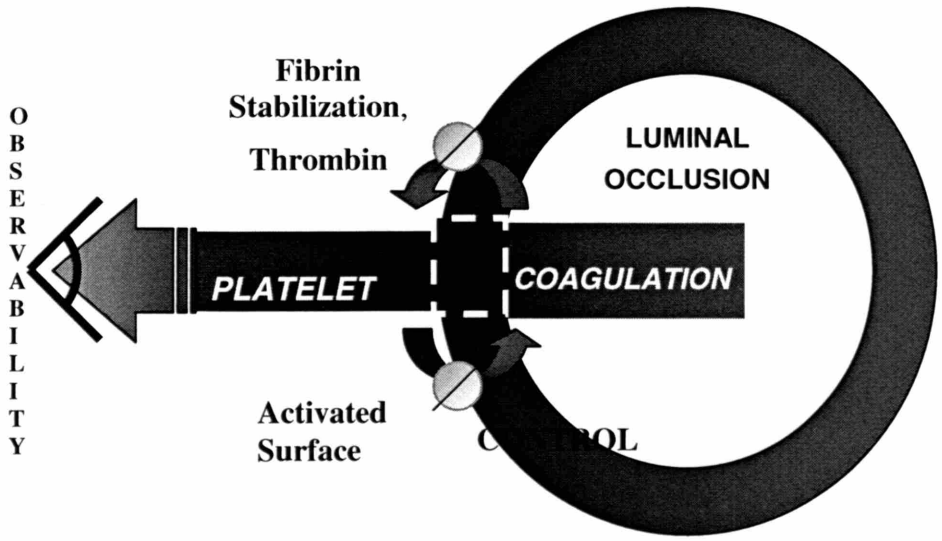

Figure 4.1. Platelet responses and coagulation interact within a black box to potentiate loop occlusion. We hope to focus on the platelet response as an important biological mediator of the thrombotic response to injury. To tease out this response, we need methods of observation and biological parameter control

In this chapter, we first review common techniques that have been used to parameterize the platelet axis in terms of methods of isolation, observation, and manipulation. We then apply such methodologies to perform a directed study on the effects of endovascular stent surface, specifically looking at the clinically relevant example of gold vs. stainless steel surfaces and how they interact in flow to mediate the reactions of thrombosis. In doing so, we show that the body's response to implanted devices such as vascular stents is a multifaceted phenomenon where complex dynamics take place and that several distinct reactions may occur which may be coupled through various biological and physical mechanisms, the balance of which determines the integrated biological response.

4.1 Platelet Function

4.1.1 Observing Platelet Function

Phenomenological loop occlusion is readily observed in our model. To focus on the platelet, we need more directed methods of observation and assessment. Platelets adhere, activate, and aggregate on reactive surfaces during which time they undergo morphological and functional changes. Each step in this process offers a handle by which to assess platelet function. Broadly speaking, we can divide observational techniques into two categories: volume measures and surface measures of platelet function.

Volume Observation

Clinically, circulating markers of platelet activation are valuable given their accessibility. Accordingly, many volumetric techniques have been developed and correlated with clinical disease and platelet function. The two principle methods of detecting platelet function through volumetric screening include assaying soluble plasma factors or assessing free stream platelets themselves.

Upon activation, a variety of soluble products (granule products, cleaved membrane glycoproteins, and metabolic factors) are released from platelets. The generation of these factors and innate clearance mechanisms create a dynamic plasma pool which can be tapped for insight into the activating source. To be effective, platelet-specific factors with low clearance rates are required due to the integrated nature of the pool. Plasma products such as platelet factor 4, β thromboglobulin, P-selectin, and thromboxane A2 can be readily monitored by isolating and assessing platelet poor plasma samples through various immunoassays (enzyme-linked, ELISA, radio-labeled, RIA). While these techniques are relatively straightforward and inexpensive, isolating the plasma samples tends to generate high levels of background activation making it difficult to observe small signals.

Flow cytometry is powerful method of analyzing platelet function by observing individual particles as they pass through a laser. Through the use of fluorescence labeled

antibodies, populations of cell suspensions (whole blood, platelet rich plasma, etc.) can be assessed for particular cell types and activation status (Fig. 4.2). This technique results in minimal artefactual activation and background noise (particularly if samples are fixed soon after collection) with added ability to distinguish subpopulations and distributions of activation status on individual cells. By selecting and observing discrete cells of interest, flow cytometry thus offers a highly sensitive, highly specific method of detecting volumetric cell parameters.

To assess a population, constitutively expressed and activation dependent markers are required. GPIb or components of the αIIbβIII integrin (GPIIb, GPIIIa) are commonly used constitutive platelet markers. Depending on the motivation, a slew of activation targets can be used to monitor different pathways of the activation process (P-selectin, activated αIIbβIII, annexin V, CD40L, etc.). Flow cytometry also allows cells to be distinguished on physical measures of forward or side scatter (representing light refraction and reflection respectively). These additional axes make it easy to detect platelet aggregates and microparticle formation, which have been associated with platelet activation and correlated with thrombotic disease [80, 110]. The versatility of flow cytometry in distinguishing multiple parameters on a single particle has also been used to observe platelet-leukocyte microaggregates, which has been recently shown to be a good marker of platelet activation in vivo [111].

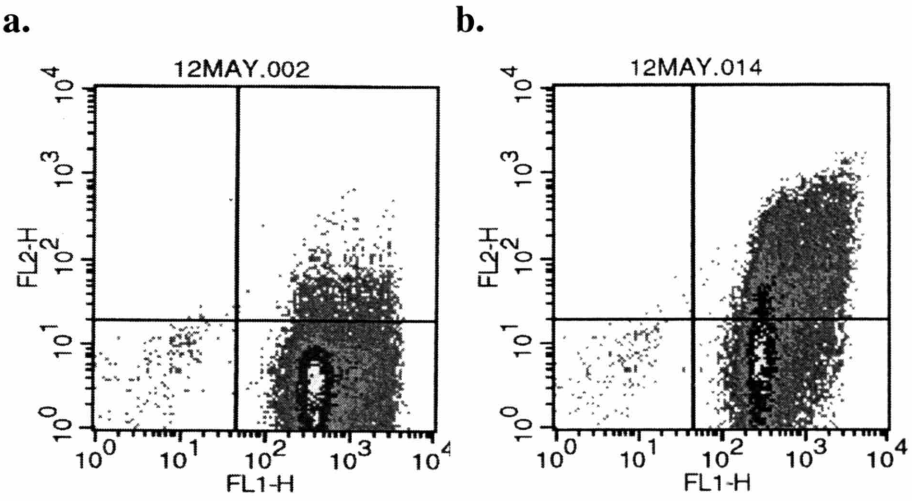

Figure 4.2. Flow cytometry where the x-axis, FL1-H, indicates presence of CD61 marker (GPIIIa constitutively present on platelets) and the y-axis, FL2-H indicates presence of CD62 marker (P-selectin present on activated platelets); a. Sample of resting platelets, and b. ADP activated platelets

Surface Observation

While volumetric measures of platelet function are readily obtainable and have proven valuable in both clinical and research settings, a fundamental concern is that volume measurements only provide an indirect indication of the platelet/surface reaction. Being a function of activation, embolization, and clearance rates from multiple potential sources, no volumetric standard has been accepted as the holy grail of surface activation. To obtain a more direct handle on the surface reactions, various strategies have been employed that directly assess the surface itself.

There are many methods of detecting platelets that have adhered and aggregated on a surface. One technique is to strip surface adherent cells from the surface and count them directly through a cell counter. While this technique has been widely used, the use of an extra surface removal step increases the possibility of introducing noise and bias into the measured signal.

One common technique that doesn't require surface removal is with the use of radio labeled platelets which requires the isolation and incorporation of a radio labeled marker such as ^{111}In (indium-111) or ^{51}Cr (cromium-51) into a subset of platelets [21, 112-114]. Subsequently, this set is recombined with the total pool and circulated over a

test surface. Upon reacting with the surface, a proportionate amount of the surface bound platelets will have a radioactive signal. While the surface count can easily be obtained and quantified in either *in vivo* or *in vitro* systems, the subset isolation/marking process can significantly affect the labeled platelets, thus creating atypical surface reactions and the accumulation of unexpected population proportions [114].

Another technique that doesn't require subset isolation is via the employment of specific cellular enzymes such as lactase dehydrogenase or acid phosphatase [115, 116]. These hardy enzymes are constitutively expressed in platelets and their activity can be detected through simple, inexpensive, colorimetric assays providing a robust, quantitative measure of cell number. However, the enzymes are generally not platelet-specific and the signal is more a marker of total thrombus rather than platelet mass. Accordingly, care must be taken when interpreting results, particularly at long time points when significant leukocytes may be incorporated into a growing thrombus. Specificity can be improved by labeling the surface adherent cellular layer with platelet specific antibodies and detecting their presence through a variety of quantitative assays (enzyme, radio labeled).

Perhaps the most direct technique comes with visualizing platelet/surface interactions. Visualization not only gives information on basic platelet adhesion, but on other important cellular and global aspects such as cytoskeletal rearrangements and thrombus height/stability. Techniques range from the use of basic histological preparations and staining with standard light field microscopy which offers a broad tissue level perspective, to more involved surface and tunneling electron microscopy where significantly greater information can be obtained at the cellular level [21, 47, 117]. In the past, many of these visualization techniques have required time-consuming fixation and sample preparation procedures. Recently, the use of unintrusive, fluorescent labeling (mepacrine, platelet-specific antibodies, calcium dies, etc.) has enabled the real time observation of platelet interactions with a variety of surfaces (curved, rough, opaque), providing much needed insight into the dynamics of thrombus growth [97, 117].

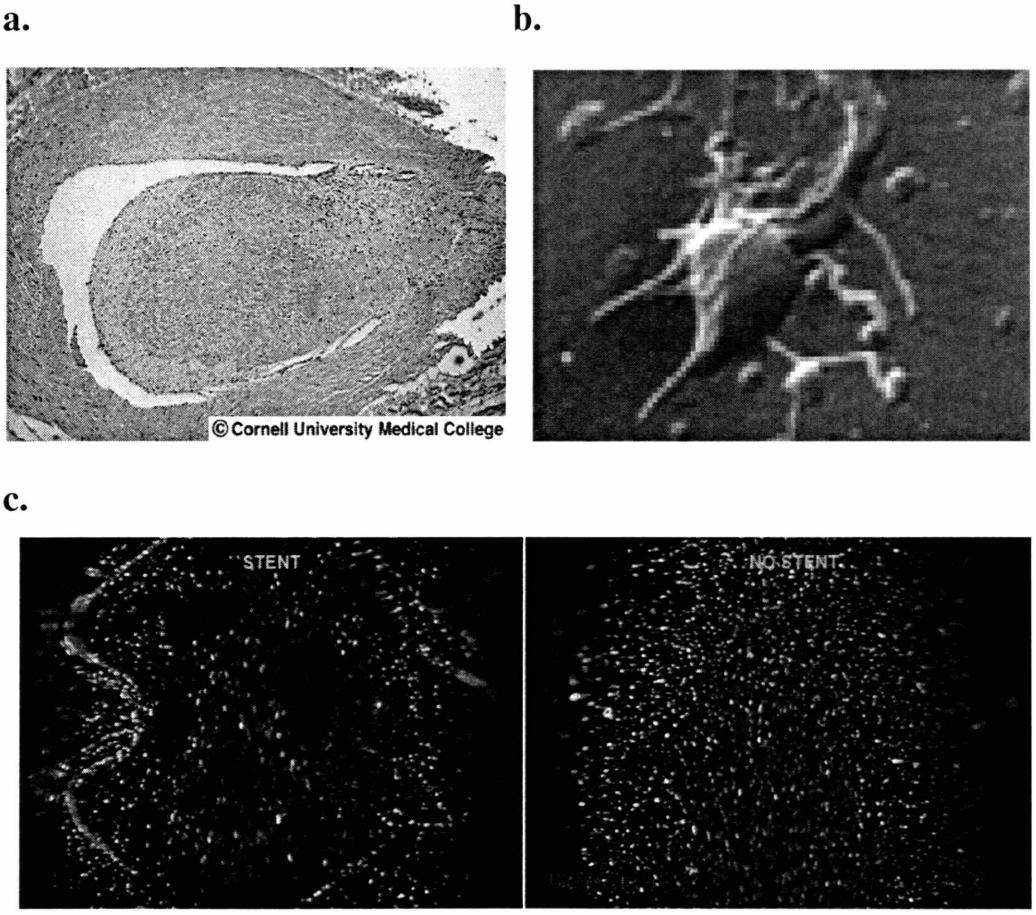

Figure 4.3. Visual examples of surface platelet responsiveness a. Light field microscope of thromboses coronary artery (© Cornell University Medical College); b. Scanning electron micrograph of platelet adherent to stent surface. c. Fluorescence actin stained image of platelet adhesion to stented and non stented collagenized surfaces.

4.1.2 Parameterizing Platelet Function

Observational tools allow us to assess biological responses. However, understanding these results within a web of multiple interactions is not straightforward. While *in vitro* systems diverge from physiological settings making complex outcomes increasingly difficult to interpret, the huge advantage of these models is that tangled situations can be unwound, parameterized and investigated in a thorough fashion using techniques which isolate and manipulate specific subsets of components.

Isolating Platelet Function

Isolating the platelet axis allows it to be studied independently of other components. So long as the relevant processes are left intact, such separation can make observations more lucid by focusing and enhancing the pertinent biological signal. There are several levels of platelet isolation that can be performed *in vitro*. A most basic isolation is the extraction of whole blood along with its innate platelet component from its typical vascular surround. Blood-borne effects can thus be studied without the added complexity of an active vessel wall. To further isolate the effects of platelets, platelet rich plasma can be readily separated from whole blood (as in our initial biological analysis of section 3.2), removing the effects of erythrocytes and leukocytes. Fully isolated platelets can be generated from PRP through a series of pelleting and washing steps or via a platelet filtration column, leaving only the intact cell sons its reactive protein environment [21]. Oftentimes, these physical isolation processes cause significant background levels of activation and thus, are typically performed in the presence of anti-platelet agents (i.e. prostaglalandins. PGE1) which themselves can have a significant impact on the observed platelet response [23].

Another method of component isolation that doesn't require physical separation comes with the use of powerful inhibitory agents. However, it is imperative to consider the effectiveness and specificity of potential agents. When isolating platelets from the effects of coagulation, citrate or EDTA work by chelating divalent cations which are required in several coagulation reaction [39]. However, these cations are also an important mediator of platelet function and their sequestration can have unwanted effects on platelet surface reactions [33]. Other agents, such as the commonly used clinical drugs heparin and coumadin, are also not ideal for *in vitro* studies as heparin's actions are far reaching, while the mechanism of coumadin's action requires an *in vivo* system [21, 39]. A good strategy for in vitro platelet isolation is through the use of specific serine protease blocking agents such as corn trypsin inhibitor (CTI) and PPACK or hirudin which target activated Factor XII and thrombin respectively [23, 118, 119]. The isolated or combined synergistic use of such agents can be used to strongly suppress coagulation,

thereby functionally isolating platelets without traumatic, physical component removal (Fig 4.4).

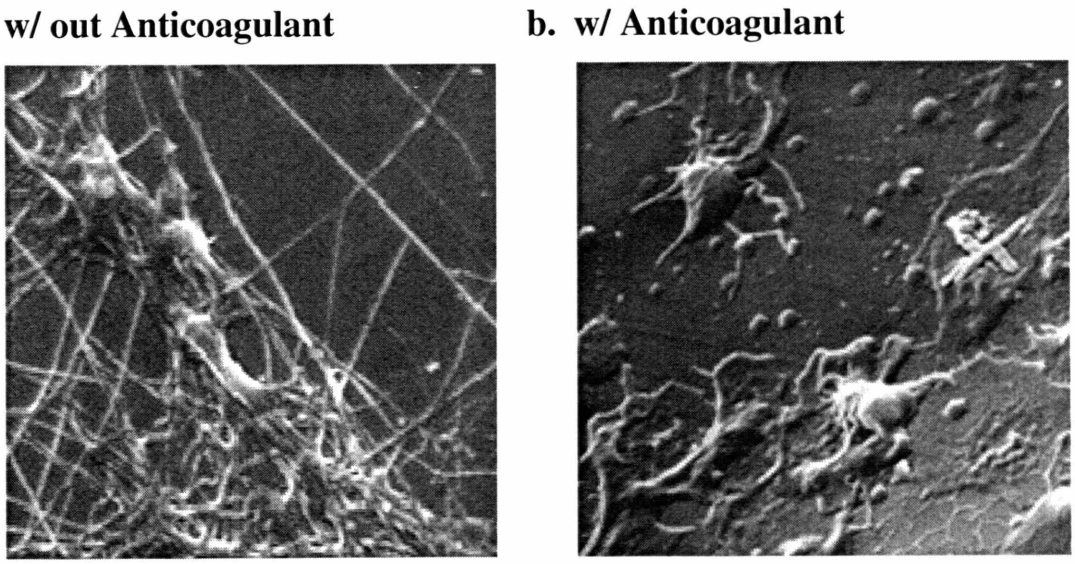

Figure 4.4. a. Surface platelet reaction with coagulation; b. Platelet Reaction with coagulation suppressed (80 ug/ml CTI + 3 U/ml Hirudin)

Manipulating Platelet Function

Once trimmed, isolated subsystems can be mechanistically studied through causative manipulation and observation. This can be accomplished by either adding back (knocking in) and/or removing (knocking out) specific components.

To observe the importance of platelet function, a fundamental manipulation is to remove platelets altogether through the use of serial centrifugations, filters and component recombination to obtain the desired, platelet poor medium. To observe which platelet functions were pivotal, individual platelet components can be added back to this depleted scheme. For example, as detailed in section 1.2, activated membrane serves as an essential catalyst for coagulation reactions. Thus, `activated' membrane analogs (such as cephalin) can be added as a functional substitute [119, 120]. Alternatively, platelets are known to play a role in supporting leukocyte surface reactions through P-selectin.

The importance of this interaction can be observed by removing platelets and using P-selectin coated surfaces to mechanistically observe this platelet function [121].

Rather than complete removal (which, but for a matter of perspective, creates a new subsystem of observation), more pointed methods can be used to study particular platelet reactions. Genetic variants with enhanced or diminished functions (polymorphic surface receptor expression levels, point mutations, etc.) are sometimes accessible [97, 122, 123]. In the modern era of genetics, directed gene over expression or knockouts have greatly expanded the library of such genetic anomalies.

It is oftentimes easier to create manipulations through the addition of external agents rather than searching for or developing specific genetic alterations. For instance, cyclooxygenase inhibitors or thienopyridine derivatives are known to knockdown the thromboxane axis or block ADP receptors respectively, greatly reducing platelet activatability in flow environments. Alternatively, function blocking antibodies have offered a highly versatile strategy of inhibiting specific platelet events from adhesion (anti-GPIb, GPVI, αIIbβIII, a2B1, avB3) to activation (anti-a2B1, PY2, GPVI, GPIb) to aggregation mechanisms (anti- αIIbβIII). While potential side effects must always be considered when using external agents, their use allows a degree of versatility not readily possible with genetic mutation. Dose-dependent effects can be readily studied, helping to distinguish causative relations while adding great insight into the underlying system kinetics and function (binary vs. graded interactions, etc.). Additionally, the combined use of multiple agents facilitates the directed investigation of complex interactions, not readily possible with genetic mutation [(concurrent blockade of αIIbβIII and GPIb].

In this section, we have reviewed methods of platelet isolation, observation, and manipulation. Together, these techniques allow us to parameterize the platelet axis to gain access and insight into this key factor in the thrombotic process. As we have already begun to explore (section 3.2.3) material surface can have a significant impact on the device dependent thrombotic response. These initial results considered the loop occlusion time of endovascular stents as a marker of device thrombotic potential. However, these coarse measures are the result of a complex interplay of surface mediated

interactions. Parameterization is an essential strategy with which to begin to unravel findings that are otherwise limited to phenomenological, model occurrences. We now apply these methods towards a more in depth study of stent surface interactions.

4.2 Dynamic Bio-Implant Platelet Reactions

When a foreign structure comes into contact with tissue and blood, a variety of biological consequences occur which can result in acute or long-term device failure. Vascular patency relies on a careful balance of chemical mediators and local fluid dynamics. The thrombotic reactions of the foreign surface are initiated by surface protein absorption followed by cellular and enzymatic interactions with this modified surface. Different surfaces have different absorption rates for various plasma proteins which eventually reach a surface dependent steady state distribution [124, 125]. The deposited proteins subsequently interact with other components of thrombosis (platelets, coagulant proteins), generating the potential for varied surface dependent responses. For instance, surfaces which preferentially bind fibrinogen have been shown to be pro-thrombotic while relatively inert albumin deposition confers a reduced potential [126-131]. Overtime, trace proteins such as coagulative or compliment proteins can accumulate on the surface, promoting their respective biological reactions and can greatly influence the overall foreign surface response.

Flow can further dynamically affect the components of thrombosis either through physical shear dependent mechanisms, such as von Willebrand's Factor (vWF) dependent platelet adhesion, or through the mass transport of cellular and molecular substances into and out of a given region (section 1.3). Such physical involvement is complicated by the fact that several interactions exist between platelets and coagulation. Activated platelet membrane is essential for sequestering and localizing coagulation reactions from the flowing blood to the site of injury, which in turn can potentiate further platelet activation and stabilization the aggregating platelet mass through the production of thrombin and fibrin (section 1.2).

The biological and physical interactions taking place at a prosthetic surface must be considered when assessing device biocompatibility as implantation can occur in a variety of biophysical settings [127, 132]. We currently address such surface interactions by developing *in vitro* techniques to parameterize the thrombotic response. We then apply strategies these to study platelet reactivity between stainless steel endovascular stents of

identical geometry, coated with dissimilar surface materials as a function of fluid flow conditions and coagulative interactions.

4.2.1 Methods

Hemodynamic Environment

For the current work, a high flow, typical coronary pattern, was approximated with a peak flow of 200 ml/min and a mean pulse flow rate of 100 ml/min along with a low flow pattern with a peak of 40 ml/min and a mean of 20 ml/min (Fig. 4.5).

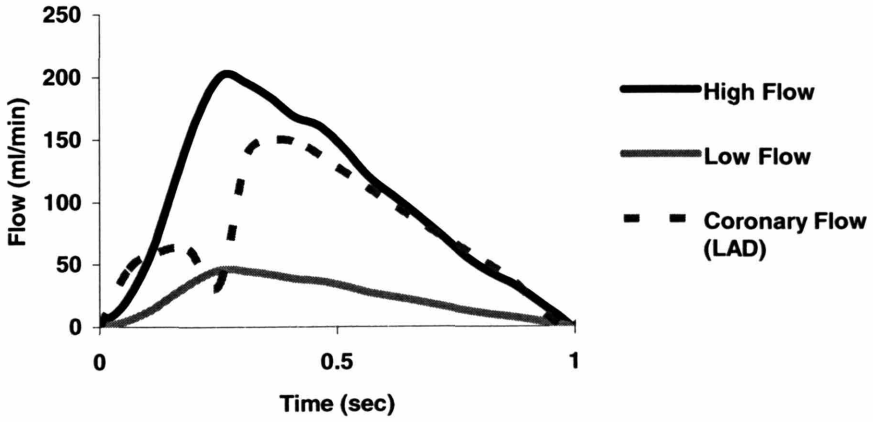

Figure 4.5. Generated coronary-like triangular flow profiles (200 ml/min High; 40 ml/min Low Peak Flow); ** It should be explicitly noted that these figures only represent one cycle of a bidirectional flow as previously shown in Fig. 3.3.

Stainless steel stents left intact or coated with a 7 + 2 um layer of gold were examined as a relevant clinical comparison (section 3.2.3) [107, 133-136]. Surface roughness of the two surfaces was determined using atomic force microscopy, showing a significant increase in surface roughness with coating (coated average roughness, Ra=154.6±5.4 nm vs. uncoated Ra=48.4±2.2 nm).

These geometrically identical stents [107] were all 9 mm in length and were expanded directly within a flood loop to a 3.5 mm post-inflation diameter under 12 atm of pressure via a balloon catheter (Fig. 3.6). Subsequently, the 24.0 cm long tubes (3.2

mm ID / 4.8 mm OD silicone tubing1) were closed into their loop format, filled with the appropriate blood components (see below; Parameterizing Thrombotic Subsystems) and run at 37°C under the desired flow conditions. The flow was monitored and motion of the loops could be stopped at any time to assess specific biological markers.

Parameterizing Thrombotic Subsystems

Along with these physical factors of flow and stent surface, we hoped to study the synergistic effects of coagulation as a potential influencer in determining endovascular stent platelet reactivity. To accomplish this, we needed mechanisms of isolating and observing the platelet and coagulative systems as well as methods of recombining them in a controlled fashion to observe their interactions. Blood components were derived from whole blood obtained from healthy volunteers drawn via a 20-gauge needle into a 1/10 dilution of ACD anticoagulant. To decrease the complexity of the situation, platelet rich plasma (PRP) was used as a source of platelets by centrifuging the blood at 200g for 15 min and colleting the top, platelet rich layer.

Decoupling the Platelet Subsystem

The decoupled platelet response was measured using PRP anticoagulated with 5 U/ml hirudin and 80mg/ml Corn Trypsin Inhibitor (CTI; specific thrombin and activated Factor XII inhibitors respectively). Significantly prolonged activated partial thromboplastin times and electron microscopy studies of post-run stent surfaces indicated the effectiveness of this method in eliminating coagulative function (Fig 4.4 depicts surface visualization).

Decoupling the Coagulative Subsystem

To consider the decoupled coagulative response, the platelets were removed by further centrifugation of the PRP at 1500g for 15 minutes. The platelet-free supernatant was recentrifuged at 2500g for 20 minutes to ensure platelet free plasma. To test the discrete

coagulation response, 100 µl/tube of 8mg/ml phosphadidylethanolamine was added to the platelet-depleted plasma to function as a decoupled phospholipid source [120].

Coupling Platelet and Coagulative Subsystems

To probe the coupled effects of coagulation on platelet reactivity, graded amounts of the specific activated Factor XII inhibitor, CTI (0-40 mg/ml), were added to PRP with higher levels of anticoagulant corresponding to diminished levels of coagulation presence.

Platelet Assessment

To measure volumetric platelet activation, 100 µl of each post-run PRP sample was suspended in 1 ml of 1% paraformaldehyde/PBS fixing solution and stored at 4 °C for 24 hours. 50 µl of the fixed sample was incubated for 20 minutes with 20 ul of CD61-FITC (anti-gpIIIa) and CD62p-PE[2] (anti-p-Selectin) as constitutive and activation dependent platelet markers respectively. The reaction mix was quenched with 1 ml 1% paraformaldehyde and assessed via flow cytometery[3] (FAC) by determining percentage of CD62p+ counts in the total CD61+ population (% activation).

For an index of surface activation, a platelet extraction protocol was developed. Briefly, the flushed tubes were filled with 1% paraformaldehyde fixative and stored at 4 °C for 24 hours. After fixing, the tubes were again flushed with HBSS and closed. Each loop was filled with 0.05% trypsin w/ 0.02% EDTA and spun in the flow setup under high shear conditions (500 ml/min peak flow rate) for 2.5 hours (25 °C) to extract adherent platelets. The loops were emptied into 200 µl trypsin inhibitor (60mg/ml; Sigma). The platelets were pelleted (2500g for 15 minute; 4 °C) and concentrated in 100 µl PBS (pH 7.2). Following the antibody staining protocol, total CD61+ counts and

[2] Beckton Dickinson
[3] FACscan™,Becton Dickinson

counts expressing both CD61 and CD62p were determined through FACs analysis as measures of surface adherent and activated platelets respectively. Fixation and trypsinization procedures were found not to alter CD61 or CD62p labeling.

Coagulative Assessment

While platelets are required for the catalytic progression of coagulation, the enzymatic cascade can be initiated directly by a surface through classical intrinsic and extrinsic mechanisms. These two pathways of activation then join in a common pathway that leads to the production of thrombin and subsequent fibrin clot.

This cascading enzymatic process generates activated proteases and cleavage byproducts which can be assessed by specific enzymatic assays or through antibody detection (ELISA, RIA). We currently assessed decoupled coagulative function by detecting the prothrombin fragment, PT1+2 (formed upon enzymatic cleavage of prothrombin by activated Factor X), using a prothrombin fragment ELISA kit (Behring-Dade).

4.2.2 Decoupled Platelet/Coagulation Responses

Anticoagulated, PRP was recalcified (13mM) and injected into the fluid loops to assess decoupled platelet reactivity to stent surface. Twelve stents of either plain or gold coated stainless steel and 4 non-stented controls were run at high flow conditions to assess platelet responsiveness. The anticoagulated runs were stopped at 1 hour and both the tube and bulk fluid were assessed for platelet reactivity.

To test the discrete coagulation response, platelet-depleted plasma enriched with phosphadidylethanolamine was recalcified (13mM) and injected into the respective fluid loops. Six stents of each type and 4 stentless controls were run in total under the high flow conditions. The tubes were all stopped after 1 hour and the circulant fluid was assessed for PT1+2 fragment levels. All values were normalized to the mean, stainless steel values of the specific run.

In these decoupled trials, plasma exposed to the bare stainless steel stents contained higher normalized PT1+2 levels (Fig. 4.6, 1.00±0.13) than plasma with gold-coated stents (0.50±0.07, $p<0.001$). Conversely, using highly anticoagulated PRP, we found significantly more normalized surface bound, activated platelets in the gold stented loops as compared to the stainless steel stented loops (1.45±0.10 vs. 1.00±0.08, $p<0.05$). This increase in platelet response was not well represented in the normalized bulk percentage activation (gold 1.21±0.16, steel 1.00±0.14, control 1.19±0.24).

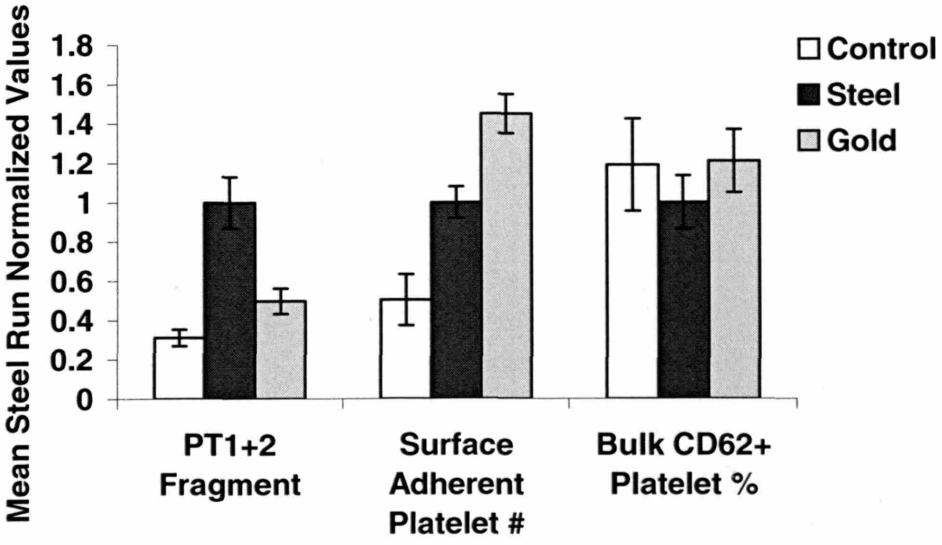

Figure 4.6. Decoupled coagulation (PT1+2) and Platelet (Surface adhesion, Bulk activation) responses. All results presented after normalization to the average stainless steel values for a given run to account for inter-run variability.

The effect of surface in differentially mediating isolated limbs of the thrombotic response is intriguing and alludes to the richness that underlies bio-implant reactions. We found that stainless steel stents had a higher independent coagulation response, while exhibiting reduced independent platelet reactivity as compared to gold stents. While stainless steel is known to form a protective oxide layer on its surface, gold does not, enabling strong, chemical surface protein interactions to highly abundant plasma proteins such as fibrinogen [107, 126, 129]. On less reactive, oxidizable surfaces such as stainless steel, the Vroman effect may occur allowing less abundant proteins such as high molecular

weight kininogen (HMWK) and FXII to accumulate on the surface [124, 126, 129, 131]. Such effects could account for the enhanced coagulative action of stainless steel devices, while the enhanced platelet reactivity of gold-plated stents could be in part due to tightly binding fibrinogen mechanisms. In addition, surface roughness (whose importance is indicated by the decreased thrombotic response upon stent polishing; Section 3.2.3), was found to be greater on the gold-coated stents, and may also play a role.

4.2.3 Coupled Platelet Response

Effect of Coagulation Strength on Stent Platelet Reactivity

To evaluate the effects of coagulation on platelet reactivity, varying levels of CTI anticoagulant (40, 20, 4, 0 μg/ml) were added to recalcified PRP. Stainless steel stents were run under the high flow conditions until a reduction in the flow recordings could be detected under any of the CTI conditions. All loops were subsequently stopped and analyzed for surface and volumetric platelet response as described above (section 4.2.1). This procedure was repeated for a total of four runs.

When we combined PRP with reducing amounts of CTI, the normalized surface bound platelet number rose (Fig. 4.7). This is likely due to synergistic interactions between the two thrombotic limbs. Although surface measures of platelet response were observable in each of these platelet reactivity trials, changes in bulk platelet activation that have been used as a marker in various other studies [94, 137, 138] were not appreciable. This discrepancy may reflect the generalized low degree of platelet activation within our flow system and the adherence of the activated platelet population to the circuit wall. One exception is in the most highly coupled condition (0 mg CTI), where observable thrombus formation occurred. Here, we see a dramatic increase in the number of surface bound platelets, accompanied by an increase in bulk activation levels. For such a progressed thrombotic stage, there is likely an explosive accumulation of coagulative products within our closed, *in vitro* system. Such uncontained coagulation could lead to volumetric platelet activation, creating a situation that may no longer be representative of surface thrombotic phenomenon. That levels of bulk activation were relatively constant

in our trials indicates that we were indeed studying the proposed, "pre-explosive", surface thrombotic phenomenon.

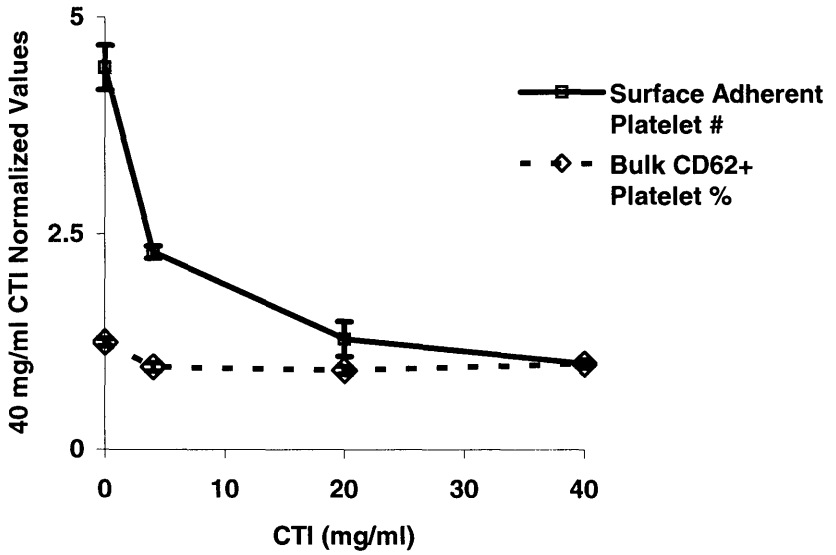

Figure 4.7. Surface and Bulk platelet response with increasing CTI anticoagulant (0-40 mg/ml CTI; decreasing coagulation). Results have been normalized to the 40 mg/ml CTI condition to account for inter run variablility.

Interactions of Flow and Coagulation on Stent Platelet Reactivity

The interactive influence of coagulation and flow on determining the relative platelet reactivity of the biomaterial surfaces was considered by performing 4 1-hour runs of 4 steel and 4 gold stents using recalcified PRP supplemented with 20 μg/ml CTI anticoagulant. In each run, 2 of each stent type were run under the high flow and 2 under the low flow conditions. Platelet response was measured as described above. Four similar runs were performed at a lower, 4 μg/ml CTI condition. In each of these trials, an additional 20 μg/ml CTI, high flow, stainless steel case was tested to allow relative scaling between the 4 and 20 μg/ml anticoagulant conditions (section 4.2.1).

Two-way ANOVA analysis revealed significant dependence on both flow and CTI levels, with significant interaction effects in the gold group. At low flow there was an increase in normalized platelet activation with increased coagulation strength for both gold (0.89±0.09 vs. 2.38±0.27; $p<0.001$) and steel (0.59±0.08 vs. 1.77±0.20; $p<0.001$) stents (Fig. 4.8). Similarly, at low coagulation levels (20mg/ml CTI), a generalized increase in platelet reactivity was observed with the higher flow rate for both gold (0.89±0.09 vs. 1.28±0.14; $p<0.05$) and steel (0.59±0.08 vs. 1.00±0.07; $p<0.01$). At high flow, there is an increased trend in platelet reactivity with decreased anticoagulation reaching significance for the steel group (1.00±0.07 vs. 2.13±0.30; $p<0.01$). At 4mg/ml CTI, we do not witness a common trend with gold showing a significant decrease in platelet reactivity with increased flow (2.38±0.27 vs. 1.44±0.12; $p<0.05$), while the steel group showed a non-significant increase.

In three of the four test conditions (Low Flow, 20mg/ml CTI; Low Flow, 4mg/ml CTI; High Flow, 20mg/ml CTI), gold reacted more strongly with platelets (first condition significant: 0.89±0.09 vs. 0.59±0.08; $p<0.05$), while at low levels of CTI and high flow, the steel stent reacted more strongly (2.13±0.03 vs. 1.44±0.12; $p<0.05$ using a one-tailed Student t test to assess this directional change). In all of these conditions, CD62+ bulk platelet activation levels (data not shown) did not significantly vary between the different groups.

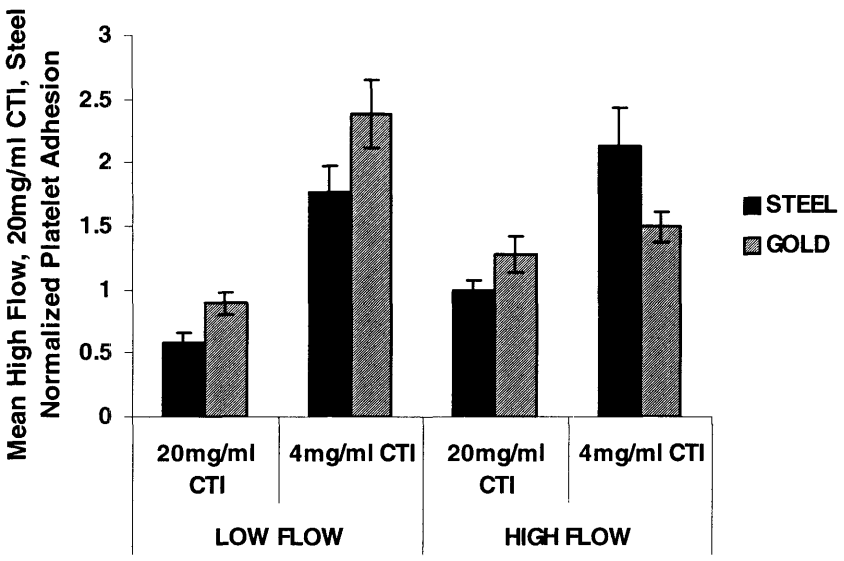

Figure 4.8. Effects of flow and coagulation strength on platelet reactivity to bare stainless steel and coated gold surfaces.

With decreased coagulative function, stent platelet reactivity increased with flow. It is known that platelets adhere and activate more effectively at higher shear rates [50, 62, 139]. In our studies, average estimated wall shears were 500 s^{-1} and 100 s^{-1} for the high and low flow cases respectively (with peak shears reaching significantly higher values), well within the dynamic range of shear-dependent platelet activity. However, it must be pointed out that the shear rates at the stent surface may vary considerably as suggested by finite element studies [82, 84].

Under conditions of low flow consistent with those found within the venous vasculature or impeded arterial flow, we witnessed an increase in platelet function when coagulative function was added. Such a coupled increase is expected as the coagulative process leads to the production of substances that can promote platelet activation, adhesion, and aggregation [39, 40]. However, with the role of coagulation increased, the flow-dependent increase of platelet reactivity was no longer evident. This may reflect the complex mutual interactions between the various components of thrombosis, flow, and the instigating surface. Increased flow could alter the balance of coagulation products within the stent vicinity, as evidenced in the case of platelet rich arterial versus fibrin rich venous thrombi [60]. Whereas the higher independent coagulative potential of stainless

steel may compensate for such clearance causing a non-significant increase in platelet reactivity, the lower potential of the gold may not.

.

4.2.4 Richness in the Thrombotic Response

Implanted devices are increasingly used to combat complex diseases in a range of pathophysiological settings. Issues of biocompatibility must now encompass far more than the inert nature of the reaction to local implantation. Among the most commonly used devices are intravascular implants which are subject to a multitude of biological responses taking place within a dynamic flow field. As implanted devices are made of multiple and composite materials, it must be recognized that devices of dissimilar compositions may stimulate different aspects of thrombosis to a variable degree [126, 127, 131]. Here we provide an example of the complexity underlying body/device interactions. By parameterizing aspects of the biological and physical setting, we demonstrate that various independent device responses may exist *in vitro*. It is a dynamic balance of these normally interactive components in the context of a local biological and physical environment that determines measures of biocompatibility such as stent-mediated platelet-reactivity.

Based on a reduced theoretical coagulative network model, Basmadgian et. al. have shown that the effects of flow and surface are intertwined. [60, 140]. Their calculations revealed the possibility of multiple steady states and regions of high and low parameter sensitivity in coagulative function, but they were limited to a single surface interaction. In physiological systems, several, distinct prosthetic reactions occur (platelets, coagulation, etc.) creating the possibility for more complex, divergent outcomes. Such dynamic interactions can have a significant impact on integrated biocompatibility measures of devices.

A surface plot presenting the parametric flow and coagulation data (Fig. 4.9) depicts the continuity of platelet reactivity, with each plane representing the biological activity of a particular device. That these formed planes are not parallel infers the existence of various biocompatibility regimes. Although more platelets adhered to the gold-coated stents under most conditions tested, the stainless steel adhered more platelets under our conditions of high flow and low anticoagulant. Practical device rankings can be made

only if the depicted reactivity surfaces are close to parallel or far enough apart over some range.

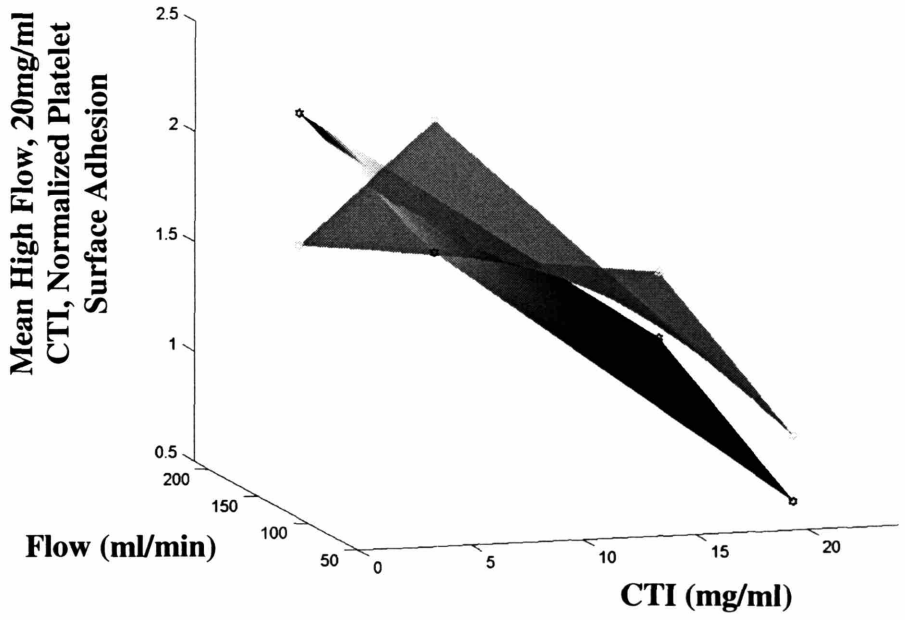

Figure 4.9. Potential platelet reactivity surfaces as a function of flow and coaglation depiciting dynamic biocompatibility.

Recognizing the dynamic nature of biocompatibility is valuable as there are several ways (both *in vitro* and *in vivo*) that parameters may be varied over considerable scales. For instance, the use of anti-thrombotic agents or considering patients or blood deficient in certain thrombotic components could dramatically affect biological variables leading to different biocompatibility regimes. When performing studies, it is important to keep such parameters in mind as these biases could help to explain discrepancies found both within and between various *in vivo* and *in vitro* systems [107, 127, 134-136]. Alternatively, human physiology encompasses a wide range of physical conditions. For vascular devices, materials suited for high flows may not be best suited for low flow conditions [132]. Dynamic biocompatibility knowledge could not only lead to such a situation-optimized use of implants and materials, but the optimization of concurrently administered drug regimes. These issues become especially relevant when considering

the present day push to locally deliver drugs from implant surfaces, where the local dynamic environment can be directly and specifically modulated.

While addressing dynamic issues is important, as they undoubtedly play a key role in determining biological outcomes (which have evolved under dynamic conditions), we must also acknowledge the difficulty in doing so. As more axes are parameterized the number of tests grows exponentially and to fully characterize these dynamic regimes would negate the cost-effectiveness of bench-top methodologies. These studies must be performed selectively and restrictively. One bound which we can impose is to aim for predictive relevance. While the use of simplistic in vitro models precludes any certainty, it is a reasonable direction in which to head (at least as good as any other).

Prediction, Parameterization and Placement

In this chapter, parameterization of the biological and physical environments has allowed us to extend the use of our model from coarse observations of loop occlusion time to a more mechanistic appreciation for the interplay of thrombotic surface reactions. Whereas non-treated gold initially seemed a less suitable candidate in terms of thrombotic response (Fig. 3.8), we show that this ranking is not necessarily the case (Fig. 4.8, 4.9). Predictive statements based on *in vitro* model outcomes must be made with caution as responses are highly dependent on condition. While model-based prediction is an important goal given the increased societal cost (money, time, risk, and ethics) of studying real-world situations, the same reductive simplicity that enables comprehensible studies acts as a double edged sword, inherently detracting from predictive relevance.

Models may be adjusted to compensate for unrealistic, skewed parameters. In engineering systems, this established process is formally referred to as dimensional analysis. When considering situations such as the lift of a model airplane wing or the fuel efficiency of a model car, dimensional analysis ensures that relevant, dimensionless parameters are equivalently scaled, bringing real-world relevance to model outcomes. In chapter 3, we go through a similar procedure to create real-world, coronary-like flow conditions by maintaining key dimensionless flow parameters (Re, Wo, De; see section) within our hemodynamic model.

While dimensional analysis is applicable to well characterized engineering systems, biological models are formed through empirical evidence and deal with incompletely characterized, qualitative concepts rather than quantitative parameters. As a result, these systems are adrift somewhere between predictive and reductionist goals. Progress generally occurs through gradual movements from *in vitro* to *in vivo* to clinical environments as predictive statements are projected over safe, stable experimental distances (Fig. 4.10). In the rapidly advancing medical arena, it is important to attempt to optimize this process by establishing firm i*n vitro* foundations in appropriate settings and making well-directed vertical projections towards increasingly complex, increasingly relevant systems. Although thorough dimensional analysis is not possible, model parameterization and placement help in this optimization via a kind of dimensional consideration.

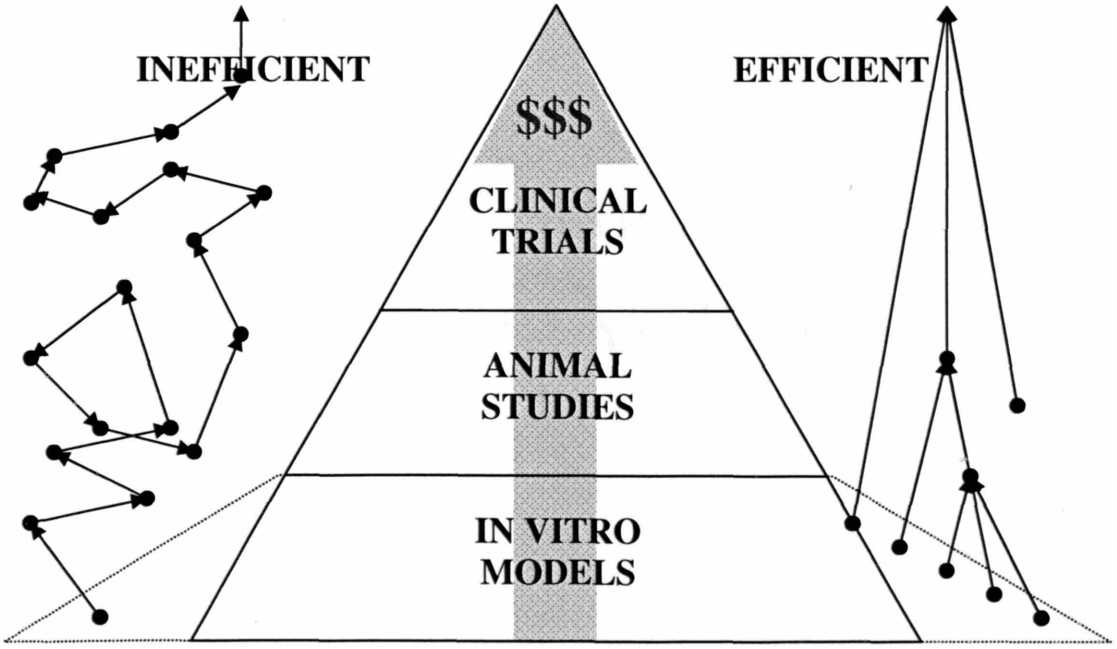

Figure 4.10. Pyramidal representation of the path to clinically pertinent developments. Given the increased societal expense at higher levels, more trials are performed at base levels, though at the expense of potential relevance. To maintain the efficiency of this scheme, well directed vertical projections from stable foundations must be attempted.

Already, we have seen that parameterization allows reductive, mechanistic studies. From another vantage point, model parameterization also adds predictive insight into biological models. While a rigorous understanding of the involved processes and parameters is not established, the underlying principles of dimensional analysis and model scalability are still valid and may be considered by varying parameters (handles; i.e. coagulation strength, flow rate; section 4.2) over a range of possibilities and observing outcomes. Such scaling offers a handle on hidden, dimensionless functions (much the same way varying fluid velocity may vary the Re). As in more rigorous engineering examples, if the necessary hidden dimensionless functions are preserved, predictive relevance can be maintained. However, since the hidden functions are not known or quantifiable, handles must be parametrically searched, in essence scanning a space of experimental possibilities. If similar findings are obtained over large parameter scale changes then predictive robustness is increased allowing safer projections to increasingly complex, relevant scenarios (i.e. *in vivo* / clinical situations). On the other hand, findings that change with handle manipulation indicate potential directions for further reductionist understanding and model stabilization, which indirectly benefits future predictive efforts by establishing firm foundations. To search such experimental spaces many tests must be performed and strategies that accommodate quick, efficient testing are important in order to maintain the effectiveness of these *in vitro* trials. The small loop volumes and multi-rotor, multi-axis design which we developed allows the consideration of multiple loops run under multiple conditions at once, greatly enhancing the efficiency of the described strategy making parametric studies feasible.

Along with efficient tests which potentiate model parameterization, model placement is essential to consider to maintain the efficacy of *in vitro* studies. While parameterization allows indirect manipulation on hidden functions, some of these functions may be only weakly dependent on (or completely independent of) the available handles. The potential experimental space may altogether exclude pertinent regions. While inclusion of relevant regions cannot be guaranteed in complex, incompletely characterized biological models, it is important to carefully consider the qualitative dynamics of the situation as the benefits of reductive simplicity are balanced with promoting predictive relevance.

By developing and applying techniques of parameterizing the biological and physical axes of our *in vitro* system, the current example of endovascular stenting shows the richness underlying vascular responses. While this is of great relevance in studying foreign surface thrombotic reactions, it is limited in making statements about complex thrombotic situations where devices are placed within a complex vascular environment. Not only do blood components interact with the stent surface and with each other, but with the vessel wall itself. Not considering the wall component could significantly affect the local response, potentially placing our findings outside the regimes of viable responses. Given the amount of energy that must be spent in parametrically studying dynamic environments, it is important to attempt to place models well to maximize the chance of predictive relevance. We now turn to the development of a model of wall reactivity with the goal of increasing the real-world applicability of our *in vitro* system.

CHAPTER 5 The Coronary Lesion Environment

5.1 *Reactive Site Development*

Model parameterization promotes the effective use of *in vitro* systems by enabling mechanistic reduction and testing predictive robustness. In chapters 2-4, we have begun to parameterize both physical and biological axes of our system, using handles on coagulation, platelets, flow, and foreign surface to study aspects of endovascular device thrombosis. While such reduction reveals the complexity underlying more blunt, loop occlusion time measures (section 3.2.3), these parameterized experiments do not consider vessel wall interactions. Not including this important wall component in our model could result in a significant, qualitative misrepresentation of the vascular situation. The geometry and surface of the vessel wall serves as a boundary to both the physical and biological environments and thus plays a critical role in determining local reactions (see sections 1.2, 1.3). Before the true power of parameterization can be realized, careful consideration must be given to proper model placement. To gain a parametric handle on critical aspects of the vessel wall, we incorporated discrete reactive sites into our previously homogenous fluid loop model as a more complete biophysical model of localized vascular lesions.

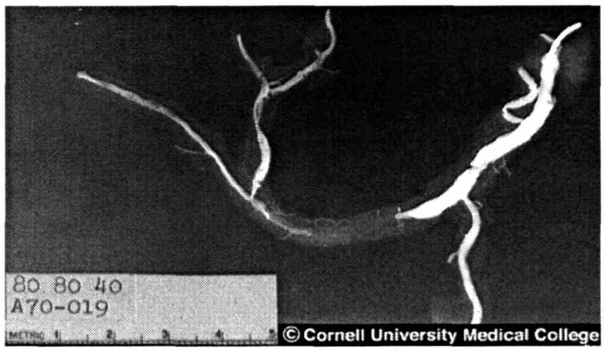

Figure 5.1. Angiogram (© Cornell University Medical College) despicting a coronary lesion (near total occlusion). Note the lengh of the lesion (LReactive Site) in relation to both the vessel diameter (D) and the vessel length (LArtery); D<LReactive Site<LArtery.

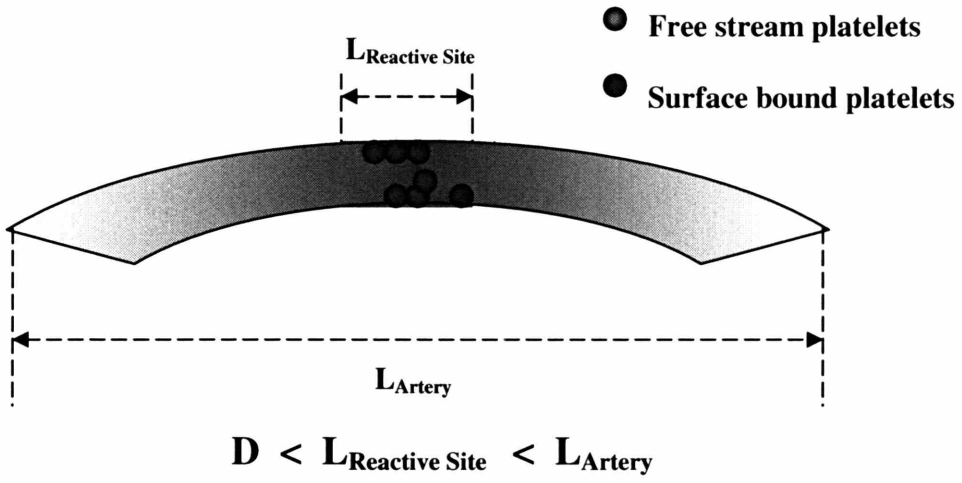

Figure 5.2. Schematic, idealized representation of a localized reactive site within an extending vessel.

Typically, individual coronary lesions are on length scales of several arterial diameters with this aspect ratio imposing a basic geometric constraint on lesion architecture. Current AHA/ACC classification stratifies Type A, B and C lesions as <10 mm, 10-20 mm, and > 20 mm respectively [141, 142]. Stents have accordingly been designed to treat these lesions, with typical lengths ranging from ~10-30 mm [143]. Although with diffuse disease these lesions may overlap and extend over considerable distances, isolated cases of disease or instances presenting upon plaque rupture or post intervention are characterized by a localized, spatial change in wall surface and/or geometry (Figs. 5.1, 5.2). To accommodate such situations, we used both glass and silicone reactive sites coated with various physiologically relevant substrates allowing both wall geometry and surface features to be individually isolated and controlled. In doing so, we positioned our model to study not only foreign surface reactions, but more generalized vascular situations.

5.1.1 Geometry

Geometry plays an important role in determining the local hemodynamic environment. In states of pathology and intervention, geometries can be significantly altered (section 1.3). To accommodate such local changes in wall geometry, we developed a discrete 3 cm reactive segment as a prototypical embodiment of an isolated vascular lesion. This segment was placed inline with a 21 cm length of 1/8" ID 3350 Tygon tubing, retaining the overall total fluid loop circumference (Fig. 5.3). The ~0.1:1 aspect ratio of vessel radius to reactive site length fit within our scheme of lesion geometry (Fig. 5.2) and was selected to provide a standardized reactive site geometry. Although the dimensions could be easily tailored to satisfy other conditions as desired, such standardization was important to create a nominal situation that could be functionally characterized and perturbed for investigating the role of altered hemodynamic situations. Using our same total loop circumference as in our homogenous fluid loop model (imposed by rotor design; Fig 2.15), we obtained a reactive site length to loop circumference ratio of 1:8 which reasonably modeled the discrete vascular lesion setting.

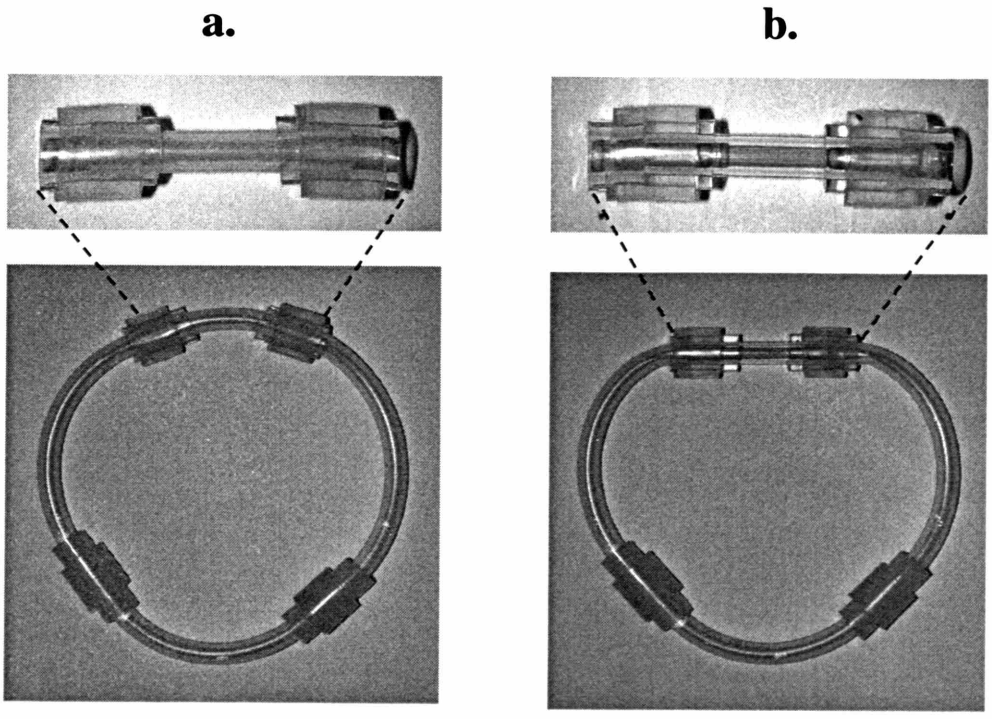

Figure 5.3 Reactive sites and fluid loops. a. Silicone; b. Glass

In these modified fluid loops, co-axial layers serve as either injection or withdrawal ports (section 2.2.2). Two additional sleeves are required to secure the reactive site in place. By eliminating the need for inline valves and connectors and by maintaining square segment ends for flush juxtapositioning, luminal flow and surface disruptions can be minimized.

While the reactive site can be made of any material, two options we considered were glass and silicone as their material properties allowed us to develop an array of geometrically relevant situations. Upon heating, glass is easily and permanently shapeable into a variety of pathological geometries (stenotic constrictions, aneurismal expansions; Fig. 5.4a-d). As the geometry is altered, blood contact surface area can be maintained by properly adjusting the reactive site length. Though the properties of glass allow tight control of the wall boundary, the glass surface is non-yielding and thus not able to support proper endovascular stent expansion. Typically, these devices require some wall elasticity for proper wall apposition (Fig. 5.5 *a*, *b*). Silicone on the other hand is complaint and thus suitable for modeling endovascular interventions by enabling proper device expansion and wall contact. While the altered physical properties on glass and silicone were selected for their ability to model certain vascular conditions, compliance changes have been shown to play a role in affecting pulsatile pressure driven flows by enabling time-dependent wall expansions [75, 103, 144]. However, in our system, which is driven by wall shear as opposed to pressure forces, we did not notice a significant effect on flow as a result of these changes in wall properties (Fig. 5.6).

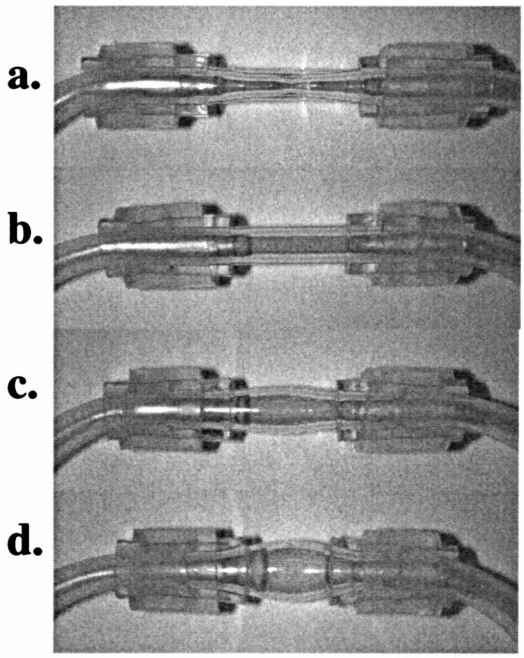

Figure 5.4. Potential reactive site geometries. a. 50% stenosis; b. constant diameter; c. 25% aneurysm; d. 50% aneurysm

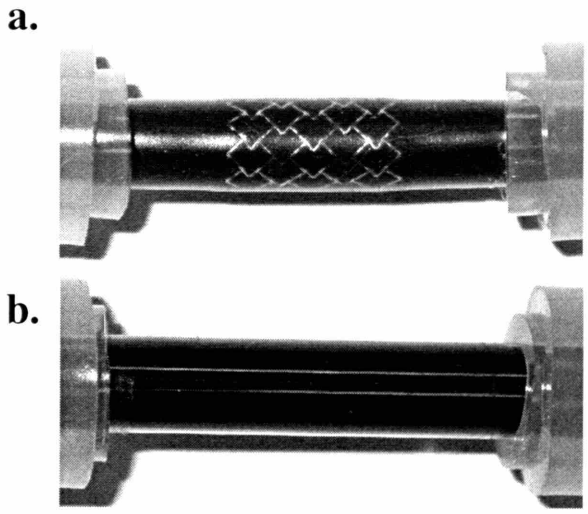

Figure 5.5. Stented reactive sites. a. Silicone (good stent-wall apposition is visualized through diplaced dye); b. Glass (poor wall apposition).

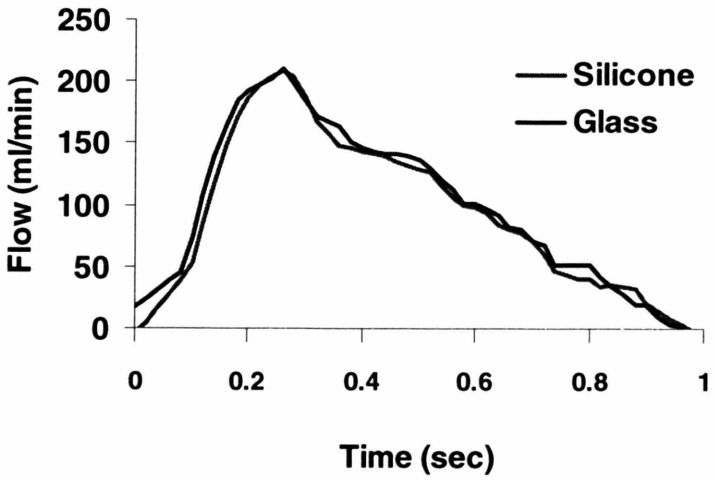

Figure 5.6. A typical triangular flow pulse (200 ml/min peak flow) generated in reactive sites of silicone and glass material using identical wall motion profiles.

5.1.2 Surfaces

We selected glass and silicone tubing as their varied structural qualities allow easy manipulation through molding (when heated) and elastic deformation respectively. However, it is widely recognized that the blood contacting surface itself interacts with blood components, playing an important role in dictating vascular responses (as we further explore in chapters 3 and 4). To move our model away from an investigation of foreign surface response (be they glass, silicone, or otherwise) and towards an investigation hemodynamic vascular situations, we coated the reactive segments and fluid loops with passive, biologically reactive, protein layers. An immense variety of potential biological substrates exist, and in the current model development, we immediately restricted ourselves to those of known physiological relevance with regards to platelet / substrate interactions (Fig 5.7).

Platelets exhibit a wide array of surface moieties which interact with their environment (section 1.2). In addition to mediating intercellular function, a portion of these mediate surface adhesion responses by interacting with specific vascular wall subsubstrates upon endothelial presentation (P-selectin, fibrinogen, vWF, etc.) or subendothelial exposure (collagen, fibronectin, laminin, vWF, etc.). By coating the glass and silicone reactive sites with individual components or subsets of these, specific interactions can be explored. As the primary focus of this work was to develop and study hemodynamic effects of endovascular thrombosis, we currently focused on the well characterized substrates collagen and albumin, which provided simple models of a reactive and unreactive vessel wall.

Collagen

Collagen is an important component of the subendothelial layer that initiates platelet adhesion when exposed to blood. Adhesion is supported by specific binding sites that enable direct interactions with vWF and platelet collagen receptors [24, 26, 29, 115, 145]. Accordingly, collagen has been a commonly used substrate for *in vitro* studies of platelet adhesion in flow. There are several types of collagen that exist within the body, with types I. III, and

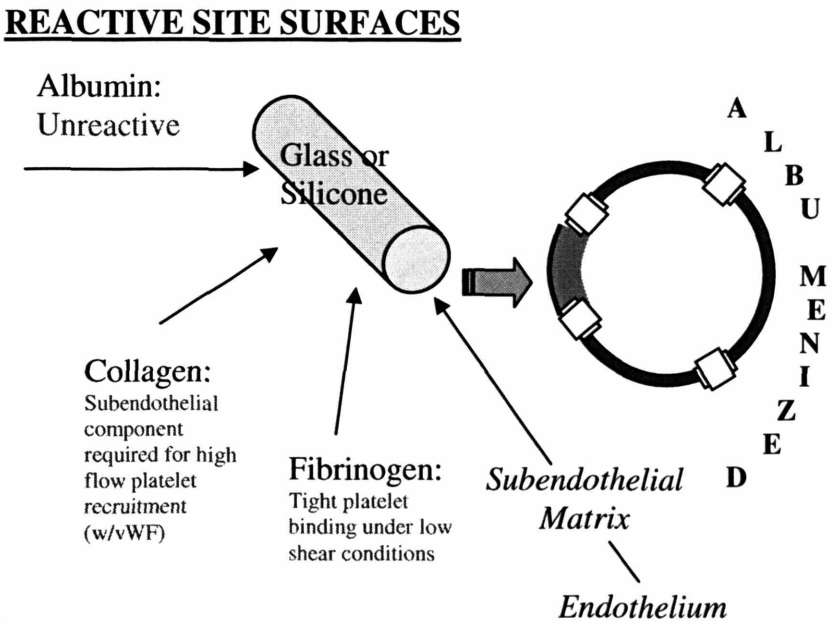

Figure 5.7. Potential reactive site surfaces to create a spatially distinct region within an otherwise, albumenized, inert fluid loop.

IV being the most prevalent in the vascular wall [21]. The various collagens each promote subtle differences in response and it is important to consider these differences when selecting surface coatings. For example, while the primary collagen integrin $\alpha_2\beta_1$ supports general, non-specific firm adhesion to collagen types I-VIII, type-specific receptors have recently been cloned for collagens I and III [36, 146]. A variety of biological processes also affect the state of collagen. It has recently been established that collagen turnover by matrix metallo-proteases (MMPs) in the fibrous cap region of atherosclerotic lesions contributes to cap and plaque weakness by degrading collagen fibrils [68, 147]. As these rupture-prone sites play an important role in the progression to acute coronary syndromes, the effects of a degraded collagen surface on vascular cell recruitment is also of great interest.

In our present work, we focus on the type I collagen surface whose platelet interactions have been well characterized through prior *in vitro* studies [26, 97, 115]. Using an established protocol, we prepared a 2.1 mg/ml collagen solution in 0.5 M acetic

acid by mixing 1 g type I acid-insoluble collagen (bovine Achilles' tendon) into 12 ml of glacial acetic acid and 198 ml water. The mixture was homogenized for two hours, 200 ml of water was added, and an additional hour of homogenization applied. The final suspension was centrifuged for 10 min at 1000 RPM, and the supernatant solution was collected and stored at 4 °C [115].

To make collagenized reactive sites, the 3 cm tube segments were filled with this solution, capped at both ends, and held at 25 °C for 90 minutes to allow surface adsorption. The segments were then uncapped, thoroughly flushed with phosphate buffered saline (PBS) to remove any loosely adherent collagen and stored at 4 °C in PBS until use. Similar amounts of collagen adsorption to either the glass or silicone surfaces (1.2 $\mu g/cm^2$ vs. 0.9 $\mu g/cm^2$) were observed using a BCA protein assay (Pierce).

Albumin

When a bare foreign surface comes into contact with blood, one of the first events to transpire is passive protein absorption. Such a protein layer can support enzymatic reactions (i.e. intrinsic coagulation, compliment activation) or cellular adhesion (i.e. fibrinogen-dependent platelet adhesion). Albumin is a large, unreactive plasma protein which can be used to saturate the surface, thus blocking unwanted surface reactions [23, 26].

Blood homeostasis is typically maintained through an active, endothelial layer which is sophisticated, dynamic, and complex. We approximate this bio-compatible surface with a passive, albumenized coating as it allows us to spatially focus the thrombotic nidus to the reactive site, though also acknowledging the simplicity of this step (Fig. 5.7) The 21 cm tubing lengths were filled with a 1% human or bovine serum albumin solution (HSA, BSA); in PBS for 60 minutes at room temperature. BSA, which is functionally indistinguishable from HSA, is preferred both from on infectious risk standpoint as well as the greatly reduced cost for the relatively large batch sizes and tubing volumes used. The tubes were flushed and stored in PBS prior to use. Following a similar protocol, albumin can also be used to saturate the reactive site surface itself, thus limiting surface reactions to those dictated by controlled, pre-coated protein layers

(i.e. collagen) or completely eliminating such interactions if used in isolation (see Section 5.2).

Other coatings

Along with the collagens and albumin, there are a slew of other potential surface coatings which can be used to capture particular platelet reactions. Individual proteins, such as fibrinogen, vWF, fibronectin, laminin, etc., interact with specialized platelet surface receptors and it is important to consider each in kind for a detailed, understanding of adhesive mechanisms. Yet, we must remember that it is a combination of interactions that orchestrates adhesion *in vivo*. Indeed, various studies have shown functional differences between single and multiple protein layers [23, 26]. As more is understood about the basic pathways of adhesion, it is important to consider these increasingly complex surfaces, moving towards a goal of considering a functional, reactive, endothelial layer. With the added layers, it is important to sufficiently characterize the surfaces to retain stable understanding and control of the *in vitro* environment. For instance, while subendothelium can be readily generated by stripping off a confluent layer of endothelial cells, the composition of the isolated material can change widely depending upon the endothelial origin, the conditions under which they are grown and the stripping technique employed. The use of complex model surfaces in conjunction with simple, pared down substrates, provides a balance between reductionist and predictive goals in understanding vascular platelet responses.

5.2 Reactive Site Characterization

In the current section, we begin to functionally characterize the platelet adhesion response to our reactive sites considering a nominal, non-stented hemodynamic setting of constant diameter (Fig. 5.3). Although many prior studies have extensively probed the interactions of platelets with collagenized and albumenized surfaces (which led us to their selection in the first place), it is important to establish the functional nature of these substrates in our specific system.

Various differences exist between our model and prior systems. By and large, other studies have considered constant flow conditions. Our flow model creates highly pulsatile conditions pertinent to the coronary flow setting, potentially resulting in observable changes. Furthermore, many of these prior studies have been performed on coated, planar, glass slides in the context of microscopic flow chambers. In our reactive site model, we consider both tubular glass and silicone surfaces which enable different vascular situations to be modeled. Although we have shown that glass and silicone both support similar amounts of protein adsorption (collagen; section 5.1.2), the functional nature of these layers may be different. Varied protein conformations may be exposed upon interaction with specific surface, either potentiating or diminishing platelet interactions. Alternatively, sensible qualities of the base material itself (charge, roughness, porosity, etc.) that are incompletely masked by the coating layer may differentially interact with blood. In the current section, we study platelet adhesion to both glass and silicone reactive sites of constant diameter (1/8") over a range of pulsatile flow conditions and compare our findings to previous platelet/substrate investigations. Through these studies, we provide an essential foundation that must be develop before we can explore how altered hemodynamic settings may affect the thrombotic platelet response.

5.2.1 Methods

Hemodynamic Environment

We applied our reactive site model to characterize the anti-coagulated platelet response over a range of [58] potential coronary-like flow rates (50-200 ml/min peak flow; Fig. 5.8) [51, 148].

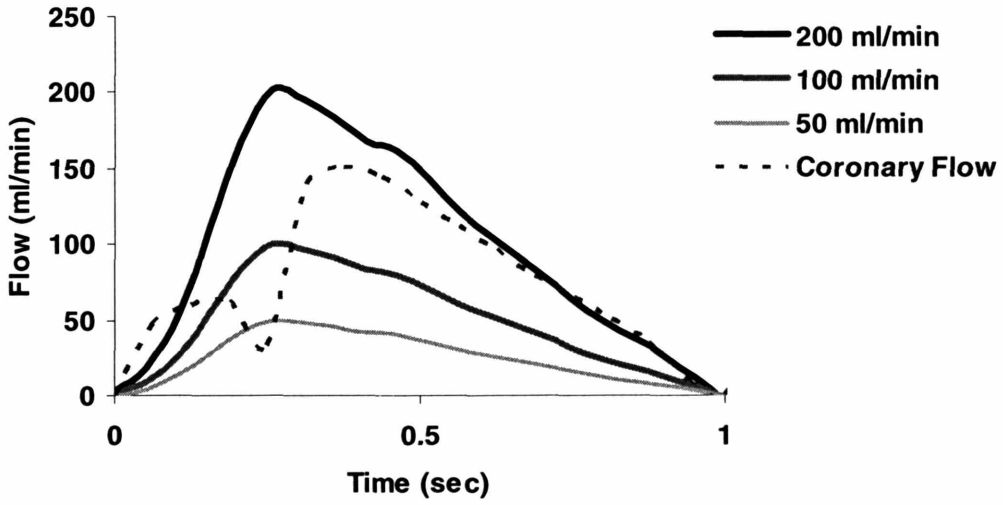

Figure 5.8. Generated flow profiles to simulate coronary conditions on a beat to beat basis. ** It should be explicitly noted that these figures only represent one cycle of the bidirectional generated flows as previously described.

The fluid loops were made from a 21 cm length of 1/8" inner diameter (ID), 3/16" outer diameter (OD) 3350 Silicone Tygon tubing into which a 3 cm reactive tubing segment (glass or silicone) was inserted (see Fig. 5.3). The reactive segments (glass or silicone) were coated with either Type I, acid insoluble bovine collagen or 1% bovine serum albumin (BSA) as models of reactive and unreactive vascular segments. The 21 cm lengths were uniformly coated with a 1% BSA blocking solution.

Platelet Source

In these studies, we used anticoagulated, leukocyte-depleted blood as a platelet source. The use of anticoagulated blood components is a required reductive step in functionally

characterizing our reactive site models. As we explore in section 4.2, coagulative synergy dramatically complicates the picture of flow dependent platelet surface interactions. Before we can begin to understand added complexities (be they with added coagulative function, altered hemodynamic environments, or otherwise) we must develop a stable understanding of the basic but highly important platelet reactions as they occur within our reactive site model. Given the recognized, clinical importance of the platelet as a key, initiating player in the vascular response to injury, the anticoagulated blood model is a well-justified point at which to develop a solid basis for further exploration.

Whole blood obtained from healthy volunteers was drawn via a 20-gauge needle into a 1/10 dilution of ACD and 80 μM (final concentration) PPACK anticoagulant. To remove the leukocyte component, the whole blood was lightly centrifuged at 200g for 15 minutes and the top platelet-rich plasma (PRP) was separated from the packed red blood cell layer. These layers were passed through appropriate, low volume leukocyte-reduction filters (Purecell™/PL, and Purecell™/Neo, Pall Biomedical) and then recombined to achieve a hematocrit of ~40%. This procedure was found to reduce the total platelet count from ~2.5% to 2.0%, while having a minimal effect on platelet activation (<2%) as assessed through P-selectin expression via flow cytometry (FACScan, Benton Dickinson). The blood was used within 30 min of withdrawal and was recalcified (2 mmol Ca^{2+}) immediately before injection into the fluid loops.

Observing the Platelet Subsystem

To assess surface platelet adhesion, we adopted a rapid LDH (lactase dehydrogenase; see section 4.1) assay as opposed to the relatively labor intensive surface extraction procedure used in section 4.2. Once a given run was complete, the fluid loops were open and the blood was emptied. When necessary, 100ul of blood was fixed in 1% paraformaldehyde for subsequent analysis of bulk platelet activation and microaggregate formation. The reactive segments were removed, and thoroughly flushed with 50ml Hanks Balanced Salt Solution (HBSS), supplemented with 2mM Ca2+. The segments were then filled with a lysis buffer to lyse any residual RBC. The segments were emptied, flushed, and again filled with a 0.09% Triton-X, 250mmol glucose solution (in

PBS,) and left for 1 hour at room temperature. 200ul of this solution was then taken and analyzed for LDH amount as an indirect marker of surface adherent platelet number (CytoTox 96® Non-Radioactive Assay, Promega) [115]. Adherent leukocytes were assumed to be minimal in comparison to the platelet number due to the leukocyte reduction process and verified by the absence of nuclear staining (as described below) on collagenized glass samples. While providing an indirect marker of surface platelet number, the speed and cost-effectiveness of theses LDH protocol greatly promoted parametric studies, justifying its use over the more platelet specific surface extraction / flow cytometric strategy used previously.

When required, other tests of surface analysis and platelet function were performed. To visually assess the adherent layer, flushed reactive sites were filled with a 3.7% paraformaldehyde solution and fixed for 20 minutes at room temperature. The reactive sites were then washed twice with PBS and filled with a 0.1% of Triton-X in PBS. After 3.5 minutes, the segments were again emptied, washed twice with PBS, and filled with a blocking 1% BSA solution for 20 min. Subsequently, the sites were drained and incubated with a staining solution of 5 U/ml BODIPY FL phallacidin (for actin staining; Molecular Probes, Eugene, OR) and bis-benzimide (for nuclear staining; Sigma), and 1% BSA in PBS at room temperature for 20 minutes in the dark. The stained samples were then washed twice with PBS, filled with a 1:1 solution of PBS and glycerol, capped, and visualized with a fluorescence microscope equipped with fluorescein and ultraviolet filters (Leica Microsystems Inc., Bannockbum, IL).

To assess bulk activation.PE (Beckton Dickinson). The reaction was stopped with 1 ml 1% paraformaldehyde after 20 minutes and the samples were assessed in a flow cytometer (FACscan™, Becton Dickinson). The platelet population was determined from CD61 binding in conjunction with forward and side scatter measurements (FSC, SSC). Bulk platelet activation, was assessed from percentage of CD62p+ platelets.

5.2.2 Functional Validation

Glass vs. Silicone Base Substrates

Collagen

We first compared the functionality of collagen coated glass versus silicone substrates in the absence of stenting. To functionally compare the two base substrates, 4 collagenized glass and 4 collagenized silicone reactive sites were run for 3.5 min at each of the 4 flow conditions. After each run, the total adherent platelet number was determined via LDH quantification, revealing similar levels of platelet adhesion to both substrates after 3.5 min of flow (Fig. 5.9).

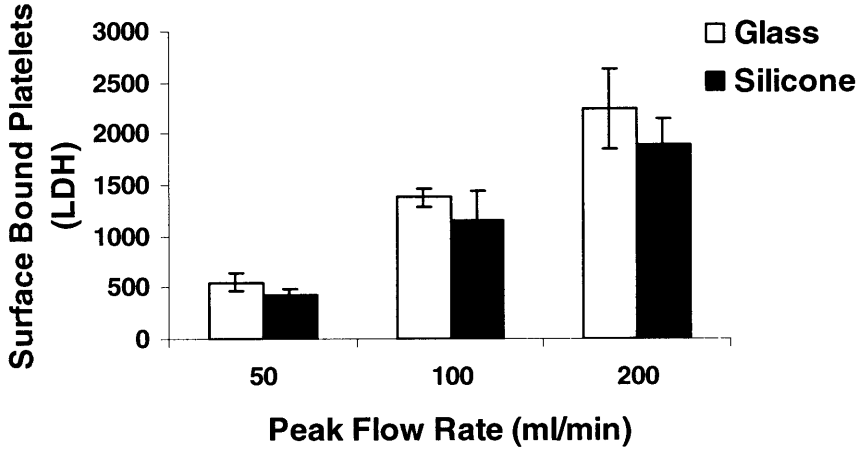

Figure 5.9. Comparison of LDH quantified platelet/thrombus adhesion to glass and silicone reactive site materials at varying flows following a 3.5min run. (Mean ± SD)

Additionally, we witness a significant increase in surface adherent thrombus/platelets with flow for both the collagenized glass and silicone sites. Although we could not visualize through the porous, translucent silicone surface, these studies were qualitatively confirmed through actin staining and visualization of glass reactive sites at both the 50 and 200 ml/min peak flow condition where we again see a significant increase in surface bound thrombus with flow (Fig 5.10 a, b). Furthermore, the lack of significant nuclear staining indicates the lack of a leukoctytic component (Fig 5.10 c, d).

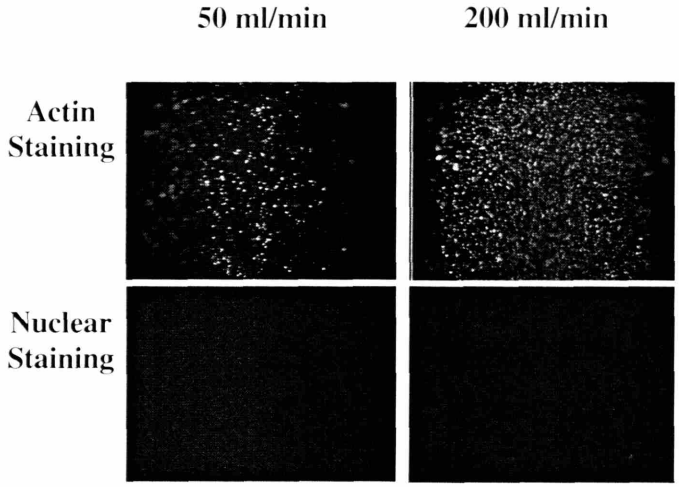

Figure 5.10. Glass reactive site surface visualization post exposure to whole blood at either 50 or 200 ml/min peak flow conditions (left/right) depicting actin staining (top) and nuclear staining (bottom). Note the lack of nuclear staining, which indicates a lack of a leukocytic component.

Albumin

To investigate the effectiveness of albumin in blocking reactive site adhesion, we ran 3 albumenized and 3 non-albumenized (non-coated) reactive sites for both the glass and silicone base surfaces at the median 100 ml/min peak flow condition for 3.5 min. Again, the LDH analysis was carried out (Fig. 5.11). Comparing these results with those of the collagenized surface (Fig. 5.9), we see a significant decrease in bound thrombus for both the non-coated and albumenized surface. Although there is a small degree of adhesion present in the non-coated cases, this signal is totally abolished with albumin coating on both the glass and silicone substrates. Again, we visually confirmed this by the lack of actin staining to albumenized glass reactive sites (results not shown).

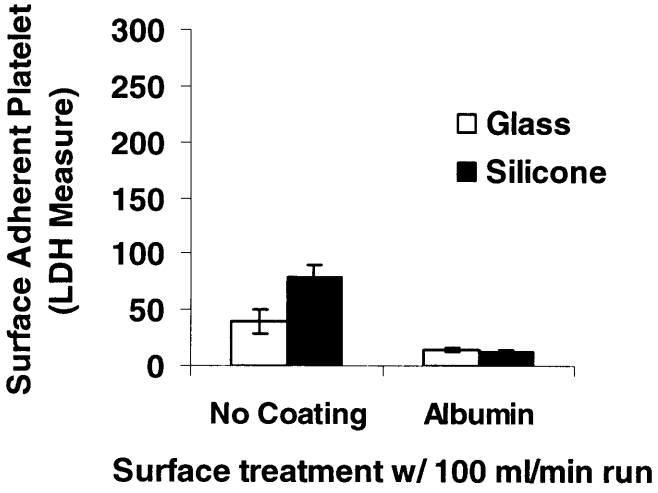

Figure 5.11. Comparison of LDH quantified platelet adhesion to non-coated and albumin coated reactive sites composed of glass or silicone material following a 3.5 min run at the 100 ml/min condtion, showing the effectiveness of albumin in creating an unreactive surface. While the non-coated cases were low as well (compare LDH scale to Fig. 5.9), they exhibited detectable signals. (Mean ± SD)

Adhesion Time Course

To determine the time dependent nature of platelet adhesion to our reactive sites, we performed a time course study (3.5, 10, 30, 60, 90 min) using collagenized silicone reactive segments (a signal was not detectable on the albumenized surfaces for +90min; results not shown). At each of the three flow rates, 2 runs of 10 segments were performed. For each run, 2 segments were stopped and analyzed for total number of adherent platelets at each of the five prescribed time points (yielding a total of four samples per time point for each of the three flow rates). We see that the level of surface adherent platelets climbs from the initial, 3.5 min time point, reaching a plateau for the 50 and 100 ml/min peak flow conditions by ~30 and 60 min respectively (Fig. 5.12). The 200 ml/min flow condition peaks more quickly (10 min), but then decreases significantly at the longer time points. In all cases, the anticoagulated platelet (thrombus) signal does not grow indefinitely, but is composed of an initial transient phase followed by a steady state response.

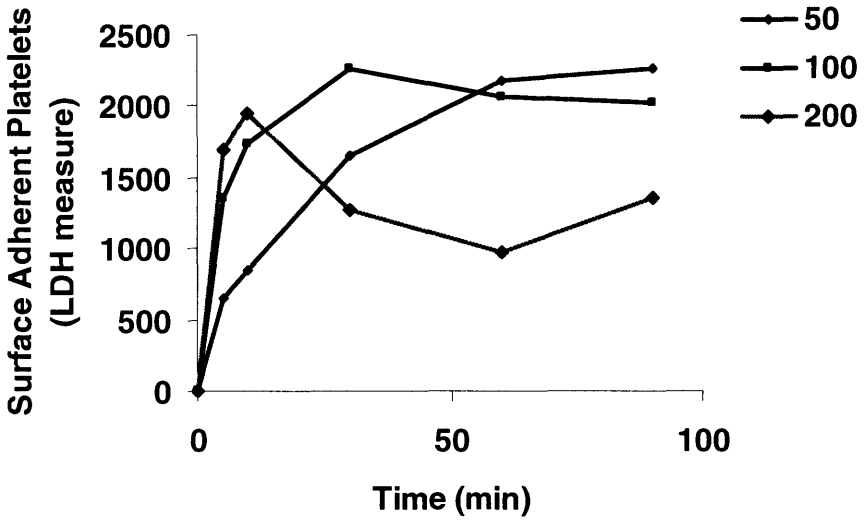

Figure 5.12. Time course of platelet response (quantified by LDH measurement) at 50, 100, and 200 ml/min peak flow rates.

5.2.3 Discussion

It is important to establish how platelets adhere in a nominal reactive site model of constant diameter coated with simple, reductive surfaces (collagen, albumen) before expanding to more complex issues of pathological and interventional geometries or surfaces. Here we have validated our techniques of reactive site preparation along with the LDH assay protocols that enable fast, efficient platelet quantification.

While non-coated glass sites exhibited negligible platelet adhesion, plain silicone sites yielded a small but noticeable signal. Such discrepancies could be the result of differential plasma protein adsorption to the bare surfaces upon blood contact or other qualities of the materials themselves such as altered roughness, porosity, etc. that may be sensible through the rapidly adsorbed protein layer. These material dependent differences were largely masked upon individual collagen or albumin coating. Basic functional similarities to both the collagenized glass and silicone segments were observed as transient platelet adhesion increased over a range of potential coronary-like flow rates. Similar flow-dependence of platelet / collagen adhesion has been widely shown using constant shear parallel plate chambers and is a result of increased surface transport and

flow-dependent platelet activation . When coated with albumin, the platelet response is completely eliminated on both surfaces.

Time is an important parameter to recognize in dynamic responses such as thrombosis. While the 3.5 min results represent a fairly early time point, we were also interested in characterizing the time dependent nature of platelet accumulation to collagen surfaces given the possibility of various outcomes. For instance, platelet / thrombus accumulation may grow unrestrained, eventually blocking off the lumen as with acute occlusive thrombotic events or in our loop occlusion time trials (sections 3.2.3, 3.2.3). Alternatively, a sub-occlusive state may be reached. In our collagenized reactive site model, we observe significant restraint on surface thrombus accumulation as the platelet/thrombus signal does not grow indefinitely, but rather is composed of an initial transient phase followed by a steady state response. The discrepancies between these findings and our previous occlusive trials are likely a result of the potent inhibition of coagulation via PPACK used in the present study (indeed collagenized reactive site loop occlusion was observed to occur <20 min with coagulation present; results not shown). In the presence of anticoagulation, growing thrombus cannot be stabilized with a fibrin mesh or potentiated by other coagulative functions (section 1.2, 4.2).

The time course response represents a balance between platelet surface capacity, accumulation (adhesion and aggregation) and removal (micro/macro embolization) and can be characterized by various features. From our studies, we see that accumulation rates, steady state signals, peak signals, time to steady state and time to peak response are required to sufficiently describe our time dependence. Appreciating these features of the dynamic response is important as different situations may affect only a portion of them, leaving others unaltered. For instance, while the accumulation rate of platelet adhesion under the 50 ml/min peak flow condition was less than that of the 100 ml/min conditions (which resulted in lower 3.5 min observations at the low flow condition), a similar steady state level was eventually reached. Dynamic changes may go unappreciated (or conversely be over-appreciated) if a more detailed picture is not recognized.

Using real time observations, various investigations have shown similar results, where a constant surface platelet level is attained under moderate shear levels. With high shear conditions (similar to levels attained during the peak of our high flow condition),

platelet adhesion initially rises, with a subsequent decay as a result of surface microembolization [72, 73, 97, 115]. Although the current embodiment of our system did not allow us to perform real time analysis to further document this occurrence, both the increased standard deviation indicative of a more complex, stochastic process and the decrease in surface bound platelets are suggestive that such embolizations are taking place within our system at high flow. Still, these are only loose relationships. Given the importance of embolization as a thrombotic outcome, strategies of further observing this phenomenon in our hemodynamic model would be of significant use.

When developing and applying *in vitro* models, it is important to consider their placement with respect to real-world scenarios given the goal of potentiating studies of predictive relevance. In previous chapters, we studied interactions of blood components with specific endovascular devices in a simple, homogenous fluid loop. While novel findings are undoubtedly possible using such a scheme, we hoped to increase the applicability of our system in studying vascular situations, recognizing the model's unique nature of setting up a highly controllable, pulsatile flow environment within relevant arterial geometries.

In the current chapter, we have considered model placement by introducing reactive segments into our fluid loops as a model of discrete vessel wall injury. Using glass and silicone materials, we developed models to support various applications requiring a moldable (pathological vessel architecture) or compliant (endovascular device implantation) vessel wall and coated them with individual protein layers to reductively model vascular situations. Specifically, we show how collagen and albumin can be used as simple models of reactive and unreactive vascular segments. In these models of vascular injury, we have begun to characterize and explore the important platelet adhesion reaction occurring within our *in vitro* setting as a key mediator of the biological response. Given this background, we now turn to more pointed investigations concerning issues of the local hemodynamic environment and how real-world factors such as spatial and temporal flow disturbances may play an important role in directing local biological responses.

CHAPTER 6 Real-World Hemodynamic Environments

The local hemodynamic environment plays a critical role in directing the local thrombotic response. While many of the fundamental, flow mediated interactions have been delineated through prior *in vitro* and *in vivo* work (section 1.3), much remains to be learned with regards as to how these factors play out in real-world scenarios. Deeper, situational studies require highly controllable, highly observable systems which recapitulate both the flow and geometric conditions present within specific vascular environments. Such systems could help to bridge the gap between overly reductive and overly complex models, optimizing the path from bench top discovery to bedside application. In preceding chapters, we have established methods to parameterize important biological and physical properties of the platelet response within our *in vitro,* reactive site model. In doing so, we have begun to characterize the platelet response within a coronary-like, pulsatile, hemodynamic setting, thus establishing a foundation from which we can further explore aspects of the hemodynamic environment.

Real-world hemodynamic scenarios exhibit a high degree of spatial and temporal variability. As blood flows through the vasculature, it experiences a multitude of environments that change over time and length scales of varying magnitudes. Given that platelets are responsive to their shear environments, we must delineate the levels at which they can sense local changes in environment. In some cases, spatio-temporal fluctuations may go by unperceived, while in other situations, they may play a crucial role in mediating the local biological reaction. In this chapter, we investigate the platelet response to variations in the hemodynamic environment induced by highly idealized situations which we develop in our reactive site model. Specifically, we more closely look at the effects of coronary-like flow pulsatility and those induced by endovascular stent presence as examples of temporal and spatial variability respectively. Given that these highly relevant hemodynamic factors create observable differences in the local platelet response, we also begin to explore the efficacy of antithrombotic agents whose mechanisms of action target specific platelet/wall interactions. As the mechanisms governing thrombotic processes change, the effectiveness of inhibitory strategies which

work to block such occurrences must be confirmed, and if needed, new strategies implemented.

6.1 Temporal Variations in Hemodynamic Environments

Mechanistic platelet wall adhesion to collagen has been widely studied in other steady flow *in vitro* models (section 1.2). At steady shear rates greater than 1500 s^{-1}, GPIb-vWF interactions are essential in mediating initial platelet recruitment to vascular surfaces. Antibodies, specific agents or component removal (depletion, genetic defects, knockouts, etc.) directed against this axis can totally abolish high flow adhesion [24, 26]. Alternatively, agents directed against the αIIbβ3 integrin significantly reduce wall adhesion across all flows by blocking firm vWF mediated collagen adhesion, as well as subsequent fibrinogen cross linking and aggregation [35, 149]. Considering the diversity of vascular environments encountered within the body, mechanistic investigations into flow dependent platelet adhesion have proven essential to our understanding of vascular thrombosis, as well as in the development of anti-thrombotic strategies that are effective throughout the vascular compartment (i.e. in settings of both arterial high flow or venous low flow thrombosis).

Along with region-specific shear variations, temporal variations in flow exist with flow pulsatility being recognized as an important modulator of vascular states [58, 66, 112, 150, 151]. Understanding the mechanisms of platelet adhesion in pulsatile flow is an important goal, particularly considering the vital coronary environment where periodic low and high flow conditions exist on a beat to beat basis. In section 5.2, we have begun to consider the pulsatile environment, observing qualitatively similar, flow dependent platelet adhesion in our flow model as compared to findings made in other constant shear systems. However, these studies only begin to explore the platelet surface reaction. Just as total loop occlusion (section 3.2) results from the integration of many thrombotic responses, platelet adhesion is the integration of many platelet responses. Even when isolated, the richness of the platelet response cannot be fully appreciated without further reductive, mechanistic studies.

No study to our knowledge has investigated the specific, mechanistic role of platelet receptors under physiologically relevant, pulsatile flow conditions. Given that important flow-dependent responses such as wall tethering and adhesion are enabled and controlled at the receptor level, we sought to focus our investigations deeper, specifically

considering the role of the GPIb tethering axis in pulsatile flow. We hypothesized that the mechanisms of platelet adhesion under coronary-like, highly pulsatile conditions would be different than those under constant shear conditions. In contrast to the later the former would allow specimens to be exposed in an alternating fashion to both high and low shear phenomenon, potentially bypassing the need for GPIb tethering.

6.1.1 Methods

Hemodynamic environment

Previously (section 5.2), we related our observational platelet adhesion studies to prior findings obtained in other model systems. To more rigorously establish the effects of pulsatility on platelet wall interactions, we must have more suitable internal controls. As rotor accelerations are required to maintain relative fluid/wall motion, we could not recreate steady flow conditions for comparison (see section 2.12). Instead, we hoped to use square wave profiles to approximate constant wall shearing conditions on a beat to beat basis. While we have previously discussed the use of square wave wall accelerations to induce flow (section 2.1), we must more fully develop and characterize this important control pulse to understand the use and potential limitations of such a strategy for approximating the constant flow condition.

Approximating the Steady Shear Condition: The Boosted Square Wave

Relatively gradual time responses (with respect to our system time constant of ~0.1 sec) are simple to generate with our methodology. Al though we sought to create square type waves of a low (1 Hz) fundamental frequency, high frequency components are required to accommodate the discontinuous boundaries of each pulse. To approximate the effects of these discontinuities, we can reconsider the results obtained from our analytical straight tube model given a square wave wall acceleration profile (Fig 2.6; section 2.2), where a 95% rise time of ~0.3 sec was determined (30% of pulse duration). This type of pattern only provides a rough approximation of a constant shear condition.

To generate these profiles, a square *wall* acceleration was applied. As we hope to maintain square *fluid* motion characteristics which inertially lag behind the driving wall

velocities (recall the square profile example in Fig.3.2), we can modify the wall profiles in an effort to counterbalance the sluggish effects of fluid inertia. The simplest method is to provide an impulsive spike near the beginning of the square acceleration profile. Given the additive nature of the Fourier series, these impulsive spikes can simply be added to the square profiles (Eq. 12), yielding a summed wall acceleration of:

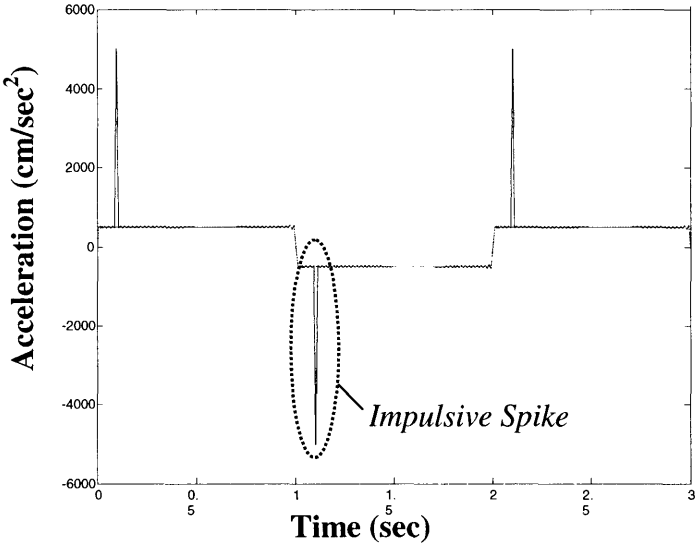

Figure 6.1. Impulsively boosted square wave wall acceleration profile (black) overlain on a plain square profile (red).

$$\frac{d^2Z(t)}{dt^2} = \sum_{n=1,3,5...}^{\infty} \frac{A_1}{n} e^{in\omega t} + \sum_{n=1}^{\infty} e^{in\omega t} \qquad (18)$$

Figures 6.1 and 6.2 show the driving wall motion profile (overlain on a simple square profile) and the resultant relative fluid velocity profile respectively.

To more clearly witness the effects of these impulsive spikes, we can integrate the axial velocity over the tube cross section for both the simple and boosted square wave conditions, obtaining the bulk flow rate (Fig. 6.3). Comparing the two profiles, it is clear how the impulsive function indeed works at the point of discontinuity to create a much better approximation of a square wave pattern.

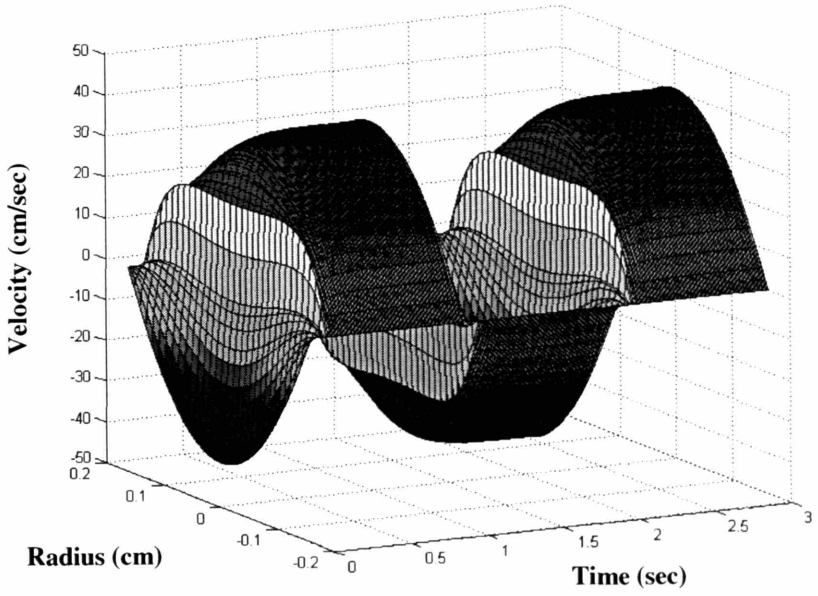

Figure 6.2. Relative axial fluid velocity over a radial distribution as a function of time given a boosted square wall motion using Eq. 17 to drive Eq. 7; R=0.16 cm, v=0.04 dynes cm/sec. This solution may be compared to the simple square driving motions on Fig. 2.6.

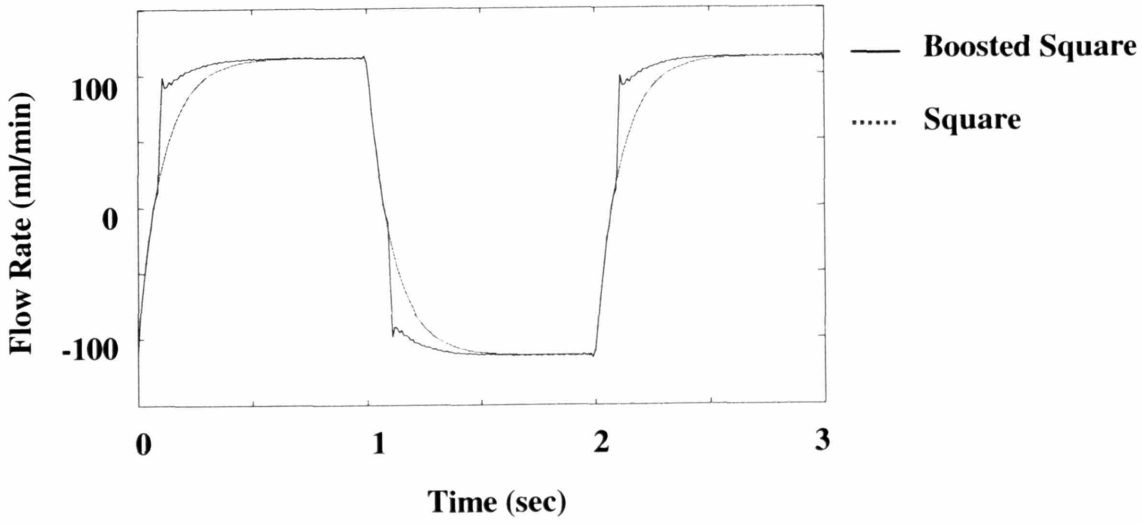

Figure 6.3. Integrated bulk flow profiles for the boosted (black solid line) and plain (red dashed line) square wave wall driving conditions. The boosted condition provides a much better approximation of a square flow pattern.

Appreciating the nature of bulk flow is important as this is the output of our Transonic flow transducers and thus, the principle handle through which we develop and observe fluid motion within our loops. However, the flow parameter that interacts most apparently at the level of platelet receptors is the shear rate. Indeed, parallel plate flow chambers which have largely been used to characterize shear dependent platelet functions enable high shear rates at low flows. Although the square and modified square wall acceleration pulses can be used to approximate near-steady flow conditions (in an absolute sense), we must consider their effects on wall shear as well. In figure 6.2, we can see that brief portions of flow reversal and increased wall velocity result at the points of flow discontinuity. To more directly assess the effects of these disturbances on shear, we graphed wall shear rate (absolute value) as a function of time for both the square and boosted square profiles (Fig. 6.4).

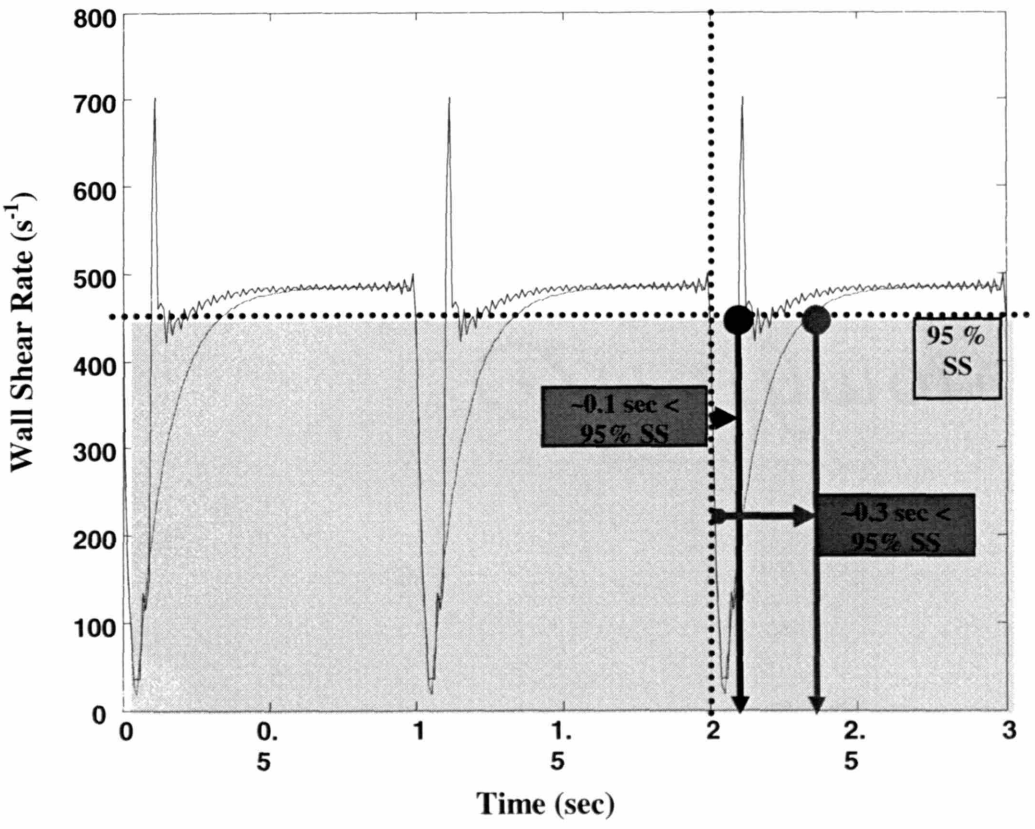

Figure 6.4. Wall shear rates for boosted (black solid line) and plain (red dashed line) square wall driving profiles. While providing a greatly reduces 95% rise time (~0.1 sec vs. ~0.3 sec), the boosted signal shows a large overshoot error (75%)

From this analytically derived figure, we can get a sense of the magnitude and duration of the flow disturbance on directional change. In the non-boosted case (red dotted line), we see an expected 95% steady state (SS) shear rise time of 0.3 sec (note the use of SS in this case is defined over an individual pulse). With the superimposed impulses (black solid line), this 95% rise time is reduced to 0.1 sec though at the expense of a brief but considerable overshoot (~75% for the depicted conditions).

While a single, well placed impulse, allows wall shear rates and flow to be maintained above a certain level for the vast majority of the flow cycle, the resultant overshoot error in wall shear creates an unwanted departure from our goal of modeling constant shear conditions. To minimize this magnitude error, we can further modify our wall motion profile, decreasing the amplitude of the impulse function and temporally spreading it out over a train of impulses (Fig. 6.5). These increasingly complex functions allow wall shear rates (black solid line; Fig. 6.6) to be quickly changed and maintained throughout the flow cycle, at the same time minimizing overshoot error to within 5% of SS value for 90% of pulse cycle (for the conditions presented).

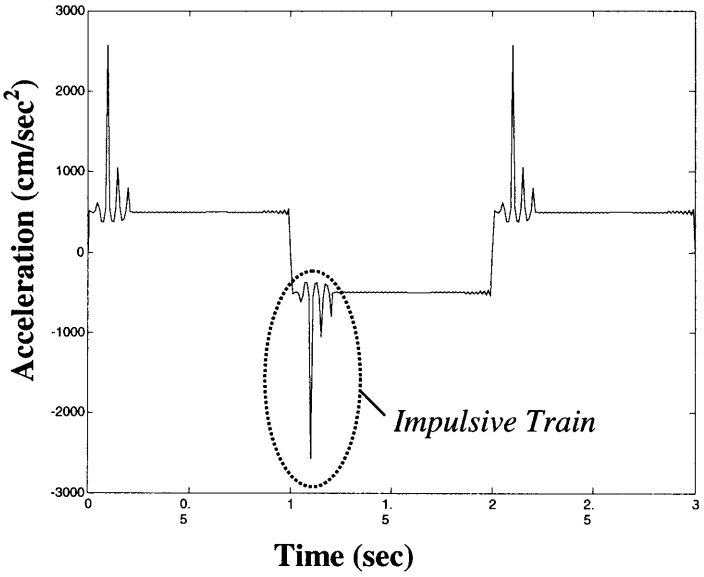

Figure 6.5. Boosted square wave with a train of discrete impulsive functions.

In our bench top model, such complex boosting functions are readily produced as practical limitations on rotor response automatically smear impulsive functions over a finite interval (~0.1 sec; section 3.1). Moreover, this spreading occurs in a continuous fashion as opposed to a chain of discrete impulse functions. Though we could not

directly observe wall shear in our system to provide the ideal feedback for creating our near constant shearing conditions, we satisfied ourselves with matching the integrated bulk flow profile pattern found through the (black dashed line; Fig 6.6), noting principally the need for a fairly rapid rise time to peak flow as compared to the relatively sluggish flows generated using an ordinary square-driving profile (red dashed line).

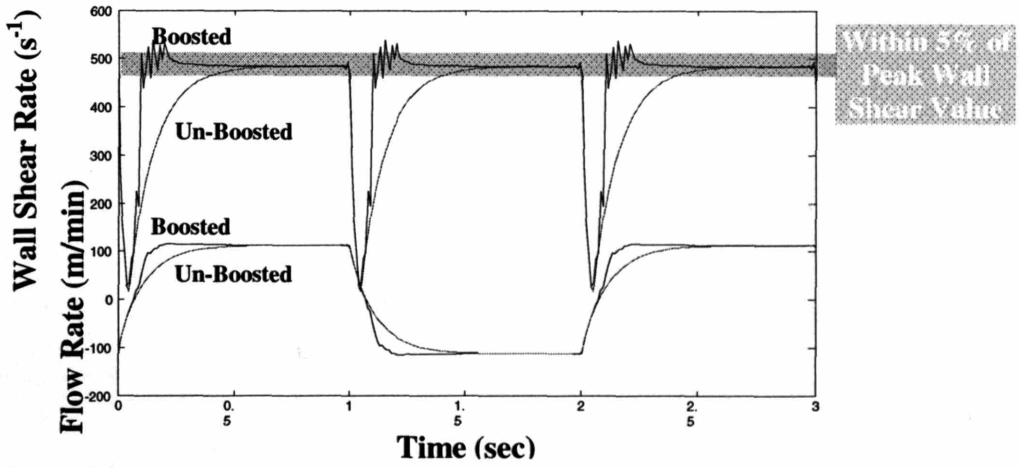

Figure 6.6. Calculated wall shear rate (top set of curves; solid lines) and fluid flow profiles (bottom set of curves; dashed lines) for a square wave wall motion boosted with an impulsive train, showing the rapid rise time and minimal overshoot error in wall shear.

Generated Flow Waveforms

To analyze the effects of coronary-like pulsatility on platelet adhesion, we used 1 Hz triangular pulses to roughly approximate the coronary wave form (section 3.1) characterized by gradual flow onset and depletion rather than abrupt flow disruptions (red line; Fig. 6.7). These gradual temporal changes were readily accommodated for considering the relatively fast response time of our system. Square waves of half the amplitude (equivalent mean flow) were developed using a strategy of boosted, square-type wall accelerations. In an effort to model absolute constant shear conditions, our acceleration strategy allowed us to quickly (minimizing duration error), though steadily (minimizing overshoot error) reach the peak flow condition (black line; Fig 5.19).

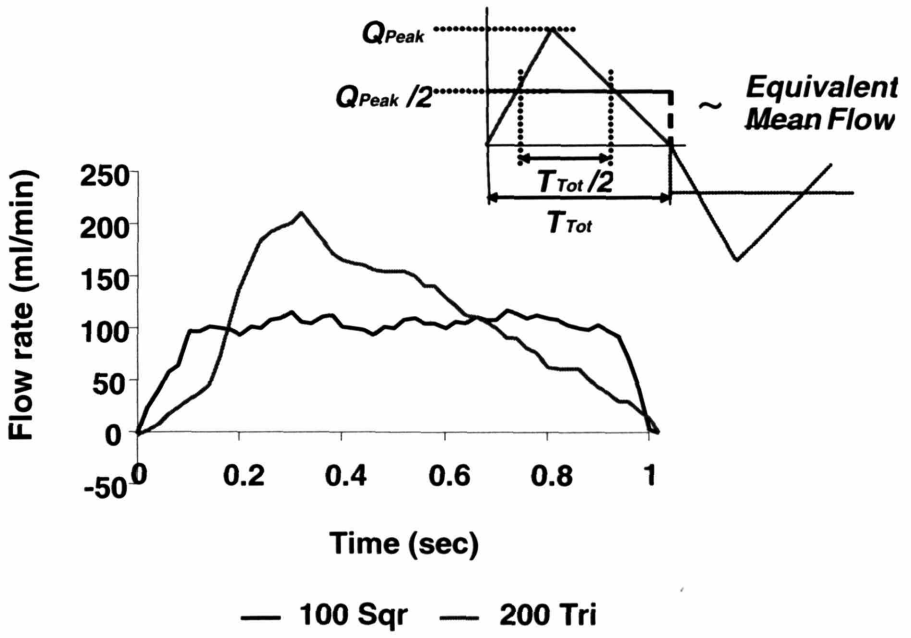

Figure 6.7. One cycle of generated triangular and square-like pulsatile profiles of equivalent mean flow rates, providing a representation of coronary-like pulsatility and an absolute constant shear condition respectively.

With these prototypical shapes, we spanned a range of shearing conditions relevant to physiological to pathological settings (section 1.3). Every triangular pulse was matched with a control square pulse of identical mean flow (Fig 6.8; 50-400 ml/min mean flow, ~250-2000 s^{-1} mean shear rate; peak shear rates of 4000 s^{-1}).

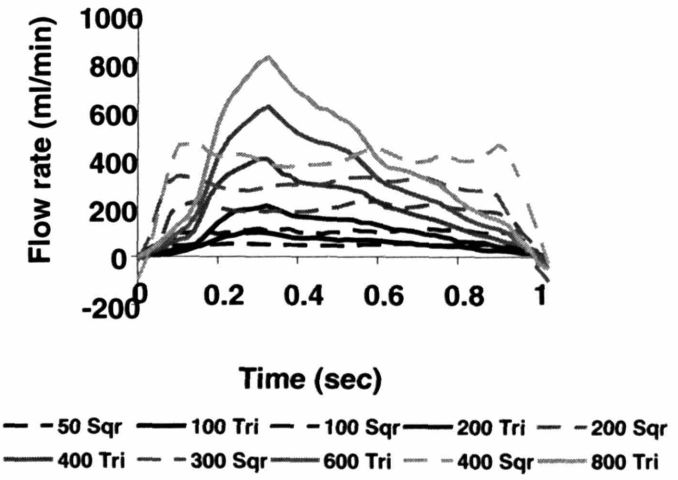

Figure 6.8. Generated triangular square flow patterns spanning a physiological to pathological range of pulsatle flow conditions; ** Note one cycle of the bidirectional profiles is shown.

Reactive Sites

Reactive segments were used as a reductive model of vessel injury. Briefly, fluid loops were made from a 21 cm length of 1/8" inner diameter (ID), 3/16" outer diameter (OD) 3350 Silicone Tygon tubing into which a glass reactive tubing segment was inserted (glass was used to enable surface visualization). The reactive segments were coated with Type I, acid insoluble bovine collagen and the 21 cm lengths were uniformly coated with a 1% BSA blocking solution (section 5.1).

Platelet Isolation, Manipulation, and Observation

Whole blood was drawn from healthy volunteers using D-Phe-Pro-Arg chloromethyl ketone (PPACK, 80 μM final concentration; Calbiochem-Novabiochem Corp. La Jolla, CA) as an anticoagulant and used within 30 min of withdrawal as source of platelets. Given that we were investigating initial (5 min) adhesion processes during which time little leukocyte incorporation could take place, whole blood (as opposed to the leukocyte depleted blood; section 5.2) was chosen to minimize handling. To study the effect of GPIb mediated wall tethering, the blood was incubated with 20 μg/ml AK2 or 20 μg/ml IgG1 isotype control (both from Serotec, Oxford, UK) for 15 minutes prior to a run. The murine monoclonal anti-GPIb antibody AK2, has been previously characterized and shown to functionally block GPIb-vWF interactions at these concentrations [152].

Platelets were quantitatively assessed through LDH staining and qualitatively through surface visualization (BODIPY FL phalloidin staining) as previously detailed (section 5.2.1).

6.1.2 Platelet Adhesion in Pulsatile Environments

Dependence of platelet adhesion on flow profile shape

To determine the effects of pulsatility on platelet tethering, we incubated PPACK anti-coagulated whole blood with either the function blocking anti-human GPIb antibody (AK2) [152] or IgG1 isotype control and circulated the blood over the reactive sites for 5 minutes to allow thrombus growth. We characterized the importance of the GPIb axis on platelet adhesion under pulsatile flow conditions over the range of physiological and pathological flow rates by quantitatively assessing the surface adherent layer using the

LDH assay as a marker of thrombus size and indirect platelet adhesion (these surface adherent layers were found to be predominantly composed of platelets given the lack of significant nuclear staining; data not shown).

In the absence of inhibition, both square and triangular profiles supported similar degrees of flow dependent platelet adhesion and thrombus growth (Fig. 6.9; grey lines). These results are agreement with our previous findings where we show an increase in adherent platelets with flow (transient case; section 5.2). That the increase occurs with both triangular and square flow patterns of identical mean flow rates indicates that this observation is relatively profile independent, supporting similar observations which have been made in a variety of other settings as well [26, 97].

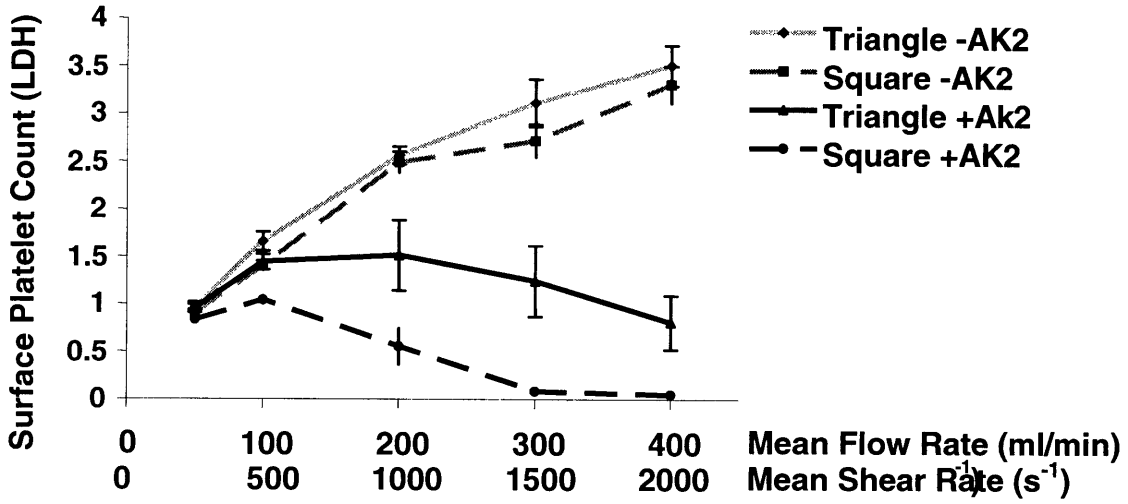

Figure 6.9. Triangular and square pulsatile flow dependent platelet adhesion (as quantified by LDH measure) with and without GPIb axis blockade using the monoclonal antibody AK2. (Mean ± SEM)

In the presence of AK2, thrombus formation was uniformly eliminated with increasing flow rates under square flow conditions (our model for constant shear), while the coronary-like triangular profiles allowed significant platelet accumulation (Fig. 6.9; black lines). These findings were visually confirmed through actin staining of reactive sites run under the extreme flow conditions (50 and 400 ml/min mean flow; Fig. 6.10).

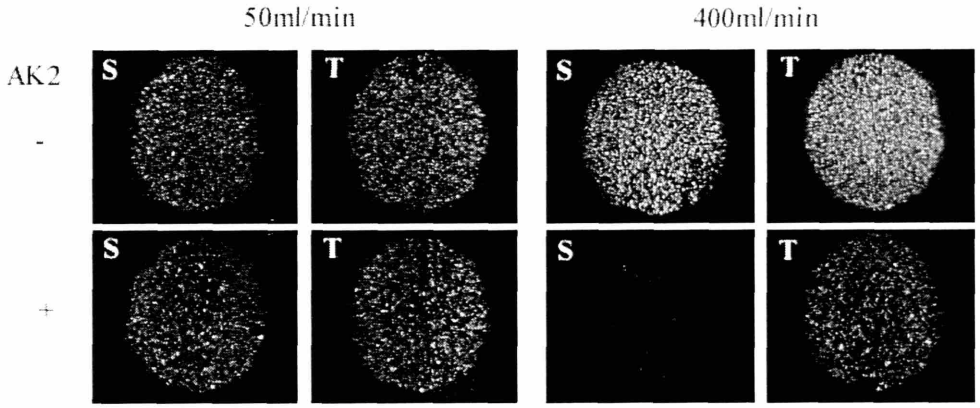

Figure 6.10. Actin visualization of surface thrombus formation at extreme (50 ml/min; 400 ml/min mean flow) pulsatile flow conditions with and without AK2 treatment. S indicates square profiles; T indicates triangular profiles.

Comparing surface platelet accumulation between the triangular and square wave flow patterns at either mean or peak shear rates, we witness a dramatic divergence that occurs between 1000 and 2000 s^{-1} for the GPIb inhibited pulses (normalized to the respective – AK2 condition; Fig. 6.11). That the jump occurs at a similar limit considering either peak or mean values is indication that profile shape (triangular vs. square) is the robust difference in mediating the GPIb-bypass effect. The divergence is a result of the complete blockade of platelet adhesion with the GPIb inhibition under high, square conditions ($\geq$ 300ml/min, 1500 s^{-1}, black dashed line; Fig. 6.9), This correlates well with the limiting 1500 s^{-1} shear rate above which GPIb tethering has been shown to be essential under steady shear conditions.

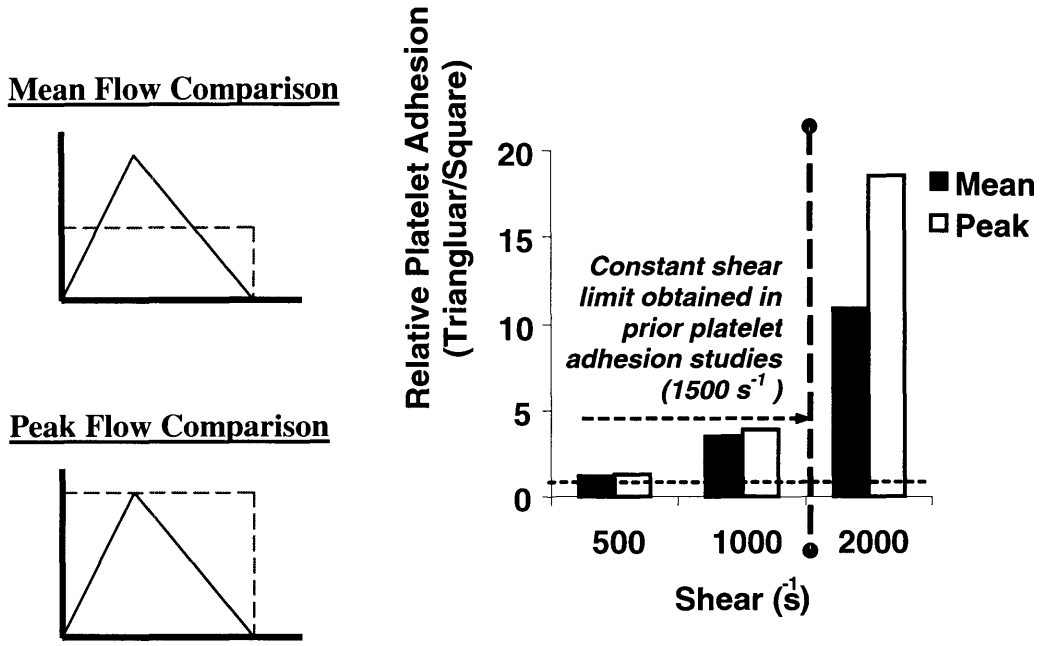

Figure 6.11. Ratio of relative platelet burden under triangular flow conditions to those under square flow conditions of either equivalent mean (black) or peak (white) pulse flow rates.

Importance of Low Flow Phase in Bypassing GPIb axis

A major difference between triangular and square wave patterns that we hypothesized may account for our observations is the significant fraction of triangular flow profiles that can be spent in low flow regimes, during which time platelets may adhere independently of GPIb tethering. We can characterize the portion of the cycle spent in the low flow phase, T_{Low}, by determining the duration of the cycle that is less than some threshold flow rate Q_{Low}, below which GPIb/vWF independent adhesions are supported (Fig 6.12). Considering our square profile dynamics (black dashed line; Fig. 6.9), we can approximate this level to be ~200 ml/min, above which GPIb inhibition dramatically reduces platelet adhesion.

If the peak flow rate, Q_{peak} never exceeds the prescribed threshold, Q_{Low}, then the entire cycle is within the low flow bounds. If on the other hand, Q_{peak} exceeds Q_{Low}, then the time spent in the low flow regime is simple given by the simple ratio:

$$T_{Low} = \frac{T_{Total} \times Q_{Low}}{Q_{Peak}} \quad (19)$$

where T_{Total} is the full pulse period (1 sec). Thus, for the 100, 200, 400, and 800 peak triangular flow rates, T_{Low} was 1.0, 1.0, 0.5, and 0.25 sec respectively.

.

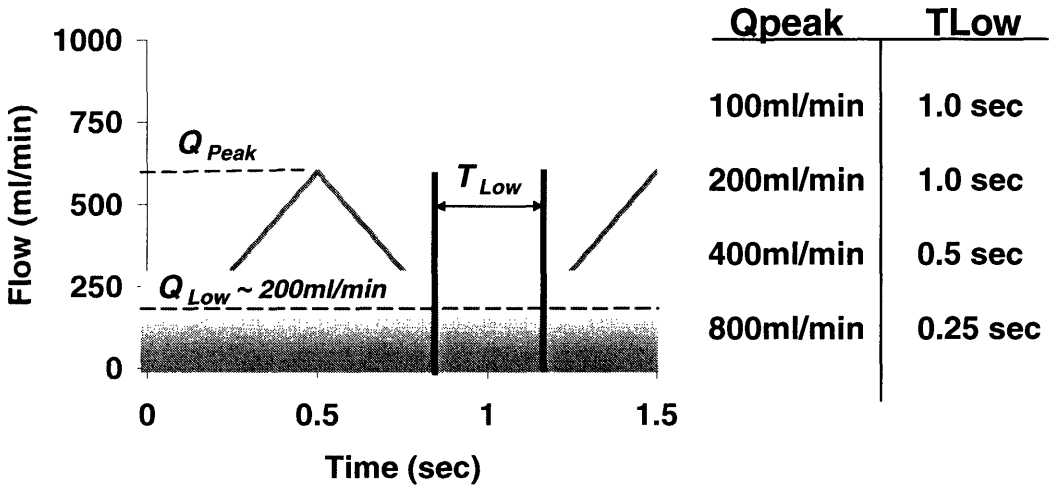

Figure 6.12. Definition of TLow.. Note that while QPeak is a function of the considered flow profile, QLow is purely of function of platelet physiology, and is given by the flow rate that is capable of supporting GPIb independent adhesion (Fig 6.9).

To isolate the importance of such alternating high and low flow conditions in a given pulsatile flow waveform and see if these could account for a profile mediated circumvention of the GPIb-vWF axis, we sought to find a minimal low flow period required for platelet adhesion to occur ($T_{Adhesion}$).

Modified Flow Profiles for Determining Platelet Adhesion Time ($T_{Adhesion}$)

To isolate and explore these temporal parameters, we developed a series of truncated square flow patterns with a variable duty cycle (low flow period/total flow period) retaining an overall 1 Hz frequency (Fig. 6.13). In each of these profiles, high (above which platelets could not bind given GPIb inhibition; > 300 ml/min) and low (nominal; << 300 ml/min) flow magnitudes of 350 and 50 ml/min were used for the high and low

flow periods (TH, TL; as defined in Fig. 6.13) respectively. Non-zero flows were used for the duration of the low flow phase to eliminate flow stagnation.

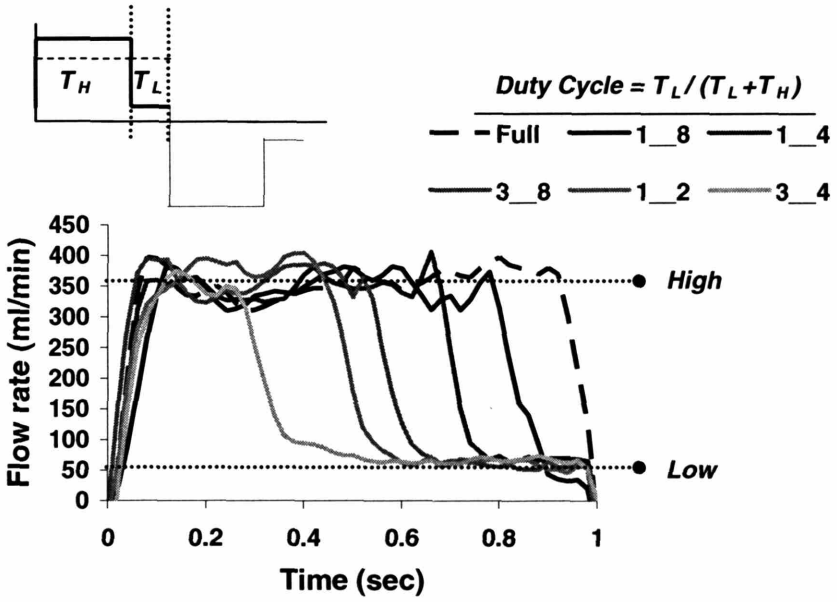

Figure 6.13. High / Low phasic flow profiles with changing duty cycle, Tl/(TL+TH) where TL is the portion of the cycle spent in the low flow regime and TH is the remander spent at the high flow condition

Characterizing $T_{Adhesion}$ given GPIb blockade

GPIb inhibited, anti-coagulated whole blood was run for 5 and 10 minutes under the varied duty cycle conditions and platelet/thrombus accumulation was quantified through LDH measurement. Each condition was compared to a control, high flow square pulse case (0 duty cycle; 350 ml/min) for 8 individuals. Platelets uniformly failed to accumulate when the low flow period, TL, was ≤ 0.125 s. This indicated that under the shortest duty cycle condition, platelets did not have sufficient time to firmly adhere and accumulate before the onset of high flow at which point platelet adhesion would no longer be supported in the absence of GPIb function. As TL was further increased, individuals began to variably respond by 0.25 s, with all showing significant thrombus formation by 0.75 s (Fig. 6.14). These results yield an estimate of intrinsic platelet adhesion time, $T_{Adhesion}$, (between 0.125 and 0.25 sec).

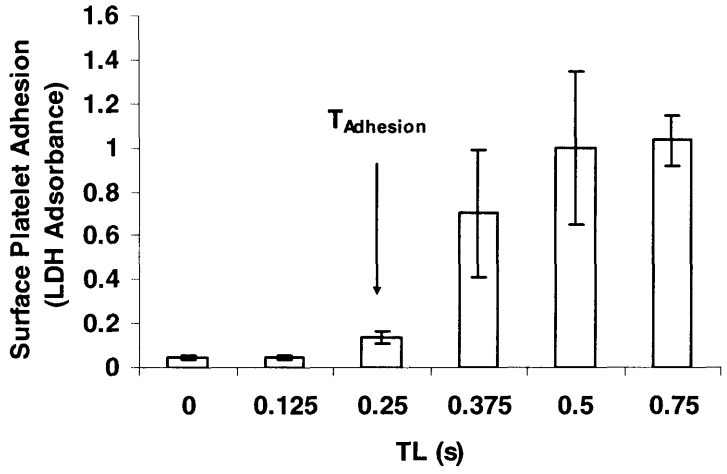

Figure 6.14. Platelet adhesion (quantified via LDH) as a function of TL and normalized to a full square pulse condtion (0 TL). These results depict the minimum adhesion time, TAdhesion, required for platelet accumulation given GPIb inhibition (0.125→0.25 sec); 1.01 value at TL=0.125.**

6.1.3 Discussion

By parametrically considering hemodynamic environments relevant to the coronary circulation and through inhibition of the GPIb platelet tethering receptor, we have mechanistically investigated the effects of pulsatility on surface platelet adhesion. To do this, we developed square flow profiles as a comparative control. However, these square profiles do not exactly produce steady absolute shear levels as the flow briefly jumps from one level to the next. While these rapid discontinuities upon directional change may be postulated to mediate the profile dependent differences observed between our square wave and our more slowly changing triangular profiles, the ability of altered duty cycle square waves (which also create such abrupt discontinuities; Fig. 6.13) to support platelet adhesion indicates that this is not the case. Furthermore, we observed that the limiting shear rate above which platelets could not adhere with GPIb blockade occurred similarly at 1500 s^{-1} for both our square flow profiles as well as the constant shear pattern which they sought to approximate, providing additional support for validity of these controls.

We compared triangular and square flow pulses over a range of magnitudes. In the absence of GPIb inhibition, platelet accumulation was found to increase with flow rate, but in a manner that was independent of profile shape. Also, under low flow conditions, pulsatile profile shape does not significantly affect platelet adhesion irrespective of GPIb blockade. This corroborates numerous other studies which show that under conditions of low flow, GPIb mediated tethering is not essential. However, under higher flow, pulsatility can bypass the GPIb-vWF tethering axis (Fig. 6.9, 6.10). The effect seems to be dependent largely on the presence of low flow periods of sufficient duration, during which time GPIb-independent adhesion can occur. So long as the cycle's low flow phase is greater than the time required for platelet attachment, $T_{Adhesion}$, platelet accumulation and thrombus growth are supported.

From our studies using modified square profiles of varying duty cycle (Fig. 6.13), $T_{Adhesion}$ with GPIb blockade was determined to be between 0.125 and 0.25 sec (Fig. 6.14). These results give important insight into understanding the varied responses observed between our triangular and square pulse profiles at high flow. Using our boosted square wave wall motion strategy, we were able to maintain near constant flow conditions (in an absolute sense), theoretically keeping wall shears to within 5% of the steady state values throughout all but 0.1 sec of the pulse. That this time is less than the observed $T_{Adhesion}$ time (0.125-0.25 sec) is a likely rational for the effectiveness of our square profiles in modeling the constant shear condition. Given triangular pulse patterns which exhibit gradual rise and fall characteristics, considerably longer portions of the cycle can be spent in low flow regimes (Fig. 6.12). For the maximum, 800 ml/min peak triangular flow wave considered, this low flow time would be around 0.25 sec, greater than the $T_{Adhesion}$ time required to support GPIb inhibited adhesion. Indeed, GPIb axis inhibition yielded significant platelet adhesion under these conditions. To test triangular waves with a low flow period less than the 0.125 sec, we would need to generate pulses with a maximum flow rate of 1600 ml/min. Though this extreme condition would further confirm the importance of low flow duration on bypassing the GPIb axis, these profiles were not possible given the current motor specifications and system embodiment. Still, considering the reducing trend of platelet adhesion by the higher flow rates under GPIb inhibited triangular pulse conditions (black solid line; Fig. 6.9), it is reasonable to

postulate that these lines would project to the eventual elimination of platelet adhesion by 1600 ml/min.

Many studies considering platelet adhesion have taken place in constant shear settings, showing the critical nature of shear on platelet receptor function. In the body, blood flow is far from constant, exhibiting widely varying temporal fluctuations. Using our pulsatile flow system, we have shown that temporal variations in flow profile shape, similar to those in a coronary arterial setting, may mediate mechanistic differences in platelet adhesion pathways as compared to a constant flow setting (modeled with our square flow patterns). Accordingly, when investigating complex, situational thrombotic events flow profile is an important parameter to consider. Given this understanding, we revisit the scenario of endovascular stenting. Using our reactive site model, we can now consider not only device/blood interactions, but the induced hemodynamic situation, as the structure of the stent creates spatial variation in the local shears experienced by the reactive vessel wall.

6.2 Spatial Variations in Hemodynamic Environments

In section 6.1, we show how pulsatility can lead to altered mechanisms of platelet adhesion, specifically through a bypass effect of the GPIb tethering axis which is typically required for high shear platelet adhesion. Along with temporal changes, abrupt disturbances in vessel geometry can also affect the local hemodynamic situation, having further implications on localized mechanisms of platelet adhesion and thrombosis. While the previous example (section 6.1) considered a reactive site and fluid loop model of constant internal diameter, the unique nature of our *in vitro* system allows us to not only establish carefully controlled flow environments, but geometrical ones of relevance to the arterial setting. We now consider the case of interventionally induced spatial changes as modeled in our idealized *in vitro* environment and how these may affect the dynamics of local platelet/wall interactions.

Coronary Interventions: Angioplasty and Stenting

Percutaneous interventions (PCI) have become the mainstay of treatment for acute coronary syndromes (ACS). Over the past two decades, the beneficial effects of percutaneous transluminal coronary angioplasty (PTCA; Fig. 6.15*a*) versus thrombolytic strategies have been shown [153, 154]. More recently, numerous clinical trials

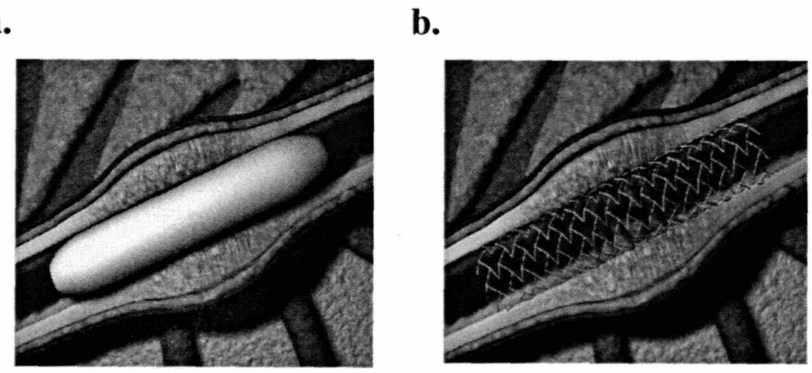

Figure 6.15. Coronary interventions. a. Percutaneous Transluminal Coronary Angioplasty (PTCA) ; b. Endovascular Stenting

have shown coronary stenting (Fig. 6.15*b*) to be an effective technique in achieving even greater post-procedural luminal gains while offering a lower incidence of recurrent ischemia and a resultant reduction in the need for target vessel revascularization [155-157]. While the marked success of these catheter-based approaches has led to their widespread use in both urgent and elective cases, these procedures are not without consequence.

Upon intervention, the local coronary environment can be dramatically altered. With coronary disease, the luminal surface may already be badly damaged as a result of endothelial erosion or rupture of the atherosclerotic plaque region, exposing subendothelial matrix components and atheromatous debris. Following angioplasty, what was left of the once-protective endothelial layer can be further removed leading to reactions such as those covered in chapter 5. While the local expansion of a stent can help to mechanically stabilize the lumen and prevent occlusive wall dissections, the device may also have adverse environmental effects. The mere presence of a foreign surface can interact strongly with various biological components (section 4.2). Moreover, that these devices function in a flowing environment provides a mechanism whereby the geometry can influence the local situation by inducing changes in the hemodynamic environment. Whether induced by foreign devices or injured vascular surfaces or both, the biological response to intervention is heralded by site platelet accumulation which serves as an important component in both the acute and long term response.

Recognition of the critical, targeted role of platelets in affecting high flow, arterial thrombosis has lead to the effective use of anti-thrombotic strategies that limit clinical cases of acute/subacute outcomes in the setting of coronary intervention. Still, there remains a significant risk of mortality associated with thrombotic vascular occlusion, along with a risk of hemorrhagic complications accompanying the use of powerful anti-thrombotic agents. Moreover, clinically silent mural thrombosis is an apparently ubiquitous process that serves as the inciting and promoting event for subsequent repair and remodeling that leads to pathological inflammation and restenosis. Accordingly, elucidation and control of the local thrombotic process induced by iatrogenic states is of

great importance for the continued use and optimized development of coronary therapeutic modalities such as angioplasty and stenting.

We have previously considered the effects of endovascular stent surfaces on thrombotic reactions, showing assorted interactions between biological and physical factors (chapters 3, 4). While these studies provided much needed insight required to parameterize and place our model, they raised more questions than they answered. What factors mediate the observed differences between non-polished, polished, gold, and treated gold stents? Why is does stainless steel more strongly activate the intrinsic pathways of coagulation while gold more strongly interacts with the platelet component? Why does platelet responsiveness increase with flow for both stent surfaces under conditions of low coagulation, but not under high coagulation levels? Though we can provide rationalizations for these findings, to more fully understand these issues requires considerable effort. Before spending excessive energy to mechanistically delineate such observations we must consider that they were made in the absence of a reactive wall component. Expanding our study from one of endovascular devices to one of endovascular situations, we can consider the effects of stent placement in our reactive site model, where wall interactions could specifically be enabled or eliminated. In doing so, we hoped to gain an appreciation for the functional influence of stent presence in the regional platelet response.

6.2.1 Methods

Hemodynamic Environment

We applied our reactive coronary site model to investigate the anti-coagulated platelet response to stented and non-stented situations over a range of flows typifying the physiologic, coronary-like

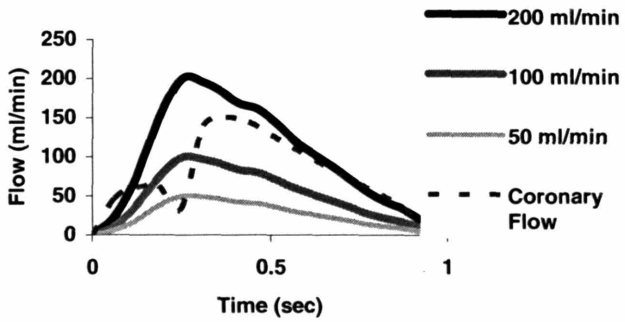

Figure 6.16. Generated triangular flow waveforms modeling coronary-like profiles.

environment (50-200ml/min; Fig. 6.16). In doing so, we provide a greatly simplified, idealized, *in vitro* model of the interventional stent and PTCA conditions. By creating an environment where the physical geometries would closely match the *in vivo* condition, we were not only able to accommodate physically relevant stents and proper mechanical expansions (section 5.1), but ensure that the developed shear profiles would closely match those found in the respective coronary interventional situations.

Qualitative effects of stenting on hemodynamic environment

In the setting of non-stented geometries, the tubular fluid flow is relatively straightforward, and while curvature effects create secondary flows that may be considered, the principle flows are those given by the analytical model which we consider in section 2.1. Although a great deal of variability may exist in time, the wall flows are axially symmetric. With the placement of a stent, the situation becomes far more complex, and simple analytical models are not suitable. Given the importance of understanding the hemodynamic environment induced with stenting, computational fluid models have been widely applied towards understanding the nature of the established conditions. From these studies, even in light of the widely varying input conditions, many qualitative similarities exist in the spatially varying flow conditions.

Although high shear rates may occur on the stent struts themselves, recirculation zones are formed in the immediate, upstream and downstream vicinity of each strut. In these regions, flow can be considered near stagnant. The sizes of these regions are largely dependent on strut dimensions and flow speed, making the conditions in the center portions of the inter strut regions far more complex. When strut spacing is close enough together (in relation to strut height) or when flow velocity is sufficiently high, the recirculation zones between two adjacent struts may connect to form a single large, near-stagnant region (Fig. 6.17*a*). Alternitively, with larger spacing or lesser flow speeds, flow reattachment may occur, thus maintaining appreciable flow between struts (Fig. 6.17*b*). Still, various numerical studies have shown the magnitudes of such flows are greatly reduced as compare to non-stented regions of similar bulk flow.

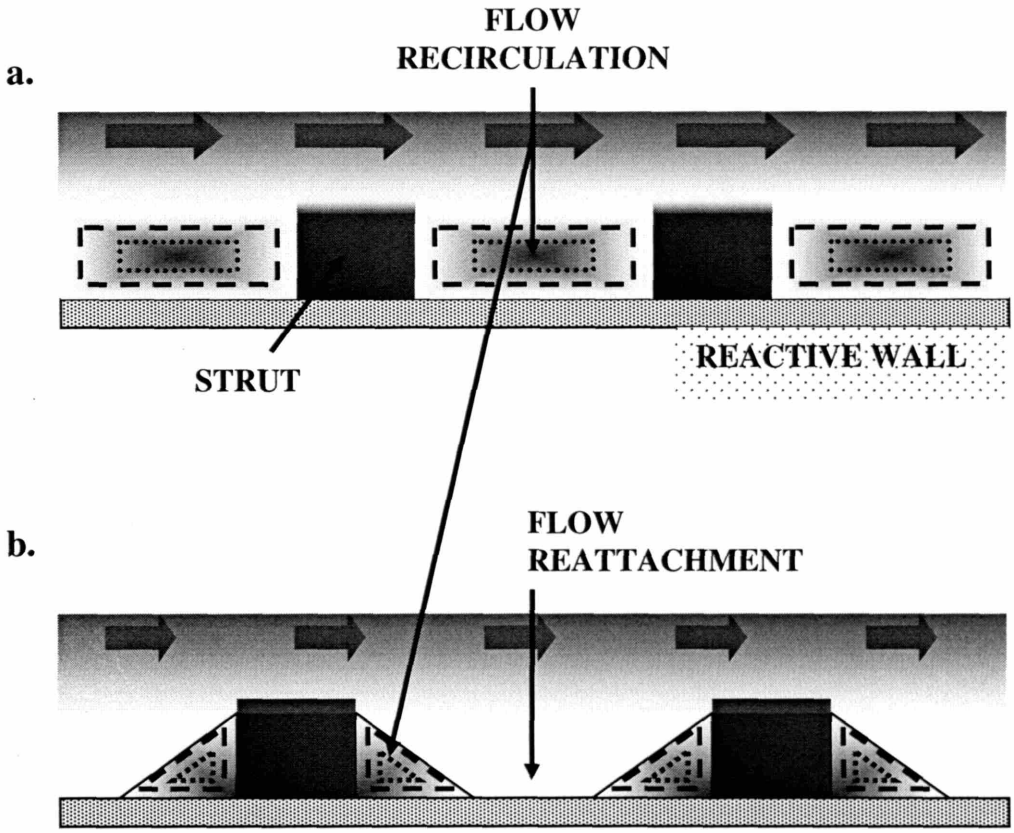

Figure 6.17. Qualitative stent induced changes in flow. a. Close strut spacing and high flow promote a single flow recirculation zone; b. Distant strut spacing and low flow promote distinct flow recirculation zones, with inter-strut regions of flow reattachment. Flow in the recirculation zones is near-stagnant, while reattachment allows reasonable shears, though still only a fraction of what would be achieved in the absence of stent placement.

As we have explored in section 6.1, pockets of low flow may create a situation where the mechanisms of platelet adhesion are different. Although the global flow condition may be indicative of the need for platelet GPIb axis tethering to enable platelet wall interaction, regions of low flow may circumvent this need. Previously, we explored the significance of temporal pockets of shear. Now we consider stent induced spatial variations. To make the effects of stent presence on GPIb tethering more clear, we generated high flow square wave forms (our model of a constant shear condition; section 6.1) of 300 ml/min flow rate (Fig 6.8). By creating conditions when GPIb function would normally be required (Fig. 6.9), this flow pattern allows us to isolate the spatial

effects of stenting from the temporal effects of flow pulsatility, which in itself, could bypass the tethering axis.

Reactive sites

Following coronary interventions, localized regions of endothelium are disrupted through the mechanical expansion of intravascular devices (balloons, stents). This provides a situation of subendothelial exposure which matches well with the idealized conditions established within our reactive site model. To make these localized sites, the fluid loops were constructed from a 21 cm length of 1/8" inner diameter (ID), 3/16" outer diameter (OD) 3350 Silicone Tygon tubing into which a 3 cm reactive tubing segment of identical diameter (ID, OD). As an initial model of the reactive coronary wall, the 3 cm silicone reactive segments were coated with Type I, acid insoluble bovine collagen while the 21 cm lengths and 3 cm unreactive segments were coated with a 1% human albumin solution to block non-specific platelet-surface interactions (section 5.1).

To make the stented segments, 9-mm, 7-cell, stainless steel NIR® stent (closed-cell design, Fig 6.18*a*; Medinol, Jerusalem ISRAEL) or Tristar® (open-cell design, Fig 6.18*b*; Guidant,) were expanded to a 3.0 mm post-inflation diameter under 10 atm of pressure via a Maxxum™ 3.0 Scimed® balloon catheter (Boston Scientific Corporation). To ensure similar handling conditions, a balloon was similarly expanded within the non-stented segments (which we found to have no observable effect on platelet response).

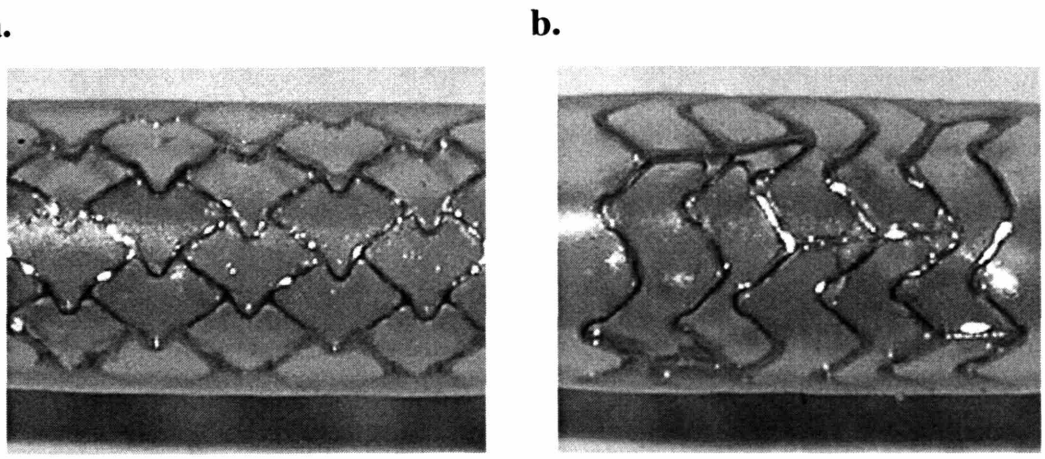

Figure 6.18. a. Closed-Cell (NIR); b. Open-Cell (TriStar) stent geometries.

Platelet Isolation, Manipulation, and Observation

To assess the effect of stent presence on the regional accumulation of platelets, we chose to consider anti-coagulated, leukocyte-depleted blood as a platelet source as we hoped to consider not only early time points (indicative of transient events) but longer time studies when platelet accumulation would saturate to surface capacity (Fig. 5.12; section 5.2). Again, this decision was made to minimize a leukocytic component in our integrative LDH measure, which could become a factor in long time studies (section 5.2). Whole blood obtained from healthy volunteers was drawn via a 20-gauge needle into a 1/10 dilution of acid citrate dextrose (ACD) and 80 uM (final concentration) PPACK anticoagulant. The leukocyte component was removed as previously described (section 5.2) and reconstituted blood components were recalcified (13mM Ca^{2+}) immediately prior to use.

For the functional studies, given the short 5 min run times, anti-coagulated whole blood was directly incubated with AK2 or IgG isotype control (20`ug/ml) and run without leukocyte removal to minimize extraneous handling as described previously (section 6.1).

To assess platelet function, LDH quantification was performed on the flushed reactive sites (section 5.2). Bulk platelet activation was also determined using platelet P-selectin, CD62p surface expression as determined by flow cytometry (section 4.2).

6.2.2 Platelet Accumulation in Stented Environments

Collagenized Reactive Sites

To assess the flow dependence of platelet accumulation to silicone segments with and without stent presence, we compared 6 closed-cell stented and 6 non-stented collagenized segments at each of the three flow conditions both after 3.5 min and 45 min runs.

At 3.5 min (Fig. 6.19), we again witness a significant, flow dependent increase in surface bound platelet number (as assessed by LDH quantification) on the non-stented segments (recall section 5.2, 6.1). In the presence of a stent, the 50 ml/min peak flow condition

promoted slightly increased surface bound platelet adhesion. However, at the 100 and 200 ml/min peak flow conditions, the stent caused a dramatic reduction in the number of 3.5 min adherent platelets as compared to the non-stented trials.

At the 45 min time point, we observed similar numbers of surface adherent platelets to our non-stented segments at the 50 and 100 ml/min peak flow conditions with a lower number at the 200 ml/min rate (perhaps indicative of increased surface embolizations as discussed previously; section 5.2). At this longer time point, the effect of stent presence in reducing local platelet adhesion was no longer apparent and in fact, there was a trend towards stent promotion of platelet accumulation.

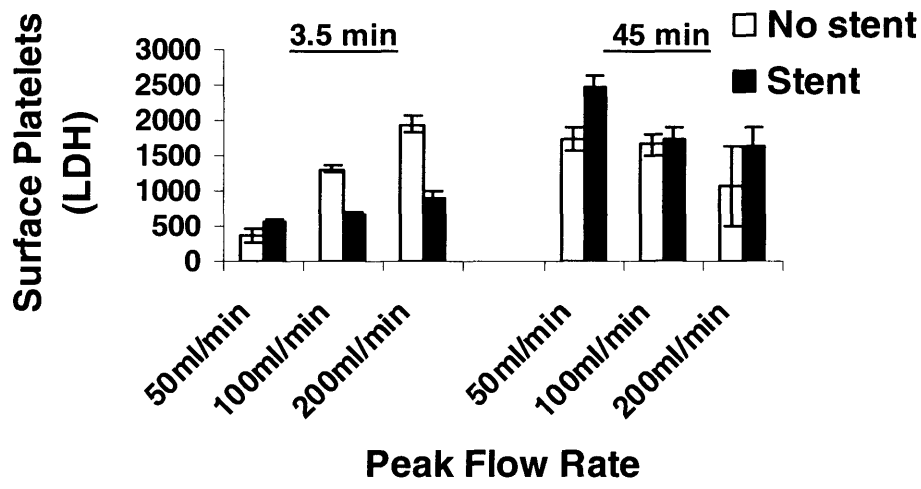

Figure 6.19. Effects of stent presence at early (3.5 min) and late (45 min) time points on platelet adhesion to a collagenized reactive site. Note a flow dependent protective effect that is eliminated with time. (Mean ± SD)

In all cases, no significant differences were noticed in the bulk fluid CD62p expression between the stented and non-stented cases (results not shown).

Albumenized Reactive Site

To study the effects of stenting without a reactive wall substrate, 4 albumenized stented and 4 non-stented reactive sites were studied at each of the 3.5 min and 45 min conditions described above.

In these trials (Fig. 6.20), we observed a dramatic, generalized reduction in surface bound platelets as compared to the reactive, collagen-coated sites. Also, we see a significant

increase in the number of bound platelets in the stented trials as compared to the non-stented cases. Given that very few platelets were adherent to the albumenized, non-stented segments, we rationalized that the majority of platelets in the stented, albumin coated cases were bound to the stent surface onto which reactive plasma proteins such as fibrinogen may adsorb to mediate stable platelet adhesions. We note that the stent-dependent rise significantly diminishes with increasing flow (as has been reported on fibrinogen treated surfaces [23]. Furthermore, noting similarity across the 3.5 min and 45 min groups, we can surmise that a steady state, low level of stent bound platelets is quickly reached, perhaps as a result of an overall diminished surface capacity.

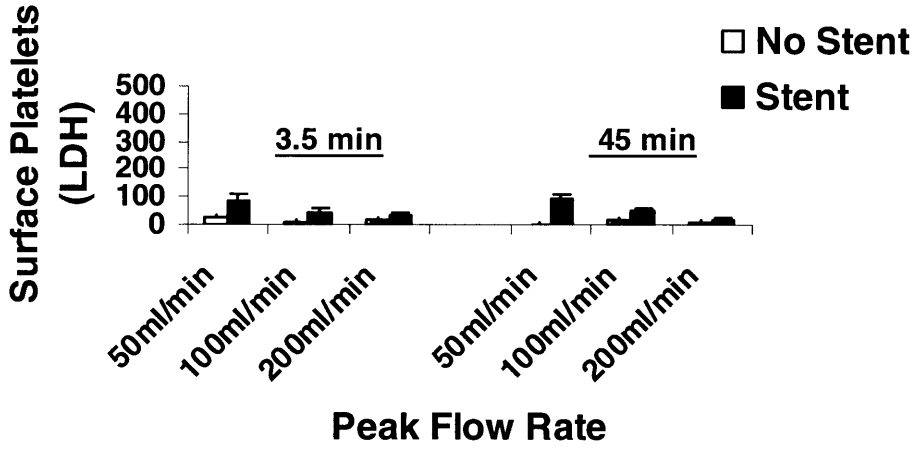

Figure 6.20 Effects of stent presence at early (3.5 min) and late (45) time points on platelet adhesion to an albumenized unreactive site. (Mean ± SD)

Robustness of findings

Testing the robustness of model findings increases confidence in their predictive value (section 4.2). Although we have witnessed significant, flow dependent effects of stent presence on platelet adhesion, these findings may be limited to particular aspects of the model system (stent type, anti-coagulated blood source, reductive protein coatings, etc). Here we consider varying stent geometry to assess the robustness of our stent dependent, reactive site platelet adhesion findings. In the preceding trials, we evaluated a stent of closed cell geometry (NIR®; Fig. 6.18a). We now present a case of significantly different geometry.

An open-cell stent design (Tristar®; Fig. 6.18b) was used to probe the robustness of platelet accumulations to collagenize and albumenized reactive sites at the more extreme 50 and 200 ml/min peak flow conditions both at 3.5 and 45 minutes. Six stented sites (4 in the albumin case) were compared with respective non-stented control sites for each flow condition and the results are given in Table 6.1.

Table 6.1. Robustness of findings to stent geometry (Mean ± SEM).

		COLLAGEN	**ALBUMIN**
		Stent vs. Non-Stented Case LDH Measure	Stent vs. Non-Stented Case LDH Measure
Time point	**Peak Flow**		
3.5 min (Transient)	**50 ml/min**	540 ± 45 vs. 417 ± 63	84 ± 8 vs. 22 ± 3
	200 ml/min	709 ± 45 vs. 1362 ± 115	33 ± 7 vs. 18 ± 3
45 min (Steady state)	**50 ml/min**	2470 ± 351 vs. 1789 ± 151	89 ± 9 vs. 17 ± 1
	200 ml/min	1017 ± 191 vs. 533 ± 150	29 ± 4 vs. 15 ± 2

These results show that the open cell geometries share similar key dynamic features with our previous closed cell results. Platelet accumulation is greatly enhanced to stented collagenized reactive wall segments as compared to the stented albuminized segments. Furthermore, at 3.5 minutes, we note a significant reduction in accumulation with stent presence, selectively at high flow. By long times (45 min) this protective effect was again eliminated. That we have observed similarities in our response for stents of significantly dissimilar geometry is indication these results are robust within the confines and considerations of our *in vitro* model.

Altered Adhesion Mechanisms in Stented Environments

These reactive site accumulation findings offer evidence that general stent presence affects the local environment in a flow dependent fashion. As in the case of flow pulsatility, where temporal variations exposed blood to functionally important pockets of both high and low shear under high, time-averaged flows, the stented environment exposes blood to positionally spaced low flow pockets (Fig 6.17). Paralleling the pulsatile case, we hypothesized that the mechanisms of platelet adhesion under such fluctuating conditions would be different than those under non-stented conditions, allowing GPIb-independent adhesion to occur in otherwise GPIb-dependent conditions.

Stented loops were filled with either blood incubated with AK2 or vehicle controls and run for 5 min under square high flow conditions (300 ml/min; 1500 s-1 mean values; Fig 6.8). Two runs of 4 stented loops (2 w/AK2, 2 w/ vehicle) were performed and the reactive sites were assessed for platelet adhesion via LDH measurement.

Normalizing to the vehicle control, we found that the AK2 inhibited stented site conditions were able to support significant platelet wall accumulation (0.34±0.05). This is in stark contrast to the complete levels of inhibition witnessed under non stented conditions (recall 300 ml/min square conditions, Fig. 6.9; section 6.1), showing that a localized spatial disturbance can indeed alter the mechanisms of platelet wall interaction, circumventing the requirement for platelet wall tethering in a global, high flow environment.

6.2.3 Discussion

By evaluating platelet accumulation to stented and non-stented sites, we considered greatly simplified, idealized models of the post-stenting and post-angioplasty situations where discrete, reactive vascular settings are iatrogenically induced through the mechanical disruption of the local endothelial layer, with or without the added presence of a stent.

We found that stenting profoundly affected local platelet surface adhesion as quantified by LDH levels. The 3.5 min time point represents a transient effect at which

point platelets are still accumulating on the surface (see time course response; Fig. 5.12). At this time, the flow dependent increase of thrombus growth was largely blunted with the presence of a stent. A simple masking of a portion of the reactive wall by the stent cannot fully explain these protective findings given that this reduction with stent placement occurred in a flow dependent fashion as well as that the reduction exceeded 50% in the high flow conditions (the stent had an expanded footprint of ~0.15cm^2 while the total reactive site surface area was 3.0 cm^2). By verifying these results on stents of significantly dissimilar closed and open cell geometry (Table 6.1), we show these findings are robust, albeit in our pared down reactive site model.

These protective effects are in opposition to the widely accepted notion that stenting creates a greater thrombotic risk than angioplasty through the added presence of a foreign surface [157]. To put these findings in context, we must stress our use of an anti-coagulated, pre-occlusive model and that a decrease in transient accumulation (or growth rate) does not imply a decrease in final accumulation. Indeed, the stented trials supported similar or greater amounts of platelet accumulation as compared to the non-stented cases by 50 minutes (perhaps by altering surface embolization properties as discussed above). Moreover, these studies were performed under stringently anticoagulated conditions. As we have witnessed (section 4.2), synergistic coagulative presence could significantly affect the local thrombotic situation (of note, we have observed similar reduced 5 min thrombotic growth rates with stenting in the presence of coagulation, which by 10 min had reversed to a situation where there is increased thrombus accumulation with stenting).

These measurements of platelet accumulation are interesting, but give an integrative view of the local situation where stent and vessel wall interact in some fashion to affect these responses. To more closely consider the situation and compare the relative importance of the stent with that of the reactive vessel wall in mediating these altered platelet accumulations, we can consider the closed cell, stented results for both the albumenized and collagenized surfaces where wall reactions were either disabled or enabled respectively. Taking the albumenized case to be reflective of stent surface accumulation (as rationalized in section 6.2.2), we show the relatively minor importance of the stent

surface as compared to the reactive wall regions in supporting local platelet adhesion (Fig. 6.21). It also is clear that the importance of stent surface decreases with increasing flow and with time (albumenized/collagenized stented site peak ratio of 0.15 at the 3.5min, 50 ml/min flow condition).

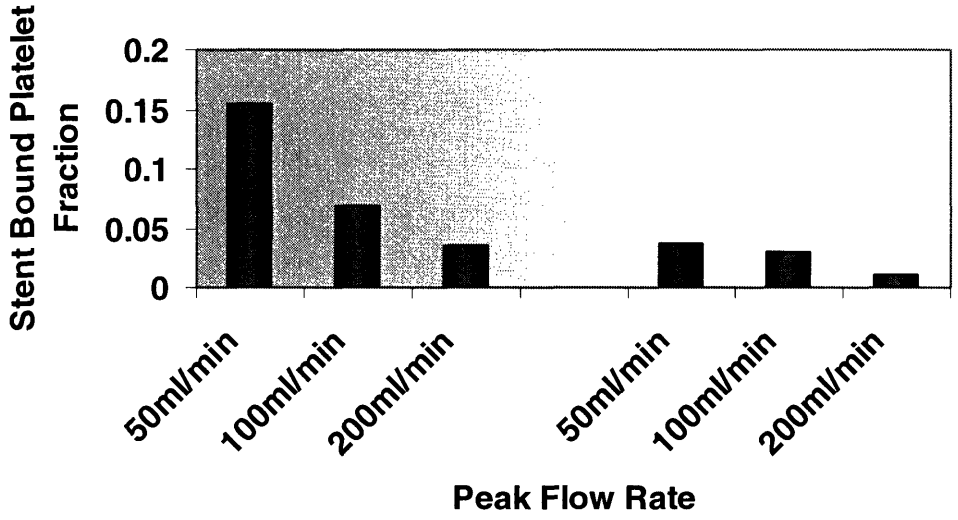

Figure 6.21. Ratio of platelet site accumulation (LDH quantified) of the albumenized/collagenized stented conditions. Right half of graph shows results at 3.5 min; Left side shows 45 min results. The low fractions indicate the relative importance of the reactive vessel wall as compared to the strut surface itself in adding to regional platelet surface capacity

The small contribution of stent surface adhesion to total site accumulation implies that the major impact of stent presence (consider the greater than 50% reduction under early, high-flow conditions) is brought about through altered wall interactions. That the stent can have such an impact on the local platelet response while only supporting low platelet adhesion onto itself is remarkable and likely results from stent-induced flow variations over the vessel wall (reduced shear zones, recirculant flow patterns) and altered transport phenomena [59, 85, 144]. In these regions, convective mass transport, intimately tied to flow, is greatly reduced. Given that the platelet wall reaction has been shown to be governed by diffusion limited kinetics [50], reduced transport could well play a role in the reduced accumulation rates we observe with stenting (as represented in our 3.5 min transient findings; Fig.6.19). The involvement of rate limiting transport phenomena is further supported by the increased dependence of altered accumulation rates with flow (greatest at 200 ml/min, not observed at 50 ml/min peak flow), as well as the fact that

given sufficient time, the stented trials eventually achieve similar (or larger) surface accumulation.

To more directly observe the potential functional impact of induced low flow regions, we again considered the flow dependent GPIb axis, noting a significant accumulation of platelets in the presence of AK2 under conditions which were found to be prohibitive in the absence of a stent. While we have not created a numerical model of our exact stenting situation, we can consider the computational results obtained from prior work [82, 85, 144, 158]. Considering cases which used similar geometric and flow conditions as our model parameters (3 cases; Table 6.2), we see that significantly reduced wall shears are maintained within the inter-strut regions as compared to peak shears in the absence of stenting in all cases well with in the limits that can support GPIb-independent adhesion. Moreover, while these peak shear values occur in zones of reattachment (found to occur in all three cases; Fig. 6.17b), a significant fraction of the inter strut region is covered by recirculant zones where near stagnant conditions and drastically reduced wall shear rates occur.

Table 6.2. Computational Results for flow over stents using geometric and flow parameters similar to our experimental conditions. Note, that these were 2-D simulations, and precise geometries are not definable (i.e. strut spacing) for our model.

		OUR MODEL	CASE 1	CASE 2	CASE 3
GEOMETRIC PARAMETERS	Artery Diameter	3.175 mm	2 mm	4 mm	4 mm
	Strut Thickness	0.1 mm	0.070 mm	0.079 mm	0.079 mm
	Strut Spacing	~1 mm (Fig. 6.18a)	0.64 mm	0.83 mm	0.83 mm
FLOW PARAMETERS	Pulse rate	60 Hz	70 Hz	70 Hz	130 Hz
	Peak Wall Shear w/o Stent	1500 s^{-1}	1550 s^{-1}	815 s^{-1}	2504 s^{-1}
	Peak Wall Shear w/ Stent	???	205	210	310
	% Recirculation Zone Wall Coverage	???	37→49 %	34 → 41 %	35 → 59 %

Considering these computational findings, it is clear that spatially induced pockets of low flow with a structural disturbance such as a stent (as we previously have shown with temporal variations) can readily lead to situations which can bypass the GPIb axis in otherwise prohibitive flow conditions.

In this section, we have considered the flow dependent impact of stenting on the local environment. While flow variations over stents have been widely shown through computational studies, we now show that such variations yield functionally relevant biological responses. We found a major functional impact of stenting to be in the induction of low flow regions over the reactive vessel wall. Specifically we observed reduced, flow dependent wall accumulation rates with stenting, implicating reduced transport phenomena. Furthermore, we tested and found the reduced flows were capable of supporting GPIb independent platelet adhesions under conditions that would otherwise preclude such events. Given these flow dependencies, it would be interesting to more precisely delineate the actual induced flow regimes over stents of our particular geometries, rather than rely on the qualitative findings of other computation studies. However, for the purposes of these examinations, where our observations were based on integrated site accumulations and designed to test for the overall impact of stent presence in reactive wall setting, such detailed scrutiny was not warranted. To develop accurate 3-D models of the stent and flow conditions (which would be required in order to improve upon the qualitatively based understanding gleaned from other models) was prohibitive at this stage. Still, given the importance of stent induced flow-changes on our experimentally observed biological function, computational models that fit closely to experimental parameters would be of considerable value if used in sync with more discretized biological observational techniques which allow us to not only measure total accumulation, but patterns and distributions of platelet interaction, activation status, etc. Currently, we are beginning to address these issues in studies where we parameterize strut thickness. These should allow to investigate the not only the functional impact of

stent presence of the local acute platelet response, but the functional impact of stent design.

In section 6.1, we have seen how temporal variations in flow are an important factor in determining the local hemodynamic environment, resulting in mechanistic differences in platelet adhesion. Currently, we show how the presence of a stent structure can also spatially affect the local hemodynamic setting, altering platelet / wall interactions. Both of these examples (flow pulsatility and stenting) offer situations that are highly pertinent to real-world scenarios and show that global hemodynamics may not be indicative of local, instantaneous conditions. When considering the effects of hemodynamic environment in real-world thrombosis, this level of detail is important to recognize. We now consider an example where these issues come to bare.

6.3 Optimizing Platelet Inhibition to Hemodynamic Settings

Anti-thrombotic agents have proven invaluable in the treatment and management of prothrombotic conditions. In cases of acute coronary thrombosis, such as those following plaque rupture or induced by interventional procedures, some of the most effective strategies work by inhibiting platelet function (section 1.2). However, the benefits of these and other anti-thrombotic drugs are tempered by an increased risk of hemorrhagic complications [148, 159]. To limit this risk, continued effort has been placed on identifying targeted anti-thrombotic strategies whose functions are limited to a particular vascular setting. That platelets exhibit receptor-based mechanistic differences under varying shear conditions is indication that the flow environment can be used as a handle by which specific environments can be separately considered and targeted. It is for these reasons that much attention has been given to the GPIb-vWF axis [12, 160-162]. Given that this axis is selectively critical in high flow regimes, its inhibition has been proposed as a method to deliver powerful anti-thrombotic effects to high flow settings as found in the arterial circulation, while still allowing lower flow thrombosis to occur. Such a strategy offers the potential to minimize bleeding complications while maintaining anti-thrombotic efficacy.

Care must be taken when considering therapies which are isolated to specific hemodynamic settings. In the case of flow sensitive GPIb/vWF axis inhibition in arterial environments, efficacy studies have been inconclusive [51, 87, 162-165]. Many possible explanations for these varied responses exist (severity of disease, inhibitor concentrations, species variability, etc.) [87]. In sections 6.1 and 6.2, we have further explored the possibility that real-world fluctuations in the hemodynamic environment likely serve as additional confounding factors. Both flow pulsatility and the mere placement of a stent were shown to affect platelet / wall interactions. That these `disturbances' can be perceived by platelets has important implications on the potential for the GPIb/vWF axis to be used as a therapeutic target in pulsatile conditions or other situations where the global, time-averaged fluid flow conditions are not indicative of local, instantaneous shears. Indeed, our studies reveal that both temporal and spatial

pockets of low flow can bypass the need for the GPIb axis under otherwise high flow, GPIb-dependent conditions.

To inhibit platelet adhesion to these surfaces in the presence of periodic low flow, one potential strategy is to target the integrin family of surface receptors. These molecules, when activated, mediate firm adhesion to specific ligands (αIIbβ3/fibrinogen; α2β1/collagen; αVβ3/ fibronectin, etc.) and it is a combination of these interactions which orchestrate the development of stable aggregates (section 1.2) [26, 35]. We sought to examine the role of specific integrin inhibition on platelet thrombus formation in pulsatile flow environments. Given our collagenized reactive site model, we focused on the collagen integrin receptor, α2β1, given our collagenized reactive site model, as well as the clinically relevant fibrinogen receptor, αIIbβ3, essential for platelet cross-linking and thrombus growth [166, 167]. In doing so, we consider therapeutic strategies that may be of use in localizing anti-thrombotic effects to pulsatile, high flow environments by taking advantage of the redundancy of adhesion pathways and kinetics of platelet response. Specifically, we develop and test the potential of dual receptor blockade ($\alpha_2\beta_1$ in conjunction with GPIb) in enabling selective, high flow inhibition in the presence of temporal fluctuations relevant to real world hemodynamic settings. Finally, we consider the utility of such a strategy in the added presence of a stent.

6.3.1 Methods

Hemodynamic Environment

We applied our reactive coronary site model to investigate the effectiveness of platelet inhibitory strategies in blocking platelet wall interactions under temporally and spatially fluctuating flow conditions. As we wanted to test

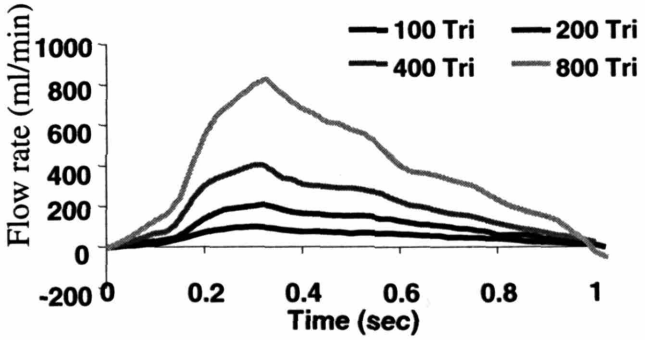

Figure 6.22. Generated triangular flow wave forms spanning a range of physiological to pathological coronary like flow conditions (100-800 ml/min peak; 50-400 ml/min mean flow rates). **One pulse shown.

the ability of these strategies to selectively target specific flow environments regardless of pulsatility, we developed triangular flow patterns that spanned a range from low to high flow conditions (100-800 ml/min peak, 50-400 ml/min mean flow rate Fig. 6.22).

Reactive segments were used as a reductive model of vessel injury. Briefly, fluid loops were made from a 21 cm length of 1/8" inner diameter (ID), 3/16" outer diameter (OD) 3350 Silicone Tygon tubing into which a glass reactive tubing segment was inserted (glass was used to enable surface visualization). The reactive segments were coated with Type I, acid insoluble bovine collagen and the 21 cm lengths were uniformly coated with a 1% BSA blocking solution (see section 5.1).

For the stented trials, 3 cm silicone (rather than glass; Fig. 5.5) reactive segment were prepared in a similar fashion, into which 9-mm, 7-cell, stainless steel NIR® stents (Fig 6.18*a*; Medinol, Jerusalem ISRAEL) were expanded to a 3.0 mm post-inflation diameter as previously described (section 6.1).

Platelet Isolation, Manipulation, and Observation

Whole blood was drawn from healthy volunteers using D-Phe-Pro-Arg chloromethyl ketone (PPACK, 80 μM final concentration) as an anticoagulant and used within 30 min of withdrawal was used as a platelet source. The blood was incubated with the specified antibodies (20 μg/ml AK2, 10 μg/ml Gi9, 20 μg/ml abciximab, PBS vehicle; Table 6.3) for 15 minutes prior to run to block specific platelet receptors. The murine monoclonal anti-GPIb antibody, AK2 as previously described has been shown to functionally block GPIb-vWF interactions [152]. The anti-integrin $\alpha_2\beta_1$ monoclonal antibody Gi9 (Immunotech International, Marseilles, France) functionally blocks collagen adhesion to this receptor [168, 169]. The anti-chimeric Fab fragment of the monoclonal antibody 7E3 (c7E3 Fab-abciximab; Eli-Lilly Centocor, Leiden, The Netherlands) inhibits $\alpha_{IIb}\beta_{III}$/fibrinogen interaction.

Platelet surface adhesion was quantitatively assessed through LDH staining as described previously (section 5.2).

Table 6.3. Platelet receptors and specific functional blocking strategies.

RECEPTOR	LIGAND	FUNCTION	BLOCKING ANTIBODY
GPIb	vWF	Platelet Tethering, Activation	AK2 (20 μg/ml)
AIIbβ3	Fibrinogen, vWF	Platelet Adhesion, Aggregation	Abciximab (20 μg/ml)
α2β1	Collagen	Platelet Adhesion	Gi9 (10 μg/ml)

6.3.2 Platelet inhibition in complex hemodynamic environments

Inhibition in temporally varying conditions (Flow Pulsatility)

To study the effects of blocking specific platelet/wall interactions through targeted receptor inhibition, we incubated anti-coagulated whole blood with the function blocking anti-human α2β1 antibody (Gi9) [168, 169], either alone or in combination with AK2, or with the inhibiting anti-human αIIbβ3 Fab fragment, abciximab alone. We ran 4-6 loops per inhibitor condition for 5 minutes under the triangular profiles over the entire range of flow rates along with PBS vehicle controls. We then analyzed the reactive sites for surface adherent platelets/thrombi via LDH quantification (Fig. 6.23).

Abciximab dramatically reduced platelet accumulation at all flow rates as compared to vehicle control, with ever increasing effectiveness at higher flow rates. Incorporating the previous AK2 findings (Fig. 6.9; section 6.1) blocking the GPIb axis alone partially reduced platelet accumulation at increasing flow rates. Remarkably, while α2β1 blockade (Gi9) had little effect by itself, co-inhibition of GPIb and α2β1 allowed full platelet accumulation at the lower pulsatile flow conditions (50, 100 ml/min mean flow), while uniformly eliminating it under the high triangular flow conditions (200, 400 ml/min).

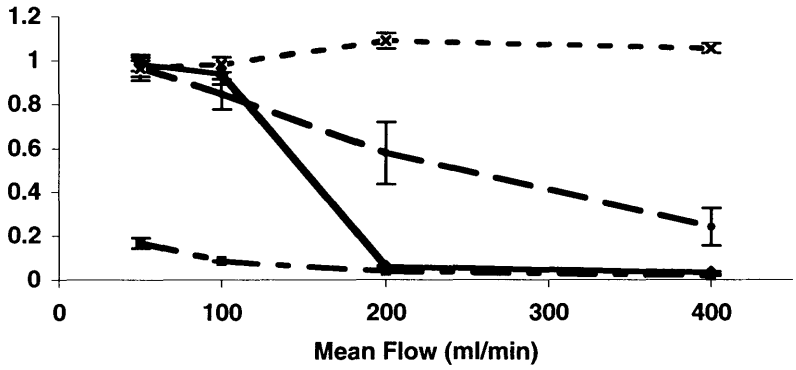

Figure 6.23. Effect of specific receptor blockade on pulsatile, triangular flow dependent platelet adhesion to collagenized reactive sites. Reopro (abxicimab) blocked platelet adhesion across all flow rates with ever-increasing effectiveness at the higher rates. While AK2 showed a reducing trend, neither it nor Gi9 (showing no inhibitory effect at any flow rate) were able to block surface site adhesions completely at any flow level tested. The combination of AK2+Gi9 powerfully inhibited high flow platelet binding, while allowing low flow accumulation to occur.

Kinetic Mechanism of GPIb/a2b1 coinhibition

Modified Flow Profiles for Determining Platelet Adhesion Time ($T_{Adhesion}$)

To determine whether the dramatic anti-platelet effect with GPIb/a2b1 coinhibition was a result of an incapacitated ability to resist high shear forces or a more subtle kinetic effect of prolonging the time required for firm wall adhesion to occur ($T_{Adhesion}$; recall section 6.1), we again generated a set of pulses of varying duty cycle. To test the hypothesis of prolonged $T_{Adhesion}$, duty cycle patterns with extended periods of low flow were needed. Such pulses require sustained periods of constant acceleration which would lead to rapidly compounding rotor velocities (Fig 2.4). To accommodate these prolonged low flow situations while maintaining rotor velocities to reasonable limits, we generated 1 Hz, bidirectional, square pulses of low magnitude (50 ml/min) through out the prescribed low flow portion (Fig. 6.24). With this strategy, we generated flow waveforms with a fixed 0.5 s T_H phase (350 ml/min) and a variable duration T_L phase (50 ml/min), ranging from 0.5-∞ s (T_H and T_L are the periods spent at high and low flow states respectively).

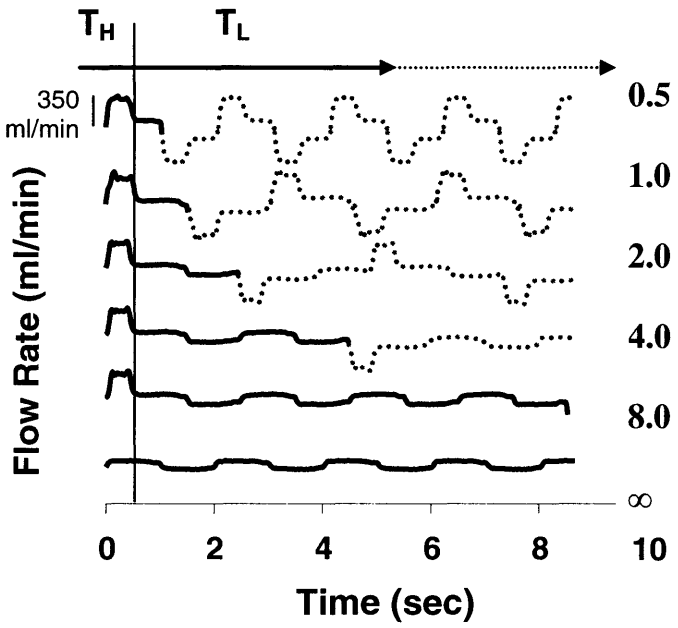

Figure 6.24. Modified High/Low phasic flow profiles of varying duty cycle. Lengthened T_L periods through the use of bidirectional low flows have been employed to test prolonged TAdhesion times.

We ran collagenized reactive sites for 5 minutes with anti-coagulated whole blood incubated with AK2+Gi9, and subsequently assessed them for platelet adhesion. As a result of variability in individual responses, we adopted a screening strategy to determine the minimal time required for platelet adhesion to occur. For each individual (n=8), platelet accumulation was determined via LDH quantification under the 0.5 s and 4 s T_L conditions. If significant platelet adhesion occurred under the 4 s condition, we performed another trial with the 1 and 2 s conditions (there was uniformly no detectable response at 0.5 s). Otherwise, a final trial was performed under the 8 s and ∞ T_L conditions. Given the clear, high (> 0.50 LDH absorbance) or low (< 0.05 LDH absorbance) nature of these responses, we represented our findings with the % of people who supported platelet adhesion (> 0.50 LDH) by a given T_L. Individuals began to respond by 2 s, with all individuals responding by 8 s (Fig. 6.25). These results implicate a finite $T_{Adhesion}$ (2-8 sec) and hence, the kinetic nature of the GPIb, $\alpha 2\beta 1$ co-inhibitory strategy as opposed to a total elimination of firm adhesion.

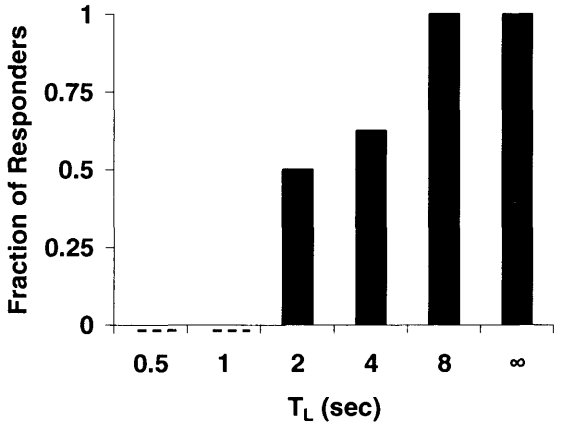

Figure 6.25. Platelet TAdhesion given dual GPIb / α2β1 axis blockade

Inhibition in spatio-temporally varying conditions (Coronary stenting)

In section 6.2, we found that similar to flow pulsatility, stent presence was able to circumvent the effectiveness of GPIb blockade in inhibiting high-flow platelet wall accumulation. Interestingly, we currently have the shown that GPIb, α2β1 coinhibition can maintain anti-adhesive effects in selective, high flow environments under pulsatile flow conditions. To see if this dual inhibitory strategy was also capable of maintaining blockade in the added presence of a stent, where both spatial and temporal pockets of low flow exist, stented, collagenized segments were considered under low and high flow conditions (50, 200 ml/min mean flow rate) using the triangular pulse profiles (Fig. 6.22) under conditions of either dual GPIb/α2β1 or αIIbβ3 inhibition. For each condition, two 5 min runs of 3 stented segments (2 inhibited, 1 non-inhibited control) were performed (total of 4 stents/ condition). Again, platelet / thrombus adhesion was assessed by LDH quantification.

Considering our results (Fig. 6.26), we see dramatically reduced platelet adhesion with αIIbβ3 blockade at both high and low flows regardless of stent presence as compared to uninhibited controls (non-stented conditions carried over from Fig. 6.23). Given GPIb/ α2β1coinhibition, we observe a significant amount of platelet adhesion under low flow

conditions as compared to aIIbB3 blockade, again irrespective of stenting condition. However, considering the high flow case, we observe reduced, but significant platelet accumulation in the presence of a stent, which was eliminated in the absence of the device. While the dual inhibitory strategy was effective in eliminating pulsatile flow adhesion selectively at high flow in a non-stented environment, it was no longer sufficient given the added presence of a stent (in marked contrast to blocking levels achieved by αIIbβ3 inhibition)

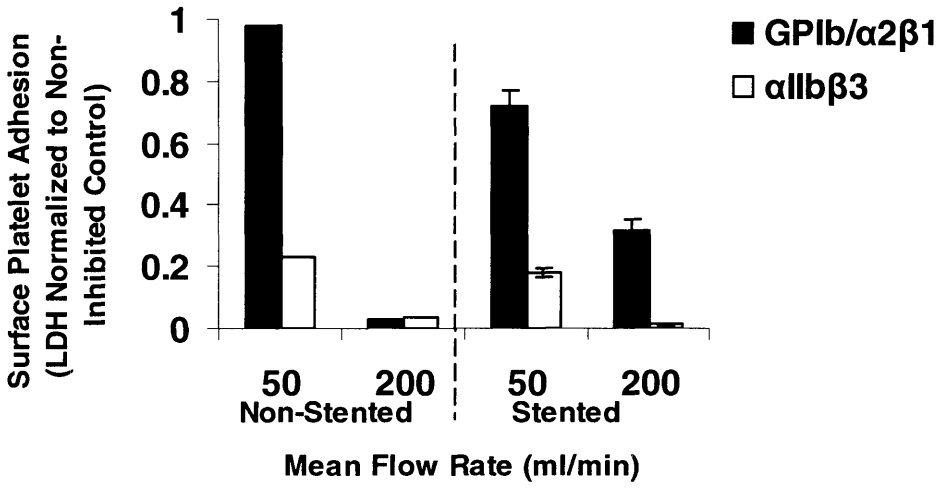

Figure 6.26 Effectiveness of GPIb/α2β1 vs. αIIbβ3 blockade in stented and non stented pulsatile environments. Mean ± SEM

6.3.3 Discussion

Blocking clot formation at the same time minimizing hemorrhagic risk is an important goal in the optimized prevention of thrombotic events. Although the GPIb-vWF axis has been harnessed as a potential high flow anti-thrombotic target, finding stable, high flow settings possess a concern. Real world hemodynamic settings are complex, exhibiting wide fluctuations in both space and time. Even within settings that can globally be defined as high flow, pockets of low flow may exist which can bypass GPIb pathways (section 6.1, 6.2). While it is important to optimize thrombotic inhibitors to a specific prothrombotic setting, it is even more critical to insure sufficient levels of inhibition.

One way to achieve robust anti-thrombotic effects is to forego the goals of targeting specific environments altogether through the use of unselective, systemic strategies. Agents that block the platelet αIIbβ3/fibrinogen receptor accomplish such a goal. The effectiveness of αIIbβ3 blockade on platelet inhibition across a wide range of shear rates has been shown through numerous in vitro and in vivo studies [170]. Moreover it has proven valuable in a variety of thrombotic clinical settings where the hemodynamic situation is far from certain, including the complex coronary stent environment [12, 167, 171]. In our current reactive site study, we also show strong inhibition at both high and low flow conditions both in the presence of pulsatile disturbances as well as to the compounded spatial disturbance of a stent. While the inhibitory strength seems to increase with flow, the significant blocking effects even under low flow, can be attributed to the role of the aiib3 receptor in mediating platelet-platelet fibrinogen cross-linking, without which the crucial aggregation step cannot take place. While a slew of antibody-derived and small molecule agents directed against the αIIbβ3/fibrinogen axis are in use, their potent effect on platelet inhibition brings with it the increased risk of bleeding complications [12, 159]. Balancing the potential benefits with these adverse outcomes tempers the circumstances where the use of such agents is warranted.

Another technique to achieve robustness is to find strategies that are specifically insensitive to the fluctuations (rather than insensitive to the hemodynamic setting altogether). In this section, we assessed the possible efficacy of GPIb/α2β1 dual inhibition and remarkably found high flow adhesion was completely and selectively eliminated given highly pulsatile, triangular flow patterns (our model of coronary-like flow conditions). This inhibition was observed even under conditions when the low flow duration would be approximately half the pulse cycle (~0.5 sec for the 200 ml/min mean flow rate triangular pulse; Fig 6.12, section 6.1). By considering specialized flow profiles of varying low flow duration, we propose that a likely mechanism which can explain the effectiveness of this dual inhibitory technique is through an increased time required for firm platelet adhesion to take place ($T_{Adhesions}$). On a background of GPIb inhibition, we found $T_{Adhesions}$ to be ~0.125-0.25 sec in the absence of α2β1 coinhibition (Fig. 6.14; section 6.1) while in the presence of α2β1 coinhibition we obtained a

considerably prolonged adhesion time between 2-8 seconds (Fig. 6.25). These prolonged $T_{Adhesions}$ may offer a mechanism of `skipping' through temporary pockets of low flow. Interestingly, the minimum $T_{Adhesions}$ of 2 seconds given GPIb/ α2β1 coinhibition suggests that this is a potentially effective strategy for naturally pulsatile, high flow conditions where the pulse rate is greater than 30 bpm (time spent in low flow is necessarily less than 2 sec). Still, larger studies are needed to both to verify this lower bound (we observed large variations over a limited sample size), as well as to delineate the frequency independence/dependence of these methods.

The effect of α2β1 in playing a participatory, non-essential role in platelet adhesion to collagen has been recognized [172-175]. In our reactive site model, sole α2β1 blockade with Gi9 did not have a noticeable effect at any flow rate. With additional blockade of GPIb, we found that adhesive events still took place, given sufficient time spent in a low flow regime (2-8 sec). These findings are in agreement with a recently proposed matrix model of platelet collagen adhesion/activation [176, 177]. In a dynamic, parallel process, weak GPVI (an essential collagen activation receptor) and α2β1 / collagen associations allow GPVI to interact increasingly efficiently with collagen by promoting receptor clustering, enhanced signal transduction, and platelet activation. Activating signals cause α2β1 and a slew of other integrins to adopt their high affinity conformation, supporting firm substrate adhesions while further potentiating GPVI/collagen associations. In such a scheme, α2β1, while enhancing the efficiency of surface collagen interactions, serves a non-essential role in mediating firm adhesive events, so long as sufficient time is allowed for GPVI activation and parallel pathways of integrin mediated firm adhesion to occur. Under conditions when only α2β1 is inhibited, GPIb tethering interactions could slow platelet translocation, thus enabling the necessary surface interactions to take place (while promoting integrin and general platelet activation in its own right). When GPIb is concurrently inhibited and tethering is disabled, platelet translocation must be slowed physically through reduced flow to allow sufficient time for reactions to take place.

The effect of $\alpha_2\beta_1$ in altering the kinetics of firm platelet adhesion raises the question as to the possible efficacy of other dual GPIb/vWF + X inhibitory strategies which may alter platelet wall interactions such that the time required for firm adhesion to

take place is greater than the times spent in regions of low flow ($T_{Adhesion} > T_{Low}$). Recently, co-inhibition of GPIb and αIIbβ3 has been shown to synergistically inhibit platelet adhesion in both *in vitro* and *in vivo* settings, allowing relatively low doses of each to be used, while retaining maximal effects [27, 162]. Other methods, such as aspirin or clopidigrel administration, which alter platelet activatability, would also be interesting, potential strategies [12]

While increasing TAdhesion seems to be an effective strategy for inhibiting high flow platelet adhesion regardless of pulsatility, we found that with the added disturbance of a stent, significant surface platelet accumulation was permitted (0.32±0.03, normalized to uninhibited stented case; Fig. 6.26). Though it is hard to predict what sufficient or insufficient levels of inhibition would be from an *in vitro* model, these findings are clearly increased from levels achieved with either dual inhibition in the absence of stenting, or with αIIbβ3 blockade.

To understand why GPIb/α2β1 coinhibition, whose mechanism of action seems to lie in prolonging the time needed for firm adhesion to take place, works in pulsatile settings but not in the stented case, we can consider the nature of the induced regions of low flow. With purely pulsatile conditions, the time platelets spend in low flow/low shear is uniform and easily definable. With each pulsation, all platelets in contact with the wall experience the same pattern of high and low shear. In the case of stenting, the platelet residence time in low flow zones is far more complex secondary to altered transport phenomena. Some platelets may spend seconds in recirculant zones, while others (as we see here) may never leave. In such complex, spatial diverse flow where platelet wall residence times are hard to predict on an individual basis, finding unique, targetable hemodynamic parameters may not be feasible. In the face of these issues, strategies such as aIIbB3 blockade that are relatively flow independent and have already shown their utility may be required.

Using our in vitro model, we have studied the effectiveness of potential anti-thrombotic strategies in the context of specific real-world situations (pulsatility, stenting). In doing so, we have found the coinhibitory strategies such as GPIb/α2β1 may prove

useful in more selectively defining targeted areas. That this particular combination seems to work well in settings of high flow, regardless of pulsatility is intriguing, particularly given the nature of coronary flow. However, we must recognize the limitations of our study. The same reductive strategies, which we used to simplify and test specific hypothesis also make our findings for less predictive. The pulsatile conditions under which we observed an effect were in an idealized, geometric setting. As we have seen, even the simple insertion of a stent can reduce the observed levels of inhibition likely through the induction of stationary pockets of low flow and prolonged platelet residence times. The actual coronary environment is far more complex and spatial and temporal effects can not be separated as they can in our in vitro system. Furthermore, we have currently only considered a simplified, collagen coated reactive layer. Realistic subendothelial layers (not to mention endothelial layers) are far more complex, with components that interact with several other platelet receptors (section 5.1). Accordingly, on more complete substrates, $T_{Adhesion}$ may no longer be as prolonged as more parallel pathways of adhesion enabling GPIb-independent stable adhesions to take place during periods of low flow. Before we can be more confident in making real-world predictions, we must test the robustness of this strategy by parametrically studying other surfaces, as well as delineate geometric conditions when the strategy breaks down. Furthermore given the importance of $T_{Adhesion}$ in mediating this strategy, we must also recognize the highly variable results that we found and the limited population size considered. Accordingly, larger populations must be observed, both to test model robustness, but also to more fully characterize the nature of the variance. Given its importance in promoting or preventing adhesion in our idealized pulsatile settings, we must consider more generally, its diagnostic potential.

The local hemodynamic environment plays a critical role in directing the local thrombotic response. While many of the fundamental, flow mediated interactions have been delineated through prior *in vitro* and *in vivo* work (section 1.3), much remains to be

learned with regards as to how these factors play out in real-world scenarios. Deeper, situational studies require highly controllable, highly observable systems which recapitulate both the flow and geometric conditions present within specific vascular environments. Such systems could help to bridge the gap between overly reductive and overly complex models, optimizing the path from bench top discovery to bedside application. In preceding chapters, we have established methods to parameterize important biological and physical properties of the platelet response within our *in vitro,* reactive site model. In doing so, we have begun to characterize the platelet response within a coronary-like, pulsatile, hemodynamic setting, thus establishing a foundation from which we can further explore aspects of the hemodynamic environment.

CHAPTER 7 Limitations, Conclusions, and Future Directions

Thrombosis is a crucial physiological response that helps to maintain vascular integrity. However, when harnessed inopportunely or pathologically, it can result in devastating outcomes. One setting which it is especially important to consider is that of acute coronary thrombosis. Formation of clot within the coronary arteries occurs in states of both pathology (atherosclerotic plaque rupture; acute coronary syndromes) and intervention (angioplasty, stenting). The involved thrombotic reactions are complex and involve an intimate partnership of both biological and physical components. Accordingly, understanding and control of thrombosis requires the establishment and control of models that recapitulate relevant aspects of these biophysical environments.

While many of the fundamental, flow mediated interactions have been delineated through prior *in vitro* and *in vivo* work (section 1.3), much remains to be uncovered with regards as to how these factors play out in real-world scenarios. Deeper, situational studies require highly controllable, highly observable systems that can recapitulate and parameterize both the flow and geometric conditions present within specific, local vascular environments. Such systems could help to bridge the gap between overly reductive and overly complex models, optimizing the path from bench top discovery to bedside application.

In the current thesis, we have established a novel method of creating oscillating flow patterns that can match coronary-like flows on a beat-to-beat basis. The method of producing flow is atraumatic to the blood, even at the considerable shear and flow rates found in the arterial setting. The technique allows the flow environment to be easily varied and parameterized through modulating wall acceleration. Importantly, the system offer the uniquely ability to maintained these atraumatic flows in highly relevant, physiological arterial geometries. Not only is wall shear rate considered (as in standard parallel plate systems), but the overall hemodynamic setting.

One limiting aspect of the current system that must be kept in mind as a departure from true flows generated in the coronary setting is the oscillatory, recirculant nature of

the generated flows. While flow in the coronary artery is highly pulsatile, there is net directionality to the flow. However, as the current system's inertial tube flows are generated through wall accelerations, net directional flows would necessarily mean net accelerations and hence, unbounded motor velocities. The bidirectional strategy employed allows coronary flow's to be matched on a single beat, after which flow is driven in an opposite, but symmetric fashion as discussed in chapters 2 and 3. Such oscillations could alter flow sensitive processes such as thrombosis through a variety of mechanisms, from altered wall transport as in a `breathing' reactor, to phenomenon such as cell wall rolling. One method of creating uni-directionality would be through the introduction of a one-way valve (discussed in chapter 3). However, the inclusion of such a mechanism in the flow path would have create additional disturbance in measurement and alternate divergence from an in vivo setting. Thus, while flow oscillation represents an undeniable limitation in the embodied system, it was felt that the ability to generate temporal and spatial flow fluctuations offers a sufficiently novel handle to explore interesting, relevant hemodynamic phenomena. However, in light of such departures, as in the case of any in vitro system, the significance of derived results must eventually be substantiated in the in vivo setting.

In chapters 3, 4, and 5, we established methods to parameterize important biological and physical properties of the platelet response within our oscillating *in vitro,* reactive site model. In particular, we characterized the platelet response within our coronary-like, oscillating, hemodynamic setting, thus establishing a foundation from which we can further explore aspects of the hemodynamic environment. Subsequently, we considered aspects of real-world hemodynamic scenarios, which exhibit a high degree of spatial and temporal variability. Given that platelets are responsive to their shear environments, it is important to delineate the levels at which they can sense local changes in environment. In some cases, spatio-temporal fluctuations may go by unperceived, while in others situations, they may play a crucial role in mediating the local biological reaction.

In chapter 6, we investigated the platelet response to variations in the hemodynamic environment induced by highly idealized situations which we develop in our reactive site model. Specifically, we focused on the effects of coronary-like flow pulsatility and endovascular stent presence as examples of temporal and spatial variability respectively

and found both to significantly affect the manner in which platelets accumulate at a local site on injury. One limitation in the spatial variation stent study was that we were limited to using stents provided by industrial manufacturers and thus, did not truly parameterized the geometric setting. Indeed, while we noted significant variation given the presence of a stent, no significant variations were noted in between stent geometry. To further explore this important issue, we are currently generating methods to create highly controllable geometries of stent dimension directly onto our reactive site surfaces.

Given our findings that highly relevant hemodynamic factors create robust, observable differences in the local platelet response, we further explored the efficacy of anti-thrombotic agents in these temporally and spatially varying settings. This allowed us to consider both the mechanisms by which platelet/wall interactions occur in given settings, as well as explore the potential efficacy of important clinical agents in real world scenarios. Notably, we found that the clinically relevant αIIbβ3 inhibitor was highly effective in a wide variety of settings, regardless of flow rate or spatially and temporally inhomogeneous flows. GPIb axis inhibition selectively blocked high flow adhesions but not in slowly changing pulsatile conditions. Interestingly, GPIb/α2β1 co-inhibition was selectively effective under high flow conditions regardless of pulsatility offering a potential strategy for creating selective blockade in specific hemodynamic settings. Perhaps most interesting was the manner in which various platelet receptors worked together in a given hemodynamic setting to create stable platelet adhesions, especially in light of the many subtle platelet receptor polymorphic variations known to exist in the normal population Still, much work remains to be done to further delineate these phenomena and to establish their relevance in the in vivo setting.

The developed in vitro model has allowed us to consider both flow and geometry as critical aspects of the hemodynamic environment and in doing so, has allowed us to gain insight into the importance of real-world temporal and spatial flow fluctuations on aspects of local thrombosis. We will continue to use the system to gain further insight and hypothesis that can subsequently be substantiated through in vivo consideration. It is our hope that such an in vitro model will be of use in accelerating the pace of bench-top discovery to bed-side understanding and therapy.

Appendix A: IQ Master Programs

Basic IQ Master program files for generating rotor motion profiles/flow waveforms. Initial programs were created using general knowledge of how loop accelerations lead to fluid velocities as determined through straight tube approximations. These examples were then fine-tuned through real-time flow observations until the desired flow profiles were generated. The final programs for generating flows are given. The functions: "Impulse", "Square", "Triangle", "Sine" were applied to tubes using PRP as a test fluid, while the "50" , "100", "200", "400" ml/min peak flow functions were applied to whole blood.

IMPULSE FUNCTION

```
title "impulse"
;assign variables
assign vcity v1
assign accl v2
assign decl v3
assign tc v4

;SET CONSTANTS
reset;
fdr=100;              100% federate
scale=4000;                   1 rev=4000 encoder counts
fel=3;                        following error limit

;start motor at init velocity
accl=500
tc=.3
vcity=50

main:

jaccel=accl
jdecel=accl

forward:
delay=tc
movv=(vcity)
if  vel1<vcity jump forward

reverse:
delay=tc
movv=(-vcity)
if  vel1>(-vcity) jump reverse

jump main
end
```

SQUARE FUNCTION

```
title "square"
;assign variables
assign vcity v1
assign accl v2
assign decl v3
assign vcity2 v4
assign vcity3 v5
assign vcity0 v6
assign sclvel v7
assign scltme v8

;SET CONSTANTS
reset;
fdr=100;              100% federate
scale=4000;                   1 rev=4000 encoder counts
fel=.2;                       following error limit
;start motor at init velocity
accl=5

scltme=.5
sclvel=1

main:
d=-.08/scltme, v=280/sclvel
d=-.055/scltme, v=257/sclvel
d=-.18/scltme, v=165/sclvel
d=-.13/scltme, v=55/sclvel
d=-.02/scltme, v=0/sclvel
d=-.15/scltme, v=155/sclvel
d=-.15/scltme, v=220/sclvel
d=-.2/scltme, v=270/sclvel
d=-.17/scltme, v=300/sclvel

d=.06/scltme, v=280/sclvel
d=.055/scltme, v=257/sclvel
d=.18/scltme, v=165/sclvel
d=.13/scltme, v=55/sclvel
d=.02/scltme, v=0/sclvel
d=.15/scltme, v=155/sclvel
d=.2/scltme, v=220/sclvel
d=.2/scltme, v=270/sclvel
d=.17/scltme, v=300/sclvel
jump main
end
```

TRIANGULAR FUNCTION

```
title "triangle"
;assign variables
assign vcity v1
assign accl v2
assign decl v3
assign vcity2 v4
assign vcity3 v5
assign vcity0 v6
assign sclvel v7
assign scltme v8

;SET CONSTANTS
reset;
fdr=100;              100% federate
scale=4000;                   1 rev=4000 encoder counts
fel=.2;                       following error limit
;start motor at init velocity
accl=5

scltme=1
sclvel=1.2

main:
d=-.16/scltme, v=294/sclvel
d=-.11/scltme, v=285/sclvel
d=-.36/scltme, v=225/sclvel
d=-.26/scltme, v=143/sclvel
d=-.15/scltme, v=0/sclvel
d=-.25/scltme, v=200/sclvel
d=-.25/scltme, v=250/sclvel
d=-.5/scltme, v=270/sclvel
d=-1/scltme, v=300/sclvel

d=.16/scltme, v=294/sclvel
d=.11/scltme, v=285/sclvel
d=.36/scltme, v=225/sclvel
d=.26/scltme, v=143/sclvel
d=.15/scltme, v=0/sclvel
d=.25/scltme, v=200/sclvel
d=.25/scltme, v=250/sclvel
d=.5/scltme, v=270/sclvel
d=1/scltme, v=300/sclvel
jump main
end
```

SINUSOIDAL FUNCTION

```
title "sine"
;assign variables
assign vcity v1
assign accl v2
assign decl v3
assign vcity2 v4
assign vcity3 v5
assign vcity0 v6
assign sclvel v7
assign scltme v8

;SET CONSTANTS
reset;
fdr=100;              100% federate
scale=4000;                   1 rev=4000 encoder counts
fel=.2;                       following error limit
;start motor at init velocity
accl=5

scltme=1
sclvel=1.2

main:
d=-.1/scltme, v=287/sclvel
d=-.075/scltme, v=270/sclvel
d=-.25/scltme, v=190/sclvel
d=-.18/scltme, v=110/sclvel
d=-.1/scltme, v=0/sclvel
d=-.2/scltme, v=155/sclvel
d=-.2/scltme, v=220/sclvel
d=-.25/scltme, v=270/sclvel
d=-.2/scltme, v=300/sclvel
d=-1/scltme, v=300/sclvel

d=-.1/scltme, v=287/sclvel
d=-.075/scltme, v=270/sclvel
d=-.25/scltme, v=190/sclvel
d=-.18/scltme, v=110/sclvel
d=-.1/scltme, v=0/sclvel
d=-.2/scltme, v=155/sclvel
d=-.2/scltme, v=220/sclvel
d=-.25/scltme, v=270/sclvel
d=-.2/scltme, v=300/sclvel
d=-1/scltme, v=300/sclvel
jump main
end
```

TRIANGULAR FUNCTION (50ml/min peak)

```
title "50tri" ; 50 ml/min peak triangular wave
;assign variables
assign vcity v1
assign accl v2
assign decl v3
assign vcity2 v4
assign vcity3 v5
assign vcity0 v6
assign sclvel v7
assign scltme v8

;SET CONSTANTS
reset;
fdr=100;                100% federate
scale=4000;                     1 rev=4000 encoder counts
fel=.2;                         following error limit
;start motor at init velocity
accl=5

scltme=3.4
sclvel=4.5

main:

o1=off
o2=on
o3=off
d=-.2/scltme, v=320/sclvel
d=-.3/scltme, v=290/sclvel
d=-.3/scltme, v=110/sclvel
d=-.05/scltme, v=0/sclvel
dac1=5
d=.3/scltme, v=190/sclvel
dac1=0
d=.3/scltme, v=250/sclvel
d=.3/scltme, v=290/sclvel
d=.3/scltme, v=310/sclvel
d=.2/scltme, v=320/sclvel
d=.3/scltme, v=330/sclvel
d=.4/scltme, v=330/sclvel

o1=off
o2=on
o3=off
d=.2/scltme, v=320/sclvel
d=.3/scltme, v=290/sclvel
d=.3/scltme, v=110/sclvel
d=.05/scltme, v=0/sclvel
dac1=5
d=-.3/scltme, v=190/sclvel
dac1=0
d=-.3/scltme, v=250/sclvel
d=-.3/scltme, v=290/sclvel
d=-.3/scltme, v=310/sclvel
d=-.2/scltme, v=320/sclvel
d=-.3/scltme, v=330/sclvel
d=-.4/scltme, v=330/sclvel

jump main
end
```

TRIANGULAR FUNCTION (100ml/min peak)

```
title "100tri" ; 100 ml/min peak triangular wave
;assign variables
assign vcity v1
assign accl v2
assign decl v3
assign vcity2 v4
assign vcity3 v5
assign vcity0 v6
assign sclvel v7
assign scltme v8

;SET CONSTANTS
reset;
fdr=100;                100% federate
scale=4000;                     1 rev=4000 encoder counts
fel=.2;                         following error limit
;start motor at init velocity
accl=5

scltme=1.5
sclvel=2

main:

o1=off
o2=on
o3=off
d=-.2/scltme, v=320/sclvel
d=-.3/scltme, v=290/sclvel
d=-.3/scltme, v=110/sclvel
d=-.05/scltme, v=0/sclvel
dac1=5
d=.3/scltme, v=190/sclvel
dac1=0
d=.3/scltme, v=250/sclvel
d=.3/scltme, v=290/sclvel
d=.3/scltme, v=310/sclvel
d=.2/scltme, v=320/sclvel
d=.3/scltme, v=330/sclvel
d=.4/scltme, v=330/sclvel

o1=on
o2=off
o3=on
d=.2/scltme, v=320/sclvel
d=.3/scltme, v=290/sclvel
d=.3/scltme, v=110/sclvel
d=.05/scltme, v=0/sclvel
dac1=5
d=-.3/scltme, v=190/sclvel
dac1=0
d=-.3/scltme, v=250/sclvel
d=-.3/scltme, v=290/sclvel
d=-.3/scltme, v=310/sclvel
d=-.2/scltme, v=320/sclvel
d=-.3/scltme, v=330/sclvel
d=-.4/scltme, v=330/sclvel

jump main
end
```

TRIANGULAR FUNCTION (200ml/min peak)

```
title "200tri" ; 200 ml/min peak triangular wave
;assign variables
assign vcity v1
assign accl v2
assign decl v3
assign vcity2 v4
assign vcity3 v5
assign vcity0 v6
assign sclvel v7
assign scltme v8

;SET CONSTANTS
reset;
fdr=100;                100% federate
scale=4000;                     1 rev=4000 encoder counts
fel=.2;                         following error limit
;start motor at init velocity
accl=5

scltme=0.8
sclvel=1

main:

o1=off
o2=on
o3=off
d=-.2/scltme, v=320/sclvel
d=-.3/scltme, v=290/sclvel
d=-.3/scltme, v=110/sclvel
d=-.05/scltme, v=0/sclvel
dac1=5
d=.3/scltme, v=190/sclvel
dac1=0
d=.3/scltme, v=250/sclvel
d=.3/scltme, v=290/sclvel
d=.3/scltme, v=310/sclvel
d=.2/scltme, v=320/sclvel
d=.3/scltme, v=330/sclvel
d=.4/scltme, v=330/sclvel

o1=on
o2=off
o3=on
d=.2/scltme, v=320/sclvel
d=.3/scltme, v=290/sclvel
d=.3/scltme, v=110/sclvel
d=.05/scltme, v=0/sclvel
dac1=5
d=-.3/scltme, v=190/sclvel
dac1=0
d=-.3/scltme, v=250/sclvel
d=-.3/scltme, v=290/sclvel
d=-.3/scltme, v=310/sclvel
d=-.2/scltme, v=320/sclvel
d=-.3/scltme, v=330/sclvel
d=- 4/scltme, v=330/sclvel

jump main
end
```

TRIANGULAR FUNCTION (400ml/min peak)

```
title "400tri" ; 400 ml/min peak triangular wave
;assign variables
assign vcity v1
assign accl v2
assign decl v3
assign vcity2 v4
assign vcity3 v5
assign vcity0 v6
assign sclvel v7
assign scltme v8

;SET CONSTANTS
reset;
fdr=100;                100% federate
scale=4000;                     1 rev=4000 encoder counts
fel=.2;                         following error limit
;start motor at init velocity
accl=5

scltme=.35
sclvel=.45

main:

o1=off
o2=on
o3=off
d=-.2/scltme, v=320/sclvel
d=-.3/scltme, v=290/sclvel
d=-.3/scltme, v=110/sclvel
d=-.05/scltme, v=0/sclvel
dac1=5
d=.3/scltme, v=190/sclvel
dac1=0
d=.3/scltme, v=250/sclvel
d=.3/scltme, v=290/sclvel
d=.3/scltme, v=310/sclvel
d=.2/scltme, v=320/sclvel
d=.3/scltme, v=330/sclvel
d=.4/scltme, v=330/sclvel

o1=on
o2=off
o3=on
d=.2/scltme, v=320/sclvel
d=.3/scltme, v=290/sclvel
d=.3/scltme, v=110/sclvel
d=.05/scltme, v=0/sclvel
dac1=5
d=-.3/scltme, v=190/sclvel
dac1=0
d=-.3/scltme, v=250/sclvel
d=-.3/scltme, v=290/sclvel
d=-.3/scltme, v=310/sclvel
d=-.2/scltme, v=320/sclvel
d=-.3/scltme, v=330/sclvel
d=-.4/scltme, v=330/sclvel

jump main
end
```

Appendix B: Experimental Data

Stented Loop Occlusion Time Data

Stented loop occlusion time data expressed in minutes:

	Polished	Unpolished
Trial 1	33.90365	36.8
	34.60707	32.8
	51.48928	24.8
Trial 2	32.06226	30.4
	35.77335	25.84
	46.16439	27.36
Trial 3	45	26.1
	44.41558	29.25
	45.58442	35.55

Table B.1: Comparison of polished and unpolished stainless steel 7-9 NIR® endovascular stents.

	Polished	Gold		Polished	Gold + Heat
Trial 1	58.75	33.79	Trial 1	41.47	33.79
	70.27	36.67		46.27	41.47
		40.51		59.71	52.99
Trial 2	46.27	39.55	Trial 2	62.59	49.15
	47.23	43.39		62.59	62.59
	70.27				79.87
Trial 3	38	30	Trial 3	38	40
	39	31		39	53
Trial 4	66	36	Trial 4	66	66
	68	37		68	72

Table B.2: Comparison of gold-coated and gold-coated+heat treated stainless steel 7-9 NIR® endovascular stents with polished stents of identical geometry

Parameterized Stent Data (Gold vs. Steel comparisons)

	Control	Gold	Steel
Trial 1	0.444	0.562	1.899
	0.46	0.586	1.847
		0.663	1.312
Trial 2		0.766	1.268
	0.491	1.128	1.807
	0.608	1.053	1.55

Table B.3: Pre-normalized omparison coagulation activation (assessed through production of PT1+2) of non-stented control, gold-coated and stainless steel 7-9 NIR® endovascular stents.

	Control	Gold	Steel
Trial 1	267	950	565
		750	469
		833	710
Trial 2	386	975	692
		750	414
		642	448
Trial 3	311	1100	529
		1140	774
		850	786
Trial 4	286	1072	681
		924	734
		1140	933

Table B.4 Pre-normalized omparison surface bound platelets of non-stented control, gold-coated and stainless steel 7-9 NIR® endovascular stents.

	Control	Gold	Steel
Trial 1	0.0103	0.009904	0.009909
		0.011444	0.010089
		0.010383	0.008482
Trial 2	0.01012	0.010066	0.00976
		0.01384	0.012784
		0.011035	0.013518
Trial 3	0.01015	0.011507	0.008644
		0.009258	0.009417
		0.008222	0.008296
Trial 4	0.01103	0.010383	0.009875
		0.00956	0.008783
		0.01274	0.001016

Table B.5: Pre-normalized comparison of bulk platelet activation of non-stented control, gold-coated and stainless steel 7-9 NIR® endovascular stents.

STENT	0CTI	.1CTI	.5CTI	1CTI

1	5790	3449	1685	1444
2	5589	3249	1615	1391
3	6715	3180	2642	1480
4	6974	3107	1355	1350

Table B.6: Pre-normalized platelet surface adhesion data for stainless steel 7-9 NIR® endovascular stents with increasing amounts of CTI anticoagulant.

STENT	**0CTI**	**.1CTI**	**.5CTI**	**1CTI**
1	0.043478	0.033003	0.034483	0.033582
2	0.043478	0.031034	0.028571	0.035971
3	0.039007	0.029221	0.031746	0.032374
4	0.041667	0.035714	0.029032	0.032143

Table B.7: Pre-normalized platelet bulk activation data for stainless steel 7-9 NIR® endovascular stents with increasing amounts of CTI anticoagulant (mg/ml).

	STEEL		**GOLD**	
Stent	**High Flow**	**Low Flow**	**High Flow**	**Low Flow**
1	4256	3918	6926	3616
2	3006	2236	2456--	
3	4701	1796	5020	3234
4	3605	1882	5532	4384
5	3672	1716	4422	4038
6	3186	1686	4044	1842
7	3654	2221	5035	2853
8	3892	2185	4986	3456

Table B.8: Pre-normalized platelet surface accumulation data for stainless steel and gold-coated 7-9 NIR® endovascular stents at high CTI anticoagulant concentration (0.5mg/ml) for high (200ml/min peak flow) and low (40ml/min peak flow) flow conditions.

	STEEL		**GOLD**	
Stent	**High Flow**	**Low Flow**	**High Flow**	**Low Flow**
1	6715	1876	2982	2500
2	4974	4094	2876	5000
3	2915	2930	2565	5425
4	3500	3260	2560	3905
5	3449	3040	2746	4208
6	3249	4235	2650	4975
7	3180	3305	2845	3500
8	3107	3100	2579	5235

Table B.9: Pre-normalized platelet surface accumulation data for stainless steel and gold-coated 7-9 NIR® endovascular stents at low CTI anticoagulant concentration (0.1mg/ml) for high (200ml/min peak flow) and low (40ml/min peak flow) flow conditions.

Effect of Coronary-Like Flow Pulsatility Data

Run	800T	800T+AK2	400S	400S+AK2
1	3.545	0.154	2.805	0.07
2	3.405	0.758	3.005	0.074
3	3.538	0.649	3.82	0.065
4	3.52	0.07	3.55	0.064
5	2.886	0.645	2.915	0.068
6	2.939	2.287	2.795	0.062
7	4.467	2.134	3.967	0.07
8	4.4	0.08	4.095	0.061

Table B.10: Triangular (T) and Square (S) pulsatile flow dependent platelet adhesion values (as quantified by LDH absorbance) with and without AK2 treatment at a mean flow of 400ml/min.

Run	600T	600T+AK2	300S	300S+AK2
1	2.143	0.277	2.61	0.144
2	2.367	0.975	2.332	0.168
3	2.956	2.43	2.29	0.181
4	2.827	0.896	2.347	0.19
5	3.543	2.765	3.105	0.088
6	3.563	0.365	3.375	0.095
7	4.354	2.327	3.547	0.14
8	3.546	0.131	2.592	0.156

Table B.11: Triangular (T) and Square (S) pulsatile flow dependent platelet adhesion values (as quantified by LDH absorbance) with and without AK2 treatment at a mean flow of 300ml/min.

Run	400T	400T+AK2	200S	200S+AK2
1	2.938	1.975	2.911	0.54
2	2.891	2.934	2.909	0.428
3	2.548	2.76	2.513	1.405
4	2.694	1.875	2.515	1.368
5	2.288	0.305	2.225	0.061
6	2.392	0.295	2.225	0.06
7	2.867	0.945	2.243	0.353
8	2.345	0.865	2.805	0.388

Table B.12: Triangular (T) and Square (S) pulsatile flow dependent platelet adhesion values (as quantified by LDH absorbance) with and without AK2 treatment at a mean flow of 200ml/min.

Run	200T	200T+AK2	100S	100S+AK2
1	2.092	1.787	1.649	1.34
2	1.982	1.543	1.688	1.402
3	1.299	1.124	1.493	1.197
4	1.317	1.154	1.473	1.234
5	1.696	1.386	1.333	1
6	1.877	1.418	1.367	1.12
7	1.695	1.599	1.313	1.077
8	1.75	1.593	1.354	1.085

Table B.13: Triangular (T) and Square (S) pulsatile flow dependent platelet adhesion values (as quantified by LDH absorbance) with and without AK2 treatment at a mean flow of 100ml/min.

Run	100T	100T+AK2	50S	50S+AK2
1	1.004	0.971	0.905	0.876
2	1.05	1.047	0.961	0.903
3	1.122	0.998	1.095	0.984
4	0.956	1.152	1.11	0.821
5	1.35	1.178	0.814	0.756
6	1.204	1.27	0.865	0.79
7	1.051	1.015	0.875	0.956
8	1.362	1.205	1.051	0.766

Table B.14: Triangular (T) and Square (S) pulsatile flow dependent platelet adhesion values (as quantified by LDH absorbance) with and without AK2 treatment at a mean flow of 50ml/min.

	TL					
Run	0 sec	0.125 sec	0.25 sec	0.375 sec	0.5 sec	0.75 sec
1	0.038	0.04	0.091	0.059	0.041	0.94
2	0.043	0.044	0.078	1.766	0.045	1.015
3	0.04	0.022	0.065	0.147	1.132	1.315
4	0.014	0.019	0.064	1.77	1.507	1.215
5	0.085	0.076	0.125	0.135	2.405	0.874
6	0.075	0.092	0.149	0.132	2.23	0.753
7	0.03	0.023	0.285	1.458	0.183	0.536
8	0.067	0.074	0.224	0.132	0.285	1.586

Table B.15: Pre-normalized platelet adhesion values (as quantified by LDH absorbance) as a function of TL (0-0.75 sec) for 8 individuals.

Platelet Inhibitor Data

	50ml/min		100ml/min		200ml/min		400ml/min	
RUN	--	+G19	--	+G19	--	+G19	--	+G19
1	1.123	1.005	1.756	1.819	2.544	2.749	3.654	3.595
2	0.876	0.765	1.865	1.765	2.355	2.57	2.987	3.323
3	0.995	0.998	1.535	1.498	2.055	2.477	3.867	4.185
4	0.985	1.064	1.256	1.105	2.767	2.713	3.97	4.075
5	1.155	1.12	1.423	1.527	2.624	2.845	3.132	3.324

Table B.15: Effect of G19 (a2B2 inhibitor) on platelet adhesion to collagen reactive site (quantified by LDH measurement) as a function of pulsatile, triangular flow rate.

	50ml/min		100ml/min		200ml/min		400ml/min	
RUN	--	+G19,AK2	--	+G19,AK2	--	+G19,AK2	--	+G19, AK2
1	1.086	1.021	1.982	2.114	2.929	0.161	3.399	0.065
2	1.097	1.085	2.092	2.125	2.912	0.162	3.128	0.14
3	0.814	0.895	1.299	1.138	2.545	0.12	3.356	0.154
4	0.872	0.818	1.317	1.212	2.467	0.135	3.587	0.098
5	1.234	1.175	1.511	1.227	1.897	0.155	2.985	0.076

Table B.16: Effect of co-administration of G19 (a2B2 inhibitor) and AK2 (GPIb inhibitor) on platelet adhesion to collagen reactive site (quantified by LDH measurement) as a function of pulsatile, triangular flow rate.

	50ml/min		100ml/min		200ml/min		400ml/min	
RUN	--	+Reopro	--	+Reopro	--	+Reopro	--	+Reopro
1	0.678	0.133	1.345	0.111	1.877	0.077	3.145	0.068
2	1.12	0.145	1.435	0.121	2.254	0.089	3.455	0.077
3	0.956	0.165	1.123	0.098	2.545	0.105	3.56	0.067
4	0.675	0.12	0.928	0.088	2.765	0.076	3.987	0.058
5	0.765	0.205	1.423	0.108	1.928	0.077	3.745	0.058

Table B.17: Effect of Reopro (IIbIIIa inhibitor) on platelet adhesion to collagen reactive site (quantified by LDH measurement) as a function of pulsatile, triangular flow rate.

	50ml/min			200ml/min		
	G19/AK2	Reopro	Control	G19/AK2	Reopro	Control
Trial 1	0.489	0.122	0.638	0.315	0.077	0.855
	0.525	0.134		0.274	0.067	
Trial 2	0.398	0.118	0.575	0.333	0.095	0.939
	0.41	0.105		0.267	0.088	

Table B.18: Effect of co-administration of G19 (a2B2 inhibitor) and AK2 (GPIb inhibitor) or Reopro (IIbIIIa inhibitor) on platelet adhesion to stented, collagenized reactive sites (quantified by LDH measurement) at 50 and 200 ml/min peak pulsatile, triangular flow.

REFERENCES

1. van Breugel, H.H., J.J. Sixma, and R.M. Heethaar, *Effects of flow pulsatility on platelet adhesion to subendothelium.* Arteriosclerosis, 1988. **8**(3): p. 332-5.
2. Jen, C.J., et al., *Flow-induced detachment of adherent platelets from fibrinogen-coated surface.* Am J Physiol, 1996. **270**(1 Pt 2): p. H160-6.
3. Hsiai, T.K., et al., *Pulsatile flow regulates monocyte adhesion to oxidized lipid-induced endothelial cells.* Arterioscler Thromb Vasc Biol, 2001. **21**(11): p. 1770-6.
4. Hsiai, T.K., et al., *Endothelial cell dynamics under pulsating flows: significance of high versus low shear stress slew rates (d(tau)/dt).* Ann Biomed Eng, 2002. **30**(5): p. 646-56.
5. Blackman, B.R., G. Garcia-Cardena, and M.A. Gimbrone, Jr., *A new in vitro model to evaluate differential responses of endothelial cells to simulated arterial shear stress waveforms.* J Biomech Eng, 2002. **124**(4): p. 397-407.
6. Dong, J.F., et al., *Ristocetin-dependent, but not botrocetin-dependent, binding of von Willebrand factor to the platelet glycoprotein Ib-IX-V complex correlates with shear-dependent interactions.* Blood, 2001. **97**(1): p. 162-8.
7. Armstrong, P.W. and M.J. Mant, *Bleeding risks, risk factors and management of bleeding complications after treatment with anticoagulants, specific antithrombins, thrombolytics IIb-IIIa receptor blockers.* Eur Heart J, 1995. **16 Suppl L**: p. 75-80.
8. Blankenship, J.C., *Bleeding complications of glycoprotein IIb-IIIa receptor inhibitors.* Am Heart J, 1999. **138**(4 Pt 2): p. 287-96.
9. Ikeda, Y., et al., *A new approach to antiplatelet therapy: inhibitor of GPIb/V/IX-vWF interaction.* Haemostasis, 2000. **30 Suppl 3**: p. 44-52.
10. Ruggeri, Z.M., *von Willebrand factor as a target for antithrombotic intervention.* Circulation, 1992. **86**(6 Suppl): p. III26-9.
11. Wu, D., et al., *Inhibition of platelet glycoprotein Ib, glycoprotein IIb/IIIa, or both by monoclonal antibodies prevents arterial thrombosis in baboons.* Arterioscler Thromb Vasc Biol, 2002. **22**(2): p. 323-8.
12. Bhatt, D.L. and E.J. Topol, *Scientific and therapeutic advances in antiplatelet therapy.* Nat Rev Drug Discov, 2003. **2**(1): p. 15-28.
13. Nichols, T.C., et al., *Role of von Willebrand factor in arterial thrombosis. Studies in normal and von Willebrand disease pigs.* Circulation, 1991. **83**(6 Suppl): p. IV56-64.
14. McGhie, A.I., et al., *Abolition of cyclic flow variations in stenosed, endothelium-injured coronary arteries in nonhuman primates with a peptide fragment (VCL) derived from human plasma von Willebrand factor-glycoprotein Ib binding domain.* Circulation, 1994. **90**(6): p. 2976-81.
15. Denis, C.V. and D.D. Wagner, *Insights from von Willebrand disease animal models.* Cell Mol Life Sci, 1999. **56**(11-12): p. 977-90.
16. Kageyama, S., et al., *Anti-human vWF monoclonal antibody, AJvW-2 Fab, inhibits repetitive coronary artery thrombosis without bleeding time prolongation in dogs.* Thromb Res, 2001. **101**(5): p. 395-404.

17. Badimon, L., et al., *Platelet thrombus formation on collagen type I. A model of deep vessel injury. Influence of blood rheology, von Willebrand factor, and blood coagulation.* Circulation, 1988. **78**(6): p. 1431-42.
18. Moroi, M. and S.M. Jung, *Integrin-mediated platelet adhesion.* Front Biosci, 1998. **3**: p. D719-28.
19. Savage, B., F. Almus-Jacobs, and Z.M. Ruggeri, *Specific synergy of multiple substrate-receptor interactions in platelet thrombus formation under flow.* Cell, 1998. **94**(5): p. 657-66.
20. Cannon, C.P., *Small molecule glycoprotein IIb/IIIa receptor inhibitors as upstream therapy in acute coronary syndromes. Insights from the TACTICS TIMI-18 trial.* J Am Coll Cardiol, 2003. **41**(4 Suppl S): p. S43-8.
21. Moliterno, D.J. and A.W. Chan, *Glycoprotein IIb/IIIa inhibition in early intent-to-stent treatment of acute coronary syndromes: EPISTENT, ADMIRAL, CADILLAC, and TARGET.* J Am Coll Cardiol, 2003. **41**(4 Suppl S): p. S49-54.
22. Nishiya, T., et al., *Reconstitution of adhesive properties of human platelets in liposomes carrying both recombinant glycoproteins Ia/IIa and Ib alpha under flow conditions: specific synergy of receptor-ligand interactions.* Blood, 2002. **100**(1): p. 136-42.
23. Moroi, M., et al., *Involvement of activated integrin alpha2beta1 in the firm adhesion of platelets onto a surface of immobilized collagen under flow conditions.* Thromb Haemost, 2000. **83**(5): p. 769-76.
24. Goto, S., et al., *Distinct mechanisms of platelet aggregation as a consequence of different shearing flow conditions.* J Clin Invest, 1998. **101**(2): p. 479-86.
1. Edelberg, J.M., P.D. Christie, and R.D. Rosenberg. 2001. Regulation of vascular bed-specific prothrombotic potential. *Circ Res.* **89**(2): 117-24.
2. Fuster, V., L. Badimon, J.J. Badimon, and J.H. Chesebro. 1992. The pathogenesis of coronary artery disease and the acute coronary syndromes (2). *N Engl J Med.* **326**(5): 310-8.
3. Fuster, V., L. Badimon, J.J. Badimon, and J.H. Chesebro. 1992. The pathogenesis of coronary artery disease and the acute coronary syndromes (1). *N Engl J Med.* **326**(4): 242-50.
4. Chesebro, J.H., V. Toschi, M. Lettino, R. Gallo, J.J. Badimon, J.T. Fallon, and V. Fuster. 1995. Evolving concepts in the pathogenesis and treatment of arterial thrombosis. *Mt Sinai J Med.* **62**(4): 275-86.
5. Hansson, G.K., P. Libby, U. Schonbeck, and Z.Q. Yan. 2002. Innate and adaptive immunity in the pathogenesis of atherosclerosis. *Circ Res.* **91**(4): 281-91.
6. Libby, P. 2002. Inflammation in atherosclerosis. *Nature.* **420**(6917): 868-74.
7. Corti, R., V. Fuster, and J.J. Badimon. 2003. Pathogenetic concepts of acute coronary syndromes. *J Am Coll Cardiol.* **41**(4 Suppl S): 7S-14S.
8. Fuster, V., B. Stein, J.A. Ambrose, L. Badimon, J.J. Badimon, and J.H. Chesebro. 1990. Atherosclerotic plaque rupture and thrombosis. Evolving concepts. *Circulation.* **82**(3 Suppl): II47-59.
9. Linton, M.F. and S. Fazio. 2003. A practical approach to risk assessment to prevent coronary artery disease and its complications. *Am J Cardiol.* **92**(1A): 19i-26i.

10. Yang, Q., G.H. Tofler, L.A. Cupples, M.G. Larson, D. Feng, K. Lindpaintner, D. Levy, R.B. D'Agostino, and C.J. O'Donnell. 2003. A genome-wide search for genes affecting circulating fibrinogen levels in the Framingham Heart Study. *Thromb Res.* **110**(1): 57-64.
11. Fox, C.S., J.F. Polak, I. Chazaro, A. Cupples, P.A. Wolf, R.A. D'Agostino, and C.J. O'Donnell. 2003. Genetic and environmental contributions to atherosclerosis phenotypes in men and women: heritability of carotid intima-media thickness in the Framingham Heart Study. *Stroke.* **34**(2): 397-401.
12. Bhatt, D.L. and E.J. Topol. 2003. Scientific and therapeutic advances in antiplatelet therapy. *Nat Rev Drug Discov.* **2**(1): 15-28.
13. Francis, G.A., J.S. Annicotte, and J. Auwerx. 2003. PPAR agonists in the treatment of atherosclerosis. *Curr Opin Pharmacol.* **3**(2): 186-91.
14. Gotto, A.M. 2003. Antioxidants, statins, and atherosclerosis. *J Am Coll Cardiol.* **41**(7): 1205-10.
15. Califf, R.M., E.J. Topol, R.S. Stack, S.G. Ellis, B.S. George, D.J. Kereiakes, J.K. Samaha, S.J. Worley, J.L. Anderson, L. Harrelson-Woodlief, et al. 1991. Evaluation of combination thrombolytic therapy and timing of cardiac catheterization in acute myocardial infarction. Results of thrombolysis and angioplasty in myocardial infarction--phase 5 randomized trial. TAMI Study Group. *Circulation.* **83**(5): 1543-56.
16. Popma, J.J., R.M. Califf, S.G. Ellis, B.S. George, D.J. Kereiakes, J.K. Samaha, S.J. Worley, J.L. Anderson, D. Stump, L. Woodlief, et al. 1992. Mechanism of benefit of combination thrombolytic therapy for acute myocardial infarction: a quantitative angiographic and hematologic study. *J Am Coll Cardiol.* **20**(6): 1305-12.
17. Califf, R.M. 2000. Combination therapy for acute myocardial infarction: fibrinolytic therapy and glycoprotein IIb/IIIa inhibition. *Am Heart J.* **139**(2 Pt 2): S33-7.
18. Chirkov, Y.Y., A.S. Holmes, S.R. Willoughby, S. Stewart, R.D. Wuttke, P.R. Sage, and J.D. Horowitz. 2001. Stable angina and acute coronary syndromes are associated with nitric oxide resistance in platelets. *J Am Coll Cardiol.* **37**(7): 1851-7.
19. Hueb, W.A., G. Bellotti, S.A. de Oliveira, S. Arie, C.P. de Albuquerque, A.D. Jatene, and F. Pileggi. 1995. The Medicine, Angioplasty or Surgery Study (MASS): a prospective, randomized trial of medical therapy, balloon angioplasty or bypass surgery for single proximal left anterior descending artery stenoses. *J Am Coll Cardiol.* **26**(7): 1600-5.
20. Dimas, A.P. and B. Healy. 1989. Coronary artery bypass surgery vs coronary angioplasty: from antithesis to synthesis. *Eur Heart J.* **10 Suppl H**: 85-91.
21. Lascalzo, J., Schafer, AJ, ed. 1994. *Thrombosis and Hemorrhage.* Blackwell Scentific Publications pp.
22. Falati, S., P. Gross, G. Merrill-Skoloff, B.C. Furie, and B. Furie. 2002. Real-time in vivo imaging of platelets, tissue factor and fibrin during arterial thrombus formation in the mouse. *Nat Med.* **8**(10): 1175-81.

23. Savage, B., E. Saldivar, and Z.M. Ruggeri. 1996. Initiation of platelet adhesion by arrest onto fibrinogen or translocation on von Willebrand factor. *Cell.* **84**(2): 289-97.
24. Ruggeri, Z.M. 2000. Role of von Willebrand factor in platelet thrombus formation. *Ann Med.* **32 Suppl 1**: 2-9.
25. Doggett, T.A., G. Girdhar, A. Lawshe, D.W. Schmidtke, I.J. Laurenzi, S.L. Diamond, and T.G. Diacovo. 2002. Selectin-like kinetics and biomechanics promote rapid platelet adhesion in flow: the GPIb(alpha)-vWF tether bond. *Biophys J.* **83**(1): 194-205.
26. Savage, B., F. Almus-Jacobs, and Z.M. Ruggeri. 1998. Specific synergy of multiple substrate-receptor interactions in platelet thrombus formation under flow. *Cell.* **94**(5): 657-66.
27. Goto, S., Y. Ikeda, E. Saldivar, and Z.M. Ruggeri. 1998. Distinct mechanisms of platelet aggregation as a consequence of different shearing flow conditions. *J Clin Invest.* **101**(2): 479-86.
28. Dopheide, S.M., M.J. Maxwell, and S.P. Jackson. 2002. Shear-dependent tether formation during platelet translocation on von Willebrand factor. *Blood.* **99**(1): 159-67.
29. Ruggeri, Z.M., J.A. Dent, and E. Saldivar. 1999. Contribution of distinct adhesive interactions to platelet aggregation in flowing blood. *Blood.* **94**(1): 172-8.
30. Perrault, C., P. Mangin, M. Santer, M.J. Baas, S. Moog, S.L. Cranmer, I. Pikovski, D. Williamson, S.P. Jackson, J.P. Cazenave, et al. 2003. Role of the intracellular domains of GPIb in controlling the adhesive properties of the platelet GPIb/V/IX complex. *Blood.*
31. Yap, C.L., S.C. Hughan, S.L. Cranmer, W.S. Nesbitt, M.M. Rooney, S. Giuliano, S. Kulkarni, S.M. Dopheide, Y. Yuan, H.H. Salem, et al. 2000. Synergistic adhesive interactions and signaling mechanisms operating between platelet glycoprotein Ib/IX and integrin alpha IIbbeta 3. Studies in human platelets ans transfected Chinese hamster ovary cells. *J Biol Chem.* **275**(52): 41377-88.
32. Yuan, Y., S. Kulkarni, P. Ulsemer, S.L. Cranmer, C.L. Yap, W.S. Nesbitt, I. Harper, N. Mistry, S.M. Dopheide, S.C. Hughan, et al. 1999. The von Willebrand factor-glycoprotein Ib/V/IX interaction induces actin polymerization and cytoskeletal reorganization in rolling platelets and glycoprotein Ib/V/IX-transfected cells. *J Biol Chem.* **274**(51): 36241-51.
33. Rosenberg, R.D. 1994.Hemorrhagic Disorders II. Platelets. In *Hematology*, W.S. Beck, Editor. The MIT Press. Cambridge, MA.
34. Nieswandt, B. and S.P. Watson. 2003. Platelet collagen interaction: is GPVI the central receptor? *Blood.*
35. Moroi, M. and S.M. Jung. 1998. Integrin-mediated platelet adhesion. *Front Biosci.* **3**: D719-28.
36. Moroi, M. and S.M. Jung. 1997. Platelet receptors for collagen. *Thromb Haemost.* **78**(1): 439-44.
37. Arderiu, G., M. Diaz-Ricart, B. Buckley, G. Escolar, and A. Ordinas. 2002. Primary arrest of circulating platelets on collagen involves phosphorylation of Syk, cortactin and focal adhesion kinase: studies under flow conditions. *Biochem J.* **364**(Pt 1): 65-71.

38. Harrison, P. and E.M. Cramer. 1993. Platelet alpha-granules. *Blood Rev.* **7**(1): 52-62.
39. Rosenberg, R.D. 1994.Hemorrhagic Disorders I. Protein interations in the clotting mechanism. In *Hematology*, W.S. Beck, Editor. The MIT Press. Cambridge, MA.
40. Coughlin, S.R. 2000. Thrombin signalling and protease-activated receptors. *Nature.* **407**(6801): 258-64.
41. Sambrano, G.R., E.J. Weiss, Y.W. Zheng, W. Huang, and S.R. Coughlin. 2001. Role of thrombin signalling in platelets in haemostasis and thrombosis. *Nature.* **413**(6851): 74-8.
42. Coughlin, S.R. 1998. Sol Sherry lecture in thrombosis: how thrombin 'talks' to cells: molecular mechanisms and roles in vivo. *Arterioscler Thromb Vasc Biol.* **18**(4): 514-8.
43. Kahn, M.L., Y.W. Zheng, W. Huang, V. Bigornia, D. Zeng, S. Moff, R.V. Farese, Jr., C. Tam, and S.R. Coughlin. 1998. A dual thrombin receptor system for platelet activation. *Nature.* **394**(6694): 690-4.
44. Kahn, M.L., M. Nakanishi-Matsui, M.J. Shapiro, H. Ishihara, and S.R. Coughlin. 1999. Protease-activated receptors 1 and 4 mediate activation of human platelets by thrombin. *J Clin Invest.* **103**(6): 879-87.
45. Dicker, I.B., D.L. Pedicord, D.A. Seiffert, G.A. Jamieson, and N.J. Greco. 2001. Both the high affinity thrombin receptor (GPIb-IX-V) and GPIIb/IIIa are implicated in expression of thrombin-induced platelet procoagulant activity. *Thromb Haemost.* **86**(4): 1065-9.
46. Ilveskero, S., P. Siljander, and R. Lassila. 2001. Procoagulant activity on platelets adhered to collagen or plasma clot. *Arterioscler Thromb Vasc Biol.* **21**(4): 628-35.
47. Schmidtke, D.W. and S.L. Diamond. 2000. Direct observation of membrane tethers formed during neutrophil attachment to platelets or P-selectin under physiological flow. *J Cell Biol.* **149**(3): 719-30.
48. Hayashi, S., N. Watanabe, K. Nakazawa, J. Suzuki, K. Tsushima, T. Tamatani, S. Sakamoto, and M. Isobe. 2000. Roles of P-selectin in inflammation, neointimal formation, and vascular remodeling in balloon-injured rat carotid arteries. *Circulation.* **102**(14): 1710-7.
49. Giesen, P.L., U. Rauch, B. Bohrmann, D. Kling, M. Roque, J.T. Fallon, J.J. Badimon, J. Himber, M.A. Riederer, and Y. Nemerson. 1999. Blood-borne tissue factor: another view of thrombosis. *Proc Natl Acad Sci U S A.* **96**(5): 2311-5.
50. Turitto, V.T. and H.R. Baumgartner. 1975. Platelet deposition on subendothelium exposed to flowing blood: mathematical analysis of physical parameters. *Trans Am Soc Artif Intern Organs.* **21**: 593-601.
51. Badimon, L., J.J. Badimon, V.T. Turitto, S. Vallabhajosula, and V. Fuster. 1988. Platelet thrombus formation on collagen type I. A model of deep vessel injury. Influence of blood rheology, von Willebrand factor, and blood coagulation. *Circulation.* **78**(6): 1431-42.
52. Goldsmith, H.L., M.M. Frojmovic, S. Braovac, F. McIntosh, and T. Wong. 1994. Adenosine diphosphate-induced aggregation of human platelets in flow through tubes: III. Shear and extrinsic fibrinogen-dependent effects. *Thromb Haemost.* **71**(1): 78-90.

53. Goto, S., N. Tamura, M. Sakakibara, Y. Ikeda, and S. Handa. 2001. Effects of ticlopidine on von Willebrand factor-mediated shear-induced platelet activation and aggregation. *Platelets.* **12**(7): 406-14.
54. Gachet, C. 2000. Platelet activation by ADP: the role of ADP antagonists. *Ann Med.* **32 Suppl 1**: 15-20.
55. Berne, R.M., Levy, M.N. 1992 *Cardiovascular physiology.* 6 ed. Mosby Year Book. pp.
56. Kolandaivelu, K. and E.R. Edelman. 2002. Low background, pulsatile, in vitro flow circuit for modeling coronary implant thrombosis. *J Biomech Eng.* **124**(6): 662-8.
57. Karnicki, K., E. Komorowicz, D.N. Fass, W.G. Owen, and R.D. McBane, 2nd. 2002. Influence of anatomical location on arterial thrombosis. *Arterioscler Thromb Vasc Biol.* **22**(2): 342-7.
58. Blackman, B.R., G. Garcia-Cardena, and M.A. Gimbrone, Jr. 2002. A new in vitro model to evaluate differential responses of endothelial cells to simulated arterial shear stress waveforms. *J Biomech Eng.* **124**(4): 397-407.
59. Basmadjian, D. 1990. The effect of flow and mass transport in thrombogenesis. *Ann Biomed Eng.* **18**(6): 685-709.
60. Basmadjian, D., M.V. Sefton, and S.A. Baldwin. 1997. Coagulation on biomaterials in flowing blood: some theoretical considerations. *Biomaterials.* **18**(23): 1511-22.
61. Mak, K.H., G. Belli, S.G. Ellis, and D.J. Moliterno. 1996. Subacute stent thrombosis: evolving issues and current concepts. *J Am Coll Cardiol.* **27**(2): 494-503.
62. Makkar, R.R., Kaul, S., Nakamura, M., Dev, V., Litvack, F.I., Park, K., Mcpherson, T., Badimon, J.J., Sheth, S.S., Eigler, N.L. 1995. Modulation of acute stent thrombosis by metal surface characteristics and shear rate. *Circulation.* **92**(8): I-86.
63. Blackman, B.R., K.A. Barbee, and L.E. Thibault. 2000. In vitro cell shearing device to investigate the dynamic response of cells in a controlled hydrodynamic environment. *Ann Biomed Eng.* **28**(4): 363-72.
64. Bao, X., C. Lu, and J.A. Frangos. 1999. Temporal gradient in shear but not steady shear stress induces PDGF-A and MCP-1 expression in endothelial cells: role of NO, NF kappa B, and egr-1. *Arterioscler Thromb Vasc Biol.* **19**(4): 996-1003.
65. Bao, X., C. Lu, and J.A. Frangos. 2001. Mechanism of temporal gradients in shear-induced ERK1/2 activation and proliferation in endothelial cells. *Am J Physiol Heart Circ Physiol.* **281**(1): H22-9.
66. Hsiai, T.K., S.K. Cho, H.M. Honda, S. Hama, M. Navab, L.L. Demer, and C.M. Ho. 2002. Endothelial cell dynamics under pulsating flows: significance of high versus low shear stress slew rates (d(tau)/dt). *Ann Biomed Eng.* **30**(5): 646-56.
67. Evangelista, V., S. Manarini, S. Rotondo, N. Martelli, R. Polischuk, J.L. McGregor, G. de Gaetano, and C. Cerletti. 1996. Platelet/polymorphonuclear leukocyte interaction in dynamic conditions: evidence of adhesion cascade and cross talk between P-selectin and the beta 2 integrin CD11b/CD18. *Blood.* **88**(11): 4183-94.

68. Huang, H., R. Virmani, H. Younis, A.P. Burke, R.D. Kamm, and R.T. Lee. 2001. The impact of calcification on the biomechanical stability of atherosclerotic plaques. *Circulation.* **103**(8): 1051-6.
69. Loree, H.M., B.J. Tobias, L.J. Gibson, R.D. Kamm, D.M. Small, and R.T. Lee. 1994. Mechanical properties of model atherosclerotic lesion lipid pools. *Arterioscler Thromb.* **14**(2): 230-4.
70. Cheng, G.C., H.M. Loree, R.D. Kamm, M.C. Fishbein, and R.T. Lee. 1993. Distribution of circumferential stress in ruptured and stable atherosclerotic lesions. A structural analysis with histopathological correlation. *Circulation.* **87**(4): 1179-87.
71. Lee, R.T. and R.D. Kamm. 1994. Vascular mechanics for the cardiologist. *J Am Coll Cardiol.* **23**(6): 1289-95.
72. Basmadjian, D. 1989. Embolization: critical thrombus height, shear rates, and pulsatility. Patency of blood vessels. *J Biomed Mater Res.* **23**(11): 1315-26.
73. Basmadjian, D. 1984. The hemodynamic forces acting on thrombi, from incipient attachment of single cells to maturity and embolization. *J Biomech.* **17**(4): 287-98.
74. Kassab, G.S., C.A. Rider, N.J. Tang, and Y.C. Fung. 1993. Morphometry of pig coronary arterial trees. *Am J Physiol.* **265**(1 Pt 2): H350-65.
75. Chang, L.J., Tarbell, J. M. 1985. Numerical simulation of fully developed sinusoidal and pulsatile (physiological) flow in curved tubes. *Journal of Fluid Mechanics.* **161**: 175-198.
76. Chang, L.J. and J.M. Tarbell. 1988. A numerical study of flow in curved tubes simulating coronary arteries. *J Biomech.* **21**(11): 927-37.
77. Nosovitsky, V.A., O.J. Ilegbusi, J. Jiang, P.H. Stone, and C.L. Feldman. 1997. Effects of curvature and stenosis-like narrowing on wall shear stress in a coronary artery model with phasic flow. *Comput Biomed Res.* **30**(1): 61-82.
78. Perktold, K., R.M. Nerem, and R.O. Peter. 1991. A numerical calculation of flow in a curved tube model of the left main coronary artery. *J Biomech.* **24**(3-4): 175-89.
79. Makkar, R.R., N.L. Eigler, S. Kaul, A. Frimerman, M. Nakamura, P.K. Shah, J.S. Forrester, J.M. Herbert, and F. Litvack. 1998. Effects of clopidogrel, aspirin and combined therapy in a porcine ex vivo model of high-shear induced stent thrombosis. *Eur Heart J.* **19**(10): 1538-46.
80. Nomura, S., N.N. Tandon, T. Nakamura, J. Cone, S. Fukuhara, and J. Kambayashi. 2001. High-shear-stress-induced activation of platelets and microparticles enhances expression of cell adhesion molecules in THP-1 and endothelial cells. *Atherosclerosis.* **158**(2): 277-87.
81. Garasic, J.M., E.R. Edelman, J.C. Squire, P. Seifert, M.S. Williams, and C. Rogers. 2000. Stent and artery geometry determine intimal thickening independent of arterial injury. *Circulation.* **101**(7): 812-8.
82. Berry, J.L., A. Santamarina, J.E. Moore, Jr., S. Roychowdhury, and W.D. Routh. 2000. Experimental and computational flow evaluation of coronary stents. *Ann Biomed Eng.* **28**(4): 386-98.
83. Eto, K., S. Goto, T. Shimazaki, M. Sakakibara, M. Yoshida, T. Isshiki, and S. Handa. 2001. Two distinct mechanisms are involved in stent thrombosis under flow conditions. *Platelets.* **12**(4): 228-35.

84. Xu, X.Y., Collins, M.W. 1996.Fluid dynamics in stents. In *Endoluminal Stenting*, U. Sigwart, Editor. W.B. Saunders Company Ltd. Philadelphia.
85. Frank, A.O., P.W. Walsh, and J.E. Moore, Jr. 2002. Computational fluid dynamics and stent design. *Artif Organs.* **26**(7): 614-21.
86. Baim, D.S. and J.P. Carrozza, Jr. 1997. Stent thrombosis. Closing in on the best preventive treatment. *Circulation.* **95**(5): 1098-100.
87. Denis, C.V. and D.D. Wagner. 1999. Insights from von Willebrand disease animal models. *Cell Mol Life Sci.* **56**(11-12): 977-90.
88. Nichols, T.C., D.A. Bellinger, D.A. Tate, R.L. Reddick, M.S. Read, G.G. Koch, K.M. Brinkhous, and T.R. Griggs. 1990. von Willebrand factor and occlusive arterial thrombosis. A study in normal and von Willebrand's disease pigs with diet-induced hypercholesterolemia and atherosclerosis. *Arteriosclerosis.* **10**(3): 449-61.
89. Schmidt, B. 1994. Experimental test systems for the assessment of the blood compatibility of materials used in extracorporeal circuits. *Nephrol Dial Transplant.* **9 Suppl 2**: 77-82.
90. Haycox, C.L. and B.D. Ratner. 1993. In vitro platelet interactions in whole human blood exposed to biomaterial surfaces: insights on blood compatibility. *J Biomed Mater Res.* **27**(9): 1181-93.
91. Engelberg, H. 1969. Studies with the Chandler rotating loop. Evidence that thrombin generation is responsible for the formation of the artificial in vitro thrombi. *Thromb Diath Haemorrh.* **22**(2): 344-50.
92. Gardner, R.A. 1974. An examination of the fluid mechanics and thrombus formation time parameters in a Chandler rotating loop system. *J Lab Clin Med.* **84**(4): 494-508.
93. Beythien, C., W. Terres, and C.W. Hamm. 1994. In vitro model to test the thrombogenicity of coronary stents. *Thromb Res.* **75**(6): 581-90.
94. Gutensohn, K., C. Beythien, J. Bau, T. Meinertz, and P. Kuehnl. 1997. Flow cytometric analysis of coronary stent-induced alterations of platelet antigens in an in vitro model. *Thromb Res.* **86**(1): 49-56.
95. Goto, S. and S. Handa. 1998. Coronary thrombosis. Effects of blood flow on the mechanism of thrombus formation. *Jpn Heart J.* **39**(5): 579-96.
96. Grabowski, E.F. 1988. Effects of contrast media on erythrocyte and platelet interactions with endothelial cell monolayers exposed to flowing blood. *Invest Radiol.* **23 Suppl 2**: S351-8.
97. Tsuji, S., M. Sugimoto, S. Miyata, M. Kuwahara, S. Kinoshita, and A. Yoshioka. 1999. Real-time analysis of mural thrombus formation in various platelet aggregation disorders: distinct shear-dependent roles of platelet receptors and adhesive proteins under flow. *Blood.* **94**(3): 968-75.
98. Bluestein, D., L. Niu, R.T. Schoephoerster, and M.K. Dewanjee. 1996. Steady flow in an aneurysm model: correlation between fluid dynamics and blood platelet deposition. *J Biomech Eng.* **118**(3): 280-6.
99. Lyne, W. 1970. Unsteady viscous flow in a curved pipe. *Journal of Fluid Mechanics.* **45**(1): 13-31.
100. Berger, S., Talbot, L, Yao, LS. 1983. Flow in Curved Pipes. *Annual Review of Fluid Mechanics.* **15**: 461-512.

101. Moore, J.E., Jr., N. Guggenheim, A. Delfino, P.A. Doriot, P.A. Dorsaz, W. Rutishauser, and J.J. Meister. 1994. Preliminary analysis of the effects of blood vessel movement on blood flow patterns in the coronary arteries. *J Biomech Eng.* **116**(3): 302-6.
102. Perktold, K., M. Hofer, G. Rappitsch, M. Loew, B.D. Kuban, and M.H. Friedman. 1998. Validated computation of physiologic flow in a realistic coronary artery branch. *J Biomech.* **31**(3): 217-28.
103. Myers, L., Capper WL. 2001. Analytic Solution for Pulsatile Axial Flow Velocity Waveforms in Curved Elastic Tubes. *IEEE Transactions on Biomedical Engineering.* **48**(8): 864-873.
104. Brodkey, R.S. 1967 *The phenomena of fluid motions.* Addison-Wesley Publishing Company. Reading, MA. pp.
105. Zapryanov, Z., Matakiev, V. 1980. An exact solution of the problem of unsteady fully-developed viscous flow in a slightly curved porous tube. *Archives of Mechanics.* **32**: 461-474.
106. Rosenhead, L. 1963.Laminar Boundary Layers. Oxford University Press.
107. Edelman, E.R., P. Seifert, A. Groothuis, A. Morss, D. Bornstein, and C. Rogers. 2001. Gold-coated NIR stents in porcine coronary arteries. *Circulation.* **103**(3): 429-34.
108. Cutlip, D.E., D.S. Baim, K.K. Ho, J.J. Popma, A.J. Lansky, D.J. Cohen, J.P. Carrozza, Jr., M.S. Chauhan, O. Rodriguez, and R.E. Kuntz. 2001. Stent thrombosis in the modern era: a pooled analysis of multicenter coronary stent clinical trials. *Circulation.* **103**(15): 1967-71.
109. Schomig, A., F.J. Neumann, A. Kastrati, H. Schuhlen, R. Blasini, M. Hadamitzky, H. Walter, E.M. Zitzmann-Roth, G. Richardt, E. Alt, et al. 1996. A randomized comparison of antiplatelet and anticoagulant therapy after the placement of coronary-artery stents. *N Engl J Med.* **334**(17): 1084-9.
110. Nomura, S., T. Nakamura, J. Cone, N.N. Tandon, and J. Kambayashi. 2000. Cytometric analysis of high shear-induced platelet microparticles and effect of cytokines on microparticle generation. *Cytometry.* **40**(3): 173-81.
111. Michelson, A.D., M.R. Barnard, L.A. Krueger, C.R. Valeri, and M.I. Furman. 2001. Circulating monocyte-platelet aggregates are a more sensitive marker of in vivo platelet activation than platelet surface P-selectin: studies in baboons, human coronary intervention, and human acute myocardial infarction. *Circulation.* **104**(13): 1533-7.
112. van Breugel, H.H., J.J. Sixma, and R.M. Heethaar. 1988. Effects of flow pulsatility on platelet adhesion to subendothelium. *Arteriosclerosis.* **8**(3): 332-5.
113. Jeong, M.H., W.G. Owen, M.E. Staab, S.S. Srivatsa, G. Sangiorgi, M. Stewart, D.R. Holmes, Jr., and R.S. Schwartz. 1996. Porcine model of stent thrombosis: platelets are the primary component of acute stent closure. *Cathet Cardiovasc Diagn.* **38**(1): 38-43.
114. Rock, G. and P. Tittley. 1990. A comparison of results obtained by two different chromium-51 methods of determining platelet survival and recovery. *Transfusion.* **30**(5): 407-10.
115. Folie, B.J., L.V. McIntire, and A. Lasslo. 1988. Effects of a novel antiplatelet agent in mural thrombogenesis on collagen-coated glass. *Blood.* **72**(4): 1393-400.

116. Bellavite, P., G. Andrioli, P. Guzzo, P. Arigliano, S. Chirumbolo, F. Manzato, and C. Santonastaso. 1994. A colorimetric method for the measurement of platelet adhesion in microtiter plates. *Anal Biochem.* **216**(2): 444-50.
117. Celi, A., G. Merrill-Skoloff, P. Gross, S. Falati, D.S. Sim, R. Flaumenhaft, B.C. Furie, and B. Furie. 2003. Thrombus formation: direct real-time observation and digital analysis of thrombus assembly in a living mouse by confocal and widefield intravital microscopy. *J Thromb Haemost.* **1**(1): 60-8.
118. Schneider, D.J., P.B. Tracy, K.G. Mann, and B.E. Sobel. 1997. Differential effects of anticoagulants on the activation of platelets ex vivo. *Circulation.* **96**(9): 2877-83.
119. Klein, S., M. Spannagl, and B. Engelmann. 2001. Phosphatidylethanolamine participates in the stimulation of the contact system of coagulation by very-low-density lipoproteins. *Arterioscler Thromb Vasc Biol.* **21**(10): 1695-700.
120. Rollason, G. and M.V. Sefton. 1992. Measurement of the rate of thrombin production in human plasma in contact with different materials. *J Biomed Mater Res.* **26**(5): 675-93.
121. Kuijper, P.H., H.I. Gallardo Torres, J.A. van der Linden, J.W. Lammers, J.J. Sixma, L. Koenderman, and J.J. Zwaginga. 1996. Platelet-dependent primary hemostasis promotes selectin- and integrin-mediated neutrophil adhesion to damaged endothelium under flow conditions. *Blood.* **87**(8): 3271-81.
122. Murata, M., K. Kawano, Y. Matsubara, K. Ishikawa, K. Watanabe, and Y. Ikeda. 1998. Genetic polymorphisms and risk of coronary artery disease. *Semin Thromb Hemost.* **24**(3): 245-50.
123. Kunicki, T.J. and D.J. Nugent. 2002. The influence of platelet glycoprotein polymorphisms on receptor function and risk for thrombosis. *Vox Sang.* **83 Suppl 1**: 85-90.
124. Vroman, L., A.L. Adams, G.C. Fischer, and P.C. Munoz. 1980. Interaction of high molecular weight kininogen, factor XII, and fibrinogen in plasma at interfaces. *Blood.* **55**(1): 156-9.
125. Leonard, E.F. and L. Vroman. 1991. Is the Vroman effect of importance in the interaction of blood with artificial materials? *J Biomater Sci Polym Ed.* **3**(1): 95-107.
126. Eriksson, C. and H. Nygren. 1997. The initial reactions of graphite and gold with blood. *J Biomed Mater Res.* **37**(1): 130-6.
127. Courtney, J.M., N.M. Lamba, S. Sundaram, and C.D. Forbes. 1994. Biomaterials for blood-contacting applications. *Biomaterials.* **15**(10): 737-44.
128. Nygren, H. 1996. Initial reactions of whole blood with hydrophilic and hydrophobic titanium surfaces. *Colloids and Surfaces B: Biointerfaces.* **6**: 329-333.
129. Kanagaraja, S., I. Lundstrom, H. Nygren, and P. Tengvall. 1996. Platelet binding and protein adsorption to titanium and gold after short time exposure to heparinized plasma and whole blood. *Biomaterials.* **17**(23): 2225-32.
130. Elam, J.H. and H. Nygren. 1992. Adsorption of coagulation proteins from whole blood on to polymer materials: relation to platelet activation. *Biomaterials.* **13**(1): 3-8.

131. Nygren, H., J.H. Elam, and M. Stenberg. 1988. Adsorption of coagulation proteins and adhesion and activation of platelets at the blood-solid interface. An experimental study of human whole blood. *Acta Physiol Scand.* **133**(4): 573-7.
132. Ratner, B.D. 1984.Contemporary Biomaterials. In *Evaluation of the blood compatibility of synthetic polymers: Consensus and Significance*, J.W. Boretos, Eden, M., Editor. Noyes Publications. Park Ridge, NJ.
133. Herrmann, R., G. Schmidmaier, B. Markl, A. Resch, I. Hahnel, A. Stemberger, and E. Alt. 1999. Antithrombogenic coating of stents using a biodegradable drug delivery technology. *Thromb Haemost.* **82**(1): 51-7.
134. Kastrati, A., A. Schomig, J. Dirschinger, J. Mehilli, N. von Welser, J. Pache, H. Schuhlen, T. Schilling, C. Schmitt, and F.J. Neumann. 2000. Increased risk of restenosis after placement of gold-coated stents: results of a randomized trial comparing gold-coated with uncoated steel stents in patients with coronary artery disease. *Circulation.* **101**(21): 2478-83.
135. Tanigawa, N., S. Sawada, and M. Kobayashi. 1995. Reaction of the aortic wall to six metallic stent materials. *Acad Radiol.* **2**(5): 379-84.
136. Alt, E., Schomig, A. 2000.The InFlow coronary stent. In *Handbook of coronary stenting*, P.W. Serruys, Kutryk, M.J.B., Editor. Martin Dunitz. London.
137. Beythien, C., K. Gutensohn, J. Bau, C.W. Hamm, P. Kuhnl, T. Meinertz, and W. Terres. 1999. Influence of stent length and heparin coating on platelet activation: a flow cytometric analysis in a pulsed floating model. *Thromb Res.* **94**(2): 79-86.
138. Shattil, S.J., M. Cunningham, and J.A. Hoxie. 1987. Detection of activated platelets in whole blood using activation-dependent monoclonal antibodies and flow cytometry. *Blood.* **70**(1): 307-15.
139. Maalej, N. and J.D. Folts. 1996. Increased shear stress overcomes the antithrombotic platelet inhibitory effect of aspirin in stenosed dog coronary arteries. *Circulation.* **93**(6): 1201-5.
140. Gregory, K. and D. Basmadjian. 1994. An analysis of the contact phase of blood coagulation: effects of shear rate and surface are intertwined. *Ann Biomed Eng.* **22**(2): 184-93.
141. Zaacks, S.M., J.E. Allen, J.E. Calvin, G.L. Schaer, B.W. Palvas, J.E. Parrillo, and L.W. Klein. 1998. Value of the American College of Cardiology/American Heart Association stenosis morphology classification for coronary interventions in the late 1990s. *Am J Cardiol.* **82**(1): 43-9.
142. Zaacks, S.M. and L.W. Klein. 1998. The AHA/ACC task force criteria: what is its value in the device era? American Heart Association/American College of Cardiology. *Cathet Cardiovasc Diagn.* **43**(1): 9-10.
143. Serruys, P.W., Kutryk, M.J.B., ed. 2000. *Handbook of Coronary Stenting*. 3 ed. Martin Dunitz. London pp.
144. Berry, J.L., E. Manoach, C. Mekkaoui, P.H. Rolland, J.E. Moore, Jr., and A. Rachev. 2002. Hemodynamics and wall mechanics of a compliance matching stent: in vitro and in vivo analysis. *J Vasc Interv Radiol.* **13**(1): 97-105.
145. Cruz, M.A., H. Yuan, J.R. Lee, R.J. Wise, and R.I. Handin. 1995. Interaction of the von Willebrand factor (vWF) with collagen. Localization of the primary collagen-binding site by analysis of recombinant vWF A domain polypeptides. *J Biol Chem.* **270**(33): 19668.

146. Monnet, E. and F. Fauvel-Lafeve. 2000. A new platelet receptor specific to type III collagen. Type III collagen-binding protein. *J Biol Chem.* **275**(15): 10912-7.
147. Loree, H.M., R.D. Kamm, R.G. Stringfellow, and R.T. Lee. 1992. Effects of fibrous cap thickness on peak circumferential stress in model atherosclerotic vessels. *Circ Res.* **71**(4): 850-8.
148. Armstrong, P.W. and M.J. Mant. 1995. Bleeding risks, risk factors and management of bleeding complications after treatment with anticoagulants, specific antithrombins, thrombolytics IIb-IIIa receptor blockers. *Eur Heart J.* **16 Suppl L**: 75-80.
149. Frojmovic, M.M., T.E. O'Toole, E.F. Plow, J.C. Loftus, and M.H. Ginsberg. 1991. Platelet glycoprotein IIb-IIIa (alpha IIb beta 3 integrin) confers fibrinogen- and activation-dependent aggregation on heterologous cells. *Blood.* **78**(2): 369-76.
150. Jen, C.J., H.M. Li, J.S. Wang, H.I. Chen, and S. Usami. 1996. Flow-induced detachment of adherent platelets from fibrinogen-coated surface. *Am J Physiol.* **270**(1 Pt 2): H160-6.
151. Hsiai, T.K., S.K. Cho, S. Reddy, S. Hama, M. Navab, L.L. Demer, H.M. Honda, and C.M. Ho. 2001. Pulsatile flow regulates monocyte adhesion to oxidized lipid-induced endothelial cells. *Arterioscler Thromb Vasc Biol.* **21**(11): 1770-6.
152. Dong, J.F., M.C. Berndt, A. Schade, L.V. McIntire, R.K. Andrews, and J.A. Lopez. 2001. Ristocetin-dependent, but not botrocetin-dependent, binding of von Willebrand factor to the platelet glycoprotein Ib-IX-V complex correlates with shear-dependent interactions. *Blood.* **97**(1): 162-8.
153. Yusuf, S. and J. Pogue. 1997. Primary angioplasty compared with thrombolytic therapy for acute myocardial infarction. *Jama.* **278**(23): 2110-1.
154. Hueb, W.A., P.R. Soares, S. Almeida De Oliveira, S. Arie, R.H. Cardoso, D.B. Wajsbrot, L.A. Cesar, A.D. Jatene, and J.A. Ramires. 1999. Five-year follow-op of the medicine, angioplasty, or surgery study (MASS): A prospective, randomized trial of medical therapy, balloon angioplasty, or bypass surgery for single proximal left anterior descending coronary artery stenosis. *Circulation.* **100**(19 Suppl): II107-13.
155. Cutlip, D.E. 2000. Stent thrombosis: historical perspectives and current trends. *J Thromb Thrombolysis.* **10**(1): 89-101.
156. Rogers, C. and E.R. Edelman. 1995. Endovascular stent design dictates experimental restenosis and thrombosis. *Circulation.* **91**(12): 2995-3001.
157. Arjomand, H., Z.G. Turi, D. McCormick, and S. Goldberg. 2003. Percutaneous coronary intervention: historical perspectives, current status, and future directions. *Am Heart J.* **146**(5): 787-96.
158. Henry, F. 2000.Flow in Stented Arteries. In *Intra and Extracorporeal Cardiovascular Fluid Dynamics*, P.K. Verdonck P, Editor. WIT Press. Boston. 333-364.
159. Blankenship, J.C. 1999. Bleeding complications of glycoprotein IIb-IIIa receptor inhibitors. *Am Heart J.* **138**(4 Pt 2): 287-96.
160. Ikeda, Y., M. Handa, M. Murata, and S. Goto. 2000. A new approach to antiplatelet therapy: inhibitor of GPIb/V/IX-vWF interaction. *Haemostasis.* **30 Suppl 3**: 44-52.

161. Ruggeri, Z.M. 1992. von Willebrand factor as a target for antithrombotic intervention. *Circulation.* **86**(6 Suppl): III26-9.
162. Wu, D., M. Meiring, H.F. Kotze, H. Deckmyn, and N. Cauwenberghs. 2002. Inhibition of platelet glycoprotein Ib, glycoprotein IIb/IIIa, or both by monoclonal antibodies prevents arterial thrombosis in baboons. *Arterioscler Thromb Vasc Biol.* **22**(2): 323-8.
163. Nichols, T.C., D.A. Bellinger, R.L. Reddick, M.S. Read, G.G. Koch, K.M. Brinkhous, and T.R. Griggs. 1991. Role of von Willebrand factor in arterial thrombosis. Studies in normal and von Willebrand disease pigs. *Circulation.* **83**(6 Suppl): IV56-64.
164. McGhie, A.I., J. McNatt, N. Ezov, K. Cui, L.K. Mower, Y. Hagay, L.M. Buja, L.I. Garfinkel, M. Gorecki, and J.T. Willerson. 1994. Abolition of cyclic flow variations in stenosed, endothelium-injured coronary arteries in nonhuman primates with a peptide fragment (VCL) derived from human plasma von Willebrand factor-glycoprotein Ib binding domain. *Circulation.* **90**(6): 2976-81.
165. Kageyama, S., H. Yamamoto, H. Nakazawa, and R. Yoshimoto. 2001. Anti-human vWF monoclonal antibody, AJvW-2 Fab, inhibits repetitive coronary artery thrombosis without bleeding time prolongation in dogs. *Thromb Res.* **101**(5): 395-404.
166. Cannon, C.P. 2003. Small molecule glycoprotein IIb/IIIa receptor inhibitors as upstream therapy in acute coronary syndromes. Insights from the TACTICS TIMI-18 trial. *J Am Coll Cardiol.* **41**(4 Suppl S): S43-8.
167. Moliterno, D.J. and A.W. Chan. 2003. Glycoprotein IIb/IIIa inhibition in early intent-to-stent treatment of acute coronary syndromes: EPISTENT, ADMIRAL, CADILLAC, and TARGET. *J Am Coll Cardiol.* **41**(4 Suppl S): S49-54.
168. Nishiya, T., M. Kainoh, M. Murata, M. Handa, and Y. Ikeda. 2002. Reconstitution of adhesive properties of human platelets in liposomes carrying both recombinant glycoproteins Ia/IIa and Ib alpha under flow conditions: specific synergy of receptor-ligand interactions. *Blood.* **100**(1): 136-42.
169. Moroi, M., I. Onitsuka, T. Imaizumi, and S.M. Jung. 2000. Involvement of activated integrin alpha2beta1 in the firm adhesion of platelets onto a surface of immobilized collagen under flow conditions. *Thromb Haemost.* **83**(5): 769-76.
170. Wang, X., R.T. Dorsam, A. Lauver, H. Wang, F.A. Barbera, S. Gibbs, D. Varon, N. Savion, S.M. Friedman, and G.Z. Feuerstein. 2002. Comparative analysis of various platelet glycoprotein IIb/IIIa antagonists on shear-induced platelet activation and adhesion. *J Pharmacol Exp Ther.* **303**(3): 1114-20.
171. Adgey, A.A. 1998. An overview of the results of clinical trials with glycoprotein IIb/IIIa inhibitors. *Am Heart J.* **135**(4): S43-55.
172. Jung, S.M. and M. Moroi. 2000. Activation of the platelet collagen receptor integrin alpha(2)beta(1): its mechanism and participation in the physiological functions of platelets. *Trends Cardiovasc Med.* **10**(7): 285-92.
173. Nieswandt, B., C. Brakebusch, W. Bergmeier, V. Schulte, D. Bouvard, R. Mokhtari-Nejad, T. Lindhout, J.W. Heemskerk, H. Zirngibl, and R. Fassler. 2001. Glycoprotein VI but not alpha2beta1 integrin is essential for platelet interaction with collagen. *Embo J.* **20**(9): 2120-30.

174. Goto, S., N. Tamura, S. Handa, M. Arai, K. Kodama, and H. Takayama. 2002. Involvement of glycoprotein VI in platelet thrombus formation on both collagen and von Willebrand factor surfaces under flow conditions. *Circulation.* **106**(2): 266-72.
175. Massberg, S., M. Gawaz, S. Gruner, V. Schulte, I. Konrad, D. Zohlnhofer, U. Heinzmann, and B. Nieswandt. 2003. A crucial role of glycoprotein VI for platelet recruitment to the injured arterial wall in vivo. *J Exp Med.* **197**(1): 41-9.
176. Kuijpers, M.J., V. Schulte, W. Bergmeier, T. Lindhout, C. Brakebusch, S. Offermanns, R. Fassler, J.W. Heemskerk, and B. Nieswandt. 2003. Complementary roles of platelet glycoprotein VI and integrin alpha2beta1 in collagen-induced thrombus formation in flowing whole blood ex vivo. *Faseb J.*
177. Clemetson, K.J. and J.M. Clemetson. 2001. Platelet collagen receptors. *Thromb Haemost.* **86**(1): 189-97.